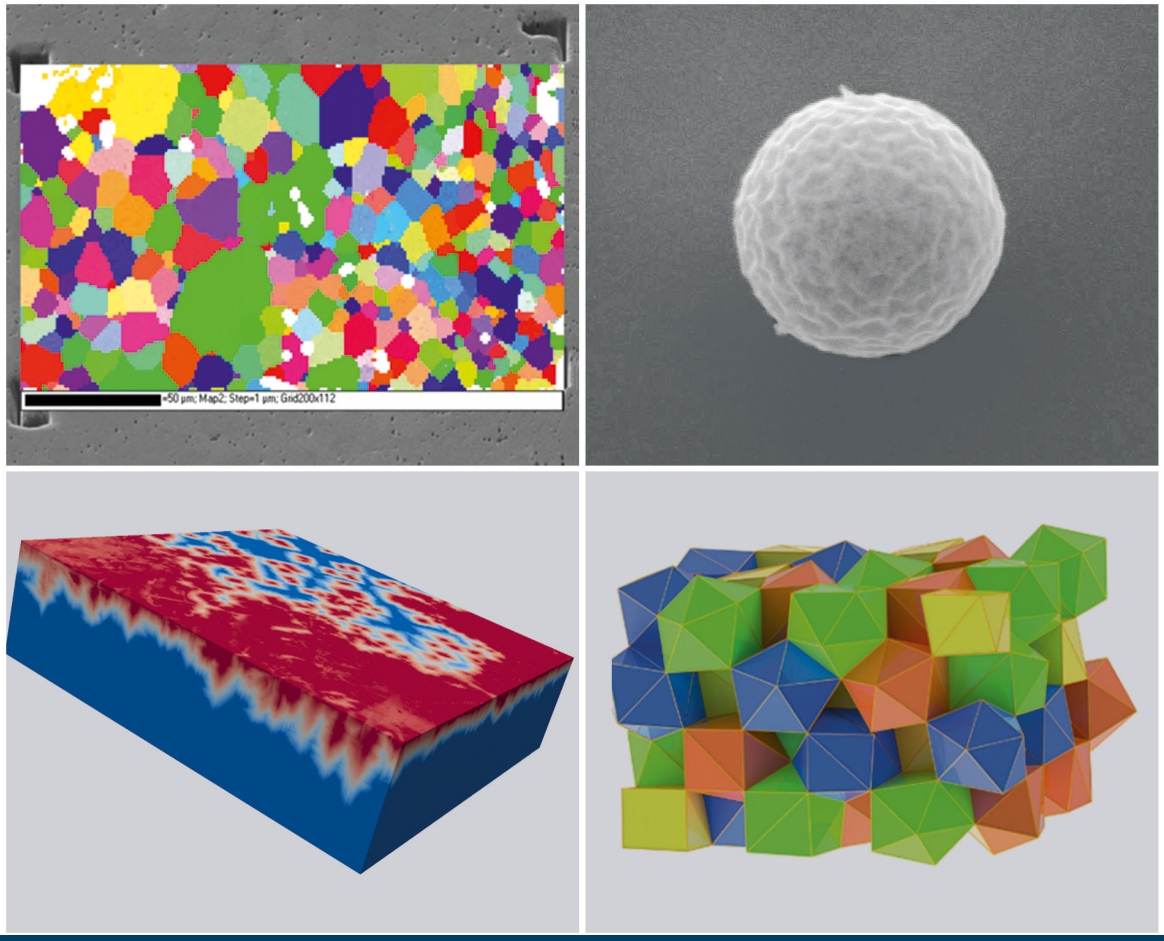

Institute of Energy and Climate Research
IEK-6: Nuclear Waste Management
Report 2015 / 2016

Material Science for Nuclear Waste Management

S. Neumeier, H. Tietze-Jaensch, D. Bosbach (Editors)

Energie & Umwelt / Energy & Environment
Band / Volume 406
ISBN 978-3-95806-293-1

Mitglied der Helmholtz-Gemeinschaft

JÜLICH
Forschungszentrum

Schriften des Forschungszentrums Jülich
Reihe Energie & Umwelt / Energy & Environment Band / Volume 406

Forschungszentrum Jülich GmbH
Institut für Energie- und Klimaforschung
Nukleare Entsorgung und Reaktorsicherheit (IEK-6)

Institute of Energy and Climate Research IEK-6: Nuclear Waste Management Report 2015 / 2016

Material Science for Nuclear Waste Management

S. Neumeier, H. Tietze-Jaensch, D. Bosbach (Editors)

Schriften des Forschungszentrums Jülich
Reihe Energie & Umwelt / Energy & Environment Band / Volume 406

ISSN 1866-1793 ISBN 978-3-95806-293-1

Bibliografische Information der Deutschen Nationalbibliothek.
Die Deutsche Nationalbibliothek verzeichnet diese Publikation in der
Deutschen Nationalbibliografie; detaillierte Bibliografische Daten
sind im Internet über http://dnb.d-nb.de abrufbar.

Herausgeber und Vertrieb:	Forschungszentrum Jülich GmbH Zentralbibliothek, Verlag 52425 Jülich Tel.: +49 2461 61-5368 Fax: +49 2461 61-6103 zb-publikation@fz-juelich.de www.fz-juelich.de/zb
Umschlaggestaltung:	Grafische Medien, Forschungszentrum Jülich GmbH
Druck:	Grafische Medien, Forschungszentrum Jülich GmbH
Copyright:	Forschungszentrum Jülich 2018

Schriften des Forschungszentrums Jülich
Reihe Energie & Umwelt / Energy & Environment, Band / Volume 406

ISSN 1866-1793
ISBN 978-3-95806-293-1

Vollständig frei verfügbar über das Publikationsportal des Forschungszentrums Jülich (JuSER)
unter www.fz-juelich.de/zb/openaccess.

TABLE OF CONTENTS

1 Research for the safe management of nuclear waste

The safe management of nuclear waste and ultimately its disposal in a deep geological repository is one of the grand challenges of our times - with strong links to societal as well as scientific-technical aspects. Without a doubt, excellent research contributes to its solution.

The nuclear phase out until 2022 is an integral part of the transition of the German energy system ("Energiewende"). The decommissioning of the nuclear power plants will take several decades. The German nuclear waste repository Konrad for radioactive waste with negligible heat generation (all low level and some of the intermediate level radioactive waste) will start operation in the next decade. The new site selection act in its most recent form (2017) re-defines the site selection procedure for the German high level nuclear waste repository. Based on a broad societal consensus, a science based comparative site selection process has been defined. This world-wide unique approach poses major scientific challenges, which have not been addressed before.

Contributing to solving these challenges, our basic and applied research for the safe management of nuclear waste is focused on radiochemistry and materials chemistry aspects within the back-end of the nuclear fuel cycle. It is organized in four areas: (1) research supporting the scientific basis of the safety case of a deep geological repository for high level nuclear waste, (2) R&D on waste management concepts for special nuclear wastes (prior to disposal), (3) international safeguards and (4) fundamental structure research of radionuclide containing (waste) materials as a cross-cutting activity. This is the fourth bi-annual report of the Nuclear Waste Management section of the Institute of Energy and Climate Research (IEK-6) at Forschungszentrum Jülich since 2009. In general, our research is contributing to the research program NUSAFE (Nuclear Waste Management, Safety and Radiation Research) of the Helmholtz Association together with the Karlsruhe Institute of Technology and the Helmholtz-Zentrum Dresden-Rossendorf.

A number of excellent scientific results have been published in more than 80 contributions to international peer-reviewed scientific journals in 2015 – 2016, some of them highlighted in this report. The institute was very successful in obtaining third party funded projects and has received substantial funding for a number of national, European and international projects. Collaborative projects funded by BMWi (Federal Ministry of Economic Affairs) and BMBF (Federal Ministry of Education and Science) included the projects ImmoRad, Neutronen Imaging, f-KOM, PGAA-Actinide, Conditioning, PROMETEUS, ThermAc. IEK-6 has been involved in several European projects: ANETTE, ASGARD, CEBAMA, G-SEXTANT, SACSESS and since 2017 in DISCO, THERAMIN, INSIDER, CHANCE and GENIORS. Sarah Finkeldei received the Cutting-Edge-Idea Award of the Forschungszentrum Jülich for her Projekt "COCO-SNUF: Unravelling the Corrosion Complexity of Spent Nuclear Fuel: "Understanding fundamental reaction mechanisms using UO_2 based model systems", 2015. IEK-6 supported the work of the "Kommission Lagerung hoch radioaktiver Abfälle" (engl. commission on disposal of high level radioactive waste) by compiling a report on a P&T strategy for Germany elaborating its pros and cons.

In recent years, the network of collaborators in research organizations, universities, waste management agencies and industry was significantly strengthened. In particular, a strong collaboration with the Belgian nuclear research center SCK.CEN at Mol, was established

including the use of hot cell facilities for studies regarding spent nuclear fuel behaviour in a deep geological repository.

The scientific staff of IEK-6 Nuclear Waste Management is committed to support universities in educating and training students in topics related to nuclear waste management. Currently, eight graduate students are working on their PhD projects. In 2015 and 2016 seven graduate students have finished their dissertation – most of them at RWTH Aachen University: George Beridze: Feasible and reliable *ab initio* atomistic modeling for nuclear waste management, 2016 RWTH Aachen University, Julia Heuser: Keramiken des Monazit-Typs zur Immobilisierung von minoren Actinoiden und Plutonium, 2015, RWTH Aachen University, Christoph Genreith: Partial neutron capture cross sections of actinides using Cold Neutron Prompt Gamma Activation Analysis, 2015, RWTH Aachen University, Alexander Knott: Production and characterization of monodisperse uranium particles for nuclear safeguards applications, 2016, RWTH Aachen University, Tangy Nicol: Caractérisation des colis de déchets radioactifs par activation neutronique, 2016, Université Grenoble Alpes, France, Bin Xiao: The Crystal Chemistry of Thorium and Uranium Compounds with Oxo-anions from Group VI of Periodic Table (S, Se, Te, Cr, Mo and W), 2016, RWTH Aachen University, Na Yu: New insights into thorium and uranium oxo-arsenic(III/V) and oxo-phosphates(V) crystal chemistry, 2015, RWTH Aachen University.

Giuseppe Modolo was awarded the status as adjunct professor at RWTH Aachen University in 2016 – thus being the third member in the faculty of georesources and materials engineering from IEK-6, in addition to Prof. Bosbach and Prof. Alekseev. Recently, Prof. Modolo received the Fritz Straßmann-Prize 2017 of the Gesellschaft Deutscher Chemiker (GDCh), Nuclear Chemistry Divison, in recognition of his outstanding research achievement in the area of actinides separation and -extraction chemistry. Sarah Finkeldei received the Ph.D Award of the German Chemical Society, Nuclear Chemistry Division (Promotionspreis der Fachgruppe Nuklearchemie der Gesellschaft Deutscher Chemiker (GDCh)) for her thesis "Pyrochlore as nuclear waste form: actinide uptake and chemical stability", 2015 and the Excellence Award of the Forschungszentrum Jülich, 2016. Thomas Krings, Julia Heuser, and Sarah Finkeldei received the Borchers Award of the RWTH Aachen for their Ph.D. theses rated “summa cum laude”.

For the future, we will establish a strong link to the research field Earth and Environment within the Helmholtz Association to broaden our multidisciplinary repository research in order to support the re-started site selection procedure in Germany. Research on reactive transport phenomena (coupled processes and scaling) will pave the way towards a more realistic view on repository systems, needed for the comparative site assessment.

Dirk Bosbach

2 Institute's profile

Forschungszentrum Jülich makes a vital contribution to solving major challenges facing society in the fields of information, energy, and bioeconomy. It focuses on the future of information technologies and information processing, complex processes in the human brain, the transformation of the energy system, and a sustainable bioeconomy. Forschungszentrum Jülich develops simulation and data sciences as a key research method and makes use of large, often unique, scientific infrastructures. Its work spans a range of topics and disciplines and it exploits synergies between the research areas. With some 5,600 employees, Jülich – a member of the Helmholtz Association – is one of Europe's large research centres. Research at the Nuclear Waste Management section of the Institute of Energy and Climate Research (IEK-6) of Forschungszentrum Jülich contributes to the Helmholtz program NUSAFE (Nuclear Waste Management, Safety and Radiation Research) and focuses on topics related to the safe management of nuclear wastes and international safeguards.

The safe management of radioactive waste and its final disposal in a deep geological repository is one of the grand challenges of our times and an integral part of the "Energiewende", the transition of the German energy system. The related research is multidisciplinary – though at IEK-6 research mainly focuses on nuclear aspects, addressing the behaviour of radionuclides and the relevant waste form materials by combining radio-, geo- and materials chemistry aspects and by integrating experiment and simulation. Research at IEK-6 covers the complete chain from nuclear waste generation to waste disposal. This includes in particular: (1) research in support of the long-term safety of deep geological disposal with a focus on the repository near-field, incl. nuclear waste forms (e.g. spent nuclear fuel), engineered and geological barrier materials, and in particular the radionuclide uptake by secondary alteration phases (i.e. addressing the radionuclide source term), (2) research on unresolved issues prior to waste disposal, i.e. pre-disposal management, focusing on waste treatment, decontamination/hydrometallurgical separation chemistry, and waste conditioning, with a strong emphasis on special radioactive wastes, for which up to now no management solutions have been developed, and (3) research on international safeguards, incl. the scientific coordination of the German IAEA Safeguards Support Program and qualification for the IAEA Network of Analytical Laboratories. These research activities are supported by the cross-sectional task "structure research", covering the fields of solid state chemistry and physics of radionuclide-bearing phases, research into long-range and short-range order phenomena in crystalline, nano-crystalline and amorphous materials, and application of supercomputing-aided atomistic modelling to issues related to nuclear waste management. IEK-6 operates radiochemistry laboratories and is strongly linked on campus to the Ernst Ruska-Centre for microscopy and spectroscopy with electrons, ER-C, to the Helmholtz Nanofacility, HNF / Helmholtz Energy Materials Characterization Platform HEMCP, with atom probe tomography, to the Jülich Supercomputing Centre, JSC, providing access to world-class supercomputers, and the Central Institute for Engineering, Electronics and Analytics, ZEA. Future research at IEK-6 will focus in particular on reactive mass transport phenomena at chemically perturbed interfaces within nuclear waste repositories, the development of solutions for special "problematic" radioactive wastes and the development of analytical methods for nuclear safeguards and security applications.

Complementary to the research activities related to nuclear waste management and disposal, IEK-6 places particular emphasis on the promotion of earlier-carrier scientists and the education of the next generation of scientists, to maintain and expand competence and know-how in all fields of nuclear waste management. In this context, senior scientists of the institute are involved in lecturing and teaching activities mainly at RWTH Aachen University as well as at other universities in Germany and abroad.

3 Key research topics

3.1. Safety research for nuclear waste disposal

The safe management of radioactive wastes and their final disposal is one of the grand challenges of our times and an integral part of the transition of the German energy system (“Energiewende”). In particular the safe disposal of heat-generating high-level radioactive wastes arising from nuclear power generation requires that the waste is isolated from the geo-/biosphere for extended timescales, in order to protect humans and the environment against dangers arising from ionising radiation. At the technical and scientific level, it is generally accepted that disposal in deep geological formations using a multi-barrier concept comprising man-made barriers ("engineered barrier system") combined with a suitable repository host rock ("geological barrier"), represents the safest and most sustainable option for the management of high-level radioactive wastes and spent nuclear fuels.

However, the geological disposal of nuclear wastes faces major scientific and societal challenges to demonstrate the long-term safety of the repository for the required timescales of up to one million years. The related research is multidisciplinary – while our research mainly considers nuclear aspects, addressing the behaviour of radionuclides and the relevant waste form materials under repository relevant conditions by combining radiochemical, geochemical and materials chemistry aspects. Our cutting-edge research with respect to the long-term safety of nuclear waste disposal includes work on spent nuclear fuel corrosion under disposal conditions, the formation of secondary phases, and radionuclide transport and retention processes – the radio(geo)chemistry of the near field of a deep geological repository. Combing innovative experimental approaches and advanced simulations on various time and length scales, from the molecular scale to the macroscale, we unravel complex coupled processes and mechanism that control the release of radionuclides from the wastes and their migration behaviour in a repository system, thus contributing to the scientific basis of the safety case for deep geological disposal.

Contact: Prof. Dr. Dirk Bosbach
d.bosbach@fz-juelich.de

3.1.1 High-level radioactive waste

The safe management of high-level radioactive wastes (HLW) arising from electricity production from nuclear energy is one of the great challenges of our times, in particular for countries with large nuclear programmes. It is generally accepted from the technical and scientific level that deep geological disposal is the safest and most sustainable option for the management of HLW, such as spent nuclear fuels (SNF) – if declared as waste – or reprocessing wastes (e.g. nuclear waste glasses, compacted wastes, etc.). The HLW containers emplaced in deep geological repositories built in clay formations or crystalline rocks will inevitably come into contact with groundwater post-closure. Even for repositories in salt rocks, the presence of water cannot be completely ruled out for less probable scenarios, for example, early failure of shaft seals and plugs. As a consequence, after container failure due to aqueous corrosion, radionuclides can be released from degrading waste forms and subsequently migrate into the geo-/biosphere via the water pathway. Thus a detailed mechanistic understanding of the relevant processes that govern the corrosion behaviour of and the radionuclide release from HLW under the (hydro)geochemical conditions encountered in the disposal facility is indispensable to substantiate the long-term safety of a geological repository for HLW for the required timescales of up to one million years.

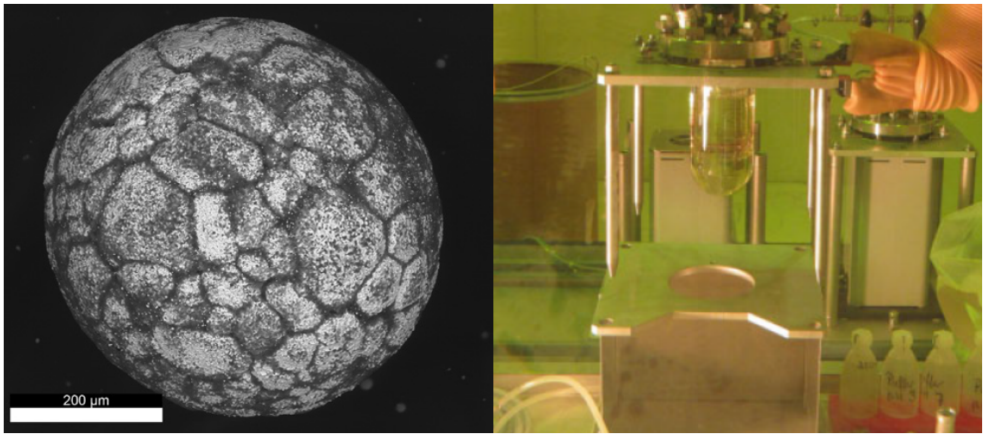

Fig. 1: Irradiated UO_2-fuel kernel (left) and static leaching experiment with spent nuclear fuel (right).

The research activities on HLW at IEK-6 are focused on materials science aspects of the behaviour of waste forms under repository relevant conditions, addressing in particular interactions of SNF with groundwater (Fig. 1). This comprises research into the fast or "instant" release of some volatile radionuclides (e.g. fission gases, and parts of the Cs and I inventories) from SNF immediately after contact with water (so-called instant release fraction IRF) as well as into long-term SNF matrix corrosion processes. These activities aim at an enhanced mechanistic understanding of processes that govern the radionuclide release from SNF in the repository environment (i.e. the radionuclide source term) on a molecular level to reduce uncertainties and conservatisms in performance assessments (PA), and to improve the confidence in system understanding beyond a simple phenomenological description.
However, due to the chemical and structural complexities of SNF and its high radiation field, studies on "real" SNF samples cannot unravel all of the various mechanisms and processes

contributing to the long-term oxidative matrix corrosion of SNF in the nominally reducing repository environment entirely. Therefore, we investigate also various simplified UO_2-based model systems in a tiered bottom-up approach to complement investigations on irradiated "real" SNF. These single-effect studies render to unravel and quantify the contributions of diverse processes to the overall long-term SNF matrix corrosion. Complementary to the various experimental approaches, atomistic simulations on the chemical states of fission and activation products in SNF aim at providing further insight into the behaviour of these materials. These innovative approaches pursued at IEK-6 aim at a refined understanding of SNF behaviour in the repository environment and contribute to the scientific basis of the safety case for deep geological disposal, by reducing uncertainties with respect to the matrix dissolution of and the radionuclide release from SNF.

Contact: Prof. Dr. Dirk Bosbach
d.bosbach@fz-juelich.de

3.1.2 Secondary phases

Deep geological repositories for high level nuclear waste are by their design complex multiphase systems. Geochemical gradients will occur - especially at the interfaces between the different components of the engineered barrier system (EBS). Depending on the host rock and ¬design of the repository, the EBS can contain components such as the waste package (waste form and container), backfill material (bentonite, crushed rock and/or mortar) and a concrete liner (Fig. 2).

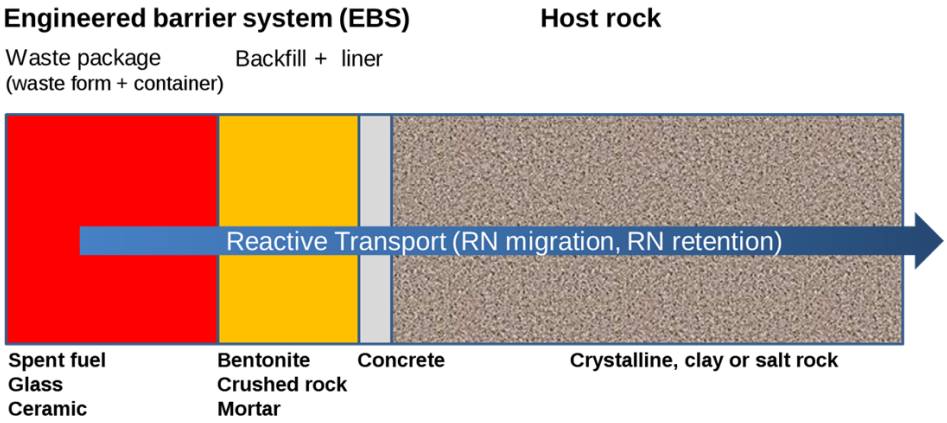

Fig. 2: Schematic of the materials and components foreseen for a deep geological waste repository.

In contact with water, the geochemical conditions are to a large extent determined by the corrosion of metal components and the groundwater chemistry of the host rock. Corrosion and alteration of the waste form and the EBS also lead to the formation of new phases which need to be considered to avoid unnecessary conservatisms in the evaluation of radionuclide mobility in future safety assessments for deep geological repositories. With respect to these new phases, different mechanisms of radionuclide retention need to be considered, (1) adsorption and (2) structural uptake, (3) precipitation of a pure radionuclide phase.

We investigated the immobilization of radionuclides by a structural uptake on a mechanistic level with a focus on the formation of solid-solutions which can have a major impact on radionuclide solubility and retention. One example is the solid solution of $^{226}RaSO_4$ and other sulphate minerals which were studied in detail within a project funded by the Swedish waste management agency SKB. The formation of $(Ba,Ra)SO_4$ solid-solutions was studied applying state of the art high resolution spectroscopic and microscopic approaches in combination with atomistic simulations.

Another example is the retention of radionuclides by cement based systems as studied in the EU-funded CEBAMA project. Here, the sorption mechanisms of radium, molybdenum and iodine species on cement phases was studied in a bottom-up approach, where the adsorption or structural uptake on well-defined model systems is investigated.

Layered double hydroxides (LDH) are studied due to their capability of retaining anionic species of selenium or iodine. Within the framework of the projects ThermAc and VESPA, the structural uptake and thermodynamic properties of LDH was studied.

Contact: Dr. Felix Brandt
f.brandt@fz-juelich.de

3.1.3 Reactive transport modelling

The long-term evolution of the geochemical conditions in a geological repository system, the release of radionuclides from the emplaced wastes, and the radionuclide migration behaviour in the repository near- and far-field are governed by various strongly coupled thermo-hydraulical-mechanical-chemical-biological (THMCB) processes. The radionuclide transport driven either by diffusion and/or advection involves multi-phase flow phenomena under hydraulic and geochemical gradients. The transport phenomena are affected by various complex reactions including dissolution, (co)precipitation and adsorption, redox processes, and gas evolution, which are partly induced and catalysed by microbial activity.

Reactive Transport Modelling (RTM) entails the integration of hydrogeology and geochemistry and the prediction of chemical reactions along transport pathways in space and time. RTM has been increasingly employed in the last decades in various applications such as subsurface contaminant transport and environmental remediation, in the oil and gas industry, or in the field of radioactive waste management. However, for a rigorous comparative analyses of long-term safety aspects of geological repository systems an in-depth understanding and close to reality description of the strongly coupled THMCB processes that affect the radionuclide transport on different time and length scales is required – a so far largely unresolved scientific challenge.

Research on RTM at IEK-6 focuses on the development of complementary experimental and computational approaches to analyse and interpret the complex coupled THMC-processes relevant to radionuclide release and transport in the near- and far-field of geological repositories for radioactive wastes on different scales, employing the high performance computing (HPC) environment provided by the Jülich Supercomputing Centre (JSC) where required. This work aims at an enhanced process and system understanding across scales as well as at the reduction of uncertainties and conservatisms in performance assessments (PA), contributing thus to the scientific basis for an in-depth comparison of different repository concepts and sites as required for the German site selection procedure.

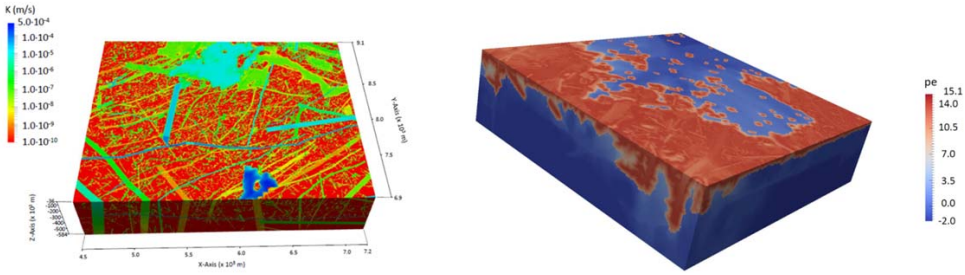

Fig. 3: Conceptual hydrogeological model of the Forsmark repository site (left) and simulated redox perturbation induced by the infiltration of oxygenated melt water during a glaciation event (pe after 350 years) (right).

Contact: Dr. Jenna Poonoosamy
j.poonoosamy@fz-juelich.de

3.2. Structure research

The topic structure research entails fundamental molecular level studies of material properties with the aim to deliver crucial information for the final disposal of high-level nuclear waste. This includes joint experimental and theoretical investigations of chemical, structural and thermodynamic properties addressing specific questions of final disposal (secondary phase formation, waste forms and spent fuel evolution), pre-disposal (extraction efficiency as a factor of coordination chemistry of lanthanides and actinides) and safeguards (e.g., characterization of nuclear materials). This basic research provides the solid scientific basis for successful applied materials research being performed at IEK-6 in general.

The solid state chemistry group is currently revealing fundamental crystal-chemical trends for actinides and selected fission products aiming into better understanding of complex chemical processes taking place in nuclear waste disposal scenarios. The structural analytics group aims into the development of novel and sophisticated diffraction and spectroscopic methods of solid state materials characterization. The atomistic modeling group utilizes and develops advanced methods of computational materials science for reliable computer-aided characterization of nuclear waste materials and processes on atomic scale. The research follows an interdisciplinary approach based on parallel and correlated work.

The studies are performed within the framework of the NUSAFE program in cooperation with partners from HZDR (Dresden) and KIT (Karlsruhe) and various external partners, with the Jülich strong points on solid state chemistry, structural characterization of ordered/disordered materials and utilization of high performance computing infrastructure for molecular-level modeling of complex solids.

Contact: Prof. Dr. Dirk Bosbach
d.bosbach@fz-juelich.de

3.2.1 Solid state chemistry - Helmholtz Young Investigator Group

The actinide elements are of particular concern due to their long half-life and their high radiotoxicity. Knowledge of the stability and the reactivity of actinide compounds under conditions relevant for a waste repository system require a deep understanding of their chemistry in different conditions including solid state. From a solid state chemistry perspective, the actinides with their characteristic ***5f*** electrons, exhibit an extremely complex redox and binding behaviour in general and in the solid state in particular. The relationship between structure of actinide based materials and their properties is one of the most important questions of fundamental actinide science. The research of the proposed "Solid State Chemistry of Actinides" group is oriented on understanding fundamental properties of actinide in solid state oxo-phases in respect to their composition and structure. The research includes understanding oxo-phases formation, their structures, spectroscopic, thermodynamic and some materials properties. The priority in research is given to mineral-like and naturally occurring materials. Mostly, those phases are based on oxo-anions or they are simple or complex oxides. State-of-the-art techniques are used for structure characterization and thermodynamic characterization of synthetized phases. The work is mostly focused on U and Th but some experiments are carried out with transuranic elements such as Np and Pu. The formation of materials is studied under normal and extreme conditions (high-temperature/high-pressure). The potential behaviour of Am^{3+} and Cm^{3+} under extreme conditions is studied with using Ln^{3+} as surrogates.

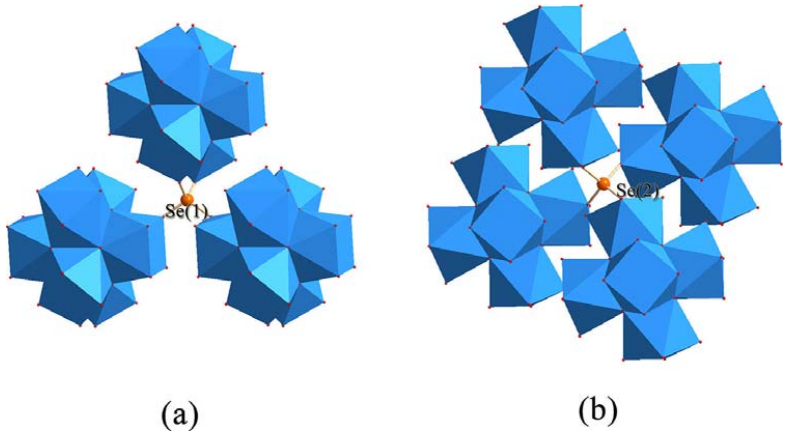

Fig. 4: Representation of the structural position of Se atom surrounded by tree (a) and four (b) $[Th_6(\mu3\text{-}O)_4(\mu3\text{-}OH)_4]^{12+}$ clusters in $Th_3O_2(OH)_2(SeO_4)_3$ phase forming in water solutions. Se atoms are shown in orange, ThO_8 polyhedra are blue. Xiao B. et al. Inorg. Chem. 2015, 54, 3022-3030.

Contact: Prof. Dr. Evgeny Alekseev
e.alekseev@fz-juelich.de

3.2.2 Atomistic modelling - Juelich Young Investigator Group

Safe Management of radioactive waste is a challenging process that involves in-depth characterization of different radionuclide-bearing materials on the atomic scale. Understanding of the atomic-scale processes that govern the interaction of radionuclides with different materials is still limited. This is in large part caused by the limitations of the experimental techniques that are restricted to the specific laboratory conditions. Experiments on active samples are in general also problematic. On the other hand, the continuous improvement of computers performance allows for simulations of even complex materials using first principles (*ab initio*) methods. Such studies provide valuable information on the chemical and physical properties of radionuclide-bearing materials, which is often difficult to obtain by experimental techniques. The aim of our atomistic modeling studies is to use the powerful supercomputing resources located at Forschungszentum Jülich and allied institutions to perform virtual experiments that reveal crucial information on the atomic-scale mechanisms that govern the interactions of radionuclides with various materials, including these constituting the storage and disposal environments.

In order to perform meaningful research we develop computational methodologies that allow for reliable and feasible simulations of nuclear materials. These computational techniques are used for derivation of various structural, thermochemical and thermodynamic parameters of waste forms and secondary phases as well as for simulations of radiation damage and defects formation processes, to name but a few. Our ultimate goal is to complement the ongoing experimental work to obtain more complete understanding of radionuclide-bearing materials. The long-term goal of such a joint modeling and experimental studies aims at providing solid scientific basis for safe management of nuclear waste.

Fig. 5: Left: one of the electronic orbitals responsible for bonding between U atom (grey) and neighboring O atoms (red) in $Ba_2(UO_2)_3(PO_4)_2$ borophosphate. Interaction between Uranium f orbital and Oxygen p orbitals is clearly visible. An atomic scale analysis of charge distribution provides information on the bonding environment. Right: Computer cluster at RWTH Aachen used in the investigation within Jülich-Aachen research alliance (JARA-HPC).

Contact: Dr. Piotr Kowalski
p.kowalski@fz-juelich.de

3.2.3 Structure analytics

The chemical and physical properties of a material are determined by its chemical composition, chemical bonds and particularly by its structure. Ceramic materials and glasses are considered as waste forms for the immobilization of radionuclides. For the disposal of some special waste streams alternative materials can be considered, e.g. so-called Geopolymers and APTM (acid phosphates of tetravalent metals), where the latter can serve as precursor materials for the synthesis of several diphosphates. For the purpose of understanding material properties and for the development of such new materials, knowing the structure is an indispensable prerequisite. As an example monazite (Ln,An)PO_4 can be considered as a solid solution with varying amounts of lanthanide (Ln) and actinide (An) cations. The crystal structures of such mixed phases are determined as a function of chemical composition, temperature, pressure and e.g. radiation damage, using X-ray diffraction and spectroscopic methods (Raman, IR, MAS-NMR, XANES/EXAFS, XPS). The structures of amorphous phases like geopolymers are analyzed by the determination of pair distribution functions (PDF) using synchrotron diffraction data.

At the IEK-6 structure research is performed using the analytical methods mentioned above and additionally thermal analysis, leaching experiments and computer simulations. X-ray synchrotron diffraction and spectroscopy experiments are performed at large research facilities like HASYLAB (Hamburg) or ESRF (Grenoble). Neutron diffraction experiments are performed in cooperation with the RWTH Aachen, e.g. at the nuclear research reactor FRM II (Garching). Structure models are generated directly from crystal structure refinements or by computer simulations (Reverse Monte Carlo for amorphous phases).

Fig. 6: Top view of the large experimental hall at the ESRF/Grenoble (left picture), and experimental setup of powder diffraction experiments on geopolymers using a 2D-detector at beamline ID22 at the ESRF (right picture).

Contact: PD Dr. Hartmut Schlenz
h.schlenz@fz-juelich.de

3.3. Waste management concepts for special radioactive wastes

An increasing number of facilities that use radioactive materials for scientific, health care and industrial purposes are in the process or to be shut down in the next decades. Decommissioning of a nuclear facility is always accompanied by generation of special radioactive wastes streams divers in their composition, radionuclide inventory and chemical behaviour and chemotoxic constituents (e.g. mercury or beryllium). Application of routine methods for characterization, handling, treatment and conditioning of these special wastes is not appropriate, and therefore requires a special consideration during selection of a management option for every waste stream.

Among the waste from decommissioning the intermediate and low level nuclear wastes (LILW), like constructional reactor and cleaning materials, comprise up to 95% waste volume carrying only 1% of specific activity. In Germany the low and some part of the intermediate level waste will be disposed of in the underground repository Schacht Konrad (a former iron ore mine in the Federal State of Lower Saxony), which will go into operation in the next decade. However, a huge necessity for R&D activities in this field still exists, particularly regarding the waste volume reduction and conditioning. As these “problematic” wastes were not properly addressed in the past, some of them failed to meet the acceptance criteria for processing or final disposal. The current R&D approach suggests a detailed characterization of every waste stream for development of an individual approach for treatment for waste minimization, waste encapsulation technology and safe disposal.

The research of our department focuses on comprehensive characterization of special nuclear waste streams, optimization of complex and time consuming procedures for the waste treatment for minimization of the waste volume and secondary waste streams. The emphasis is made on the decontamination of irradiated or contaminated materials (e.g. nuclear graphite, mercury) in order to achieve a clearance level, significant reduction of radioactive waste to be disposed of and potential reuse of treated materials. This also includes the development of advanced technologies for recovery of long-lived radiotoxic constituents, such as the minor actinides or ^{14}C, and their subsequent conditioning in stable matrices.

Contact: Prof. Dr. Giuseppe Modolo
g.modolo@fz-juelich.de

3.3.1 Characterisation of nuclear waste

The Waste Characterization group at IEK-6 develops innovative passive and active non-destructive analytical techniques (Fig. 7) for the accurate and reliable characterization of radioactive waste and other materials. R&D activities focus on neutron interrogation techniques for the determination of chemotoxic elements using Prompt and Delayed Gamma Neutron Activation Analysis (P&DGNAA) and for the localization of large shielding structures by fast neutron imaging in 200 L waste packages. Simulation tools such as MCNP and GEANT4 are applied for system design and optimization.
In the field of technology transfer industrial applications of P&DGNAA for recycling of conventional waste and for quality control of products and raw materials are also investigated.

P&DGNAA – MEDINA Facility

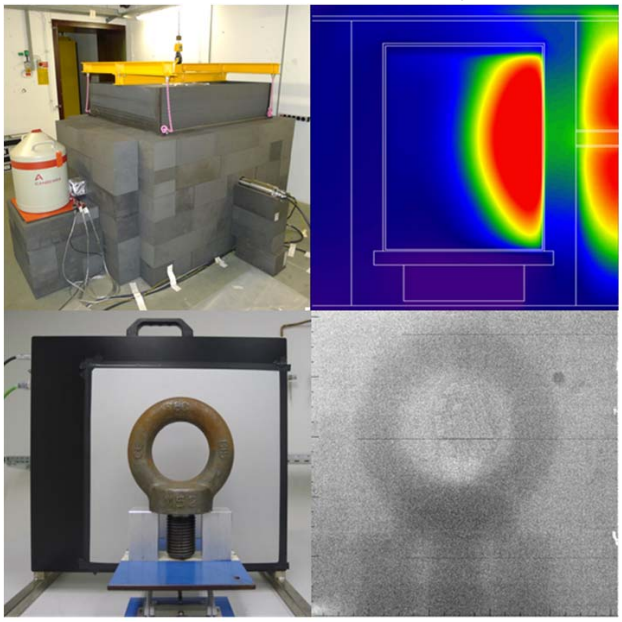

Fast Neutron Imaging

Fig. 7: Non-destructive analytical techniques: MEDINA (Multi-Element-Detection based on Instrumental Activation Analysis) and Fast Neutron Imaging.

Contact: Prof. Dr. Giuseppe Modolo
g.modolo@fz-juelich.de

3.3.2 Nuclear waste treatment

The group of Nuclear Waste Treatment at IEK-6 focuses its research activity on fundamental investigation of “problematic” nuclear wastes arising from commercial and research reactors, like irradiated graphite (i-graphite), spent ion exchange resins (SIERs), radioactive toxic metals (e.g. mercury, beryllium). Our research activity addresses primarily the characterization of material properties, such as (1) structure, which is extensively effected by irradiation performance in the reactor, (2) inventories and distribution of activation products (APs), which to a large extent stem from the impurity in the original inactive material used in the reactor construction, and (3) chemical properties in order to develop an efficient treatment approach for waste minimization and encapsulation. This information represents the boundary conditions for theoretical modelling of waste stability in the long-term and enables the development of a waste minimization technology, providing a safe and economic solution to the worldwide problem of nuclear waste accumulation. Modern analytical techniques (e.g. SEM, XPS, SIMS, HPLC, GC, ICP-MS, etc.) are used along with radioanalytical methods (α- and α-spectrometry, LSC, autoradiography etc.) in order to achieve a high precision in identification of radionuclide vectors, radionuclide localisation and speciation in irradiated materials. Fig. 8 demonstrates an example of a successive application of autoradiography and SEM for localization of APs in i-graphite.

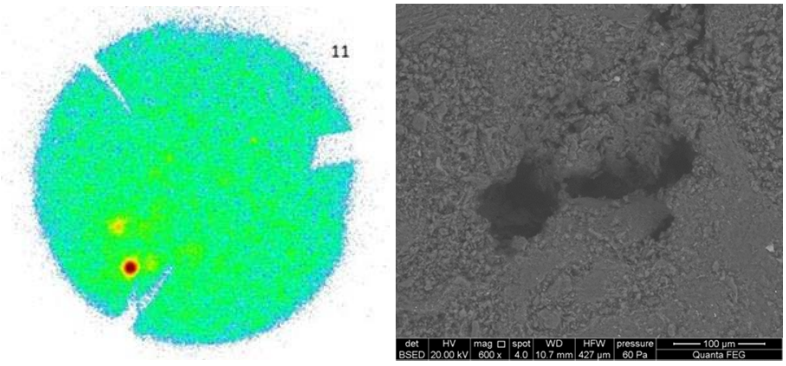

Fig. 8: Autoradiography (a) and SEM imaging of a hot-spot (b) in i-graphite, demonstrating an approach for localization of some APs in nuclear graphite.

Contact: Dr. Natalia Shcherbina
n.shcherbina@fz-juelich.de

3.3.3 Separation chemistry

Our research focuses on minimization of the volume of the radiotoxic waste, to safely condition residual waste and to optimize complex and time consuming procedures. This includes also the development of advanced technologies to potentially recover long-lived constituents, such as the minor actinides from highly radioactive spent fuel for a subsequent conditioning in stable matrices. Research on the separation of radionuclides from nuclear waste solutions is based on highly selective hydrometallurgical separation processes.

Hydrometallurgical separation technologies also concentrate the radionuclides destined for geologic disposal into a smaller volume. The main objectives of our research are on the one hand fundamental research on solvent extraction, to improve the knowledge of the chemistry of the radionuclides and the extraction ligands and on the other hand process development involving testing of continuous extraction devices (Fig. 9) with inactive and with spiked radioactive waste solutions. For a successful separation of specific waste components, a fundamental understanding of the principles of the complexation of radionuclides in aqueous and organic extractant solution is a crucial issue. Research covers the fields of thermodynamics, hydrodynamics and kinetics of liquid-liquid extraction as well as the long-term operation of the solvent (hydrolysis and radiolysis). This includes also recycling and cleaning of the solvent and the management of secondary waste. This knowledge is important to develop multi-scale models to be used in a simulation code, which is an indispensable tool to operate such processes in a safe manner. The flow-sheets are tested and evaluated by comparing them with model predictions.
Solvent extraction processes are also capable of very high throughputs, with minimal generation of secondary wastes, because a relatively small volume of solvent can be used and continuously recycled.

Fig. 9: Centrifugal contactors installed in the fume hood of IEK-6 laboratory

Contact: Prof. Dr. Giuseppe Modolo
g.modolo@fz-juelich.de

3.3.4 Ceramic waste forms

In the last decades, various ceramic materials have been proposed as potential waste forms for the immobilisation of special nuclear waste streams, such as separated plutonium from civilian or military sources unsuitable for further use. At IEK-6, a research program has been developed (Fig. 10) in order to investigate systematically the correlation between structure and properties of ceramic waste forms with the aim to gain a refined understanding on the atomic scale of the long-term behaviour of these materials under conditions relevant to disposal in a deep geological repository.
The research focuses on single phase ceramics such as monazite-type and zirconium and hafnium oxide based materials due to their specific physico-chemical properties including high structural flexibility, high chemical durability, and high radiation resistance and cover:

- development and optimisation of wet chemical synthesis and sintering methods suitable for the immobilisation of radionuclides in and the densification of ceramic waste forms with well-defined microstructure,
- structural and microstructural characterisation of the ceramic materials using state-of-the-art diffraction (powder and single crystal XRD), spectroscopic (Raman, TRLFS, EXAFS) and microscopic (SEM, FIB/TEM) methods,
- determination of thermodynamic and physical properties,
- investigation of radiation damages invoked by heavy ion irradiation,
- investigation of aqueous durability,
- development of synergies between experimental investigations and atomistic simulations (e.g. regarding structure, physical properties and radiation damages).

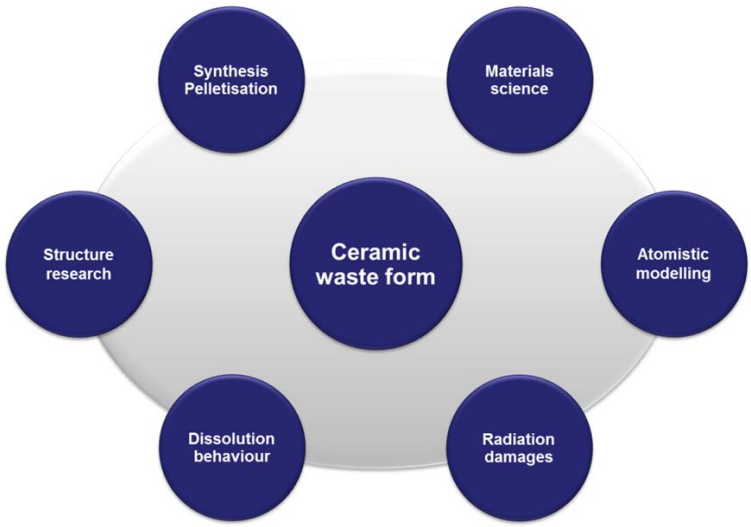

Fig. 10: Scheme of methodology for systematic investigation of ceramic waste forms at IEK-6.

Contact: Dr. Stefan Neumeier
s.neumeier@fz-juelich.de

3.4. Nuclear safeguards and security

Safeguards are activities by which the International Atomic Energy Agency (IAEA), in accordance with the Treaty on the Non-Proliferation of Nuclear Weapons (NPT), can verify that a State is in compliance with its international commitments to use nuclear material and technologies only for peaceful purposes. In order to implement safeguards efficiently and effectively, the IAEA needs to deploy 'state of the art' tools, techniques, methodologies and expertise. As the IAEA has no dedicated budget for R&D, support from States is required in this regard.

Germany provides R&D support though the "Joint Programme on the Technical Development and Further Improvement of IAEA Safeguards between the Government of the Federal Republic of Germany and the International Atomic Energy Agency", also known as the "German Member State Support Programme" (GER MSSP). On behalf of the Federal Ministry of Economic Affairs and Energy (BMWi), IEK-6 is in charge of the scientific coordination of this programme, which typically includes about 20 joint R&D projects with the IAEA. At the same time, IEK-6 is also the principal investigator of many of these projects. In this line, IEK-6 carries out R&D activities in the following areas: Safeguards analytical techniques (cf. 3.4.2), systems analysis, geospatial information analysis, sealing systems, and verification concepts (cf. 3.4.2).

On the national level, the safeguards project "New and further development of safeguards techniques and methods" (Neu- und Weiterentwicklung von Safeguardstechniken und -methoden) consists of R&D activities in primary support of the German safeguards stakeholders and the European Commission (Euratom).

Recently, the scope of R&D activities at IEK-6 related to nuclear non-proliferation has been extended to also take nuclear security aspects into consideration. Nuclear security measures are put in place to ensure the physical protection of nuclear installations and material. These measures are designed to prevent, detect, and respond to theft, sabotage, unauthorized access, illegal transfer or other malicious acts involving nuclear material, other radioactive substances or their associated facilities. Nuclear safeguards and security are both aimed at securing nuclear materials and preventing nuclear proliferation, including terrorism.

Education and training are also part of the nuclear safeguards and security activities at IEK-6, including partnership in the Horizon2020 project 'Advanced Networking for Nuclear Education and Training and Transfer of Knowledge' (ANNETTE), active membership in the IAEA International Nuclear Security Education Network (INSEN) and university lecturing.

Finally, national and international consultancy services and committee work is aimed at strengthening the aforementioned coordination and R&D activities. Such committees and organizations include: the IAEA Standing Advisory Group on Safeguards Implementation (SAGSI), the European Safeguards Research and Development Association (ESARDA), the Institute of Nuclear Materials Management (INMM) and the International Partnership for Nuclear Disarmament Verification (IPNDV).

Contact: Dr. Irmgard Niemeyer
i.niemeyer@fz-juelich.de

3.4.1 Concepts, methods and techniques for nuclear safeguards and security applications

R&D activities conducted at IEK-6 under the German Member State Support Programme (cf. 3.4.) focuse on a wide range of topics, including concepts and approaches; safeguards equipment and communication; information technologies, collection, analysis and security; analytical services; new mandates; and training.

In addition to improving quality control of analytical methods (cf. 3.4.2 and 6.23.), IEK-6 contributes to enhancing IAEA Safeguards through the following activities:

- Safeguards systems analysis: Using mathematical and statistical models, improved tools for implementing State-level safeguards are developed further (cf. 6.22. for more details). A case study on the nuclear fuel cycle of the Iran was conducted in order to evaluate the utility of a systems-based approach to determine inspection strategies in the context of the Joint Comprehensive Plan of Action (JCPOA).
- Geospatial information analysis: A pilot project was started to evaluate the technical changes required to implement a new process for submitting digital declaration site maps for example sites in Germany using a secure, web-based Geographic Information System (GIS). Satellite-borne video processing techniques for imagery analysis are also investigated.
- Sealing systems: Given current issues related to sealing spent fuel storage casks in the German on-site spent fuel dry storage facilities (SFSFs), options for improving techniques were investigated. In this context, suitable current and future sealing systems as well as alternative available technologies, such as laser based systems or neutron monitors, and evaluate are reviewed.
- Verification concepts and approaches: The research demonstrates that when using a systems approach, it is possible to design a transparent state-level system framework to define arms control verification objectives, processes, and timescales. This approach leads to an effective verification regime based on the strategic goals of a treaty, while taking into account restrictions from different security environments.

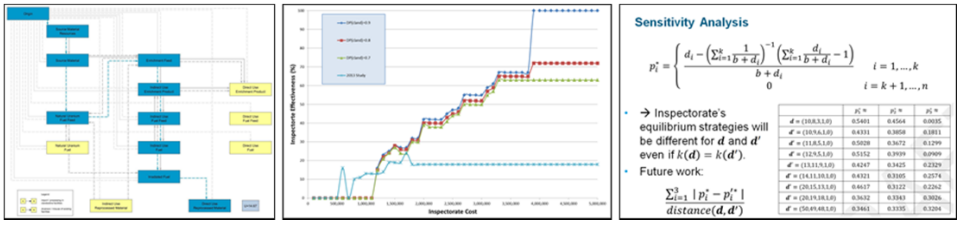

Fig. 11: Examples of analysis results from quantitative methods applied to verification approaches

Contact: Dr. Irmgard Niemeyer
i.niemeyer@fz-juelich.de

3.4.2 Analytical methods for safeguards applications

The application of safeguards by the IAEA involves analytical measurements of samples taken during inspections and requires the development and advancement of analytical techniques with support from the Member States contributing to strengthened and more efficient verification of compliance with non-proliferation obligations. To this end, the IAEA has expressed the need to acquire quality control and reference materials for particle analysis methods applied in safeguards.

In the framework of the German Member State Support Programme (cf. 3.4.) as well as dedicated cooperation arrangements between Forschungszentrum Jülich (IEK-6) and the IAEA's Office of Safeguards Analytical Services (SGAS), recent activities have been focussing on:

- The production and characterisation of particles for quality assurance and quality control. As the availability of monodisperse uranium-containing particles with well-defined properties such as size, density, elemental and/or isotopic composition (Fig. 12) is limited so far, the work at IEK-6 is aimed at assisting the IAEA in acquiring particle reference materials.
- The qualification of the Forschungszentrum Jülich (nominated by the German Federal Ministry of Economics and Technology in 2013) as a member of the IAEA Network of Analytical Laboratories for Safeguards (NWAL). In line with the above mentioned research, it was agreed with the IAEA that Forschungszentrum Jülich pursues the qualification for NWAL membership as a laboratory for provision of particle reference materials.

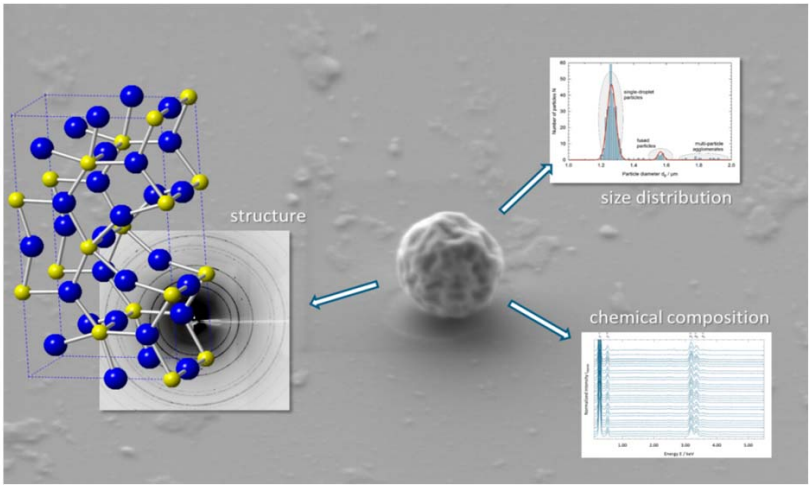

Fig. 12: SEM micrograph of a produced microparticle deposited on a Si wafer and overview of typical analytical methods of characterization: XRD (structure), EDX (chemical composition) and SEM (particle size distribution).

Contact: Dr. Stefan Neumeier
s.neumeier@fz-juelich.de

4 Facilities

The institute operates several radiochemical laboratories (750 m^2) for experimental work with radioactive material including alpha emitters (actinides). About 500 m^2 are licensed according to the German Atomic Energy Act which permits the handling of nuclear fuels. One part of the controlled area is used for the development of non-destructive characterisation methods for radioactive waste applying neutron sources. In addition to the radiochemical laboratory equipment, the controlled area provides glove boxes which enable the handling of radioactive materials. Furthermore, analytical instruments, such as α-, β-, and γ-spectrometry, as well as x-ray diffraction, Raman spectroscopy and electron microscopy are available.

4.1. Solution calorimeter Setaram C80

This machine was installed in mid-2013 in the frame of Helmholtz Young Investigator Group leading by Evgeny V. Alekseev. This equipment constructed for determination of the heat of dissolution of crystalline and amorphous materials. Especially for the solid state chemistry of actinides group, the vessels were made from Teflon to be used with highly aggressive dissolvents such as HF, conc. HNO_3 and H_2SO_4. It is due to the high stability of solid state actinide phases in normal dissolvents, especially for *An*(IV). The calorimeter allows using of very small amount of studying materials with about 2 mg. Such, we can use this machine for study not only Th and U bearing materials but also Np and Pu containing phases. Using standard methods of calorimetry we can determinate enthalpy of formation of studied materials. Combining with thermophysical measurements of third low heat capacity we can archive Gibbs free energy for the actinide based solid state materials. These data are absolute necessary for processes modeling with actinides.

Fig. 13: Calvet type Setaram C80 calorimeter.

4.2. Combined piston cylinder / Multi anvil press

In November 2013 the new high pressure/high temperature facility was established at IEK-6. The aim of the new device is to investigate the physical and chemical behaviour and properties of actinide materials under elevated pressures and temperatures. The apparatus is used for the synthesis of new actinide materials and hydrostatic sintering of new ceramic compounds.

The combined piston cylinder / multi anvil press (Voggenreiter LP 1000 – 540/50) is a tool for producing high hydrostatic pressure and high temperature simultaneously with relatively large sample volumes compared to a diamond anvil cell which usually has sample sizes in µg range. The advantage of the device is that two well established high pressure / high temperature methods (piston cylinder apparatus and walker type multi anvil press) can be used in one instrument (Fig. 14). The high-pressure modules can be replaced within a few minutes. Both technologies have different advantages that complement each other perfectly. The piston cylinder module has a relatively simple sample structure setup with a significantly increased sample volume and a very precise control of the pressure-temperature conditions. In addition, it has very short operating times between the experiments (30-60 minutes per cycle). The multi anvil module offers an ability to generate very high pressures up to 24 giga pascal (240 000 bar) and also a very precise control of the pressure-temperature conditions.

Fig. 14: Combined piston cylinder / multi anvil press. In this picture the piston cylinder module is installed under the main cylinder. On the left workbench side of the device the walker-type multi anvil module is visible.

4.3. Microparticle production set-up

There is great need for uranium oxide microparticle materials as (certified) reference materials [(C)RM's] for nuclear safeguards applications. Therefore, a microparticle generator has been constructed at IEK-6 which is used for the preparation of such materials with accurately characterized isotopic compositions and elemental contents (Fig. 15). The production is based on the preparation of an uranyl containing aerosol using a so-called vibrating orifice aerosol generator. A liquid jet consisting of an uranyl nitrate solution is prepared and by applying an oscillating frequency to the jet, the liquid jet is broken up into monodisperse aerosol droplets. The aerosol droplets with a diameter of approximately 40 μm are dried and calcined to obtain solid uranium oxide microparticles with diameters of about 1 μm.

Uranyl nitrate solutions prepared by dilution of certified reference materials with certified isotopic compositions are used as liquid feed. As no alteration of the isotopic composition is expected, the isotopic composition of the produced microparticles is comparable to the isotopic composition of the reference material. A major advantage of the system at IEK-6 in comparison to other methods is the production of monodisperse microparticles. Since the aerosol volume can be calculated as the liquid feed rate divided by the oscillating frequency and the uranium content of the liquid feed can be accurately determined by ICP-MS, the amount of uranium per particle can be calculated.

The particles are characterized by SEM/EDX to obtain information on the particle size distribution, morphology, and the chemical composition. Measurement by SIMS and ICP-MS confirmed the isotopic composition of the produced microparticles. Installation of a new optical particle sizer allows the online measurement of the particle size distribution as additional quality control measure during production.

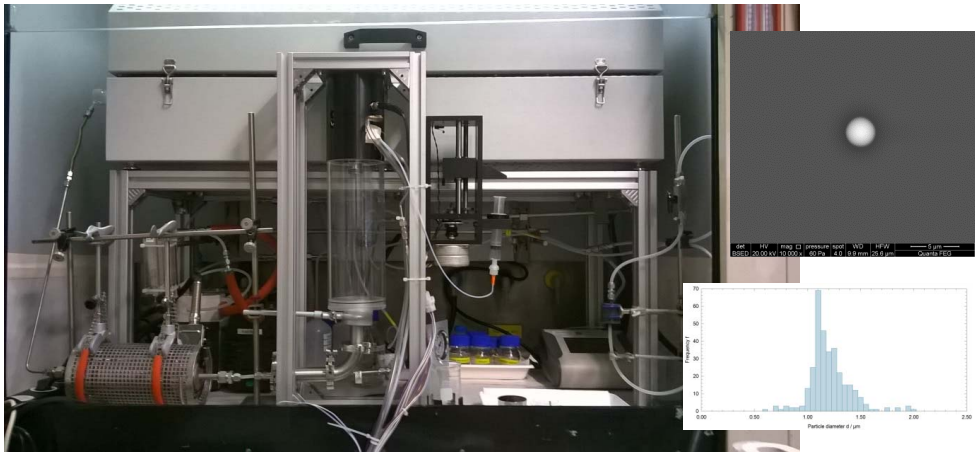

Fig. 15: Microparticle generator (left) and SEM micrograph of single particle (right-top) with particle size distribution (right-bottom).

4.4. FaNGaS, a new instrument for Fast Neutron Gamma Spectroscopy installed at FRM II in Garching

A new instrument to study fission neutron inelastic scattering reactions in elements and actinides has been designed, constructed and tested at the SR10 channel of the Forschungsneutronen-quelle Heinz Maier-Leibnitz, MLZ in Garching (Fig. 16). Together with the local support team of the FRM II the Nuclear Data and Waste Characterization groups of the IEK-6 have developed the innovative facility to apply PGAA techniques for (n,n'γ) and other nuclear reaction channels to explore possible analytical benefits for actinide and heavy metal characterization. First results obtained with FaNGaS indicate that e.g. strong neutron absorbers such as Cd, Gd (and possibly other lanthanides) can be more accurately determined using fast compare to thermal neutrons. This effect might be helpful in detecting clandestine materials or hidden sources in strong shielding structures. Additionally, some of the reactions will produce radioactive isotopes that can be measured with high sensitivity after irradiation at a close-to-detector position to extract production probabilities and other nuclear-physical properties.

The fission neutron beam created at a 93 % enriched ^{235}U converter plate of 15 x 15 cm² effective area in immediate vicinity of the tip of the beam tube delivers unmoderated fission neutrons of 2.3·108 $cm^{-2}s^{-1}$ (with 6 cm PB filter) to the MEDAPP experimental bunker where the new FaNGaS instrument is located. Two adjacent collimators in the beam channel confine the beam to 5 cm diameter and irradiate elemental or isotopic samples in front of a heavily shielded 50 % eff. HPGe detector. The shielding consists of 15 cm of lead, 1 cm of boron carbide and 40 cm of polyethylene to reduce scattered fast neutrons and gamma rays producing background in the detector. The present system allows taking spectra with sufficient sensitivity to determine systematically prompt gamma signals from (n,n'γ), and delayed gamma signatures of (n,p), (n,α) and in some cases also (n,2n) reactions.

FaNGaS has been set-up under a BMBF contract (02 S 9052A) "Bestimmung und Validierung nuklearer Daten von Actiniden zur zerstörungsfreien Spaltstoffanalyse in Abfallproben durch prompte Gamma Neutronenaktivierungsanalyse (PGAA-Actinide)" in close cooperation with the PGAA, MEDAPP and NECTAR groups of the FRM II.

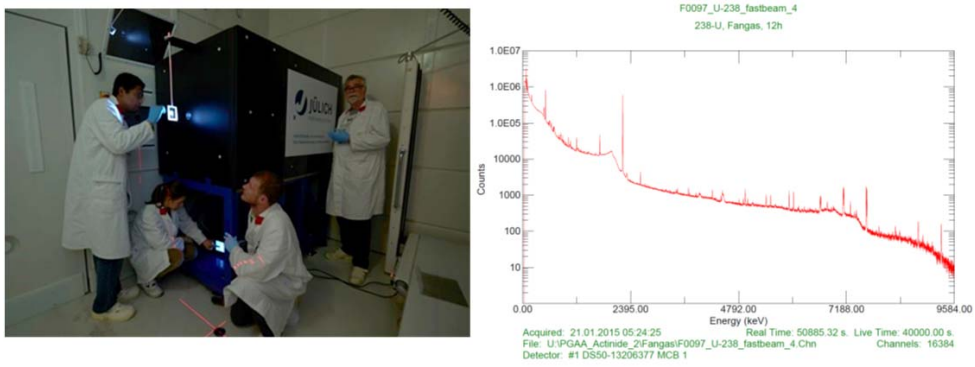

Fig. 16: Left: The FaNGaS instrument at work, right: ^{238}U prompt gamma spectrum, 12 h irradiation with fission neutrons.

4.5. Hot-cell facility

Interaction of ground water with nuclear waste forms, particularly with spent nuclear fuels, are performed by IEK-6 in the hot cell facility (operation since 1969; including a control area of 3576 m^2) within the hot cell line 1 (HZ1).
HZ1 consists of 5 working cells and 5 attached cells. The hot cell area varies from 3 x 3 m to 10.7 x 3 m and allows handling of different spent fuel geometries. In the used hot cells, the handling of radioactive material (i.e. spent UO_2 fuel (enriched in ^{235}U up to 93.2%) containing 1.37 kg of ^{235}U) is possible. The ventilation system has an output of 96.000 m^3 per hour. Each hot cell is equipped with (a) Master-Slave manipulators, (b) a manual driven manipulator and (c) a crane (3 t). To bring in/out radioactive materials glove boxes and Padirac coupling systems are equipped to the hot cells. For external transportation of radioactive material a truck sewer port and a hall, hosting a crane (30 t), is available.

Raman spectroscopy is used to identify the secondary phases formed due to corrosion processes of the fuel sample. For that reason the Raman instrument is attached to fibre-optics connected to Raman sensors which are located in the hot-cell. With one Raman sensor in-situ measurements of the fuel corrosion process can be directly performed.
In January 2015 another experiment started in the hot cell 505. Spent UO_2 fuel developed for prototype VHTR reactor is used. The used fuel samples (TRISO coated particles) are miniature fuel elements with a diameter of 1 mm. To work in a hot cell with this material a high-resolution camera was installed. In Fig. 17, TRISO coated particles and the camera are shown. The hot cell 505 possesses three windows equipped with six Master-slave manipulators. Due to this equipment, three experiments will be performed with this fuel material: (a) isolation from the graphite matrix, (b) isolation of the spent UO_2 fuel kernel from the coatings and (c) determination of the volatile/instant radionuclide release fraction.
However, due to the imminent decommissioning and dismantling of the hot-cell-facilities located at FZJ (outsourced to Jülicher Entsorgungsgesellschaft für Nuklearanlagen, JEN, in 2015) research activities on SNF had to be suspended during 2015/16, but will be revived in the near future in collaboration with the Belgian nuclear research centre SCK•CEN, using their hot-cell-facilities at Mol, Belgium.

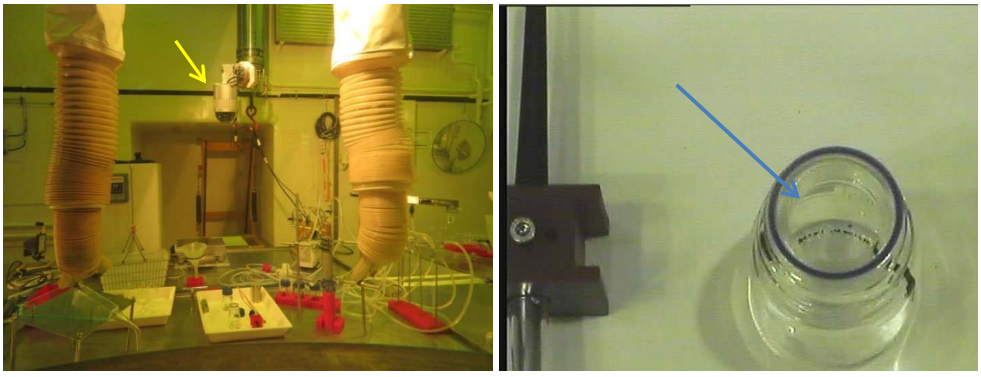

Fig. 17: Left: Installed camera (yellow arrow), Right: Glass bottle containing one mm sized TRISO coated particles (blue arrow) within the hot cell 505.

4.6. Single-pass flow through experiments

Single-pass flow through experiments (SPFT) are the most commonly applied dynamic type of experiments to determine dissolution rates of nuclear waste. The SPFT set up prevents the progressive accumulation of reaction products which may affect the element release rate. During the experiment, a continuous flow of fresh influent solution keeps up constant, well defined chemical conditions within the flow-through reactor.
Two different types of SPFT experiments were set up, (1) SPFT for the temperature range between room temperature and 90 °C and (2) a pressurized SPFT setup for temperatures above 100 °C. Around 20 SPFT experiments which mainly consist of PFA and Teflon parts are now simultaneously run in order to systematically explore the dissolution kinetics of phosphate and zirconia based ceramic waste forms.
In addition, a titanium and PEEK based setup is used to carry out experiments above 100 °C. The setup consists of a pressurized titanium mixed-flow reactor, a high-performance pressure HPLC pump (p_{max} = 60 bar) and a computer controlled high precision outlet valve which is automatically opened and closed according to a set pressure within the titanium reactor. Thus, a constant fluid flow can be guaranteed although the solution flowing into the reactor is at room temperature and the solution flowing out of the reactor may well be above 200 °C. During the experiments, the pressure can be adjusted to keep the water below the boiling point, ensuring a well-defined contact between the aqueous solution and the nuclear waste form.

4.7. X-ray diffraction analysis

In principle all kinds of analysis can be performed by the structure research group according to x-ray diffraction: qualitative and quantitative phase analysis, cell constant determination, structure analysis, structure refinement (Rietveld) and the determination of radial distribution functions are possible.

- **Single-crystal X-ray diffractometer:** is equipped with the state-of-the-art SuperNova system. It has a multi-layer X-ray optics (CuKα and MoKα). The SuperNova combines high intensity Nova X-ray micro-source with the 165 mm fast, high performance Eos™ CCD detector. Mounted on a 4-circle goniometer, the copper radiation Nova X-ray source provides up to 3x the intensity of a 5 kW rotating anode generator with optics and the data quality of a micro-focus rotating anode. Additionally, the SuperNova goniometer has been designed to accept all major open flow cryogenic sample cooling device, including CryojetJet (Oxford Instruments) liquid nitrogen device (90 – 500 K). With this equipment we are able to provide a full structural characterization of radioactive single crystals including very small objects (up to 10-15 µm) in wide temperature range.
- **Bruker X-ray powder diffractometer D8:** is equipped with a copper tube (Cu K_α), a molybdenum tube (Mo K_α) and two suitable detector systems (scintillation counter and Si semiconductor detector), in order to perform X-ray diffraction analysis on crystalline, semi-crystalline and amorphous samples. Radioactive and non-radioactive powder samples can be measured. Additionally, a climate chamber is available on request that enables *in situ* measurements at different atmospheres and humidities and at temperatures up to 250°C.

- **Bruker X-ray powder diffractometer D4:** is equipped with a copper tube (Cu Kα) and a multi-sample stage (66 samples) as well as with a fast LynXEye detector, appropriate for high throughput measurements. The D4 can also be used for any kind of analysis, with the exception of radial distribution function determination and *in situ* measurements using the climate chamber.

4.8. Electron microscopy

- **ESEM (Environmental Scanning Electron Microscope)**
  - Quanta 200 F from FEI: high resolution field emission SEM
  - High/low vacuum, and ESEM: up to 2700 Pa: Investigation of wet samples at ESEM-mode
  - Detectors: Everhart Thornley SE-detector (high vac.), Gaseous large field SE-detector (low vac.), BSE-detector (high/low vac.), Gaseous analytical detector (GAD) BSE-detector (low vac.), Gaseous secondary electron detector (GSED) (ESEM)
  - EDX: Apollo X Silicon Drift Detector (SDD) from EDAX
  - WDX: TEXS LambdaSpec from EDAX

- **FIB (Focused Ion Beam)**
  - NVision 40 Cross Beam Workstation from Zeiss
  - High resolution field emission GEMINI SEM
  - High performance SIINT zeta FIB column
  - Gas injection system
  - Detectors: In-column: EsB detector with filtering grid for BSE detection; In-lense: SE detector; chamber: Everhardt Thornley SE detector, 4Q BSE detector, GEMINI® multimode BF/DF STEM (Scanning Transmission Electron Microscopy) detector.
  - EDX: INCA energy dispersive x-ray spectroscopy from Oxford Instruments
  - EBSD: Nordlys II Electron Backscattered Diffraction detector from Oxford Instruments.

4.9. Non-destructive assay testing

Segmented Gamma-Scanner GERNOD II.

The Segmented Gamma-Scanner GERNOD II is used for the characterization of 200-L or 400-L drums radioactive waste with wide range of matrices and isotopic compositions. The Gamma-Scanner consists of a mechanical part, a control unit, a detection system and a system unit and operator interface. The mechanical system consists basically of a turntable to accommodate different waste drums (max. weight 6000 kg) and a platform for the vertical movement of the gamma detection and collimation unit. The driving units comprise stepping motors with superior positioning capabilities. The positioning of the drum and detector is handled by a SPS control unit. This offers superior positioning capabilities together with highly reliable performance and control of the system status. Scanning programs are performed either continuously (fast measurements) or in a step by step mode (long time measurements). The detection of gamma emitting nuclides is performed by an HPGe detector connected to a digital spectrometer for signal processing and data acquisition. The detector can be used together with different collimators depending on the type of application. A dose rate meter is attached to the detector to record the dose rate at the surface of the drum over the whole assay period. All routine operator interactions are carried out via a PC-based control system using the software SCANNER32 developed in cooperation with a professional software engineering company for ease operations and reliable data handling.

Transmission and Emission Tomography System

The Transmission and Emission Tomography System developed at IEK-6 is an advanced tool for the characterization of 200-L radioactive waste drums. The radiation emitted from a ^{60}Co transmission source (200 GBq in DU shielding) is collimated in the direction of 4 fast scintillation detectors located in the detector collimation shielding bank to perform 4 transmission measurements at the same time. Meanwhile, the 3 HPGe-detectors are used for the emission measurements of the waste drum. An irradiation of these detectors by the transmission source is avoided by the source and detector collimation. Two stepping motors move the drum horizontally and rotate it between two measurement steps respectively. On the data collected for each measurement a pulse height analysis is performed. This leads to the basic data sets for the algorithms used for Transmission Computer Tomography, Emission Computer Tomography and Digital Radiography.

MEDINA

MEDINA (Multi-Element Detection based on Instrumental Neutron Activation) is an innovative analytical technique based on prompt and delayed gamma neutron activation analysis for non destructive assay of 200-L waste packages.

4.10. Radiochemical analytics

- **LSC (Liquid Scintillation Counter):**
  - Analysis of aqueous and organic samples
  - Quantulus (PerkinElmer), Autosampler, Ultra low activity determination, determination of environmental activity (^{14}C), α,β discrimination
  - TRI-CARB 2020 (PerkinElmer) Autosampler > 100 samples

- **α-spectrometry:**
  - Qualitative and quantitative analysis of α-emitter, Si-detector, low level detection

- **γ-spectrometry:**
  - HP Ge-detector (N_2-cooled), NaI-detector, LaBr-detecor, Radionuclide detection with low γ-energy (^{55}Fe: E_γ < 5.9 kEV), low level detection, borehole detector

4.11. Miscellaneous

- ICP-MS ELAN 6100 DRC (PerkinElmer SCIEX)
- STA 449C Netzsch
- FTIR-spectrometer: Equinox 55 (Bruker), KBr-pellets, ATR (attenuated total reflection), TGA
- Horiba raman spectrometer LabRAM HR Vis (400 – 1100 nm), currently equipped with a He-Ne laser (wavelength λ = 633 nm, visible red light), a Diode laser (wave length λ = 785 nm, NIR), an edge filter, two gratings (600 and 1800), focus length 800 mm, a peltier cooled solid state detector, five objectives (x10, x50, x100, x50 NIR, x100 NIR), a safety energy supply system, a safety box for the microscope and a video camera for sample observation using reflected or transmitted visible light.
- Dilatometer DIL 402C (Netzsch)
- Induction furnace (Linn High Therm GmbH), max. temperature 2500 °C, mass spectrometer for analysis of combustion gases
- High temperature furnace HTK 8 (GERO GmbH), max. temperature 2200 °C
- BET AUTOSORB-1 (Quantachrome Instruments)
- Spectral photometer CADAS 100
- Granulometer CILAS 920
- Autoclaves
- Gas chromatography (Siemens AG)
- Gas chromatography PerkinElmer Clarus 580 devices
- Vacuum hot press HP W 5 (FCT Systeme), max. temperature 2200 °C, press capacity max. 50 kN, 5 x 10^{-2} mbar

5 About IEK-6

5.1 Staff

78 staff members (Dec. 2016)

32 scientists	23 PhD students	9 graduands
3 engineers & technicians	6 laboratory assistants	5 administration

5.2. Organisation chart

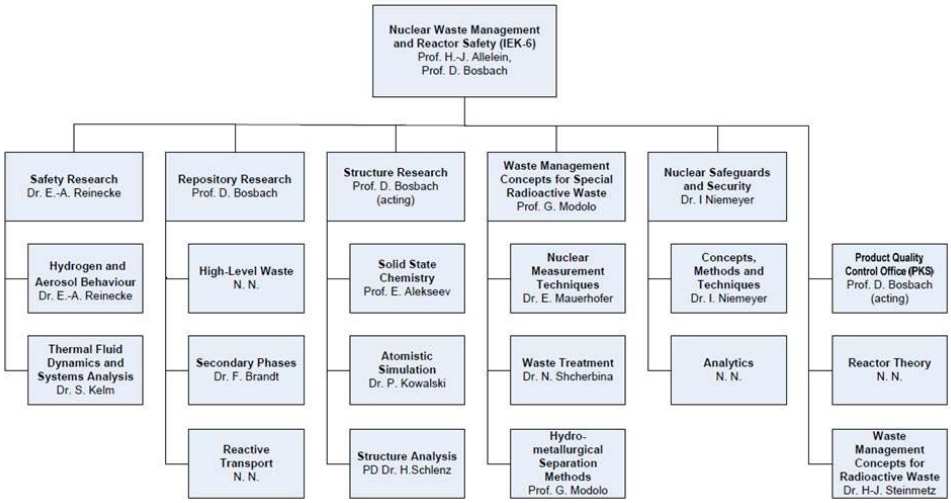

Fig. 18: Organisation chart of the Institute of Energy and Climate Research (IEK-6), Nuclear Waste Management and Reactor Safety division.

5.3. Budget

2015

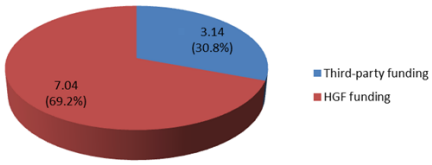

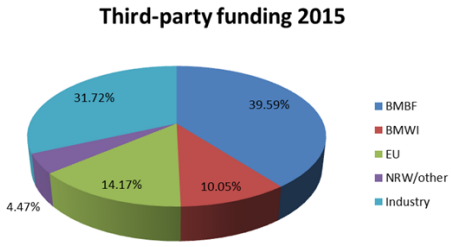

2016

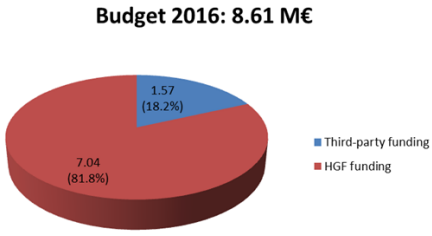

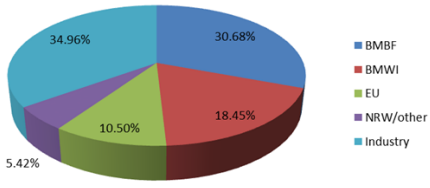

6 Scientific and technical reports 2015/2016

6.1. Unravelling corrosion mechanisms of spent nuclear fuels in the repository environment

S. Finkeldei, A. Baena, F. Brandt, H. Curtius, A. Bukaemskiy, G. Deissmann, D. Bosbach

Corresponding author: d.bosbach@fz-juelich.de

Introduction

The safe disposal of high level nuclear wastes (HLW) arising from the civilian use of nuclear energy is a challenging scientific and societal issue. Within the scientific and technical community there is a general consensus that disposal of heat-generating HLW, such as vitrified reprocessing wastes (HLW glass) and spent nuclear fuels (SNF) in a deep geological repository (DGR) represents the safest and most sustainable waste management option[1-3]. In the year 2000, Germany took the decision to terminate the (foreign) reprocessing of SNF and to opt for the direct disposal of SNF. In order to avoid undue burdens and obligations for future generations, the construction of a German DGR should be achieved as quickly as possible[4], making disposal of SNF an ongoing issue of paramount importance. The long-term safety assessment for a future DGR requires an in-depth understanding about the corrosion of and radionuclide release from SNF under the post-closure conditions expected in the repository, when water may come into contact with the SNF (i.e. after failure of the waste containers), to avoid over-conservative assumptions and to enhance public acceptance and trust into the safety case. However, many fundamental processes governing the corrosion of SNF, from molecular scale to macro scale, can at present only be described phenomenologically and are not yet fully understood[5,6].

UO_2-based SNF from light water reactors is a very complex and heterogeneous material[7-11], due to significant changes of the microstructure and chemical composition of the UO_2-based fuel pellets during power generation. After unloading from the reactor, about 5 wt.% of the SNF consist of fission products (FP) and transuranium elements (TRU) in different chemical and physical forms that are heterogeneously distributed in the SNF: (1) volatile/gaseous FPs (e.g. I, Cs, Kr and Xe), (2) oxide precipitates (grey phase) of Zr, Nb, Rb and Ba, (3) metallic precipitates (ε-particles) containing Mo, Tc, Ru, Rh and Pd immiscible with the UO_2 matrix and (4) TRU and FP (e.g. lanthanides and Zr) forming solid solutions with the UO_2 matrix. The concentrations of FP and TRU, their distribution between different phases, as well as the macro- and micro-structural features are highly dependent on the burn-up of the fuel. The release of radionuclides from SNF in a DGR upon contact with groundwater is deemed to proceed in two major stages[12,13] beginning with an initial fast release of volatile and easily soluble radionuclides (fission gases and parts of the inventories of Cs and I), the so called instant release fraction (IRF). At later stages, the radionuclide release from SNF is governed by the (slow) corrosion of the SNF matrix, which – after the relatively fast decay of β- and γ-emitters during the first thousands of years – proceeds due to the production of oxidants (e.g. H_2O_2) at the SNF-water interface due to α-radiolysis in the long-term. Recent SNF corrosion experiments indicate the long-term matrix corrosion rate might be influenced by the amount

of FPs within the UO_2 structure, and catalytic scavenging of oxidants by reaction with H_2 (produced by anaerobic metal corrosion in the DGR) on ε-particles [14,15].
The research activities at IEK-6 concerning SNF during the last years addressed both the IRF as well as the long-term (oxidative) matrix corrosion of SNF in the nominally reducing repository environment. Besides investigations on real irradiated fuels and unirradiated nuclear materials, complementary approaches using simplified model systems were pursued. These model systems enable single effect studies to unravel the complexities and couplings between processes governing the radionuclide release from SNF under disposal conditions, which cannot be assessed by experiments using "fresh" SNF.

Investigations on SNF

In the past, the research on SNF corrosion at IEK-6 was initially addressing the corrosion behaviour of non-conventional SNF, such as intermetallic plate-type uranium-aluminide and uranium-silicide fuels from research reactors, and U and/or Th based fuels from prototype high-temperature reactors[16]. Starting with the collaborative EU-project FIRST Nuclides launched in the EURATOM 7th Framework Programme, the IRF and the microstructural evolution of high burn-up UO_2-based fuels have been investigated in leaching experiments[17], using irradiated TRISO (TRI-structural-ISO-tropic) particles containing UO_2 fuel kernels as model systems for extremely high burn-up (~100 GWd/t_{HM}) SNF. However, due to the imminent decommissioning and dismantling of the hot-cell-facilities located at FZJ (outsourced to Jülicher Entsorgungsgesellschaft für Nuklearanlagen, JEN, in 2015) research activities on SNF had to be suspended during 2015/16, but will be revived in the near future in collaboration with the Belgian nuclear research centre SCK•CEN, using their hot-cell-facilities at Mol, Belgium. Investigations in Mol will focus on the dissolution behaviour of MOX fuel, with a variation of the burn-up as well as the composition of the leaching solution. In addition to monitoring of the solution and gas composition during the leaching experiments, a microstructural characterisation of the MOX-samples before and after the leaching experiments is planned. The experimental set up for these experiments will be operational in January 2018.

UO_2-based model systems

In the framework of the COCO-SNUF project “Unravelling the **CO**rrosion **CO**mplexity of **S**pent **NU**clear **F**uel: Understanding fundamental reaction mechanisms using UO_2-based model systems” these model systems are studied to complement SNF research in a tiered approach. *Via* a bottom-up approach (Fig. 19) a series of ceramics is fabricated starting with pure UO_2 ceramics serving as reference materials, moving on to the fabrication of more complex, doped and composite UO_2-based ceramics, which mimic individual aspects of SNF. These systematic sample set enables single effect studies of, for example the impact of the fission product concentration and distribution on the long-term matrix corrosion.

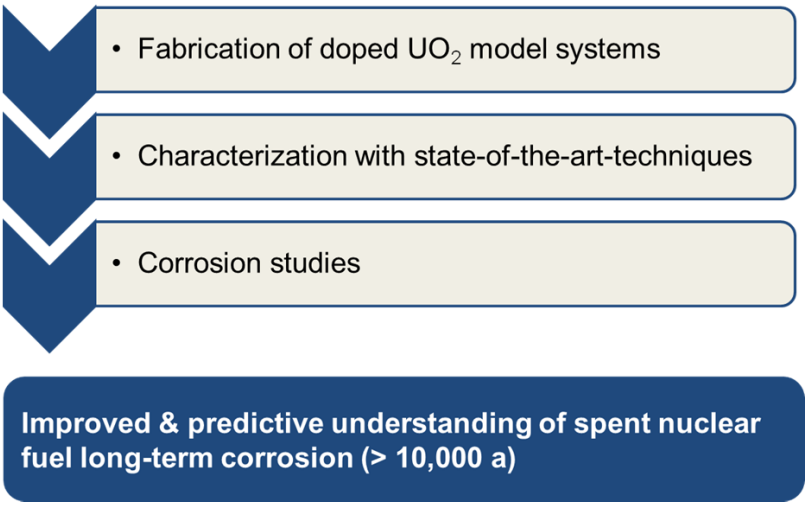

Fig. 19: Bottom-up approach followed in the COCO-SNUF project using UO_2-based model systems to understand corrosion mechanisms of aged SNF in the repository environment.

In a first step lanthanide-doped UO_2-ceramics were fabricated to address the influence of fission lanthanides dissolved in the UO_2-matrix on its crystal structure and corrosion processes. Nd was employed as representative of the fission lanthanides in SNF, with varying Nd-concentration in the UO_2 to mimic SNF with different burn-ups. As a basis for all subsequent investigations, suitable synthesis routes of *Ln* doped UO_2 powders as precursors for the fabrication of ceramics had to be developed. This precursor formulation is the key to manipulate the microstructure and homogeneity of the ceramic materials. From these precursor powders, ceramics with a microstructure representing the center region of SNF were fabricated. The systematic preparation of a range of doping levels with Nd will enable a fundamental investigation of the resulting structural and chemical modifications in the UO_2 matrix and their impact on its electrochemical properties and corrosion behaviour. In order to fabricate tailor-made ceramics for these single-effect studies, we have developed a toolbox of various wet-chemical synthesis routes such as co-precipitation, sol-gel routes and ion exchange reactions of weak acid resins to prepare appropriate precursor materials.

A thorough understanding/investigation of the ceramic materials prior to and after corrosion studies is a prerequisite to identify the role of lanthanide FPs on the long-term matrix corrosion of SNF. Complementary characterisation techniques such as XRD, density measurements, SEM and EBSD are applied. Fig. 20 shows first results regarding the microstructure (a) and the structure (b) of a $(U_{0.986}Nd_{0.032})O_{2\pm x}$ ceramic which was fabricated via a coprecipitation route. From the electron microscopy analysis as well as from the XRD pattern the formation of a solid solution is confirmed. The average grain size is ~ 11.5 µm and corresponds well to the central region of SNF[18].

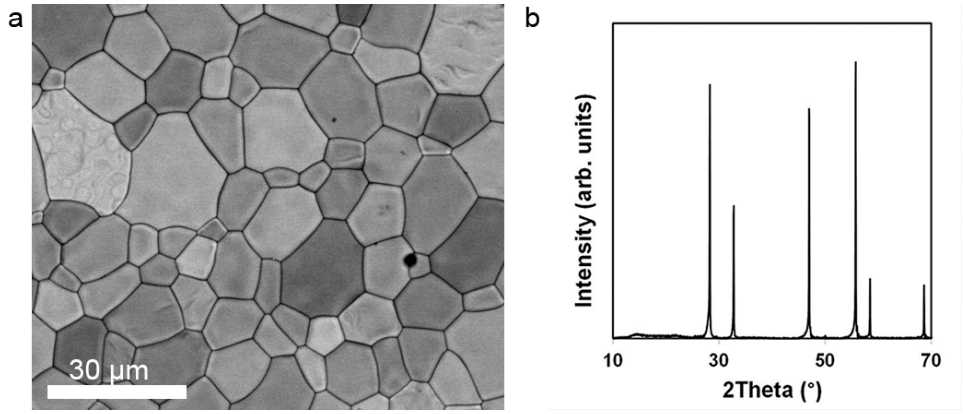

Fig. 20: Backscattered electron SEM image of a $(U_{0.986}Nd_{0.032})O_{2\pm x}$ ceramic (a) and the corresponding XRD pattern after a calcination step at 100 °C (red), after milling (green) and sintering at 1400 °C (b). Both techniques indicate a solid solution formation.

The incorporation of Nd in the oxidation state (+III) in the fluorite matrix with U(+IV) can be counterbalanced by partial oxidation of Uranium and/or the incorporation of oxygen vacancies. This affects in particular the oxygen sublattice, which is hardly accessible via conventional XRD measurements. However, the oxygen sublattice is expected to play a key role on surface electrochemical properties and matrix corrosion, due to interstitial oxygen and vacant sites. To gain an in-depth understanding of the role of FP dopants on the structural properties in particular on the oxygen sublattice of the materials, neutron total scattering at the NOMAD beamline at the SNS facility in the Oak Ridge National Laboratory has been applied recently. These structural insights into lanthanide doped UO_2-based model systems gained from the evaluation of these data will be linked to their corrosion behaviour and contribute to an enhanced mechanistic understanding of SNF long-term matrix corrosion.

Moreover, the role of the metallic epsilon particle inside SNF will be addressed via UO_2 - model systems containing metallic precipitates (using e.g. Pd as surrogate for the five metal system), mimicking these epsilon particles to understand whether they are suppressing or enhancing the SNF matrix corrosion by interacting with radiolytical oxidants. These metallic particles are finely dispersed in the SNF matrix in the nanometer-size and as larger particles at the grain boundaries. At present, we develop wet-coating procedures to fabricate UO_2 model systems with Pd particles suitable to mimic the distribution and size of epsilon particles in SNF. The next step will be the fabrication of a more complex system containing both lanthanide dopants as well as metallic (nano)particles to probe any synergistic effects between these phases and to move closer towards more complex systems such as SNF consisting of many different phases and elements. Future work will implement alpha-emitters such as ^{238}Pu to mimic the effects of alpha-radiolysis on the dissolution of aged SNF in the repository environment.
The aim of the destined single effect studies studies on UO_2-based model systems is to enhance the molecular process understanding of specific mechanisms relevant to long-term matrix corrosion of SNF, and to complement thus corrosion studies on spent UOX and MOX fuels in the future.

Acknowledgements

This work was financially supported from the internationalization funds of the Forschungszentrum Jülich under the "Cutting-Edge Ideas" grant (COCO-SNUF).

References

[1] International Atomic Energy Agency (IAEA): *Technical Reports Series* 413 (**2003**) 80 pp.
[2] Council of the European Union: COUNCIL DIRECTIVE 2011/70/EURATOM (**2011**) 56 pp.
[3] Kommission Lagerung hochradioaktiver Abfallstoffe: Abschlussbericht (**2016**) 683 pp.
[4] Federal Ministry for the Environment, Nature Conservation, and Reactor Safety: Safety requirements governing the final disposal of heat-generating radioactive waste (**2010**) 21 pp.
[5] Poinssot, C., Gras, J.M.: *Mat. Res. Soc. Symp. Proc.* 1124 (**2009**) 85–97.
[6] Poinssot, C., Gin, S.: *J. Nucl. Mater.* 420 (**2012**) 182–192.
[7] Rondinella, V.V.; Wiss, T.: *Mater. Today* 13 (**2010**) 24–32.
[8] Kleykamp, H., Paschoal, J.O., Pejsa, R., Thummler, F.: *J. Nucl. Mater.* 130 (1985) 426–433.
[9] Bruno, J., Ewing, R.C.: *Elements* 2 (2006), 343–349.
[10] Kleykamp, H.: *Nucl. Technol.* 80 (1988), 412–422.
[11] Carbol, P., Wegen, D.H., Wiss, T., Fors, P.: *Compr. Nucl. Mater.* 5 (**2012**) 389–420.
[12] Johnson, L., Ferry, C., Poinssot, C., Lovera, P.: *J. Nucl. Mater.* 346 (**2005**) 56–65.
[13] Poinssot, C.; Ferry, C.; Lovera, P.; Jegou, C.; Gras, J.-M.: *J. Nucl. Mater.* 346 (**2005**) 66–77.
[14] Ewing, R.C.: *Nat. Mater.* 14 (**2015**) 252–257.
[15] Broczkowski, M.E., Noël, J.J., Shoesmith, D.W.: *J. Nucl. Mater.* 346 (**2005**) 16–23.
[16] Curtius, H., Bosbach, D., Deissmann, G.: *KIT Scientific Reports* 7696 (**2015**) 176–180.
[17] Curtius, H., Kaiser, G., Lieck, N., Güngör, M., Klinkenberg, M., Bosbach, D.: *Radiochim. Acta* 103 (**2015**) 433–442.
[18] Hiezel, Z., Hambley, d.I., Padovani, C., Lee, W.E.: *J. Nucl. Mater.* 456 (**2015**) 74–84.

6.2. Radionuclide bandwidth calculation in the inventory of PWR-UO_2 spent fuel derived from reactor design and operating data

I. Fast, H. Tietze-Jaensch

The declared radionuclide inventory of spent fuel assemblies is derived from numerical assessment, based on the reactor and fuel design parameters and operational record. The independent verification of such estimations for spent fuel nuclide inventories requires the knowledge or good estimate of these reactor and fuel design and operational history parameters to determine the realistic concentration ranges, or bandwidths, of the radionuclide inventory. The list of final repository relevant radionuclides is based on the safety assessment for a particular repository, thus it is justified to comprise more-or-less the same radionuclides for spent fuel assemblies as those to be declared for compacted metallic waste residuals from the reprocessing of spent fuel. An estimation of the average radionuclide composition of the burnt-up fuel including the realistic inventory bandwidths for each of relevant radionuclides is highly desirable. This information is required for proof tools of product quality control (PQC) or safeguards, but also for the evaluation of various safety scenarios regarding the radionuclide mobility or contamination. Here we focus on realistic radionuclide bandwidths where no information of the reactor design and operating data are available. As burn-up (BU) and cooling time (CT) that are considered to be known, nine so-called Secondary Reactor Parameters (SRPs) that include parameters: initial enrichment (IE), fuel density (FD), fuel temperature (FT), specific power (SP), downtime (DT), irradiation time (IT), moderator density (MD), moderator temperature (MT) and boric acid concentration (BA). All the SRP values are averaged for the fuel assembly and whole irradiation time and varied independently in burn-up calculation models. The realistic range limits of each such SRP are obtained from 339 international PWR-UO_2 spent fuel assemblies with well-known fuel design and reactor operating data[1]. For the SRP analysis and determination of RN bandwidths uniform distribution of assemblies with burn-up up to 71 GWd/t_{HM} are assumed. The modelling of radionuclide inventories is carried out with the burn-up code SCALE 6.1 using the nuclear data library ENDF/B-VII.0. The input data include geometry of the fuel assembly and a set of the associated SRP values.

The calculated bandwidths are validated with experimental data[1] and the magnitude varies significantly for various radionuclides and the burn-up and cooling time. For most final disposal relevant radionuclides the realistic bandwidths can be determined accurately with only information of burn-up and cooling time. For some radionuclides (^{14}C, ^{126}Sn, ^{108m}Ag etc.) additional parameters of fuel impurities, burnable absorber exposure etc. are required.

Theoretical radionuclide bandwidths are compared with calculated data from ORNL, NAGRA, SKB and GRS that comprise more than 5000 SNF assemblies Understanding the origin of the uncertainties and bandwidths of radionuclide inventories in comparison with experimental data can be applied to address spent fuel compositions with insufficient knowledge of SRPs. This work[2] provides a realistic radionuclide bandwidth calculation method to support long-term safety analyses, the development of efficient and validated tools for the PQC of HLW disposal and for safeguard applications.

References

[1] NEA 'Spent Fuel Isotopic Composition Database (SFCOMPO)'. https://www.oecd-nea.org/science/wpncs/ADSNF/. (**2015**).

[2] Ivan Fast, Ph.D. Thesis RWTH Aachen, XI, 129 Seiten; ISBN 978-3-95806-206-1; (**2017**).

6.3. Radionuclide retention by secondary phases in the repository environment

F. Brandt[1], S. Lange[1], M. Isaacs[1,2], S. Labs[1,3], H. Curtius[1], M. Klinkenberg[1], J. Barthel[4,5], G. Deissmann[1], D. Read[2,6], D. Bosbach[1]

[1]Forschungszentrum Jülich GmbH, Institute of Energy and Climate Research – IEK-6: Nuclear Waste Management and Reactor Safety, 52425 Jülich, Germany

[2]University of Surrey, Guildford GU2 7XH, UK

[3]Currenta GmbH, 51368 Leverkusen, Germany

[4]Central Facility for Electron Microscopy (GFE), RWTH Aachen University, 52074 Aachen, Germany

[5]Forschungszentrum Jülich GmbH, Ernst Ruska-Centre for Microscopy and Spectroscopy with Electrons (ER-C), 52425 Jülich, Germany

[6]National Physical Laboratory, Teddington TW11 0LW, UK

Corresponding author: f.brandt@fz-juelich.de

Introduction

In the presence of water within the near field of a deep geological repository for high level nuclear waste, corrosion and alteration processes will occur especially at the interfaces of the different types of materials which make up the engineered barrier system (EBS). Secondary phases forming due to corrosion of near field materials including the waste canisters and waste forms or the alteration of phases present within the EBS as well as cementitious materials can provide a high retention potential for radionuclides due to adsorption or co-precipitation and subsequent structural uptake. The precipitation of secondary phases can provide for typically lower solubility limits of certain radionuclides. In order to take credit from these processes in safety assessments, an in-depth insight into the geochemical stability fields of relevant secondary phases and their thermodynamic properties as well as a mechanistic process understanding of the radionuclide uptake mechanisms are essential. In this context, at IEK-6 the retention of safety relevant radionuclides by layered double hydroxides and cementitious materials, as well as the formation of coffinite as a potential corrosion product of spent nuclear fuels have been investigated intensively throughout the last five years.

Layered double hydroxides

Layered doubled hydroxides (LDH) have been widely studied in the last decades because of their ability to control the mobility of various anions and cations in the environment. The structure of LDH consists of layers with a brucite-like structure comprising octahedrally coordinated divalent cations which form two dimensional infinite layers by edge-sharing of the octahedra (Fig. 21). Due to a partial isomorphous substitution of the divalent cations by trivalent (or more rarely tetravalent) cations, the octahedral layer of LDH carries a net positive charge, which is compensated by anions intercalated between the brucite-like layers. Additional molecular water in the interlayer provides hydrogen bonding between the brucite-like layers. Hydrotalcite ($Mg_6Al_2(OH)_{16}[CO_3]\ H_2O$), is the name-giving mineral of the supergroup of layered double hydroxides with more than 40 LDH-type mineral species[1].

LDH may be relevant to the safety case of nuclear waste repositories due to their retention potential of anionic radionuclide species, for example of ^{129}I or ^{79}Se. So far few studies were dedicated to the incorporation of Zr into LDH. Zr is relevant with respect to nuclear waste management due to the extensive use of zirconium alloys ("zircalloys") in the nuclear industry, for example as cladding material for fuel rods in water cooled nuclear reactors. The long-lived radionuclide ^{93}Zr is generated by neutron activation of stable Zr isotopes in these materials. Moreover ^{93}Zr is formed as a significant fission product due to thermal fission of ^{235}U in nuclear fuels. Thus the uptake by LDH may provide for an effective retention mechanism for ^{93}Zr in the repository near field. However, the incorporation of tetravalent cations such as Zr^{4+} into the brucite-like layers of LDH has been discussed.

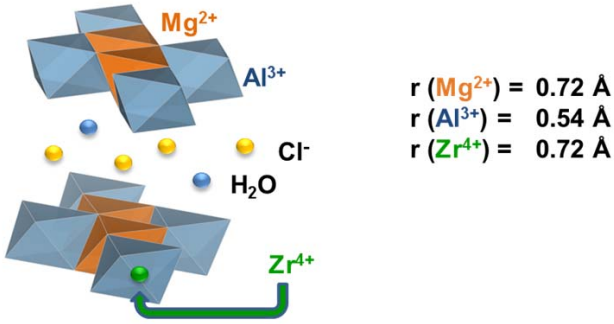

Fig. 21: Schematic representation of the LDH structure consisting of positively charged octahedral layers; the negatively charged anionic species in the interlayer compensate for the charge of the octahedral layer. Zr^{4+} is expected to replace Mg^{2+} in the octahedral layer.

In order to include LDH phases and especially their Zr-bearing solid solutions in geochemical models and take credit from their retention potential, the thermodynamic properties of these phases need to be determined. The study focused on the synthesis and structural characterization of Zr^{IV}-bearing Mg-Al-LDH containing Cl^- as interlayer anion and the derivation of their thermodynamic properties. The potential isostructural substitution was investigated at ambient conditions by synthesizing Mg-Al-Zr-LDH with variable Zr/(Zr+Al) mole fractions via a co-precipitation method[2]. The samples were thoroughly characterized using powder XRD (pXRD), Raman spectroscopy, chemical analyses and electron microscopy. The results of this study indicated a structural uptake of Zr into the LDH structure. Detailed analyses of the structural data suggest that Zr is mainly incorporated isostructurally into the octahedral layer. However, Raman spectroscopy and XRD indicate not only the structural uptake in the brucite layer but also the possible presence of a second Zr-species in the solid. Based on these observations, an additional uptake of Zr (as $Zr(OH)_5^-$) into the interlayer of the Zr-Mg-Al-LDH was suggested. Thermodynamic properties of the synthesized LDH were estimated assuming a thermodynamic equilibrium between the LDH solid and the aqueous solution. The GEMS-Selektor code was applied with the built-in NAGRA-PSI database[3-5]. The theoretical predictions indicated that the addition of Zr into the hydrotalcite structure increases the Gibbs free energy of LDH[2]. This study provided the basis for the contribution of IEK-6 to the on-going project THERMAC funded by the German Federal Ministry of Education and Research (BMBF) that focusses on temperature effects on the solubility of Zr-Mg-Al-LDH and the concentration limits for the structural uptake of Zr by LDH.

Uptake of long-lived safety relevant radionuclides by cementitious materials

Cementitious materials are widely used in nuclear waste management, for example in the barrier system of near surface repositories and geological disposal facilities, in certain waste containers (e.g. in the Belgian Supercontainer), or for solidification of low and intermediate level wastes[6-8]. Cementitious materials comprise a variety of cement hydration phases as a consequence of interaction between cement clinker and water, in particular calcium-silicate-hydrates (CSH), portlandite ($Ca(OH)_2$), and calcium-aluminate / -ferrate compounds (AFm/AFt)[9]. The migration behaviour of radionuclides in cementitious materials is controlled by radionuclide solubility phenomena, diffusion, interface processes (e.g. surface complexation or ion exchange), or incorporation into solid phases, including the formation of solid solutions. Within the EC-funded Horizon 2020 collaborative project CEBAMA (www.cebama.eu) key issues related to the use of cement-based materials in nuclear waste disposal applications are addressed, focusing on questions relevant to long-term safety such as radionuclide retention in high-pH concrete environments. In this context, we study the uptake of selected safety relevant long-lived fission and decay products (e.g. ^{226}Ra, ^{129}I, ^{99}Tc, ^{93}Mo, ^{79}Se) by various cementitious materials, aiming at an in-depth mechanistic understanding of radionuclide uptake and retention in cementitious systems. A bottom-up approach is being pursued studying radionuclide uptake both by synthesized model phases representative for hydrated cementitious materials (e.g. CSH, AFm/AFt-phases, hydrogarnet), and by hardened cement pastes made from ordinary Portland cement (OPC, CEM I) or composite cement containing silica fume and blast furnace slag. The various model phases were synthesized under argon atmosphere using well established procedures[10-13] and characterized inter alia by pXRD, SEM/EDS, and TG-DSC (Fig. 22).

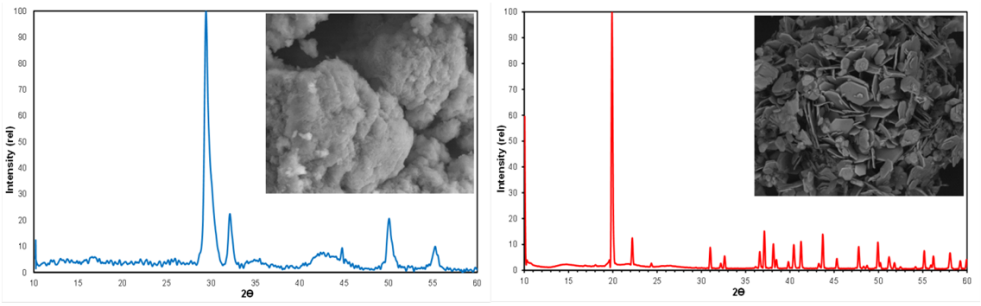

Fig. 22: SEM pictures and pXRD patterns of synthesised model phases: CSH (left) and AFm–SO_4 (right) as examples.

Radionuclide uptake kinetics were studied in static batch experiments under anoxic conditions. To address the uptake of radionuclides at different stages of concrete alteration, experiments were performed at different pH conditions. Experiments with artificial cement pore water (ACW) at pH 13.5 are deemed to be representative to address the radionuclide uptake in early stages (i.e. when young alkali-rich cement pore waters persist), while later stages of progressive calcium leaching were investigated using aqueous solutions that are in equilibrium with the solids studied. The radionuclide uptake was quantified in terms of distribution ratios (R_d-values) between solid and liquid phase according to:

$$R_d = \frac{A_{ini} - A_t}{A_t} \cdot \frac{V}{m}$$

where A_{ini} and A_t are the initial concentration of the radionuclide in solution and the concentration at time t, respectively, V is the volume of the liquid phase, and m the mass of the solid phase. Experiments performed for up to 60 days indicate a very strong retention of ^{226}Ra by CSH phases (equilibrium R_d >1000 L kg^{-1}), while the uptake of ^{226}Ra by AFt and AFm phases was significantly lower (R_d <150 L kg^{-1}). It was found that the ^{226}Ra uptake by CSH depends both on the Ca/Si ratio (C/S) and on pH (Fig. 23). CSH with lower C/S-ratios showed a stronger uptake of ^{226}Ra, potentially, by electrostatic sorption, since the negative surface charge of CSH at C/S <1.2 allows for a more pronounced uptake of cations[6]. However, this observation can also be explained in terms of cation exchange[14], due to the significantly lower competition with calcium ions in solution at lower C/S-ratios that outweighs the lower number of Ca-sites at the surface. At high pH conditions in the ACW representative for young cementitious materials (pH ~13.5), the uptake of ^{226}Ra by the CSH was generally lower than at the equilibrium pH of the CSH phases (CSH 0.9: pH 11.9; CSH 1.4: pH 12.2).

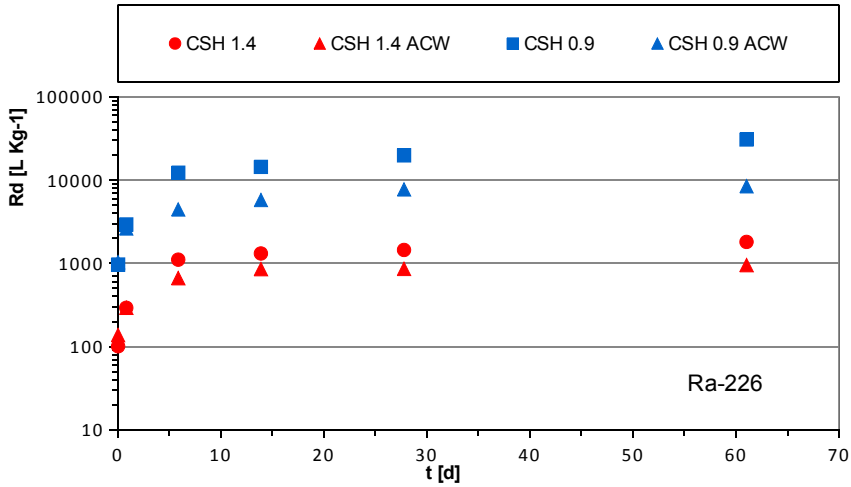

Fig. 23: ^{226}Ra uptake by CSH-phases with different Ca/Si-ratios at equilibrium pH (CSH 0.9: pH 11.9; CSH 1.4: pH 12.2) and in artificial cement porewater (ACW) at pH ~13.5.

The uptake of $^{99}Tc^{VII}$ by the various model phases was found to be negligible, since no reductants such as Fe^{II}-bearing phases were present in the systems to reduce the highly soluble pertechnetate-ions to sparingly soluble Tc^{IV}. The uptake mechanisms for iodine depend essentially on its aqueous redox speciation. A structural incorporation of iodide (I^-) was observed for AFm-SO_4 with an equilibrium R_d of about 500 L kg^{-1}. The weaker uptake of I^- by to AFm-CO_3 reveals that the uptake of anionic radionuclides by AFm-phases is dependent on the nature of the anion complex and the degree of carbonation. The uptake of iodate (IO_3^-) by AFm-SO_4 and AFt resulted in both cases in the formation of an iodate-substituted ettringite, formed by phase transformation in case of AFm or due to anion exchange.

Ettringite (AFt), which is generally known for its capability to incorporate various monovalent and divalent oxo-anions by solid-solution formation, showed a stronger affinity to incorporate monovalent iodate than the divalent molybdate oxo-anion (MoO_4^{2-}). In general, no significant uptake of molybdate by most of the model phases was observed. The slight uptake of

molybdate by AFm-SO_4 (R_d ~60 L kg^{-1}) is accompanied by an increase in the basal spacing, suggesting a structural incorporation of MoO_4-anions in the interlayer of the AFm-structure, since the size of molybdate oxo-anions (Mo-O bond length ~1.77 Å) is larger than of SO_4-ions (S-O bond length ~1.47 Å). However, the increase in the basal spacing could also be attributed to an increasing number of water molecules in the interlayer. Moreover, the precipitation of a molybdenum-containing AFm-like phase was also observed by SEM/EDS in experiments on the molybdate-uptake by hydrogarnet. Specific syntheses were performed to investigate the structure of pure AFm-MoO_4, leading to a product with hexagonal plate-like morphology (Fig. 24) and a Ca:Al:Mo-ratio of 4:2:1. However, pXRD and TEM studies revealed that the synthesized material was not pure single-phased AFm-MoO_4 but a mixture of AFm-MoO_4 with a triclinic molybdate-phase that might be structurally related to the so-called U-phase ($4CaO•0.9Al_2O_3•1.1SO_3•0.5Na_2O•16H_2O$)[15,16].

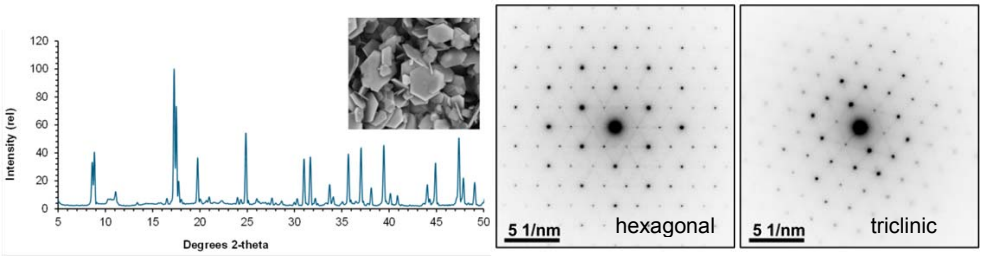

Fig. 24: SEM picture and pXRD pattern (left) of the synthesised Ca-Al-molybdate material and SAED (Selected Area Electron Diffraction) patterns recorded on hexagonal and triclinic platelets (right).

Further batch sorption experiments using hardened cement paste monoliths are in progress to compare the distribution and uptake of radionuclides with observations made in experiments using single model phases. The results of this ongoing study will lead to a refined understanding of the uptake and retention mechanisms of safety relevant radionuclides in cementitious barriers and materials and thus contribute to the scientific basis of the safety case for deep geological disposal of nuclear wastes.

Thermodynamic properties of coffinite

Coffinite ($USiO_4$ or $U(SiO_4)_{1-x}(OH)_{4x}$) is a tetragonal orthosilicate isostructural to zircon ($ZrSiO_4$) and thorite ($ThSiO_4$)[17,18] with space group symmetry $I4_1/amd$ and $Z = 4$ (Fig. 25). Coffinite is the most important U^{IV}-mineral besides uraninite (UO_2) and occurs in many sedimentary and hydrothermal uranium ore deposits as well as in igneous and metamorphic rocks[19,20], where it is assumed to have formed as alteration product from uraninite. Coexisting coffinite and uraninite were described from world class uranium ore deposits such as Cigar Lake (Canada) and Oklo (Gabon) although it is not clear to date whether the replacement of uraninite by coffinite is a result of a direct solid-state process or due to a dissolution and reprecipitation mechanism[21-25].

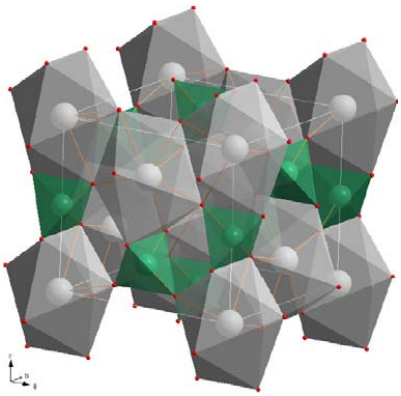

Fig. 25: Structure of coffinite ($USiO_4$) - unit cell with coordination polyhedra: grey U-atoms, green Si-atoms and coordination polyhedra, red O–atoms and coordination polyhedra[26].

Coffinite is expected to be formed as a potential alteration product of directly disposed spent nuclear fuels in contact with silica-rich groundwaters under reducing conditions[27-30]. In safety assessments for deep geological repositories, the uranium (IV) solubility in the aqueous phase is typically derived from the solubility product of UO_2. This provides for very low uranium concentrations in solution due to the expected strongly reducing conditions in the repository environment. Stable U^{IV} phases that could form as secondary phases during spent fuel corrosion would impart an even lower uranium solubility in such systems. Thus the knowledge of the thermodynamic properties of coffinite is meaningful with respect to more realistic safety assessments for deep geological disposal facilities for spent nuclear fuels. However, natural coffinites are generally not suited for the direct determination of the thermodynamic properties of $USiO_4$, due to radiation-induced amorphisation ("metamictisation") and the widespread presence of inorganic and organic impurities (e.g. uraninite, thorianite (ThO_2), rare earth elements, etc.) in these materials[26]. Moreover, the synthesis of pure $USiO_4$ has been proven to be challenging and laborious[26, 31-33]. Thus to date the thermodynamic properties of coffinite are poorly constrained.

In a recent collaborative research activity of IEK-6 with ICSM (Marcoule, France), CEA (Bagnols sur Cèze, France), the University of California (Davis, USA), Stanford University (Stanford, USA), and the University of Notre Dame (Notre Dame, USA) calorimetric measurements on synthetic $USiO_4$ samples were performed to get further insight into the thermodynamics of coffinite formation[34]. For this purpose, different coffinite samples were synthesised under hydrothermal conditions at ICSM and FZJ, respectively, and purified from a mixture of byproducts (e.g. UO_2 and amorphous silica) by treatment with HNO_3 and KOH. The enthalpy of formation of the coffinite samples was obtained by high-temperature oxide melt solution calorimetry. It was found that the standard enthalpy of formation of coffinite from the elements is -1,970.0 ± 4.2 kJ mol^{-1} at 25 °C and that coffinite is energetically metastable with respect to a mixture of uraninite and quartz (SiO_2) by 25.6 ± 3.9 kJ mol^{-1}. Moreover, the calorimetric data revealed that, in reducing environments, coffinite can form from silica-rich aqueous solutions in contact with dissolved uranium species. These thermodynamic properties corroborate that coffinitisation of uranium ores and spent nuclear fuels occurs through dissolution of UO_2 - often forming intermediate U^{VI} species - by a subsequent reaction of the dissolved uranium with a silica-rich aqueous phase[34].

Acknowledgements

The research leading to these results has received funding from the European Union's Horizon 2020 research and innovation programme under grant agreement No 662147 (CEBAMA). Moreover, financial support was provided by the German Federal Ministry of Education and Research (BMBF) through grant 02NUK019C.

References

[1] Mills, S.J., Christy, A.G., Génin. J.M.R., Kameda, T, Colombo, F.: *Min. Mag.* 76 (**2012**) 1289–1336.
[2] Rozov, K., Curtius, H., Bosbach, D.: *Radiochim. Acta* 103 (**2015**) 369–378.
[3] Kulik, D.A., Wagner, T., Dmytrieva, S.V., Kosakowski, G., Hingerl, F.F., Chudnenko, K.V., Berner, U.R.: *Comput. Geosci.* 17 (**2013**) 1–24.
[4] Wagner, T., Kulik, D.A., Hingerl, F.F., Dmytrievava, S.V.: *Can. Mineral.* 50 (**2012**) 1173–1195.
[5] Hummel, W., Berner, U., Curti, E., Pearson, F.J., Thoenen, T. NAGRA Technical Report 02-16 (**2002**) 565 pp.
[6] Atkins, M., Glasser, F.P.: *Waste Manage*. 12 (**1992**) 105–131.
[7] Drace, Z., Ojovan, M.I.: Chapter 1 in: Bart, F., Cau-dit-Coumes, C., Frizon, F., Lorente, S. (eds.): Cement-based materials for nuclear waste storage, Springer (**2013**) 3–11.
[8] Bel, J.J.P., Wickham, S.M., Gens, R.M.F.: *Mat. Res. Soc. Symp. Proc.* 932 (**2006**) 10 p.
[9] Taylor, H.F.W.: Cement chemistry, Thomas Telford Publishing (**1997**) 480 pp.
[10] Atkins, M., Macphee, D.: *Cem. Concr. Res.* 21 (**1991**) 991–998.
[11] Atkins, M., Glasser F.P.: *Cem. Concr. Res.* 22 (**1992**) 241–246.
[12] Baur, I., Keller, P., Mavrocordatos, D., Wehrli, B., Johnson, C.A.: *Cem. Concr. Res.* 34 (**2004**) 341–348.
[13] Matschei, T., Lothenbach, B.: *Cem. Concr. Res.* 37 (**2007**) 1379–1410.
[14] Tits, J., Iijima, K., Wieland, E., Kamei, G.: *Radiochim. Acta* 94 (**2006**) 637–643.
[15] Li, G., Le Bescop, P., Moranville, M.: *Cem. Concr. Res.* 26 (**1996**) 27–33.
[16] Li, G., Le Bescop, P., Moranville-Regourd, M.: *Cem. Concr. Res.* 27 (**1997**) 7–13.
[17] Fuchs, L.H., Gebert, E.: *Am. Mineral.* 43 (**1958**) 243–248.
[18] Speer, J.A.: *Rev. Mineral.* 5 (**1980**) 113–135.
[19] Plant, J.A., Simpson, P.R., Smith, B., Windley, B.F.: *Rev. Mineral.* 38 (**1999**) 255–319.
[20] Fayek, M.: *MAC Short Course Series* 43 (**2013**) 121–146.
[21] Janeczek, J., Ewing, R.: *Mater. Res. Soc. Symp. Proc.* 257 (**1991**) 497–504.
[22] Janeczek, J., Ewing, R.C.: *J. Nucl. Mater.* 190 (**1992***)* 157–173.
[23] Janeczek, J.: *Rev. Mineral.* 38 (**1999**) 321–392.
[24] Deditius, A.P., Utsunomiya, S., Ewing, R.C.: *Chem. Geol.* 251 (**2008**) 33–49.
[25] Fayek, M., Janeczek, J., Ewing, R.C.: *Appl. Geochem.* 12 (**1997**) 549–565.
[26] Labs, S.: *Schriften des Forschungszentrums Jülich, Reihe Energie & Umwelt / Energy & Environment* 267 (**2015**) 153 pp.
[27] Bruno, J., Ewing, R.C.: *Elements* 2 (**2006**) 343–349.
[28] Poinssot, C., Ferry, C., Poulesquen, A.: *Mater. Res. Soc. Symp. Proc.* 985 (**2007**) 6 pp.
[29] Baker, R.J. *Coord. Chem. Rev.* 266–267 (**2014**) 123–136
[30] Ewing, R.C.: *Nat. Mater.* 14 (**2015**) 252-257.
[31] Pointeau, V., Deditius, A.P., Miserque, F., Renock, D., Becker, U., Zhang, J., Clavier, N., Dacheux, N., Poinssot, C., Ewing, R.C.: *J. Nucl. Mater.* 393 (**2009**) 449–458.
[32] Costin, D.T., Mesbah, A., Clavier, N., Dacheux, N., Poinssot, C., Szenknect, S., Ravaux, J.: *Inorg. Chem.* 50 (**2011**) 11117–11126.
[33] Szenknect, S., Costin, D.T., Clavier, N., Mesbah, A., Poinssot, C., Vitorge, P., Dacheux, N.: *Inorg. Chem.* 52 (**2013**) 6957–6968.
[34] Guo, X., Szenknect, S., Mesbah, A., Labs, S., Clavier, N., Poinssot, C., Ushakov, S.V., Curtius, H., Bosbach, D., Ewing, R.C., Burns, P.C., Dacheux, N., Navrotsky, A.: *Proc. Natl. Acad. Sci. USA* 112 (**2015**) 6551–6555.

6.4. Retention of radium by solid-solution formation: kinetic and microstructural aspects

F. Brandt[1], M. Klinkenberg[1], E. Curti[2], J. Weber[1], J. Barthel[3], U. Breuer[4], K. Rozov[1], D. Bosbach[1]

[1]Forschungszentrum Jülich GmbH, Institute of Energy and Climate Research – IEK-6: Nuclear Waste Management and Reactor Safety, 52425 Jülich, Germany

[2]Paul Scherrer Institut, Nuclear and Safety Research Department, Laboratory for Waste Management (LES), CH-5232 Villigen PSI, Switzerland

[3]Forschungszentrum Jülich GmbH, Ernst Ruska-Centre for Microscopy and Spectroscopy with Electrons (ER-C), 52425 Jülich

[4]Forschungszentrum Jülich GmbH, Central Institute for Engineering, Electronics and Analytics (ZEA-3), 52428 Jülich

Corresponding author: f.brandt@fz-juelich.de

Introduction

The retention of radionuclides in the geosphere is to a large extent controlled by sorption processes onto minerals and colloids – including surface complexation, ion exchange as well as the formation of solid solutions. The formation of solid solutions can lead to the structural incorporation of radionuclides into a host structure. Solid solutions are ubiquitous in natural systems. In fact, most minerals in nature are atomistic mixtures of elements rather than pure compounds because solid solution formation leads to a thermodynamically more stable situation compared to the formation of pure compounds.

The formation of ^{226}Ra containing solid solutions with sulphate minerals was recently studied due to their potential for lowering the ^{226}Ra solubility in aqueous systems. In some scenarios for the direct disposal of spent nuclear fuel, ^{226}Ra dominates the dose after 100,000 years [1] (Fig. 26). Radium has a high affinity to secondary barite ($BaSO_4$), which is likely to form as a result of the reaction between sulphate bearing ground waters and Ba present as a fission and decay product in spent fuel. At ambient conditions it was shown that the formation of $(Ba,Ra)SO_4$ solid solutions can lower the Ra solubility by several orders of magnitude [2]. Therefore, the formation of $(Ba,Ra)SO_4$ solid solutions is already considered in some safety assessments for the disposal of spent nuclear fuel in a deep geological repository [3].

However, in order to take full credit of the $(Ba,Ra)SO_4$ solid solution, the details of the ^{226}Ra uptake into the barite structure need to be understood. Earlier studies indicated the uptake of ^{226}Ra into the barite structure during a surprisingly fast recrystallization process [4]. A deeper knowledge regarding the details of the kinetically driven transition from barite to $(Ba,Ra)SO_4$ and the internal microstructural features of barite relevant for the uptake of Ra were so far not understood.

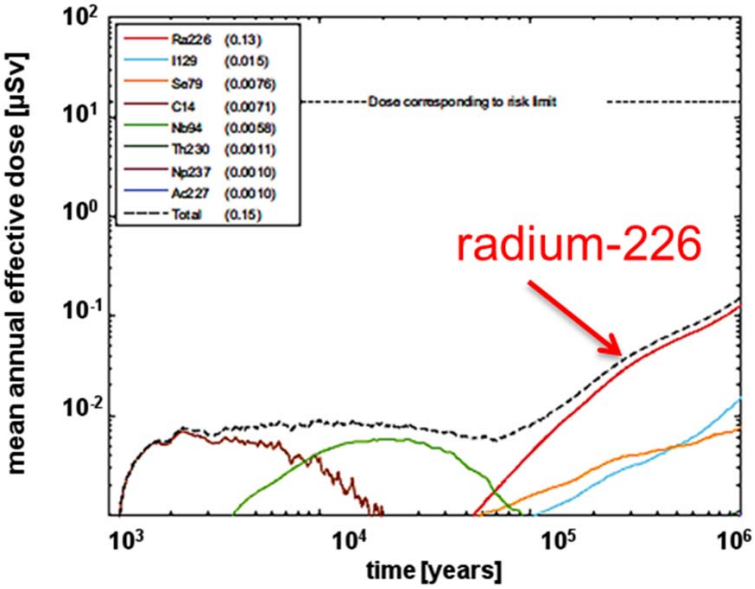

Fig. 26: Evolution of dose vs. time in a deep geological waste repository in crystalline rock from a Swedish scenario.[1]

Aims

The aim of the studies described below was to develop a deeper understanding of the transient kinetics and the microstructural pathways leading to the uptake of Ra via the formation of a $(Ba,Ra)SO_4$ solid-solution at conditions close to equilibrium, as expected for a deep geological waste repository. In order to quantify and compare the radium uptake into two different barite powders, a kinetic model and recrystallization rates for the different phases of barite replacement by the $(Ba,Ra)SO_4$ solid solution were derived for the two kinetically driven phases of radium uptake.

From the studies of Klinkenberg et al. (2014) it became clear that the uptake of radium is related to internal processes within the barite particles. A complementary microscopic approach was applied to investigate the internal microstructure of the barite particles and to identify possible pathways which could explain the surprisingly fast uptake of radium into the barite crystal volume.

Macroscopic long-term experiments and kinetic modelling

The long-term batch-recrystallization experiments were carried out by putting a defined amount of two different barite powders (0.5 g/L) of high purity into contact with a radium-containing solution at room temperature. The experimental window was carefully selected (solid/liquid ratio, grain size and specific surface area etc.) in order to follow the uptake of Ra via the decrease of the Ra-concentration in solution. The barite samples were two commercially available powders of high purity. The barite powders obtained from Sachtleben und from Aldrich were thoroughly analyzed and characterized before the experiments. Typical features of the Sachtleben barite are a blocky morphology and a grain size of more than 10 µm, whereas Aldrich barite is much finer, with a typical grain size smaller than 2 µm.

The BET-surface area differed by one order of magnitude (Sachtleben 0.17 g/m^2, Aldrich 1.7 m^2/g). Radium concentrations in solution were determined at defined times by analyzing liquid samples taken from the experiments with Gamma-spectrometry. The evolution of the radium concentration with time (Fig. 27 a) shows three kinetic regions, (1) a slow initial decrease followed by (2) a faster decrease to a minimum radium concentration and finally (3) the approach to equilibrium. At the end of the experiment, the radium concentrations in solution had decreased by more than 99% of the starting radium concentration.

The macroscopic data were interpreted using the GEMS-PSI code [5] implemented with the NAGRA/PSI thermodynamic database and a thermodynamic model derived in earlier studies by Vinograd et al. [6]. A kinetic model was derived based on the assumption of a constant specific surface area of the barite particles, considering the volume of the aqueous solution and the mass of pure barite at the beginning of the experiment. As the barite recrystallized at close-to-equilibrium conditions, the SS-AS system can be approximated by iterations of equilibrium calculations and comparing the calculated radium concentration [Ra] in solution to the experimental [Ra]. Based on, equilibrium calculations yielded pairs of [Ra] and corresponding amounts [n] of (Ba,Ra)SO_4 solid solution that were formed at different times. For each of the calculated pairs of [Ra] and [n], a reaction time can then be assigned, depending on the chosen values of the thermodynamic model and a defined reaction rate. The resulting recrystallization rates are depicted in Fig. 27 b.

The newly derived experimental recrystallization rates of the first stage were in the order of magnitude of recrystallization rates determined through ^{133}Ba exchange in experiments [7,8]. The second kinetic step takes place at much higher rates than the initial stage. This was interpreted to be related to the possible nucleation of new Ra-barite from supersaturation. During this step, [Ra] in solution decreased below the theoretically predicted equilibrium concentration, indicating a kinetically driven non-equilibrium entrapment of radium [9].

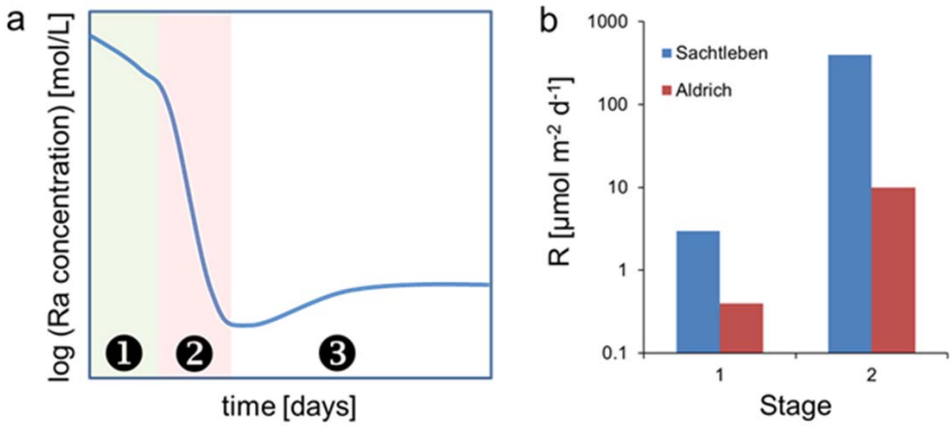

Fig. 27: (a) Typical evolution of the radium concentration in solution versus time including the initial kinetic phase 1, followed by a faster recrystallization step 2 and the approach to equilibrium 3; (b) recrystallization rates determined for stages 1 and 2 applying a kinetic model derived in this study.

During the approach to equilibrium, these precipitates are then slowly transformed in a Ra-poorer (Ba,Ra)SO_4 solid solution, approaching true thermodynamic equilibrium. A significant difference in the recrystallization rates was observed between the fine-grained Aldrich and the coarse grained barite, i.e. the recrystallization rates of Sachtleben barites are consistently higher even though its specific surface area is much smaller. This led to the microscopic study in which the internal features of Sachtleben barites were investigated.

Microscopic investigation of the internal microstructure of Sachtleben barite

The combination of earlier analyses of the final barite samples after recrystallization [4] and the kinetic discussion above lead to the conclusion that internal pathways enabling a fast uptake of radium may play an important role during the recrystallization of barite to a (Ba,Ra)SO_4. The Sachtleben barite sample was chosen because its typical grain size is very suitable for the high resolution techniques applied later.

For the first time, a complementary analytical approach including the atom probe tomography (APT) newly installed at Forschungszentrum Jülich and electron microscopy was applied to investigate the details of the internal barite microstructure which may be relevant for the recrystallization and radium uptake (Fig. 28). APT is a relatively young technique capable of providing 3-D reconstructions of the elemental composition of tip-shaped samples at near-to atomic resolution and was for the first time used to characterized barite samples.

Samples of Sachtleben barite were cut using a focused $^{69}Ga^{+}$ ion beam (FIB) device installed in the controlled area of IEK-6. Cross-section TEM lamellae were prepared perpendicular to the barite particle surfaces and in plane view, i.e. parallel to the barite particle surfaces. In addition, APT tips were prepared by similar preparation procedures as the TEM-lamellae.

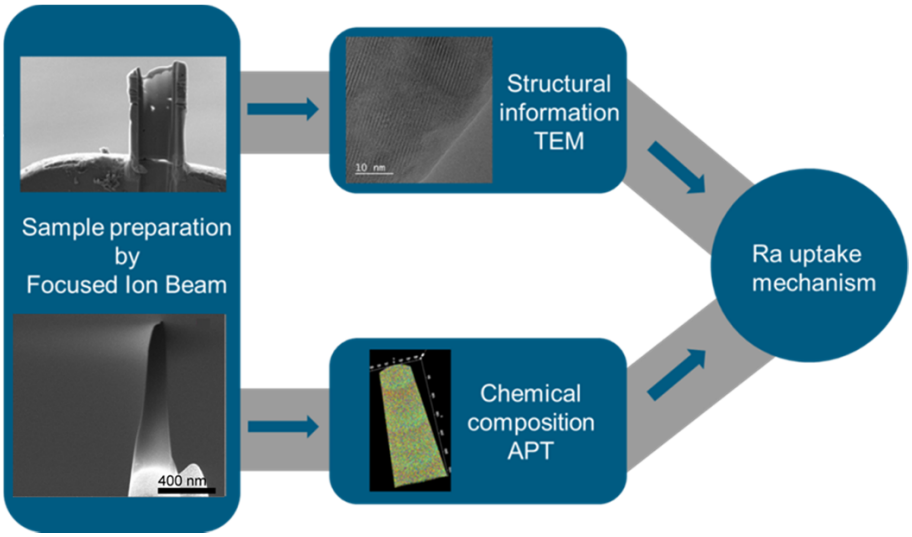

Fig. 28: Combined electron microscopy and atom probe tomography (APT) approach applied in this study.

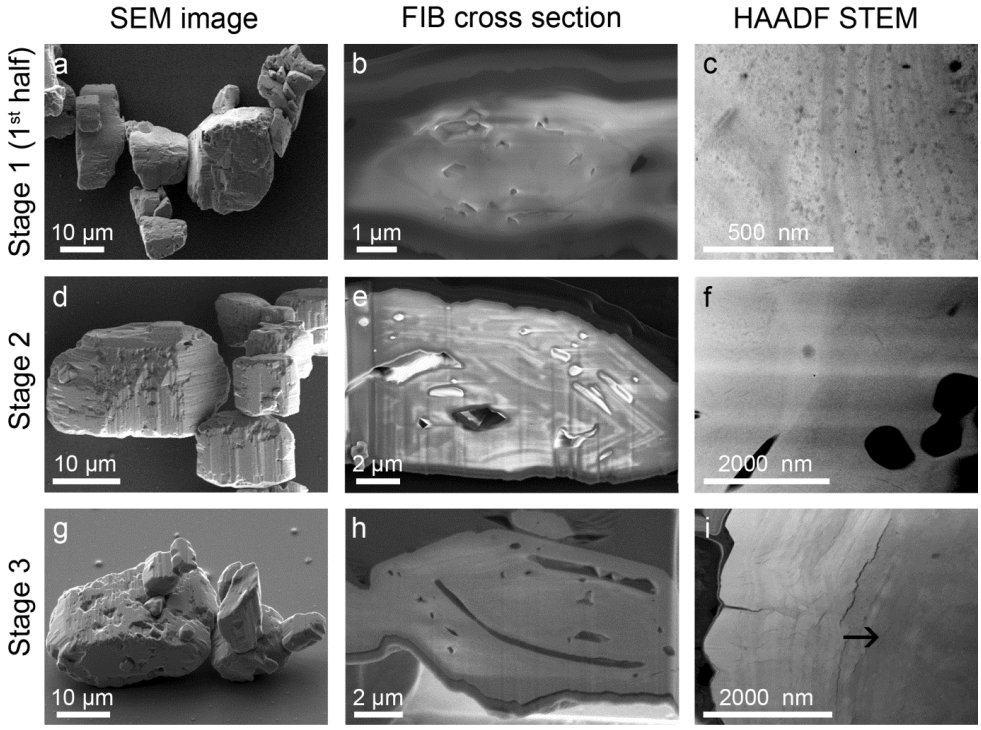

Fig. 29: Representative images demonstrating the temporal evolution of the microstructure of SL barite from Ra uptake experiments during the first half of stage 1 (a-c), at stage 2 (d-f) and stage 3 (g i). SEM images of the barite particles (a, d & g); SEM images of FIB cross-sections displaying the internal microstructure (b, e & h); HAADF STEM images of the layered structure containing nano-scaled pores (c,f & i).

Selected area electron diffraction (SAED) and scanning transmission (TEM) images were obtained with a FEI Tecnai G2 electron microscope operated at 200 kV. A high-angular dark-field (HAADF) detector setup was used for the acquisition of STEM-images. APT measurements were carried out with a LEAP 4000x HR instrument using a laser wavelength of 355 nm. Reasonable data sets were obtained with APT consisting of more than 30 Mio detected ions. This is remarkable because the optimum sample for APT should be electrically conductive or a good thermal conductor – which is not true for barite.

Already the electron microscopy observations of FIB-cross-sections revealed systematic contrast variations which were oriented parallel to the crystallographic directions of the barite particles (Fig. 29 b,e,h). No chemical variation was recorded by EDX at these layered structures. In addition to these layered structures, pores several micrometers in size and of irregular shape were observed. These macro-pores correspond well with micrometer-scale fluid inclusions in natural barites. Natural barites are often formed by precipitation, similar to Sachtleben which is industrially formed by the same mechanism. Some earlier studies (e.g. Rajabzadeh, 2007) reported fluid inclusions matching the cleavage planes of the barite crystals which could correspond to the elongated pores observed in the FIB-cross-sections of Sachtleben barite. In the case of the FIB-preparation, these pores would be opened during

the cutting and are therefore empty. No impurities were observed within the macropores of the FIB cross-sectopms.
SAED observations indicated no change in the crystallographic orientation of the barite at the layered structures but a single crystalline, coherent structure without twins, grain boundaries or other large-scaled defects. The layered structures already visible in SEM become clearly visible in HAADF-STEM observations (Fig. 29 c,f,i). At a higher magnification, HAADF-STEM observations show a structural difference between the alternating bright and dark layers. Because neither the formation of another phase nor variations of composition or orientation were detected by the electron diffraction and EDX, the layers were attributed to the presence of nano-scale porosity. Similarly to larger fluid inclusions, nano-scale porosity has already been encountered in earlier TEM studies on barite crystal growth where they were related to the currently discussed "non-ideal" nucleation mechanism of barite. In this case they would be filled with a residual fluid of the solution from which the barite was formed.
APT was carried out to understand the nature of these nanometer-scale pores. Successful APT measurements were carried out on barite for the first time, revealing new detailed chemical information obtained in the layered structure of barite. The 3D elemental composition maps of several APT measurements performed on Sachtleben barite APT tips reveal again a layered structure. In contrast to the electron microscopy, here the layered structure could clearly be attributed to chemical inhomogeneities within the APT tip. These are caused by the presence of water and Na. Therefore, the layered structures can be interpreted as agglomerations of nano-scale pores filled with fluids which may result from the reaction of

$$BaCl_2 + Na_2SO_4 \rightarrow BaSO_4 + NaCl$$

The identified composition of the chemical inhomogeneities identified by APT is consistent with the residuum of mother liquid commonly assumed to remain within barite after its formation via precipitation.
In summary of the electron microscopy and APT observation, barite crystals can contain significant internal porosity, consisting of larger macropores and nano-scale pores – both likely to be filled with the original mother liquid from which the barite crystallized. In the case of the Sachtleben, both types of pores appear to be abundant and could therefore explain the rather high recrystallization rates observed for this barite type. More details about the results summarized above are available in Weber et al. 2016 [10] and in Brandt et al., 2015 [2].

Acknowledgements

The work has been partially funded by the European FP 7 project SKIN ("Slow processes in close-to-equilibrium conditions for radionuclides in water/solid systems of relevance to nuclear waste management") and by SKB, Swedish Nuclear Fuel and Waste Management Company.

References

[1] Norrby, S., Andersson, J., Dverstorp, B., Kautsky, F., Lilja, C., Sjöblom, R., Sundström, B., Toverud, Ö, Wingefors, S.: "*SKI SITE-94 Saekerhetsanalys foer Djupfoervar iett Kristallint berg*". (**1997**).
[2] Brandt, F., Curti, E., Klinkenberg, M., Rozov, K., Bosbach, D.: *Geochim. Cosmochim. Acta* 155 (**2015**) 1–15.
[3] NAGRA: *Technischer Bericht NTW 14-03*. (**2014**). Wettingen, Switzerland.
[4] Klinkenberg, M., Brandt, F., Breuer, U., Bosbach, D.*: Environ. Sci. Technol*. 48 (**2014**), 6620–6627.
[5] Kulik, D.A., Wagner, T., Dmytrieva, S.V., Kosakowski, G., Hingerl, F.F., Chudnenko, K.V., Berner, U.R.: *Comput. Geosci*. 17 (**2013**) 1–24.

[6] Vinograd, V.L., Brandt, F., Rozov, K., Klinkenberg, M., Refson, K., Winkler, B., Bosbach, D.: *Geochim. Cosmochim. Acta* 122 (**2013**) 398–417.
[7] Curti, E., Fujiwara, K., Iijima, K., Tits, J., Cuesta, C., Kitamura, A., Glaus, M.A., Müller, W.: *Geochim. Cosmochim. Acta* 74 (**2010**) 3553–3570.
[8] Bosbach, D., Boettle, M., Metz, V.: *SKB Technical Report TR-10-43* (**2010**), Stockholm, Sweden.
[9] Thien, B.M.J., Kulik, D.A., Curti, E.: *Appl. Geochem.* 41 (**2014**) 135–150.
[10] Weber, J., Barthel, J., Brandt, F., Klinkenberg, M., Breuer, U., Kruth, M., Bosbach, D.: *Chem. Geol.* 424 (**2016**) 51–59.

6.5. Reactive transport modelling: An attractive tool to support safety assessments for nuclear waste disposal

J. Poonoosamy[1], S. Rohmen[1], A. Idiart[2], D. Bosbach[1], G. Deissmann[1]

[1]Forschungszentrum Jülich GmbH, Institute of Energy and Climate Research – IEK-6: Nuclear Waste Management and Reactor Safety, 52425 Jülich, Germany

[2]Amphos[21] Consulting, 08019 Barcelona, Spain

Corresponding author: j.poonoosamy@fz-juelich.de

Introduction

The geological disposal of nuclear wastes faces major scientific and societal challenges to demonstrate the long-term safety of the repository for the required timescales of up to one million years. For demonstrating the safety of a repository system over these time scales, a fundamental understanding and quantification of the processes governing (i) the long-term evolution of hydrogeological and geochemical conditions in the repository system, (ii) the release of radionuclides from the wastes, and (iii) the migration behaviour of radionuclides in the near- and far-field from the molecular level up to the macro scale are essential for post closure safety assessments. The evolution of the repository near-field is controlled by a number of strongly coupled thermo-hydraulical-mechanical-chemical-biological processes (THMCB-processes) affecting, for example, corrosion rates, gas generation, advective and diffusive radionuclide transport, etc. and are influenced by a variety of factors (e.g. groundwater flow and chemistry, heat output from waste, materials used in the engineered barrier system, microbial activity etc.). Hence the long-term evolution of the hydro-geochemical conditions in a repository cannot be fully assessed by respective laboratory experiments or in-situ experiments (e.g. in underground rock laboratories), for example, due to difficulties in the experimental derivation of flow fields in fractured media in the laboratory, the (experimental) inaccessibility of the pore water within the microporosity of the rock, and especially the long-time scales of the processes involved, but can be addressed by state of the art simulations of the flow regimes coupled to the relevant geo(bio)chemical processes, i.e. by Reactive Transport Modelling (RTM).

RTM provides quantitative tools to analyse the interaction between physical and geochemical processes and predict chemical reactions along transport pathways in space and time. RTM has been increasingly employed in various sub-surface applications during the last decades, for example within the fields of nuclear waste management, CO_2-sequestration, contaminant remediation and pollution prevention, or the development of oil and gas resources. However, the (realistic) description and modelling of the dynamics of solute transport is still a challenging task, due to the complexity introduced by process couplings, the non-linearity of rates at which aqueous species and solid phases interact, and the spatial scaling behaviour of the reactive systems resulting from geological heterogeneities and the ubiquitous variability in physical and geochemical properties of the subsurface, including the interfaces between the various components of a repository system.

The research activities on RTM at IEK-6 focus on complementary experimental and computational approaches to analyse and interpret coupled THMC-processes relevant to the safety of geological repositories, aiming at an enhanced process and system understanding across scales as well as at the reduction of uncertainties and conservatisms in performance assessments (PA). This work comprises the benchmarking of continuum-scale models by laboratory experiments and code comparison, the application of micro-continuum models to address safety relevant processes and phenomena in repository systems using high-performance computing (HPC), as well as the development of pore-scale models, to simulate complex coupled processes, for example, the degradation of cementitious materials or solute transport in clay rocks.

Benchmarking of reactive transport simulations through laboratory experiments

At present, a variety of commercial and purpose-built proprietary codes are available for reactive transport simulations, having different capabilities and using partly different conceptual approaches for the simulation of coupled reactive transport processes. A strict "validation" of the codes to test, for example, conceptual model capabilities, numerical implementation, process couplings, and accuracy, as well as their predictive capabilities, is in principle not feasible. Benchmarking of codes is usually done by applying different codes to selected, often simplified theoretical model problems to evaluate the suitability of the codes to describe a specific process or coupling (e.g. [1]). A different but less often adopted approach to address and compare code capabilities, for example with respect to the description of coupled processes such as permeability/diffusivity changes due to mineral dissolution/precipitation or to address inherent heterogeneities of geological media, is the comparison of simulations to well constrained laboratory[2, 3] or field scale experiments (e.g. in underground research laboratories such as Äspö, Sweden or Onkalo, Finland[4, 5]).

The modelling of coupled processes significantly affecting system evolution at continuum-scale is often not trivial[2, 6-8], for example in case of steep geochemical gradients at interfaces leading to precipitation of solids or with regard to transport phenomena in confined spaces (e.g. diffusive transport in clay rocks). The inability of continuum-scale reactive transport codes to accurately reproduce changes in porosity, permeability and/or diffusivity induced by chemical reactions is because these models consider the medium as average domains with macroscopic flow and transport properties, while the changes effecting transport properties are occurring at the pore-scale (i.e. nano-scale). Therefore, we focus on the development and application of laboratory experiments employing, for example, 1D-column experiments or microfluidic devices and using comparatively simple (geo)chemical systems to shed light onto pore-scale physicochemical processes such as nucleation mechanisms, passivation of surfaces, and creation of unconnected porosities (pore clogging). In particular, key factors affecting precipitation processes, for example pore size dependent effects, and secondary mineral formation that reduces the reactive surface area are addressed. In Fig. 30 the microstructural changes/porosity changes resulting from the injection of a $BaCl_2$ solution into a porous medium constituted initially of celestite ($SrSO_4$) with a bimodal grain size distribution are depicted[2, 3]. The newly formed phases include an epitaxial overgrowth of barite ($BaSO_4$) micro-crystals on large celestite crystals and a nano-crystalline barite phase (resulting from the dissolution of small celestite crystals) in the pore interstices.

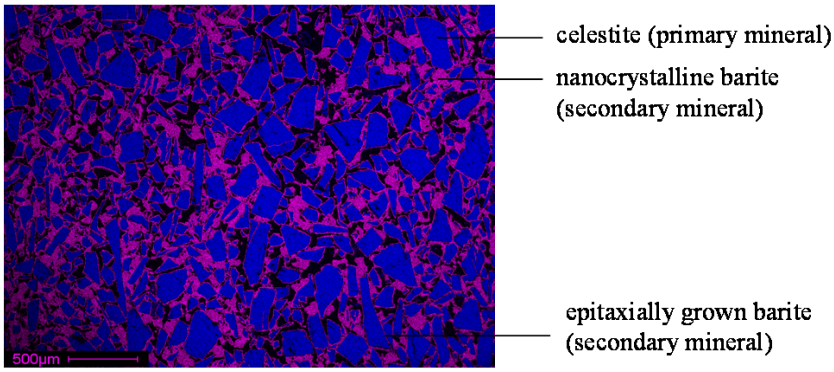

Fig. 30: False-colour SEM image of microstructural changes induced in a porous medium due to reaction of primary celestite ($SrSO_4$, dark violet) with a $BaCl_2$ solution: Precipitation of nanocrystalline barite ($BaSO_4$, pink) in the pore space and formation of epitaxial barite overgrowth on celestite[2, 3].

Pore-scale modelling is applied to investigate the aforementioned processes that are not resolved in continuum models with respect to their backcoupling on transport phenomena. The results of the numerical analyses are used to parameterise constitutive equations to introduce pore-scale corrections into macroscopic (continuum) RTM codes ("upscaling") that can be used for a more realistic macro-scale simulation of the evolution of repository systems. Though the results of laboratory experiments using relatively simple chemistry cannot be used directly for the safety assessment of nuclear waste repositories, they provide for a deeper understanding of processes occurring at the pore scale and the associated changes of (macroscopic) transport properties. Thus this approach allows via appropriate upscaling methodologies the improvement of continuum-scale reactive transport simulations including a more-realistic representation of coupled THMC-processes.

Numerical experiments relevant for performance assessment employing HPC

We apply RTM using HPC solutions to be able to include detailed descriptions of those parameters and processes that have the potential to affect the long-term hydrogeochemical conditions in a nuclear waste repository. In this context, we analyse the influence of heterogeneities present on different scales in a repository system (i.e. from site-scale to the grain-scale) on a number of relevant geochemical processes governing radionuclide transport and retention in the repository near- and far-field. The goal of this analysis, which is based on a number of numerical experiments using (micro-)continuum models, is to enhance process understanding and quantify safety relevant processes, and to provide the scientific basis for upscaling techniques for site-scale reactive transport models, which are required and typically used for the safety analysis of deep geological repositories for nuclear waste.

Effects of site-scale heterogeneities on oxygen intrusion

The ingress of oxygen (i.e. oxygen-rich waters) due to intrusion of glacial meltwaters during/after glaciation events into a geological disposal facility may result in redox transients leading to (more) oxidizing conditions in the vicinity of the emplaced wastes. The intrusion of oxygenated water can in consequence adversely affect the long-term repository performance due to (i) enhanced corrosion of metallic waste containers, (ii) increased matrix corrosion of and radionuclide release from disposed spent nuclear fuels, which are a rather stable waste

form under the prevailing strongly reducing conditions, and (iii) an increase in the mobility of certain radioelements (e.g. U, Pu, Tc) that would be retained in the repository near-field under reducing conditions. However, the presence of Fe(II)-bearing minerals such as pyrite, chlorite, and biotite in the rock matrix or in fracture fillings may lead to oxygen consumption along the flow path and provide sufficient redox buffering to sustain strongly reducing conditions in the repository environment.

The (coupled) reactive transport simulation of oxygen intrusion into fractured and (micro)porous media and the evolution of redox conditions and the depth of oxygen penetration into the repository host rock is computationally highly demanding and usually requires significant simplifications[9, 10], since these simulations suffer from numerical stiffness and require a high spatially discretization as well as small time steps[11]. Therefore we used an enhanced continuum-based approach for the modelling of groundwater flow coupled with reactive transport in crystalline fractured rocks, where flow, transport and geochemical parameters are represented onto a numerical grid using Discrete Fracture Network (DFN) derived parameters[11]. The geochemical reactions are further constrained by field observations on the distribution of minerals providing for redox buffering such as chlorite ($(Mg,Fe^{II})_5(Al,Fe^{III})[AlSi_3O_{10}](OH)_8$), using kinetic descriptions for chlorite dissolution[12] and the oxidation of aqueous Fe(II)-ions. To illustrate the applicability of this approach to include site-scale physical and geochemical complexities into RTM, the potential ingress of oxygenated glacial-meltwater in heterogeneous fractured rocks was simulated using the Forsmark site (i.e. the Swedish candidate site for a deep geological repository for spent nuclear fuel) as an example. The calculations were performed using the recently developed interface for reactive transport modelling in crystalline rocks iDP[13] that couples the hydrogeological model DarcyTools[14] to the massively parallel reactive transport simulator PFLOTRAN[15, 16]. The reactive transport simulations were run on the supercomputer JUQUEEN of the Jülich Supercomputing Centre (JSC)[17].

The results of the high-performance reactive transport calculations show that, after a quick oxygen penetration, steady state conditions are attained where abiotic reactions (i.e. the dissolution of chlorite and the homogeneous oxidation of aqueous Fe(II)-ions) can counterbalance the advective oxygen fluxes into the repository host rock (cf. Fig. 31), and that chlorite dissolution rates are higher in the highly conductive zones, i.e. where higher mineral surface are available for reactions[11]. These results suggest that the Forsmark site has enough buffering capacity to limit the extension of oxygen penetration due to the ingress of oxygenated melt water during glaciation events, even for a very large period of time (i.e. some thousands of years, which are the relevant timescales for these processes). Compared to previous modelling studies on oxygen ingress, and thanks to the use of HPC resources, the methodology applied allows for the inclusion of the full complexity of the site, thus increasing the realism of the resulting reactive transport simulations[11].

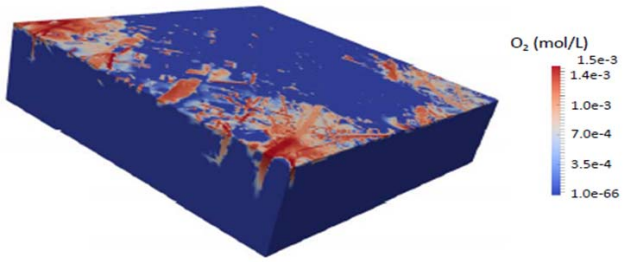

Fig. 31: Oxygen concentration in groundwaters at the Forsmark site after approx. 350 years of ingress of oxygenated melt water from the surface. A log colour scale and a vertical exaggeration of 2:1 are used (domain size 1000x1000x132 m^3 discretised by 4.125E06 cells).

Effects of grain scale mineralogical heterogeneity

In the most-advanced projects for geological disposal of high-level nuclear wastes worldwide (i.e. Olkiluoto in Finland and Forsmark in Sweden), the host formations are constituted by crystalline rocks, which are also considered as potential host rocks for geological repositories, for example, in Germany, the UK and Russia. The radionuclide retention potential of crystalline rocks is mainly related either to (i) sorption of radionuclides to fracture filling minerals (e.g. clays) or (ii) to radionuclide diffusion into the rock matrix and sorption onto the mineral surfaces available in the rock matrix. In-situ and laboratory investigations provided abundant evidence of the highly heterogeneous nature of the matrix of crystalline rocks with respect to microstructure and distribution of available mineral surfaces and pore space. This intrinsic textural and mineralogical heterogeneity of the rock matrix on the grain-scale was suggested as possible explanation for the anomalous (radio)tracer penetration profiles observed in experiments at the ONKALO underground facility in Finland and the Äspö Hard Rock Laboratory in Sweden, and to explain the large discrepancies between the radionuclide profiles modelled with continuum-scale models and the observations[18].

Therefore, we used a micro-continuum approach to study radionuclide transport in a synthetically generated heterogeneous fracture–matrix system to assess the implications of grain-scale physical and mineralogical heterogeneity on radionuclide transport and retention avoiding an averaged equivalent porous media approach[19]. Micro-continuum approaches are deemed as interesting alternatives to pore-scale models as they allow high-resolution mineralogical and microstructural data to be accurately represented while still using “standard” continuum models with bulk-derived parameters[19]. The conceptual model consists of a heterogeneous single fracture–matrix system (domain size 5x10x50 cm^3) that is discretized with 52,827,840 rectangular cuboids (cell size ~0.4x0.4x0.1 mm^3) (cf. Fig. 32). The conceptual geochemical model considers the transport of the non-redox sensitive radionuclide ^{135}Cs, which is retained by cation exchange on biotite[20], with the number of exchange sites depending on the abundance and (heterogeneous) distribution of biotite ($K(Mg,Fe)_3(Si_3Al)O_{10}(OH,F)_2$). The resulting grain-scale reactive transport model was solved using HPC technologies using the reactive transport code PFLOTRAN[15, 16] on the supercomputer JUQUEEN[17] at JSC. The results were compared to those derived from two alternative ("upscaled") models, where the abundance of the reactive mineral biotite – and thus the number of available sorption sites – was averaged over the matrix volume[19].

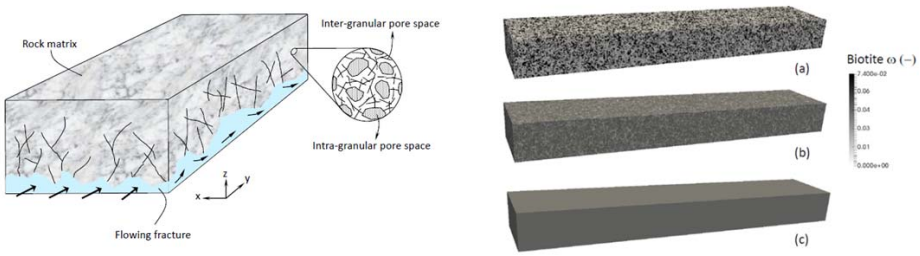

Fig. 32: Left: Conceptual model of the heterogeneous single fracture–matrix system used in the numerical analysis (the thick arrows indicate the water flowing through the open fracture)[19]. Right: Distribution of biotite volume fraction for the heterogeneous discrete mineralogical model (DM) (a), and the upscaled models (b: continuous mineralogical (CM) and c: homogeneous mineralogical (HM) model)[19].

The simulation results show that in the heterogeneous grain-scale model, the penetration of Cs into the rock matrix is faster and the penetration front uneven and finger-shaped, whereas for the upscaled models a much smoother front is observed. The analysis of the Cs breakthrough curves computed at the fracture outlet shows that the upscaled models provide significantly later first-arrival time estimates compared to the grain-scale model, with the breakthrough curves converging at late times (Fig. 33). These results suggest that spatially averaged upscaled parameters for the distribution of sorption sites can be used to predict the late-time behaviour of the breakthrough curves but could be inadequate to simulate the early behaviour, when modelling radionuclide transport in fractured crystalline rocks[19].

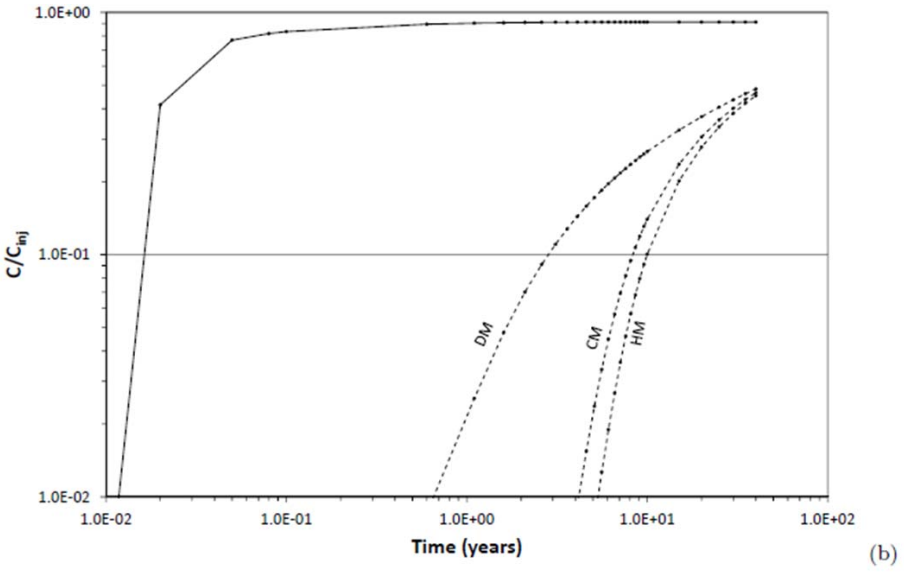

Fig. 33: Cs breakthrough curves (dashed lines) computed with the three models at the fracture outlet (DM: discrete heterogeneous mineralogy; CM, HM: upscaled models, see Fig. 3) compared to the conservative tracer (continuous line)[19]. Concentrations are normalized by the concentration of the boundary water.

Development of pore-scale models for the simulation of concrete degradation

In recent years, the development of advanced numerical algorithms and the increase in computational power have paved the way for simulations on the pore-scale. Pore-scale models utilise mechanistic approaches to incorporate the inherent heterogeneities of system properties, for example, with respect to solid phase distribution, reactive surface areas, and microstructure. Pore-scale models avoid thus the implicit spatial averaging of large-scale (continuum) models that smooth out any heterogeneity and non-linear feedbacks at a scale comparable or smaller than the representative elementary volume (grid-spacing) used in those models[21].

Cement-based materials have been widely adopted as engineered barrier materials in nuclear waste repositories both for their radionuclide fixation and immobilisation properties as well as for their low permeability and diffusivity. Cementitious materials generally consist of various hydration phases, in particular nanocrystalline calcium-silicate-hydrates (CSH), calcium aluminate/ferrate compounds (AFm/AFt), and portlandite ($Ca(OH)_2$). The phase assemblage of specific cementitious materials and their microstructure depend on the cement types used and the mixing and curing processes[22]. The macroscopic physical properties of these materials (incl. their transport properties) strongly depend on the pore structure and the (micro)structural and chemical changes resulting from long-term alteration and degradation processes. In particular chemical degradation processes such as calcium leaching and/or carbonation and their impact on physical properties, such as diffusivity, permeability, porosity, and pore-size distribution are of interest[23, 24]. However, a realistic simulation of the feedback of these long-term alteration processes (e.g. the leaching of portlandite from ordinary Portland cement based materials by groundwaters in a geological repository covers timeframes of some ten thousands of years) on transport properties and solute transport/radionuclide transport is challenging.

Therefore, within the frame of the EC-funded Horizon 2020 collaborative project CEBAMA (www.cebama.eu), a pore-scale reactive transport modelling framework for obtaining a more accurate and mechanistic description of alteration processes in cementitious materials is under development. The code development is based on the coupling of a transport code based on the Lattice-Boltzmann-Method (Palabos[25]) with a well-established geochemical code (PhreeqcRM[26]) and is called *iPP* (**i**nterface **P**alabos **P**hreeqC). The Lattice-Boltzmann method (LBM) can be used to simulate the microscopic behaviour of particles in a fluid in a discrete way where space, time and velocity vectors are discretised. The mesoscopic and macroscopic properties of the system can be recovered by choosing proper discretisation steps. Thus, LBM solves the Navier-Stokes equation for advective-diffusive transport processes[27, 28]. The coupling code *iPP* implemented using C++ template meta-programming techniques and MPI capabilities for HPC facilities, follows the operator splitting approach. Flow and solute transport are calculated using the LBM at a given time step, followed by the calculation of chemical reactions in PhreeqcRM, which calculates various solution properties including pH, redox potential and the concentrations of aqueous species, as well as the saturation indices of solid phases. Moreover, the abundance of the various solid phases in the system and their composition are obtained and the porosity values are updated after each time step.

In order to validate the current version of *iPP*, a simple symmetrical 1D diffusion-based setup was employed, consisting of a domain containing an inert tracer (NaCl) surrounded by semi-infinite regions with zero tracer concentration on both sides, with no source or sink terms considered. The concentration profiles were calculated for four different times with the LBM code and compared to the analytical solution of the diffusion problem[29], showing an excellent agreement between both approaches (Fig. 34).

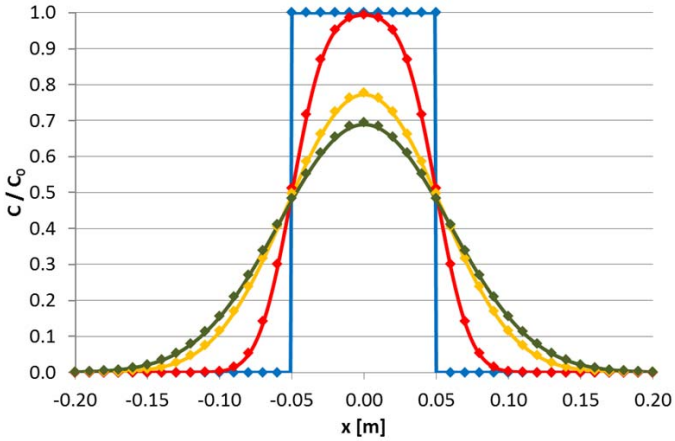

Fig. 34: Comparison of LBM diffusive transport results (diamonds) to analytical solutions (solid lines) for different simulation times (blue: initial values, red: 2 d, yellow: 10 d, and green: 14 d).

The preliminary verification and benchmarking of the code provided evidence that the tool is appropriate for the simulation of complex advective and diffusive solute transport processes. Recently, *iPP* was extended to support the simulation of heterogeneous precipitation processes leading to the formation of grain overgrowth via distance field transformation. In future development steps the simulation results with respect to changes of phase assemblage and microstructure will be compared to results of experiments performed within the CEBAMA project by research teams from the University of Sheffield (UK) and the University of Surrey (UK). In the scope of these experiments, data on the chemical and microstructural evolution in cementitious materials leached by various types of water (e.g. clay water, granite water, seawater) will be obtained. This will aid to derive a better understanding of the mechanisms that have to be implemented in the code and enhance its predictive capabilities to address long-term alteration processes in cementitious materials on the pore-scale. Moreover, the versatility of the simulation framework under development will allow to address also pore-scale processes in other porous media in the future, such as transport phenomena in clay materials.

Concluding remarks

RTM provides means to analyse and quantify coupled processes affecting the hydro-geological and hydrogeochemical conditions in the subsurface and to predict, inter alia, the migration behaviour of radionuclides in repository systems. However, in the field of nuclear waste management, the reliability and the predictive capabilities of the modelling codes are of special concern, requiring an in-depth understanding of the process couplings from the nano-scale to the macro-scale. In this context, we pursue different modelling approaches,

from pore-scale modelling via micro-continuum models to continuum formulations, complemented by information obtained from laboratory experiments and/or underground research facilities, to understand coupled reactive transport phenomena on different scales. The overall goal of this research is to derive a fundamental (quantitative) understanding of the multiple coupled processes related to long-term repository evolution, and thus to improve the scientific basis of the safety case of deep geological disposal. This work aims in particular at implementing close-to reality process descriptions in RTM codes to provide for a system understanding across scales and to reduce uncertainties and conservatisms in PA, contributing thus to the prerequisites for an in-depth comparison of different repository concepts and sites, which is, for example, mandatory in the German site selection procedure[30, 31].

Acknowledgements

The research leading to these results has received funding from the European Union's Horizon 2020 research and innovation programme under grant agreement No 662147 (CEBAMA). The authors gratefully acknowledge the computing time granted by the JARA-HPC Vergabegremium and provided on the JARA-HPC Partition part of the supercomputer JUQUEEN at Forschungszentrum Jülich. The authors are indebted to J. Molinero, P. Trinchero and H. Ebrahimi (Amphos[21] Consulting, Barcelona, Spain) for the extensive and fruitful collaboration in the field of reactive transport modelling.

References

[1] Steefel, C.I., Yabusaki, S.B., Mayer, K.U.: *Computat. Geosci.* 19 (**2015**) 439–443.
[2] Poonoosamy, J., Kosakowski, G., Van Loon, L.R., Mäder, U.: *J. Contam. Hydrol.* 177-178 (**2015**) 1–17.
[3] Poonoosamy, J., Curti, E., Kosakowski, G., Van Loon, L.R., Grolimund, D., Mäder U.: *Geochim. Cosmochim. Acta,* 182 (**2016**) 131–144.
[4] Voutilainen, M., Poteri, A., Helariutta, K., Siitari-Kauppi, M., Nilsson, K., Andersson, P., Byegård, J., Skålberg, M., Kekäläinen, P., Timonen, J., Lindberg, A., Pitkänen, P., Kemppainen, K., Liimatainen, J., Hautojärvi, A., Koskinen, L.: WM2014 Conference, March 2 – 6, 2014, Phoenix, AZ, USA (**2014**) 14 pp.
[5] Widestrand, H., Byegård, J., Nilsson, K., Höglund, S., Gustafsson, E., Kronberg, M.: SKB Report R-10-67 (**2010**) 153 pp.
[6] Tartakovsky, A.M., Redden, G., Lichtner, P.C., Scheibe, T.D., Meakin, P.: *Water Resour. Res.* 44 (**2008**) W06S04.
[7] Katz, G.E., Berkowitz, B., Guadagnini, A., Saaltink M.W.: *J. Contam. Hydrol.* 120-121 (**2011**) 27–44.
[8] Chagneau, A., Claret, F., Enzmann, F., Kersten, M., Heck, S., Madé, B., Schäfer, T.: *Geochem. Trans.* 16 (**2015**) 13.
[9] Spiessl, S., MacQuarrie, K, Mayer, K.: *J. Contam. Hydrol.* 95 (**2008**) 141–153.
[10] MacQuarrie, K., Mayer, K., Jin, B., Spiessl, S.: *J. Contam. Hydrol.* 112 (**2010**) 64–76.
[11] Trinchero, P., Puigdomenech, I., Molinero, J., Ebrahimi, H., Gylling, B., Svensson, U., Bosbach, D., Deissmann, G.: *J. Contam. Hydrol.* 200 (**2017**) 60–69.
[12] Lowson, R.T., Comarmond, M.C.J., Rajaratnam, G., Brown, P.: *Geochim. Cosmochim. Acta* 69 (**2005**) 1687–1699.
[13] Molinero, J., Trinchero, P., Ebrahimi, H., de Vries, L., Luna, M., Svensson, U., Lichtner, P.: SKB Report R-15-17 (**2015**) 64 pp.
[14] Svensson, U., Ferry, M.: SKB Report R-10-72 (**2010**) 166 pp.
[15] Hammond, G.E., Lichtner, P.C.: *Water Resour. Res.* 46 (**2010**) W09527 131.
[16] Lichtner, P.C., Hammond, G.E., Lu, C., Karra, S., Bisht, G., Andre, B., Mills, R., Kumar, J.: PFLOTRAN User's Manual (**2014**) 184 pp.
[17] Stephan, M., Docter, J.: *J. Large Scale Res. Facil.* 1 (**2015**) doi:10.17815/jlsrf-1-18.
[18] Nilsson, K., Byegård, J., Selnert, E., Widestrand, H., Höglund, S., Gustafsson, E.: SKB Report R-10-68 (**2010**) 298 pp.
[19] Trinchero, P., Molinero, J., Deissmann, G., Svensson, U., Gylling, B., Ebrahimi, H., Hammond, G., Bosbach, D., Puigdomenech, I.: *Transp. Porous Med.* 116 (**2017**) 73–90.
[20] Kyllönen, J., Hakanen, M., Lindberg, A., Harjula, R., Vehkamäki, M., Lehto, J.: *Radiochim. Acta*, 102 (**2014**) 919–929.
[21] Yoon, H., Kang, Q., Valocchi, A.J.: *Rev. Mineral. Geochem.* 80 (**2015**) 393–431.
[22] Taylor, H.F.W.: Cement chemistry. Thomas Telford Publishing (**1997**) 480 pp.

[23] Kang, Q., Chen, L., Valocchi, A.J., Viswanathan, H.S.: *J. Hydrol.* 517 (**2014**) 1049–1055.
[24] Zhang, M., Xu, K., He, Y., Jivkov, A.P.: *Constr. Build. Mater.* 64 (**2014**) 222–230.
[25] FlowKit: Palabos user guide (**2011**) http://www.palabos.org/documentation/userguide/.
[26] Parkhurst, D.L., Wissmeier, L.: *Adv. Water Resour.* 83 (**2015**) 176–189.
[27] Mohamad, A.A.: Lattice Boltzmann Method. Springer (**2011**) 178 pp.
[28] Succi, S.: The Lattice Boltzmann equation for fluid dynamics and beyond. Clarendon Press (**2001**) 304 pp.
[29] Crank, J.: The mathematics of diffusion (2nd ed.). Oxford University Press (**1980**) 414 pp.
[30] Gesetz zur Suche und Auswahl eines Standortes für ein Endlager für hochradioaktive Abfälle (Standortauswahlgesetz - StandAG) vom 23. Juli **2013**. BGBl I, 41, p. 2553, 26.07.2013.
[31] Gesetz zur Fortentwicklung des Gesetzes zur Suche und Auswahl eines Standortes für ein Endlager für Wärme entwickelnde radioaktive Abfälle und anderer Gesetze vom 5. Mai **2017**. BGBl I, 26, p. 1074, 15.05.2017.

6.6. Hydrometallurgical separation of minor actinides

G. Modolo, A. Wilden

Forschungszentrum Jülich GmbH, Institute of Energy and Climate Research – IEK-6: Nuclear Waste Management and Reactor Safety, 52425 Jülich, Germany

Corresponding author: g.modolo@fz-juelich.de

Summary of the group activities

Although the minor actinides (MA) americium and curium contribute to less than 0.1% of the initial spent fuel mass they dominate the long-term radiotoxicity and heat load of the high active waste after separation of plutonium. The R&D at IEK-6 is focused on the efficient separation of the minor actinides from nuclear waste solutions by hydrometallurgical processes. The main objectives of our research are on the one hand fundamental research on solvent extraction to improve the knowledge of the chemistry of actinides and the extraction ligands and on the other hand process development involving testing of continuous extraction processes with inactive and with spiked radioactive waste solutions in appropriate devices.
Important aspects to understand are:

- The chemistry of key fission products (lanthanides, Zr, Mo, Sr etc.) to improve the actinide/fission product separation.
- The stability of the solvent (ligand + diluent), to improve its resistance against radiolysis and hydrolysis. This includes also recycling and cleaning of the solvent and management of secondary waste.

Actinide separation by hydrometallurgical methods is strongly linked to coordination chemistry. The selectivity of extraction ligands for the separation of minor actinides is governed by the preferential formation of MA complexes with these ligands. The general methodology deployed to develop a separation process is shown in Fig. 35. The first step is the design and synthesis of new ligands and the assessment of their complexation and extracting properties on the laboratory scale. Due to the long-standing involvement in European partitioning projects we have a strong collaboration with different organic synthesis laboratories (e.g. Twente University, NL; Reading University, UK). The novel ligands are assessed in screening tests, following standardized protocols, regarding their usability in one (or more) of the hydrometallurgical separation processes (e.g. DIAMEX, SANEX etc.). These processes for actinide separation rely on the formation of either hydrophilic (cf. 5.7) or lipophilic coordination complexes. Hence, different hydrophilic and lipophilic ligands, derived from approved structures developed during the European partitioning projects (NEWPART to SACSESS) are studied in Jülich.

Many criteria must be met for the candidate ligands: high affinity for actinides, selectivity over fission products, reversibility, resistance to chemical and radiolytic environment of the highly aggressive medium etc. Only the ligands which successfully pass this assessment are considered for further process development studies.
The acquisition of distribution data of all relevant elements (e.g. fission and activation products) is the next step to understand the extraction mechanism. Highly sophisticated analytical tools are available in Jülich and at different national and international collaboration organizations to deeper understand the complexation and extraction chemistry on the

molecular level. Main objective of this task is to assess the complex structures of formed metal – ligand complexes of interest.
These analytical tools comprise e.g. single crystal X-ray diffractometry mainly involving inactive surrogate metal ions (e.g. lanthanides) to identify solid-state structures of the complexes. These results, in combination with data from speciation studies and structure analysis of the actinide complexes in solution (using TRLFS, ESI-MS, NMR, and EXAFS spectroscopy) and extraction results are used to understand and to develop thermodynamic models of the extraction processes. Quantum chemistry and Molecular Dynamics calculations are further applied to understand how selected ligands interact with targeted metal ions. These studies combined altogether help understanding the fundamental causes of the selectivity observed at the molecular level, and help to design improved ligands in a more methodical way.

The Jülich IEK-6 laboratory as partner within national and European projects (NEWPART to GENIORS, 2017 – 2021) is one of the leading laboratories in the development of innovative hydrometallurgical partitioning processes. The developed flow-sheets are tested in miniature centrifugal contactors and evaluated by comparing the results with computer code model predictions. In collaboration with European partners, successful processes are demonstrated using genuine solutions. Our knowledge of solvent extraction is transferred to non-nuclear applications, such as the recycling of precious elements or rare earth elements from primary and secondary resources.

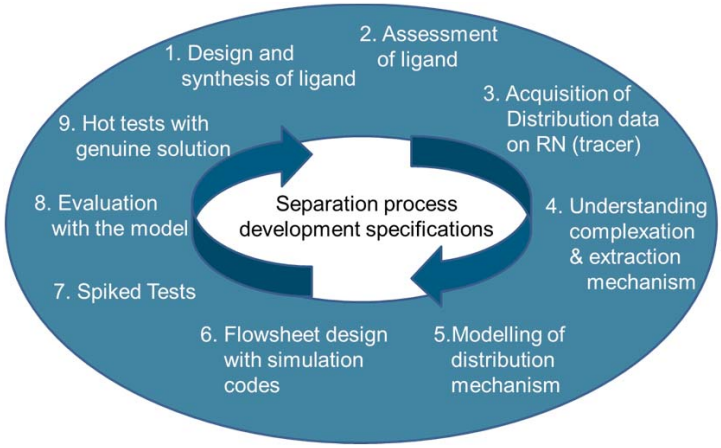

Fig. 35: Methodology deployed to develop a separation process.

References

[1] Modolo, G. et al. (2015): Chap. 10 in Reprocessing and Recycling of Spent Nuclear Fuel, Taylor, R., Woodhead Publishing: Oxford, pp. 245-287.
[2] Moyer, B.A. et al. (2015): Chap. 11 in Reprocessing and Recycling of Spent Nuclear Fuel, Taylor, R., Woodhead Publishing: Oxford, pp. 289-312.
[3] Bourg, S. et al. (2015): Nukleonika Vol. 60 (4 (Pt. II)), 809-814.
[4] Geist, A. et al. (2016): Procedia Chem. Vol. 21, 218-222.
[5] Lumetta, G.J. et al. (2015): Solvent Extr. Ion Exch. Vol. 33 (3), 211-223. Levitskaia, T.G. et al. (2017): Solvent Extr. Ion Exch. Vol. submitted. Lumetta, G.J. et al. (2017).

6.7. Diglycolamides – complex chemistry in organic and aqueous systems

A. Wilden[1,*], L. Klaß[1], P.M. Kowalski[1], G. Modolo[1], D. Bosbach[1], C. Wagner[2], A. Geist[2], P. Panak[2], W. Verboom[3]

[1]Forschungszentrum Jülich GmbH, Institute of Energy and Climate Research – IEK-6: Nuclear Waste Management and Reactor Safety, 52425 Jülich, Germany

[2]Karlsruher Institut für Technologie (KIT), Institut für Nukleare Entsorgung (INE), 76021 Karlsruhe, Germany

[3]University of Twente, Laboratory of Molecular Nanofabrication, MESA+ Institute for Nanotechnology, P.O. Box 217, 7500 AE Enschede, The Netherlands

Corresponding author: a.wilden@fz-juelich.de

Introduction

Diglycolamides are one of the most important classes of extractants used in the treatment of used nuclear fuel solutions for minor actinide separation. Since many years, lipophilic extractants of this class are successfully used in counter-current processes developed at IEK-6 and worldwide for the extraction of trivalent actinides (*An*(III)) together with the trivalent lanthanides (*Ln*(III)). TODGA (*N*,*N*,*N'*,*N'*-tetraoctyl-diglycolamide, Fig. 36) resembles the most prominent ligand.[1-5] The diglycolamide class permits a multitude of chemical derivatizations, which are synthetically easily available. E.g. the amidic side chain length has a tremendous influence on the solubility. Therefore, hydrophilic analogues of TODGA with shorter side chains are also successfully used in solvent extraction processes for the aqueous phase complexation of *An*(III) and *Ln*(III) or back extraction from loaded solvent.[6-10] Within European collaborative projects, modified diglycolamides were synthesized and tested for *An*(III)/*Ln*(III) extraction with a focus on modifying the ligand backbone.[11]

The extraction properties were evaluated in view of possible application in separation processes. Additionally, the complexation of trivalent 4*f* and 5*f* metal ions was studied on a fundamental basis using a variety of different analytical techniques comprising single crystal structure analysis, time-resolved laser fluorescence spectroscopy (TRLFS), extended X-ray absorption fine structure (EXAFS) spectroscopy, as well as DFT-based atomistic simulations.

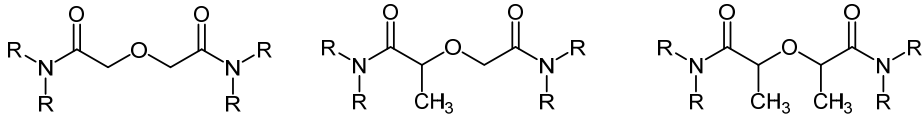

R=C_8H_{17}: TODGA
R=C_2H_5: TEDGA
R=CH_3: TMDGA

R=C_8H_{17}: Me-TODGA
R=C_2H_5: Me-TEDGA
R=CH_3: Me-TMDGA

R=C_8H_{17}: Me_2-TODGA
R=C_2H_5: Me_2-TEDGA
R=CH_3: Me_2-TMDGA

Fig. 36: Chemical structures of the ligands used in this study.

Results and Discussion

In solvent extraction experiments with the lipophilic diglycolamides TODGA and its methylated analogues it was found that the extraction of 4*f* and 5*f* metal ions follows a clear trend. The distribution ratios followed the order TODGA > Me-TODGA > Me_2-TODGA. Solvent extraction slope analysis suggested the formation of 1:3 (metal:ligand) complexes in an aliphatic diluent, which was supported by TRLFS investigations. In mono- and biphasic TRLFS measurements, the 1:3 complexation was confirmed. Conditional stability constants followed the same trend as the distribution ratios.[12] Interestingly, the same complexation mode and trend in conditional stability constants was found for the hydrophilic analogues in aqueous solution, recently.[10] Table 1 shows a comparison of the conditional stability constants for the formation of $[Cm(L)_n]^{3+}$ complexes of hydrophilic and lipophilic ligands and Fig. 37 shows normalised fluorescence spectra of the titration of Cm(III) with Me-TEDGA in $HClO_4$ as an example of the sequential formation of $[Cm(L)_n]^{3+}$ complexes.

Table 1: Conditional stability constants for the formation of $[Cm(L)_n]^{3+}$ (n = 1-3) in $HClO_4$ (TEDGA, Me-TEDGA, Me_2-TEDGA)[10, 13] and ethanol (TODGA, Me-TODGA, Me_2-TODGA, data taken from ref.[12]).

	TEDGA*	Me-TEDGA	Me_2-TEDGA	TODGA	Me-TODGA	Me_2-TODGA
log β_{01}	3.3	3.3	3.0	6.25	5.89	4.15
log β_{02}	6.3	5.8	4.7			
log β_{03}	8.3	7.8	6.1	14.92	14.85	12.72

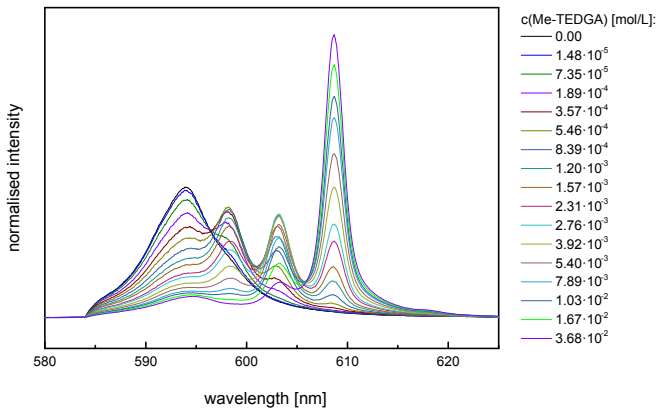

Fig. 37: Normalised fluorescence spectra of the titration of Cm(III) (initial concentration: 10^{-7} mol/L) with Me-TEDGA in 10^{-3} mol/L $HClO_4$.

EXAFS spectroscopy was used to study the metal complexation under realistic conditions, as real organic samples from solvent extraction experiments were used. The EXAFS analysis was supported by single crystal structure analysis of crystals grown from short chain diglycolamides. Fig. 38 exemplary shows the primary $k^3\chi(k)$ Eu EXAFS data and Fourier transform of the $k^3\chi(k)$ Eu EXAFS data and fit for a structure model of a 1:3 complex. A very good fit was obtained for this structural model, supporting solvent extraction and TRLFS data of 1:3 complexes being present in solvent extraction experiments.

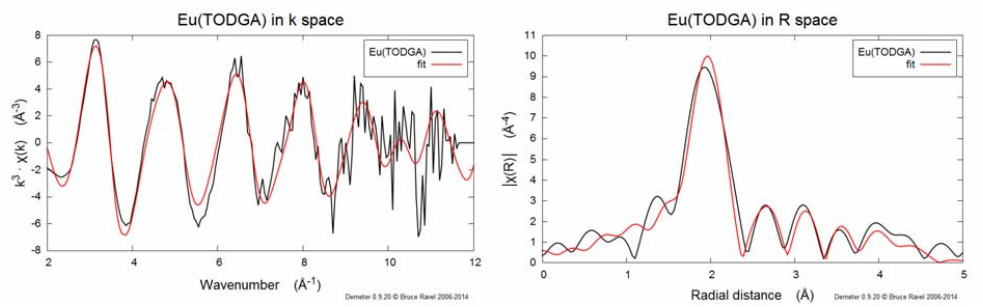

Fig. 38: Left: Primary $k^3\chi(k)$ Eu EXAFS data and fit. Right: Fourier transform of the $k^3\chi(k)$ Eu EXAFS data and fit.

DFT-based atomistic simulations were conducted to study the complexation of metal ions with diglycolamides also on a theoretical level and to support the experimental and spectroscopic results. The goal was to gain an in-depth and comprehensive understanding of the complexation of 4*f* and 5*f* metal ions on a fundamental basis. The trends observed in solvent extraction experiments were very well reproduced in these calculations.

Conclusions

The structure of metal ion complexes with different diglycolamide was studied using a variety of different complementary analytical techniques including DFT-based atomistic simulations. The results were consistent and a clear trend was observed with regards to ionic radius of the 4*f* and 5*f* metal ion and level of derivatization of the ligands. The obtained fundamental understanding of the complexation strongly supports the possible application of diglycolamides in solvent extraction processes.

Acknowledgements

Financial support for this research was provided by the European Commission (project SACSESS—Contract No. FP7-FISSION-2012-323282) and the German Federal Ministry of Education and Research (Contract No. 02NUK020A, 02NUK020B, 02NUK020D, and 02NUK020E).

References

[1] Modolo, G. et al.: *Solvent Extr. Ion Exch.* 25(6) (**2007**) 703-721.
[2] Modolo, G. et al.: *Solvent Extr. Ion Exch.* 26(1) (**2008**) 62-76.
[3] Magnusson, D. et al.: *Solvent Extr. Ion Exch.* 27(1) (**2009**) 26-35.
[4] Wilden, A. et al.: *Solvent Extr. Ion Exch*. 33 (2) (**2015**) 91-108.
[5] Taylor, R. et al.: Procedia Chem. 21 (**2016**) 524-529.
[6] Lange, S. et al.: Solvent Extr. Ion Exch. 35 (3) (**2017**) 161-173.
[7] Vanel, V. et al.: *Procedia Chem.* 21 (2016) 190-197.
[8] Chapron, S. et al.: *Procedia Chem.* 21 (**2016**) 133-139.
[9] Sasaki, Y. et al. (2015): *Solvent Extr. Ion Exch.* 33(7) (2015) 625-641.
[10] Klaß, L.: Masterthesis, RWTH Aachen (**2016**).
[11] Iqbal, M. et al.: *Supramol. Chem.* 22(11) (**2010**) 827-837.
[12] Wilden, A. et al.: *Solvent Extr. Ion Exch*. 32(2) (2014) 119-137.
[13] Klaß, L. et al.: *Solvent Extr. Ion Exch.* (**2017**) submitted.

6.8. An advanced TALSPEAK flowsheet test for the selective separation of minor actinides

A. Wilden[1,*], G. Modolo[1], F. Sadowski[1], H. Schmidt[1], D. Schneider[1], D. Bosbach[1], G. Lumetta[2], T. Levitskaia[2], A. Casella[2], G. Hall[2], J. Law[3], A. Geist[4]

[1]Forschungszentrum Jülich GmbH, Institute of Energy and Climate Research – IEK-6: Nuclear Waste Management and Reactor Safety, 52425 Jülich, Germany

[2]Pacific Northwest National Laboratory, PO Box 999, MSIN P7-25, Richland, Washington 99352, USA

[3]Aqueous Separations and Radiochemistry Department, Idaho National Laboratory, Idaho Falls, Idaho, USA

[4]Karlsruher Institut für Technologie (KIT), Institut für Nukleare Entsorgung (INE), 76021 Karlsruhe, Germany

Corresponding author: a.wilden@fz-juelich.de

Introduction

During the last decade a large amount of research has been conducted in several countries on the separation and recovery of Americium and Curium from the high-level liquid waste (HLLW) fraction of the PUREX process. Most strategies rely on the co-extraction of trivalent actinides (*An*(III)) and lanthanides (*Ln*(III)) (e.g. TRUEX, DIAMEX), followed by an *An*(III)/*Ln*(III) group separation (e.g. TALSPEAK, SANEX).[1, 2] The last step is important because it is essential to separate americium and curium from trivalent lanthanides to avoid the strong absorption of thermalized neutrons by the lanthanides, particularly if the trivalent actinides are to be recycled as new innovative fuel within a fast reactor fuel cycle strategy. Within the European collaborative project SACSESS (Safety of Actinide Separation Processes)[3] the development of hydrometallurgical actinide separation processes was addressed[4] and a transatlantic partnership between European and US-Department of Energy (DOE) researchers was established. Within this SACSESS – DOE cooperation the experimental evaluation of an Advanced TALSPEAK process was tackled. In the Advanced TALSPEAK concept, a combined system of 2-ethylhexylphosphonic acid mono-2-ethylhexyl ester (HEH[EHP], Fig. 39) and citrate-buffered *N*-(2-hydroxyethyl)ethylenediamine-*N*,*N'*,*N'*-triacetic acid (HEDTA, Fig. 39) is used to extract trivalent lanthanides, while trivalent actinides are kept in the aqueous phase.[5] This overcomes the limitations of the preceding TALSPEAK process with regards to pH dependence and complicated lactic acid chemistry.[6] Therefore, the new Advanced TALSPEAK chemical system was developed and optimized and a flow-sheet was elaborated based on batch and single centrifugal contactor tests.[7]

In the present paper the results of a 24-stages laboratory-scale Advanced TALSPEAK demonstration test at IEK-6 for the *An*(III)/*Ln*(III) separation using a simulated feed spiked with radionuclides are presented.[8] Due to the limited availability of 16 centrifugal contactors, the extraction + scrubbing part was tested first. Table 2 shows the feed composition used for the first part. The loaded solvent was collected, stored overnight and used on the consecutive day as the feed for the stripping part (Fig. 40).

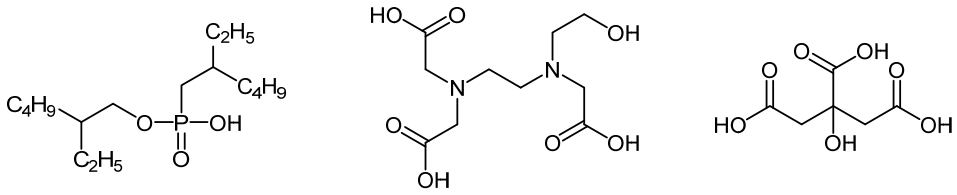

HEH[EHP]
2-ethylhexylphosphonic acid
mono-2-ethylhexyl ester

HEDTA
N-(2-hydroxyethyl)-ethylenediamine-
N,*N*′,*N*′-triacetic acid

citric acid

Fig. 39: Chemical structures of HEH[EHP] (left), HEDTA (middle), and citric acid (right).

Table 2: Composition of the Advanced TALSPEAK feed solution.

Component	Concentration	Component	Concentration	Component	Concentration
La	260.0 mg/L	Eu	39.5 mg/L	citrate	0.6 mol/L
Ce	570.2 mg/L	Gd	98.4 mg/L	HEDTA	0.125 mol/L
Pr	213.5 mg/L	^{241}Am	3.6 MBq/L	pH	2.6
Nd	1029 mg/L	^{244}Cm	3.6 MBq/L		
Sm	171.4 mg/L	^{152}Eu	10.2 MBq/L		

Results and Discussion

The Advanced TALSPEAK demonstration test was run as shown in Fig. 40 on two consecutive days. During the test samples of the effluents were taken and analyzed to follow the evolution of the steady-state. After the test the content of the mixing chambers was analyzed to measure the steady-state concentration profiles of all metal ions.

The phase separation in the centrifugal contactors was very good, as no hydrodynamic problems such as phase entrainment, precipitation or 3rd phase formation have been observed. Clean product and solvent fractions were obtained. The same applies for the loaded solvent stored overnight.

The results (Fig. 40) show that the trivalent actinides Am and Cm were nearly quantitatively routed to the aqueous *An* product fraction on the first day with an excellent selectivity towards trivalent lanthanides. The measured concentrations of *Ln*(III) in the *An* product fraction were very low (≤ 0.1%). The lanthanides were routed nearly quantitatively to the loaded solvent. On the second day of the test, the lanthanides were stripped from the loaded solvent and recovered with a high yield in the *Ln* product fraction. The recovery was very good (≥ 99.9%) and the obtained *Ln* product fraction was very clean with *An* contaminations ≤ 0.1%. The spent solvent was very clean, as ≤ 0.1% of *An* and *Ln* were found. This enables an easy recycling of the solvent, as tedious washing steps to remove remaining metal contaminations can be reduced.

The measured metal ions concentration profiles clearly showed the routing of the metal ions to the different product fractions and were in good agreement with the prediction of computer-code calculations.

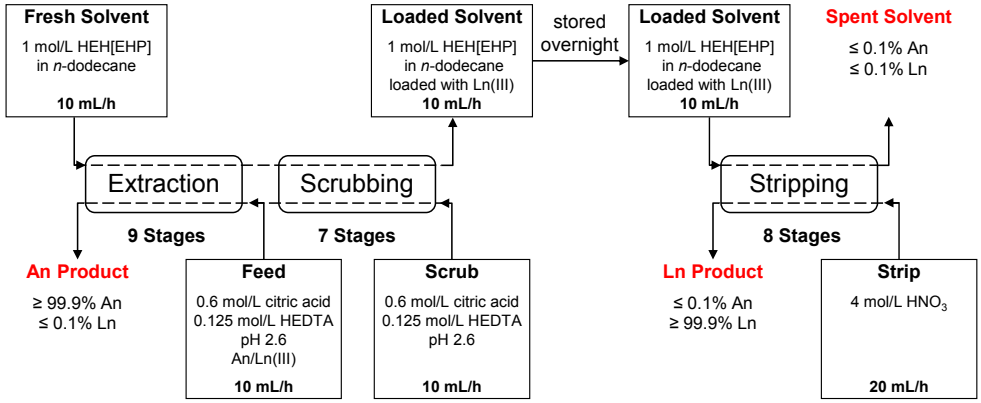

Fig. 40: Flowsheet of the Advanced TALSPEAK process demonstration test and main results.

Conclusions

The results of this spiked test were very good, as clean *An*(III) and *Ln*(III) product fractions were obtained. Very low concentrations of *Ln*(III) (≤ 0.1%) were found in the Am(III) + Cm(III) product solution, and vice versa. No hydrodynamic problems were observed during the test trials and the spent solvent was very clean enabling an easy recycling of the solvent. The experimental concentration profiles were in good agreement with the prediction of computer-code calculations.

The successful collaboration between European and US-American partners was very productive, with prospects of further collaboration on other separation systems in view of a common goal.

Acknowledgements

Financial support for this research was provided by the European Commission (project SACSESS – Contract No. FP7-Fission-2012-323-282) and the U.S. Department of Energy, Office of Nuclear Energy, through the Fuel Cycle Research and Development Program. Pacific Northwest National Laboratory is operated by Battelle Memorial Institute for the U.S. Department of Energy under contract DE-AC05-76RL01830.

References

[1] Modolo, G. et al.: Chap. 10 in Taylor, R. (ed.): Reprocessing and Recycling of Spent Nuclear Fuel. Woodhead Publishing: Oxford (**2015**) 245-287.
[2] Moyer, B.A. et al.: Chap. 11 in Taxlor, R. (ed.): Reprocessing and Recycling of Spent Nuclear Fuel. Woodhead Publishing: Oxford (**2015**) 289-312.
[3] Bourg, S. et al.: *Nukleonik*a 60(4 (Pt. II)) (**2015**) 809-814.
[4] Geist, A. et al.: *Procedia Chem.* 21 (**2016**) 218-222.
[5] Lumetta, G.J. et al.: *Solvent Extr. Ion Exch.* 33(3) (**2015**) 211-223.
[6] Nash, K.L.: *Solvent Extr. Ion Exch.* 33(1) (**2015**) 1-55.
[7] Lumetta, G.J. et al.: *Solvent Extr. Ion Exch.* 35(6) (**2017**) 377-395.
[8] Wilden, A. et al.: *Solvent Extr. Ion Exch.* 35(6) (**2017**) 396-407.

6.9. Selective separation of Am(III) from highly radioactive PUREX raffinate (HGF Milestone 2016)

P. Kaufholz[1], A. Wilden[1], G. Modolo[1,*], D. Bosbach[1], L. Harwood[2], C. Marie[3], V. Vanel[3], U. Müllich[4], P. Panak[4], A. Geist[4]

[1]Forschungszentrum Jülich GmbH, Institute of Energy and Climate Research – IEK-6: Nuclear Waste Management and Reactor Safety, 52425 Jülich, Germany

[2]Department of Chemistry, University of Reading, Whiteknights, Reading RG6 6AD, UK

[3]CEA Marcoule, Nuclear Energy Division, Radiochemistry & Processes Department, Bagnols-sur-Cèze, F-30207, France

[4]Karlsruher Institut für Technologie (KIT), Institut für Nukleare Entsorgung (INE), 76021 Karlsruhe, Germany

Corresponding author: g.modolo@fz-juelich.de

Introduction

The minor actinides (MA) Np, Am, and Cm contribute to less than 0.1% of the initial spent fuel mass, but dominate the long-term radiotoxicity and heat load of the residual high active waste (e.g., vitrified waste) after recycling uranium and plutonium using the PUREX process.[1] Within the European collaborative project SACSESS (Safety of Actinide Separation Processes) the development of a hydrometallurgical actinide separation process was addressed to separate only trivalent americium from the PUREX high active raffinate.[1] This improves the safety of the fuel cycle by avoiding the presence of curium in the fuel fabrication. Furthermore, the impact of Cm with regard to final repository long-term heat-load is limited, as the major curium isotope ^{244}Cm has a half-life of only 18 years. However, the separation of Am(III) from Cm(III) by solvent extraction techniques is a very difficult task due to their chemical similarity and only a few processes have demonstrated a successful separation, mainly based on a multi-cycle approach.[2-4] Recently, a trend can be observed for the reduction of required processes and the increased interest in potentially simpler single-cycle processes, although a more complicated chemistry and process control might be necessary.[2, 5]

The most promising systems for Am(III)/Cm(III) separation already identified in the previous European projects (EUROPART[6], ACSEPT[7]) were adapted to meet the requirements of a selective americium separation process. This paper summarizes the optimization work to design a flowsheet in preparation for demonstration tests in Jülich. This work was undertaken in a 3 year-collaboration between CEA, NNL, KIT and Jülich teams.

Results and Discussion

The first option for selective Am(III) separation is based on the 1-cycle SANEX process developed in Jülich,[8] and the French EXAm process[9]. A novel combination of the lipophilic extractant $CyMe_4BTPhen$ (2,9-bis(5,5,8,8-tetramethyl-5,6,7,8-tetrahydrobenzo[e]-[1,2,4]triazin-3-yl)-1,10-phenanthroline, Fig. 41) and the hydrophilic complexant TEDGA (*N,N,N',N'*-tetraethyl-diglycolamide, Fig. 41) was used to enhance the selectivity towards Am(III) extraction. $CyMe_4BTPhen$ shows a slight preference for the extraction of Am(III), while TEDGA shows a slight preference for the complexation of Cm(III) in the aqueous phase.

Therefore, a synergistic effect for the combination of $CyMe_4BTPhen$ and TEDGA was achieved. Within an acidity range of 0.5 – 1 mol/L HNO_3, conditions were found with rather high Am(III)/Cm(III) separation factors of 3.5 and appropriate Am(III) and Cm(III) distribution ratios ($D_{Am} > 1$ and $D_{Cm} < 1$).

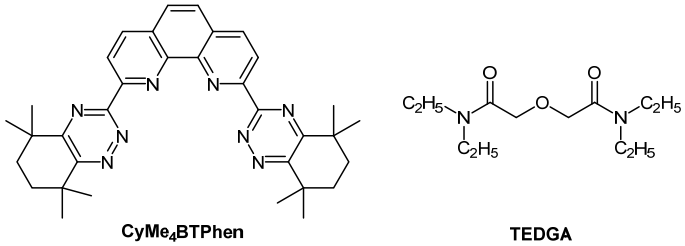

Fig. 41: Chemical structure of $CyMe_4BTPhen$ and TEDGA.

The second option is based on the innovative-SANEX process recently demonstrated at Forschungszentrum Jülich.[10] The innovative-SANEX process follows the concept of an An(III) + *Ln*(III) co-extraction using TODGA in a mixture of TPH containing 5 vol.% 1-octanol. After scrubbing some undesired co-extracted fission products, the trivalent actinides (Am, Cm) are selectively stripped using a water-soluble tetra sulfonated BTP (SO_3-Ph-BTP).[10-12] The remaining *Ln*(III) are then stripped using a buffer solution. The co-extraction and scrubbing steps of the innovative SANEX process were taken as the basis for this study. The actinide-selective stripping of the innovative SANEX process is changed to an americium(III) selective stripping step using Am(III) selective hydrophilic complexants. By combination of the lipophilic TODGA, which preferably extracts Cm(III), and hydrophilic complexants with a preference for Am(III), an americium selective process where Am(III) is separated from Cm(III) can be achieved. Fig. 42 shows the different hydrophilic complexants which showed very promising results.

The water soluble ligand H_4TPAEN (*N,N,N′,N′*-tetrakis[(6-carboxypyridin-2-yl)methyl]-ethylenediamine) was developed at CEA.[13] Used in combination with TODGA in the organic phase, H_4TPAEN shows a quite high Cm(III)/Am(III) selectivity ($SF_{Cm/Am}$ = 3.6 at 0.1 mol/L HNO_3),[14] which allows to selectively strip Am(III) while Cm(III) and *Ln*(III) remain extracted in the organic phase.[15] Additional batch data were acquired to evaluate best conditions to develop a liquid-liquid separation flowsheet with this promising TODGA/H_4TPAEN system.

TS-BTPhen (3,3‘,3‘‘,3‘‘‘-[3-(1,10-phenanthroline-2,9-diyl)-1,2,4-triazine-5,5,6,6-tetrayl]tetra-benzenesulfonic acid[16]) and SO_3-Ph-BTBP (6,6’-bis(5,6-di(sulfophenyl)-1,2,4-triazin-3-yl)-2,2’-bipyridine[17]) are complexants which were derived from the successful lipophilic extractants $CyMe_4BTPhen$ and $CyMe_4BTBP$, by introduction of sulfophenyl groups. Both extractants showed a preference for Am(III) extraction. Therefore, they were chosen as possible hydrophilic Am(III) complexants in the aqueous phase. This concept was successfully proven by the synthesis and testing of TS-BTPhen at Reading University/Jülich and SO_3-Ph-BTBP at KIT-INE. Both complexants showed increased Cm(III)/Am(III) selectivity in combination with TODGA with separation factors of 2.5 – 3.3.

These systems are currently studied for a new Am(III)-only extraction process.

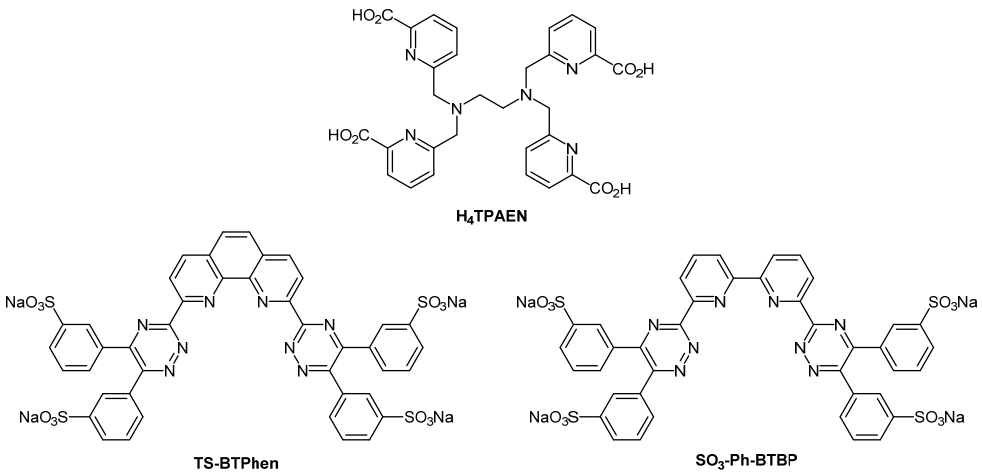

Fig. 42: Chemical structures of H_4TPAEN, TS-BTPhen, and SO_3-Ph-BTBP.

Conclusions

Several promising chemical systems were tested towards their selectivity for Am(III) separation from PUREX raffinate. Some of these systems were already defined in the ACSEPT project and were further tested for Am(III)/Cm(III) separation studies, others were developed during the SACSESS project.

In the first option, based on the 1-cycle SANEX process developed in Jülich and the French EXAm process, an Am(III)-selective extraction based on the lipophilic $CyMe_4$BTPhen extractant was proposed. Within an acidity range of 0.5 – 1 mol/L HNO_3 applicable conditions were found with rather high Am(III)/Cm(III) separation factors of 3.5.

The second option is based on the co-extraction of *An*(III) and *Ln*(III) by a TODGA based solvent in the innovative-SANEX process and a consecutive Am(III) selective stripping step using hydrophilic ligands. Several hydrophilic ligands were tested and very promising results were obtained with the H_4TPAEN, TS-BTPhen and SO_3-Ph-BTBP ligands. High Cm(III)/Am(III) separation factors of up to 3.6 were observed. The information generated to date and described in this report is currently used to further improve Am(III) alone separation studies. The most promising system with regards to hydrodynamics, kinetics, robustness, selectivity and recovery of Am(III) will be demonstrated on the laboratory scale using centrifugal contactors.

Acknowledgements

Financial support for this research was provided by the European Commission (project SACSESS – Contract No. FP7-Fission-2012-323-282).

References

[1] Geist, A. et al.: *Procedia Chem.* 21 (**2016**) 218-222.
[2] Modolo, G. et al.: Chap. 10 in Taylor, R. (ed.): Reprocessing and Recycling of Spent Nuclear Fuel. Woodhead Publishing: Oxford (**2015**) pp. 245-287.
[3] Glatz, J.-P. et al.: Chap. 3 in Taylor, R. (ed.): Reprocessing and Recycling of Spent Nuclear Fuel. Woodhead Publishing: Oxford (**2015**) pp. 49-62.
[4] Veliscek-Carolan, J.: *J. Hazard. Mater.* 318 (**2016**) 266-281.

[5] Modolo, G. et al.: *Radiochim. Acta* 100(8-9) (**2012**) 715-725.
[6] Madic, C. et al.: *Radiochim. Acta* 96(4-5) (**2008**) 183-185.
[7] Bourg, S. et al.: *Nucl. Eng. Des*. 241(9) (**2011**) 3427-3435.
[8] Wilden, A. et al.: *Solvent Extr. Ion Exch.* 31(5) (**2013**) 519-537.
[9] Rostaing, C. et al.: *Proc. Chem.* 7 (**2012**) 367-373.
[10] Wilden, A. et al.: *Solvent Extr. Ion Exch*. 33(2) (**2015**) 91-108.
[11] Modolo, G. et al.*: Progr. Nucl. Energ*. 72 (**2014**) 107-114.
[12] Magnusson, D. et al.: *Proc. Chem*. 7 (**2012**) 245-250.
[13] Borrini, J. et al.: *Solvent Extr. Ion Exch*. 33(3) (**2014**) 224-235.
[14] Heres, X. et al.: Patent (**2012**) FR2968014.
[15] Heres, X. et al. Increase in the separation factor between americium and curium and/or between lanthanides in a liquid-liquid extraction process. WO2011012579A1.
[16] Lewis, F.W. et al.: *Synlett* 27(1) (**2016**) 1-5.
[17] Müllich, U. et al.: Water-soluble bis-triazinyl-pyridines, bipyridines and terpyridines, synthesis and use of same. EP2377861, 2011-10-19.

6.10. Radiolysis studies of important solvent extraction systems

H. Schmidt[1], A. Wilden[1], G. Modolo[1,*], D. Bosbach[1], B. Santiago-Schübel[2], M. Hupert[2], J. Švehla[3], B. Grüner[3], C. Ekberg[4], B. Mincher[5], C. Zarzana[5], S. Mezyk[6], H. Galán[7]

[1]Forschungszentrum Jülich GmbH, Institute of Energy and Climate Research – IEK-6: Nuclear Waste Management and Reactor Safety, 52425 Jülich, Germany

[2]Forschungszentrum Jülich GmbH, Central Institute for Engineering, Analytics (ZEA-3), 52425 Jülich, Germany

[3]Institute of Inorganic Chemistry, Academy of Sciences, Hlavni 1001, 25068 Husinec-Rež, Czech Republic

[4]Department of Chemical and Biochemical Engineering, Chalmers University of Technology, 41296 Gothenburg, Sweden

[5]Idaho National Laboratory, Idaho Falls, USA

[6]California State University at Long Beach, Long Beach, CA 90840 USA

[7]Centro de Investigaciones Energéticas, Medioambientales y Tecnológicas (CIEMAT), Madrid 28040, Spain

Corresponding author: g.modolo@fz-juelich.de

Introduction

The radiolytic stability of organic molecules used in solvent extraction processes for the separation of radioactive elements is of major concern, as the radiolytic degradation changes the properties of solvents which have to be accounted for and potentially produces hazardous or dangerous reaction products. Therefore, the stability of the currently most widely studied ligand classes (Fig. 43) towards radiolysis was studied in the EU project SACSESS in collaboration with partners from US-DOE, which were associated partners in SACSESS, and the German federal ministry of education and research funded project “f-kom”.

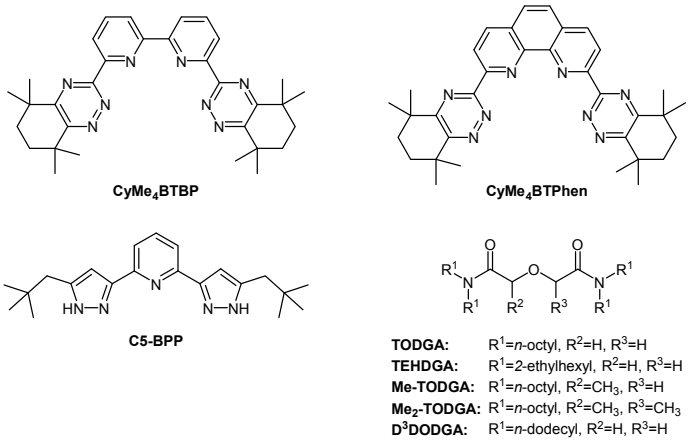

Fig. 43: Chemical structures of the extractants described in this paper.

N-Donor ligands of the BTBP, BTPhen and BPP classes show a very high selectivity towards trivalent actinides and are preferred candidates for future processes for the separation of minor actinides.[1-5] Diglycolamides on the other hands show a very high affinity for trivalent actinides and lanthanides and are therefore also studied worldwide for a potential application in separation processes.[6-9]

Results and Discussion

Within our research in collaboration with multinational international partners, the degradation mechanism of the radiolytic degradation of different N-Donor extractants and diglycolamides was elucidated. In general, an indirect radiolysis was found, i.e. the reaction of the extractants with highly reactive degradation products of the diluent. This effect is often referred to as the sensitization effect.[10] As different diluents were used, namely 1-octanol in the case of N-Donor extractants and aliphatic hydrocarbons (e.g. TPH, dodecane) in the case of diglycolamides, different reaction patterns were found.
The major reactive species formed by radiolysis of 1-octanol is the α-hydroxyoctyl radical.

$$RCH_2OH + \gamma \rightarrow \left[RCH_2OH\right]^{*} \rightarrow e^{-}_{solv} + \left[RCH_2OH\right]^{\bullet +} \rightarrow e^{-}_{solv} + \left[RCH_2OH\right]^{\bullet} + H^{+} \qquad (1)$$

We found that this radical adds to the backbone structure of the N-Donor extractants yielding addition products with higher masses than the parent molecules. This was proven by high-resolution and coupled mass spectrometric analytical methods, both qualitatively and quantitatively.

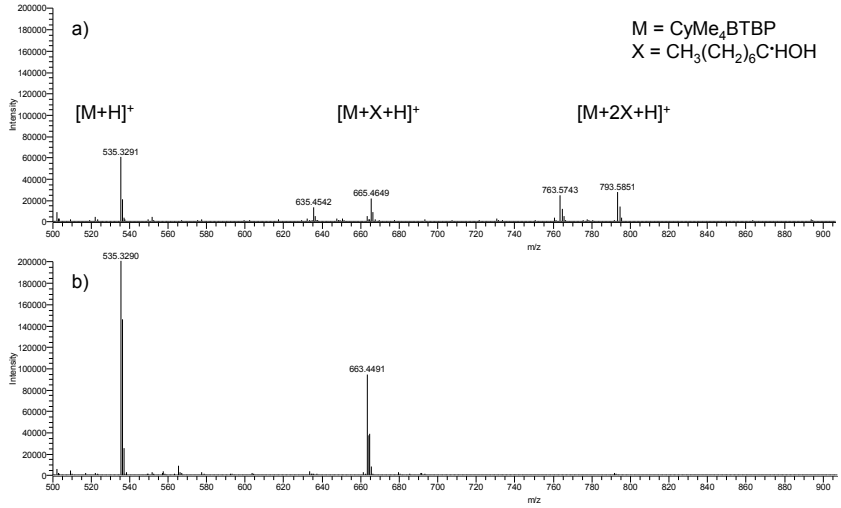

Fig. 44: CyMe$_4$BTBP irradiated without (a) and in contact (b) with 1 mol/L HNO$_3$ to an absorbed dose of 100 kGy.

In solvent extraction experiments we found that the distribution ratios generally decrease with increasing absorbed dose, but the reduction in distribution ratios is smaller than expected, taking into account the remaining concentration of extractant in solution and the extraction mechanism (Fig. 44). This finding combined with the discovery of the formation of addition products with the α-hydroxyoctyl radical let us conclude that the addition products are partly also capable of extracting the desired metal ions. Additionally, we encountered a protective effect of the addition of a nitric acid containing aqueous phase during irradiation (which is always the case in realistic scenarios), resulting in a relatively high durability of these N-Donor extractants under irradiation.[11, 12]

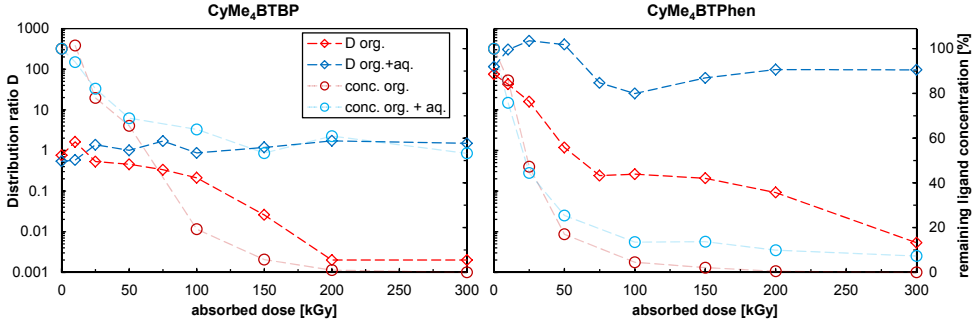

Fig. 45: Americium distribution ratios (left y-axis) for the extraction with irradiated solvents of CyMe$_4$BTBP (left diagram) and CyMe$_4$BTPhen (right diagram) and remaining ligand concentration (right y-axis) as a function of the absorbed dose.

The diglycolamides on the other hand didn't form addition products with diluent radicals. With all examples studied yet (see Fig. 45) a fragmentation of the parent molecules was found. Through qualitative and quantitative mass spectrometric analysis, the degradation paths

were clarified and the reaction rate (i.e. dose) constants were derived for irradiation without and in contact with an aqueous phase (Table 3). Here, in contrast to the N-Donor extractants, no protective effect of the addition of an aqueous phase was found.

Table 3: Dose constants for the degradation of different diglycolamides (10^{-3} kGy^{-1}).

DGA (see Fig. 43)	org. phase only	org. + aq. phase
TODGA[13]	4.1 ± 0.3	4.5 ± 0.2
TEHDGA[13]	4.3 ± 0.3	3.7 ± 0.2
Me-TODGA[14]	5.0 ± 0.3	5.8 ± 0.4
Me_2-TODGA[14]	3.0 ± 0.2	5.3 ± 0.4
D^3DODGA[15]	4.1 ± 0.3	3.4 ± 0.4

Conclusions

Within the EU project SACSESS the most important extractant classes were evaluated regarding their radiolytic stability. A very fruitful collaboration between the European partners and the partners from US-DOE was established. A major difference in the radiolytic stability of different extractants was found, as the diglycolamides decompose under irradiation and form smaller degradation fragments, while the highly selective N-Donor ligands form heavier addition products with radicals formed from diluent radiolysis. The main degradation compounds for both extractant classes were identified and the main degradation paths were clarified using qualitative and quantitative analysis. These findings contribute significantly to an enhanced understanding of the fundamental processes taking place during radiolysis and to a greater safety of processes using these extractants.

Acknowledgements

Financial support for this research was provided by the European Commission (project SACSESS—Contract No. FP7-FISSION-2012-323282), the German Federal Ministry of Education and Research (Contract No. 02NUK020E), the US Department of Energy, Assistant Secretary for Nuclear Energy, under the Fuel Cycle R&D Program, Idaho Operations Office Contract DE-AC07-05ID14517, and Office of Science, Division of Chemical Sciences, Geosciences and Biosciences under contract DE-AC02-98CH10886.

References

[1] Magnusson, D. et al.: *Solvent Extr. Ion Exch.* 27(2) (**2009**) 97-106.
[2] Lewis, F.W. et al.: *J. Am. Chem. Soc.* 133(33) (**2011**) 13093-13102.
[3] Wilden, A. et al.: *Solvent Extr. Ion Exch.* 31(5) (**2013**) 519-537.
[4] Panak, P.J. et al.: *Chem. Rev.* 113(2) (**2013**) 1199-1236.
[5] Wilden, A. et al.: *Separ. Sci. Technol.* 50(16) (**2015**) 2467-2475.
[6] Ansari, S.A. et al.: *Chem. Rev.* 112(3) (**2012**) 1751-1772.
[7] Wilden, A. et al.: *Solvent Extr. Ion Exch.* 32(2) (**2014**) 119-137.
[8] Wilden, A. et al.: *Solvent Extr. Ion Exch.* 33(2) (**2015**) 91-108.
[9] Taylor, R. et al.: *Procedia Chem.* 21 (**2016**) 524-529.
[10] Sugo, Y. et al.: *Radiochim. Acta* 90(3) (**2002**) 161-165.
[11] Schmidt, H. et al.: *Procedia Chem.* 21 (**2016**) 32-37.
[12] Wilden, A. et al.: *Solvent Extr. Ion Exch.* 34(1) (**2016**) 1-12.
[13] Zarzana, C.A. et al.: *Solvent Extr. Ion Exch.* 33 (5) (**2015**) 431-447.
[14] Galán, H. et al.: *Dalton Trans.* 44(41) (**2015**) 18049-18056.
[15] Roscioli-Johnson, K.M. et al.: *Solvent Extr. Ion Exch.* 34(5) (**2016**) 439-453.

6.11. Stabilization of defect fluorite phase in UO_2-$NdO_{1.5}$ system

A. Bukaemskiy[1], C. Schreinemachers[1,2], G. Modolo[1], D. Bosbach[1]

[1]Forschungszentrum Jülich GmbH, Institute of Energy and Climate Research – IEK-6: Nuclear Waste Management and Reactor Safety, 52425 Jülich, Germany

[2]Belgian Nuclear Research Centre (SCK·CEN), Institute for Nuclear Materials Science, Boeretang 200, B-2400 Mol, Belgium

Corresponding author: a.bukaemskiy@fz-juelich.de

Introduction

Spent UO_2-based fuel contains various fission products (FP), whereas some of them (e.g. Zr, Sr, and lanthanides) are soluble in the crystal structure of UO_2.[1] According Carbol et al.[2] it is estimated that 30% of the FP forms solid solutions with the UO_2 matrix. The chemical and mechanical characteristics of this solid solution may differ significantly from the properties of the original fuel and as a consequence lead to a change in the crystalline structure of the material. Hence, understanding the processes of formation and stabilization of solid solutions and their characterization is important for predicting the behaviour of spent fuel during geological repository environment. The lanthanide element neodymium (Nd) is generated with a high fission yield and belongs therefore to the major fission products.[1-3] In this work we studied the influence of synthesis methods and following heat treatment on the crystallographic characteristics of sintered ceramics. Moreover, a study of the UO_2-$NdO_{1.5}$ system is of considerable interest in the development of new types of fuels based on uranium and minor actinides.[4] In this case neodymium can be used as a surrogate for trivalent actinides such as americium. UO_2 - Nd_2O_3 particles with a mole fraction of neodymium from 0 to 0.43 were synthesized by the sol-gel method via internal gelation. The synthesis method, some particles characteristics and used research methods are described partially in [5, 6].

Results and discussion

All studied powders are single phase materials and crystallized in a face-centred cubic (fcc), fluorite-type structure. Our and reference experimental data[7-9] of the lattice parameter, depending on the neodymium content are shown in Fig. 46. Evidently, these data cannot be described by a single universal relationship. Independently, the results of different authors are well-described by a linear type dependence (Vegard`s law):

$$\boldsymbol{a = Ax + B} \qquad (1)$$

where *A* and *B* are empirical coefficients, $\boldsymbol{x}$ is the mole fraction of Nd in the UO_2 matrix. Lattice parameter for pure UO_2 was calculated as the average value for our and literature data and is equal to 5.4701 Å. The values of $\boldsymbol{A}$ equal -0.0615, -0.0521 and -0.0451 for [7, 8], [9] and our data, respectively. The significant variation of the lattice parameter data derived from experiments might be explained by different synthesis methods. The techniques used are summarized in Table 4.

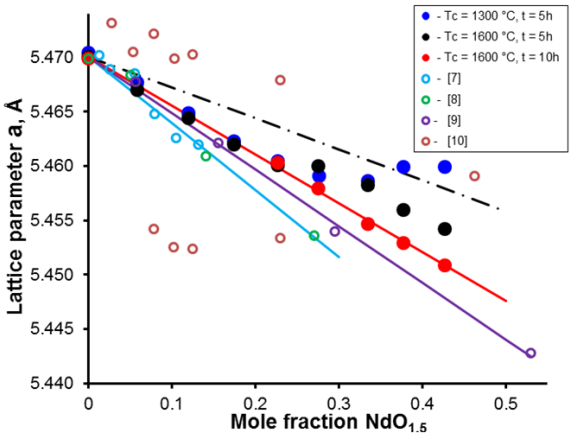

Fig. 46: Lattice parameter *a* as function of the Nd mole fraction in UO_2 matrix.

The synthesis method mainly determines important material characteristics such as the region of homogeneity of the components (oxide or hydroxide metals). In the case of solid state reaction method (SSR), the region of homogeneity is equal to the size of the initial oxide particles (~10 μm), and for modified direct denitration process (MMD) and Sol-Gel methods, it is equal to the size of the primary particles (~10 nm). Moreover, the SSR powder can be occasionally stabilized in two defect fluorite (DF) phases even after high temperature [7] and long-term annealing [10]. Apparently, the small size of the homogeneity regions contributes to a more successful formation of the equilibrium solid solution.

Table 4: Applied synthesis techniques, as well as thermal treatment conditions (calcined temperature (Tc), duration (t), atmosphere) and resulting phases.

Authors	Method	Tc, t	Atmosphere	Phase
[7]	SSR	1800 ºC (4 h)	H_2	2 phases
[8]	SSR	1700 ºC (2 h)	H_2	1 phases
[9]	MDD	1600 ºC (5 h)	H_2/Ar (4:96)	1 phases
[10]	SSR	1400 ºC (72 h)	H_2/Ar (5:95)	2 phases
This work	Sol-Gel	1600 ºC (5 and 10 h)	H_2/Ar (4:96)	1 phases

*SSR – solid state reaction; MDD – modified direct denitration process.

All studied powders are single phase; however, the crystallinity degree of the material strongly depends on the conditions of heat treatment (Tc and the duration of the annealing).
For Ndc ontents up to 0.25, all studied powders are characterized by narrow XRD reflexes and zero level of microdeformation (***ε***), see Fig. 47. For the fixed composition the values of lattice parameter differ within the experimental error (Fig. 46). Moreover, the lattice parameter has a linear relationship with the Nd content up to 0.25. The same relationship was obtained for powders with higher Nd contents annealed at 1600 ºC for 10 h. These powders are also characterized by a zero level of microdeformation, see Fig. 47.
Contrarily, the powders with the Nd contents higher than 0.25 calcined for 5 hours at 1300 ºC and at 1600 ºC are characterized by broad XRD reflexes and rather high levels of microdeformation (***ε***). Additionally, the lattice parameters of these materials annealed at 1300 ºC for 5 h or 1600 ºC for 5 h differ significantly from the corresponding values of the powders annealed for 10 hours at 1600 ºC, Fig. 46.

The observed deviation of the lattice parameter from Vegard`s law for the powders annealed at 1300 ºC for 5 h and 1600 ºC for 5 h correlates well with the dependence of lattice distortion on the Nd content ***ε(x)***, Fig. 47. This allows assuming that the deviation of the lattice parameter at high Nd contents is a consequence of a insufficient crystallization and the presence of residual stresses in the material. Longer annealing at 1600 ºC (10 h) leads to their relaxation and finally as a result to the observed decrease of the lattice parameter.

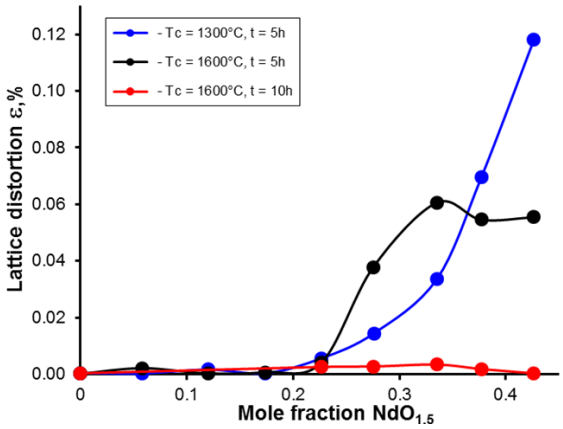

Fig. 47: Lattice distortion (*ε*) as function of the Nd mole fraction in UO_2 matrix.

Apparently, the experimentally measured lattice distortion *ε* and the derived lattice parameter can be used as an important indicator, which characterizes the stability of the crystalline phase. It turns out that the phase can be considered as equilibrated when (i) the level of microdeformation of the crystal lattice is minimized (*ε* ~ 0) and (ii) the dependence of the lattice parameter from the additive content is linear (Vegard`s law) with the R^2 value close to one.

Finally, for all studied powders with ***ε*** ~ 0 the refined linear dependence (1) is described well using:

$$a, \text{Å} = -0.0540x + 5.4701 \qquad R^2 = 0.998 \tag{2}$$

The description of the crystal structure of the fluorite phases traditionally uses ion-packing models. Adding trivalent cations to the system determines the necessity of charge compensation which can be realized by formation of vacancies, or due to changes in the valence state of uranium from U^{+IV} to U^{+V} [11,7]. In accordance with these models, the dependence ***a = a(x)*** can be written as:

$$a = \frac{4}{\sqrt{3}}\left(r_{U^{4+}} + r_{O^{2-}}\right) + x\frac{4}{\sqrt{3}}\left(r_{Nd^{3+}} - r_{U^{4+}} - 0.25r_{O^{2-}} + 0.25r_{V}\right) \tag{3}$$

$$a = \frac{4}{\sqrt{3}}\left(r_{U^{4+}} + r_{O^{2-}}\right) + x\frac{4}{\sqrt{3}}\left(r_{Nd^{3+}} - 2r_{U^{4+}} + r_{U^{5+}}\right) \tag{4}$$

The values of ionic radii of uranium, neodymium and oxygen ions ($r_{U^{4+}}$, $r_{U^{5+}}$, $r_{Nd^{3+}}$, $r_{O^{2-}}$) were taken from [12, 7]. The value of vacancy radius (r_V) is an adjustable parameter, which was determined from the value of slope (***A***) presented in equations (1, 3).

$$r_V = A\sqrt{3} - 4r_{Nd^{3+}} + 4r_{U^{4+}} + r_{O^{2-}} \quad (5)$$

Both models predict linear dependence of the lattice parameter from the Nd content. The results are inserted in Fig. 1 (black dotted line – U^{+IV}-U^{V+}-model, coloured solid lines – vacancies model).

Obviously, the ***a(x***) dependence is overestimated using the U^{+IV}-U^{+V} model. The vacancies model instead describes well the experimental results. The vacancies radii are equal to 0.828 Å[7,8], 0.844 Å[9] and 0.857 Å [this work]. Taking into account that the accuracy of the determined cationic radii is approximately 0.01 Å[12], it can be assumed that the variation of r_V is small (±0.014 Å) and the vacancies model describes well the experimental data. However, these values are significantly below the values obtained for similar Ce- and Th-based systems, r_V =1.13 Å and 1.15 Å, respectively[13] although the values of cationic radii for these metal ions are close (0.97 Å, 1.00 Å and 1.05 Å for Ce, U and Th cations respectively). Therefore, the application of the vacancies model for the U-based systems is problematic. Apparently, using a mixed model (vacancies and U^{+IV}-U^{+V}) is more appropriate, but requires an experimental determination of several independent parameters – vacancies radius, their contents and distribution in crystal lattice.

Conclusion

The investigation of the UO_2-$NdO_{1.5}$ system is of considerable interest for research on U-based spent fuel and in the development of advanced fuels based on uranium and actinides (neodymium is a surrogate for trivalent actinides). In the present work the influence of synthesis methods and following heat treatment on the properties of sintered ceramics were investigated. The crystallization processes of the material and the formation of equlibrated solid solutions were studied and suitable criteria for phase stabilization proposed. Possible models of the crystal lattice description are considered.

Acknowledgements

This work was financially supported by the European Atomic Community`s 7th Framework Programme, project ASGARD – EC-GA; grant no.: 295825.

References

[1] Kleykamp, H.: *J. Nucl. Mater.* 131 (2-3) (**1985**) 221-246.
[2] Carbol, P. et al.: Spent Fuel as Waste Material. *Elsevier Ltd. (***2012**) 389-420.
[3] Olander D.: *J. Nucl. Mater.* 389 (1) (**2009**) 1-22.
[4] Vespa, M. et al.: *J. Nucl. Mater.* 421 (**2012**) 80-88.
[5] Schreinemachers, C. et al..: Prog. Nucl. Energy 72 (**2014**) 17-21.
[6] Schreinemachers, C.: Master Thesis. *FH Aachen Campus Juelich.* (**2013**).
[7] Ohmichi, T. et al.: *J. Nucl. Mater.* 102 (**1981**) 40-46.
[8] Wadier, J.F.: *CEA-R-4507* (**1973**).
[9] Lee, S.M..: *Nucl. Tech.* 193 (**2016**) 287-296.
[10] Dottavo, G.: *J. Nucl. Mater.* 458 (**2015**) 394-405.
[11] Ho, S.M.: *Nucl. Tech. 73* (**1986**) 350-360.
[12] Shannon, R.D.: *Acta Cryst. A32.* (**1976**) 751-767.
[13] Marrocchelli, D.: *J. Mater. Chem. A.* 1 (**2013**) 7673-7680.

6.12. Dissolution behaviour of inert matrix fuel

E.L. Mühr-Ebert[1], M. Cheng[2,3], M. Steppert[2]. A. Geist[3], C. Walther[2], D. Bosbach[1], G. Modolo[1]

[1]Forschungszentrum Jülich GmbH, Institute of Energy and Climate Research – IEK-6: Nuclear Waste Management and Reactor Safety, 52425 Jülich, Germany

[2]Leibniz University Hannover, Institute for Radioecology and Radiation Protection, Herrenhäuser Str. 2, 30419 Hannover – Germany

[3]Karlsruhe Institute of Technology, Institute for Nuclear Waste Disposal, Hermann-von-Helmholtz-Platz 1, 76344 Eggenstein-Leopoldshafen – Germany

Corresponding author: g.modolo@fz-juelich.de

Introduction

The oxide dissolution and separation strategy is a fairly mature process being dealt with and optimised in the European SACSESS[1] project. New separation strategies have been tested on genuine spent fuel and the selected processes will be evaluated for industrial implementation. Whereas the above is valid for actinide oxide fuel, such as MO_X and/or Minor Actinide containing MO_X, the dissolution and separation issues for inert matrix fuel containing ceramic MgO (CerCer) or metallic molybdenum (CerMet), has not been investigated coherently. The ASGARD[2,3] project focuses therefore mainly on the Inert Matrix Fuel (IMF) with molybdenum or magnesium oxide where, except for the manufacturing, the handling of the inert component could be of a major concern in a recycling process. In the case of the MgO based fuel there is a need for removal of the bulk Mg to prevent it entering the final vitrification and in the case of Mo based fuel the recovery of the isotopic enriched faction is important.[4] This paper summarizes the work on the CerMet fuel. This work was undertaken in a 3 year-collaboration between Jülich, KIT and Leibniz University Hannover.

Fabrication and dissolution CerMet Fuel

In the case of CerMet fuel, it is of crucial importance to take into account the behaviour of the matrix elements in the dissolution and separation processes and to check their compatibility with future immobilisation methods; impact on the stability of the waste and amount of generated waste. Two types of fresh un-irradiated fuel (0, 5, 10, 25 and 40 wt.% of CeO_2, PuO_2 resp.) in molybdenum matrix have been fabricated by powder metallurgy method and fully characterized. All pellets were prepared in the same way and were sintered at 1600ºC; the bulk density (measured by immersion methods) was around 90% of the theoretical density. The actinides oxides were quite well distributed in the molybdenum matrix.

Dissolution experiments on pure Mo pellets revealed that the dissolution velocity increases with temperature and nitric acid concentration, but so does the fraction of molybdenum which precipitates. Therefore, mild conditions (1 mol/L HNO_3, RT) are considered optimal for the dissolution of Mo. Moreover, the addition of 1 mol/L ferric nitrate to the acid can prevent precipitation at low nitric acid concentrations and accelerate the dissolution. However, it is unclear whether adding such an amount of Fe^{3+} to the dissolver solution could influence the subsequent extraction process.[5] Dissolution experiments on mixed Mo/CeO_2 pellets have been performed in 20 and 100 mL 1 mol/L HNO_3 without Fe(III) or containing 1 equivalent of Fe(III) per equivalent of Mo at room temperature. Fig. 48 compares the initial dissolution rates of molybdenum and cerium from mixed Mo/CeO_2 (60/40wt.%) pellets in the different dissolver solutions. The dissolution rate of molybdenum is higher in 20 mL compared to

100 mL acid and also increases in the presence of iron. The initial dissolution rate of cerium is barely influenced by the composition of the dissolver solution. In all cases the solutions in equilibrium (prior to the molybdenum precipitation) contain about 1 mmol cerium and 7 mmol molybdenum. The difference in dissolution rate of molybdenum in 20 and 100 mL is caused by the dissolution mechanism of Mo in nitric acid. Metals (e.g. Cu, Fe, Ni, Zn, Co) are known to dissolve in nitric acid according to an autocatalytic mechanism involving the formation of nitrous acid. The first step is considered to be rate determining for the dissolution; a slow induction period followed by a more rapid dissolution was observed. The first step plays an important role in the initial formation of HNO_2 by reduction of the absorbed HNO_3 on the metal surface.

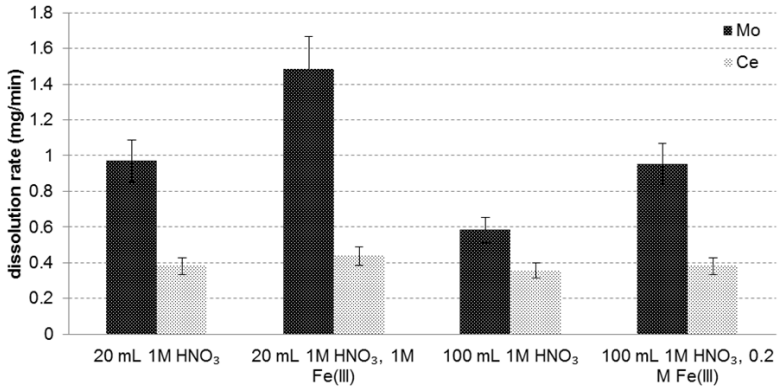

Fig. 48: Comparison of dissolution rates (mg/min) of molybdenum and cerium from mixed Mo/CeO_2 (60/40wt.%) pellets in 20 and 100 mL 1 mol/L HNO_3 without Fe(III) or containing 1 equivalent of Fe(III) per equivalent of Mo at room temperature.

The setup dissolution conditions have been applied for the dissolution study of actinides fresh fuel, pellets with PuO_2 shares of 5, 25, and 40 wt.% were dissolved in 100 mL solution. The dissolution media were 1 and 3 mol/L HNO_3 and 1 mol/L HNO_3/0.2 mol/L $Fe(NO_3)_3$. All dissolution experiments were performed at room temperature. The concentrations of Mo and Pu in the solution are determined by ICP-MS, and ^{241}Am by γ-counting. The dissolution velocity of molybdenum is similar for all pellet compositions, whereas the dissolution of plutonium is significantly faster for the pellet with the highest plutonium content. However, after about two weeks none of the pellets is dissolved completely. The concentration of molybdenum in the solution is about three orders of magnitude higher compared to plutonium. The measurement of samples is still underway. At the end of the experiments a black powder, which is expected to be PuO_2, remains as a residue and will be subject to SEM and XRD investigations.

The dissolution of molybdenum and plutonium from mixed Mo/PuO_2 pellets with 40% plutonium content in 1 mol/L HNO_3 containing 0.2 mol/L $Fe(NO_3)_3$ or 3 mol/L HNO_3 at room temperature is depicted in Fig. 49 as a function of time. The concentrations of Mo and Pu in 1 mol/L HNO_3/0.2 mol/L differ by three orders of magnitude as described above, whereas the concentrations of Mo and Pu are similar in 3 mol/L HNO_3. The overall initial dissolution is faster in 1 mol/L HNO_3/0.2 mol/L $Fe(NO_3)_3$. However, after about 24 h the Mo concentrations align, but the amount of dissolved Pu is significantly higher in 3 mol/L HNO_3. The same trends apply to the other pellet compositions.

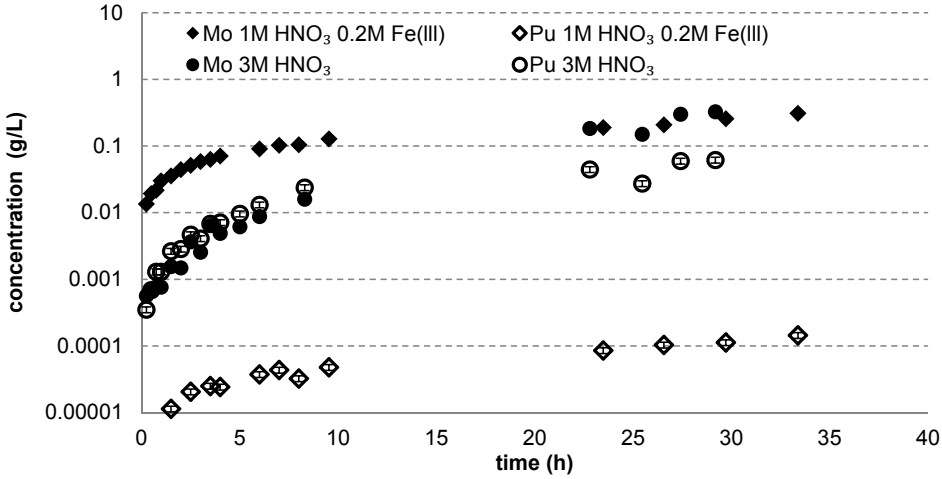

Fig. 49: Dissolution of molybdenum and plutonium from mixed Mo/PuO_2 pellets (0.8 g) with 40% plutonium share in 100 mL 1 mol/L HNO_3 containing 0.2 mol/L $Fe(NO_3)_3$ or 3 mol/L HNO_3 at room temperature.

Aqueous reprocessing of molybdenum

The dissolution behaviour of molybdenum has been comprehensively investigated by means of ESI-MS. The investigation of the kinetics of a pure ^{98}Mo-pellet dissolution was successfully performed. The Mo solution was measured by ESI-MS after 3, 5, 6, 10 days and 6 months, correlated to different Mo concentrations (Fig. 50). The concentration of ^{98}Mo in nitric acid increased with time, after 10 days the pellet was completely dissolved. The mass spectrum of the solution shows that after three days there are no large oligomers present in solution. The oligomer size and the concentration of larger oligomers increases with increasing concentrations of Mo in the nitric acid (and with time), leading to a more complicated system. The resulting system with many different species present in solution might affect reprocessing steps, as each species might behave differently for instance in liquid-liquid extraction steps. The investigation was performed in 1 mol/L nitric acid. Together with our previous investigations, we can deduce that higher acidic strengths are favourable, as this causes a less complicated species distribution. Furthermore, the Mo species tend to grow to larger species over time.

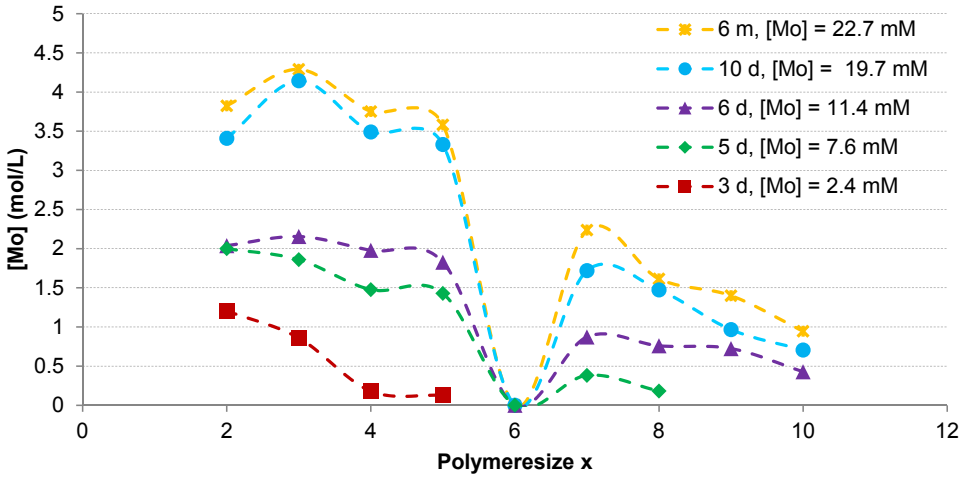

Fig. 50: Relative abundance of species in ^{98}Mo pellet dissolved solution in 3 days, 5 days, 6 days, 10 days and 6 months.

Conclusions

The dissolution issues for inert matrix fuel containing metallic molybdenum (CerMet) has been investigated. The dissolution head-end step prior to aqueous reprocessing of molybdenum based fuel has been comprehensively studied. Un-irradiated fuel with CeO_2 and PuO_2 in the matrix have been prepared and characterized. These fuel have been dissolved close to the PUREX process conditions, in some cases with addition of Fe (III) to speed up the dissolution. A selective dissolution of the matrix material at mild conditions is possible for CerMet fuels. The addition of Fe(III) is necessary to prevent the formation of Mo precipitates. Semi-warm dissolution tests revealed that while the solubility of molybdenum in nitric acid increases in the presence of iron, the solubility of the actinides is further decreased. In all cases less than 5% of the actinides dissolved. Therefore, it seems that the matrix can be dissolved selectively; remaining residue is expected to be PuO_2. The speciation of molybdenum has been studied by ESI-MS, and different molybdenum species have been identified. The method delivers unique insights into the solution speciation of molybdenum as a function of acid- and Fe(III)-concentration. The ESI-MS results hint on an increased solubility due to the formation of mixed Mo-Fe species.

Acknowledgement: This work has been supported by the European FP7 ASGARD (EC-GA No. 295825).

References

[1] S. Bourg et al.: *Nucl. Eng. Des.* 241(9) (**2011**) 3427–3435.
[2] C. Ekberg et al., ASGARD, in Sustainable Nuclear Energy Conference SNEC, Manchester, (2014).
[3] ASGARD, *Project Homepage*, http://asgardproject.eu/.
[4] N. Ouvrier & H. Boussier: *Procedia Chem.* 7 (**2012**) 322–327.
[5] Sypula, M. et al.: *Solvent Extr. Ion Exch.* 30(7) (**2012**) 748–764.

6.13. Pyrochlore and defect fluorite ceramics for nuclear waste immobilization: Structural, thermodynamic and computational insights

S. Finkeldei[1], P. Kegler[1], P.M. Kowalski[1], M. Lang[2], A. Bukaemskiy[1], V.L. Vinograd[1], A. Navrotsky[3], D. Bosbach[1], F. Brandt[1]

[1]Forschungszentrum Jülich GmbH, Institute of Energy and Climate Research – IEK-6: Nuclear Waste Management and Reactor Safety, 52425 Jülich, Germany

[2]University of Tennessee, Knoxville, Department of Nuclear Engineering

[3]University of California Davis, Peter A. Rock Thermochemistry Laboratory

Corresponding author: s.finkeldei@fz-juelich.de

Introduction

Pyrochlore- and defect fluorite-based ceramics are investigated as candidate materials for the immobilization of radionuclides.[1,2] ZrO_2-based pyrochlores are particularly suitable for this purpose due to their ability of accommodating a variety of different elements in different oxidation states (+II, +III, +IV, +V) in their crystal structures, due to their resistivity to amorphization caused by self-irradiation and their high corrosion resistance in aqueous environments. An ideal stoichiometric pyrochlore has the composition of $A_2B_2O_7$. The unit cell of such a compound contains 16 A, 16 B, and 56 O atoms as well as 8 O-vacancies (V_O). The anions (i.e. the oxygen atoms and the vacancies) form a simple cubic lattice. The vacancies, V_O, are ordered in pyrochlore such that their mutual contacts within the first and the second near-neighbor anion-anion shells are completely avoided, while all V_O-V_O pairs are at the third near-neighbor anion-anion distance. Each vacancy (small squares,Fig. 51) is surrounded by four B cations (here Zr) at the first cation – anion distance, such that the structure can be viewed as a regular alternation of A_4O (yellow) and B_4V_O (blue) tetrahedral clusters located at the corners of a cube (Fig. 51). The cube edge is equal to twice the shortest anion-anion distance or twice the unit cell parameter of fluorite. Due to this doubling, pyrochlore shows superlattice Bragg reflections in addition to those typical for the fluorite structure.

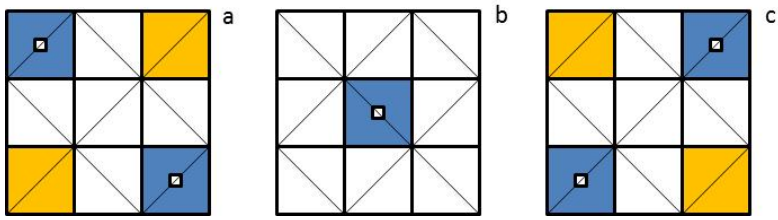

Fig. 51: Three-layer sketch of a pyrochlore structure, with the layer a on top of b and the layer b on top of c. Each square represents a tetrahedron of cations. The tetrahedra composed of four B cations or by four A cations are shown with blue and yellow colour, respectively. The vacancies (small squares) are located at the third anion-anion distance occupying B_4 clusters. The oxygen atoms occupy centers of the other tetrahedra.

The degree of order of the cation/anion distribution in defect fluorite $(A,B)_4(O,V_O)_8$ is much less certain. Consistently with the higher symmetry in comparison to pyrochlore, the superlattice reflections are absent, however the absence of these reflections does not imply a complete disorder.
In pyrochlore the distribution of A and B cations is ordered, such that a tetravalent cation, e.g. Ti, Zr, Hf, Ce, Th, Pu, occupies preferably the B site, while the trivalent cation, e.g. Y, Sc, lanthanide (*Ln*), actinide (An^{III}), finds itself in the other site with a higher probability. In defect fluorite both A and B sites are populated by tri- and tetravalent cations with equal probabilities. The order/disorder transition can be caused by different treatments, e.g. by irradiation, by a change in the sintering temperature, by applying pressure, as well as by compositional changes. Here, the structural transition from a stoichiometric $A_2B_2O_7$ pyrochlore ($Nd_2Zr_2O_7$) to a defect fluorite sample was induced by replacing a certain fraction of the A site cations (Nd) with the B site cations (Zr).
This work aimed at quantifying the thermodynamic effects due to the order/disorder transition and at a refined understanding of the degree of short-range order remaining in the defect fluorite phase after the phase transition.

Structural insights *via* neutron total scattering

To study the order/disorder transition from pyrochlore to defect fluorite along different length-scales we applied neutron total scattering at the NOMAD beamline in the Oak Ridge National Laboratory.[3] The total scattering function S(Q) contains the scattering intensity due to Bragg reflections and the diffuse scattering due to various effects of short-range ordering. In classical X-ray or neutron analyses of powders, only the Bragg-scattering is evaluated, while the information on local ordering is ignored. This loss of information can be avoided by applying a Fourier transformation to the total scattering function. The resulting pair distribution function (PDF) contains not only the Bragg scattering but also the diffuse scattering, allowing for insights into the local structure of the material of interest.[4] A combined neutron total scattering and PDF analysis thus allows for a characterization at different length scales and therefore a more complete characterization of the order/disorder transition.
A $Nd_2Zr_2O_7$ pyrochlore and a $Nd_{0.94}Zr_{2.53}O_{6.47}$ defect fluorite sample were synthesized for these measurements. Replacing part of Nd(+III) by Zr(+IV) leads to an increase in the number of vacancies in an electroneutral sample due the different oxidation states of the cations. The structural transition studied here is therefore expected to have a particular impact on the oxygen sublattice. In contrast to X-rays, neutrons are sensitive to the oxygen/vacancy distribution despite the presence of heavy elements such as Nd and Zr. This makes neutron scattering a perfect technique for following the structural consequences of the order/disorder transition from pyrochlore to defect fluorite.
The Rietveld refinement of the neutron total scattering data of the stoichiometric pyrochlore sample resolved the average structure as pyrochlore. The PDF refinement was consistent with these results showing a pyrochlore structure at the local scale. The neutron total scattering of the $Nd_{0.94}Zr_{2.53}O_{6.47}$ sample could be refined with a defect fluorite structure. However, a refinement of the PDF with a defect fluorite structure could not capture the experimentally derived data satisfactorily.[5] Thus, the assumption of complete disorder at all length-scales seemed to be an oversimplification for this sample requiring a search for a more ordered model structure than the defect fluorite. The high degree of local order, which is recorded in the PDFs, is comparable to that produced by the structure of weberite.

Weberite, ABC_2O_7, is a polymorph of fluorite and pyrochlore that has an orthorhombic symmetry. In an ideal weberite the C sublattice is disordered, i.e. randomly occupied by A and B cations, while the A and B sublattices are occupied exclusively by A and B cations, respectively. The average coordination numbers of A and B cations in weberite are 7.5 and 6.5, respectively. These values are intermediate between those of ideal stoichiometric pyrochlore (8 and 6) and of ideal completely disordered fluorite (7 and 7). Thus the degree of cation order in weberite is intermediate between that of pyrochlore and fluorite. The weberite structure also reflects the observed tendency of a vacancy to be preferably associated with the B cations in fluorite ceramics.[6] Importantly, similar to the case of pyrochlore, the vacancies in weberite are ordered such that first and second near-neighbor vacancy-vacancy contacts are avoided. This distribution is consistent with the results of first principles calculations.[7] The good fit of the weberite-type structural model to the experimental PDF suggested that the non-stoichiometric sample may consist of local weberite-type domains with different crystallographic orientations.[5] The total neutron scattering and PDF analyses thus suggest that the order/disorder transition from pyrochlore to defect fluorite proceeds *via* locally ordered weberite-type domains.

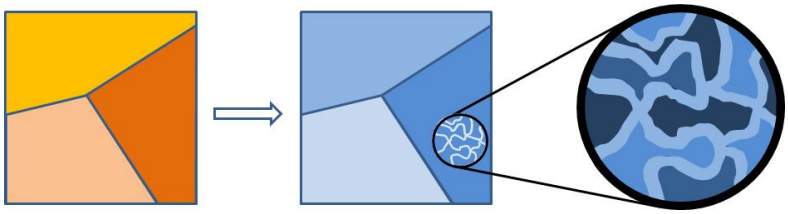

Fig. 52: Scheme of the pyrochlore/fluorite transition. Large polygonal areas denote hmogenous blocks of pyrochlore and defect fluorite which are responsible for the Bragg scattering of the pyrochlore and fluorite types. The average defect fluorite structure further consists of local weberite-type domains. The sizes of these domains are smaller than the coherence length of X-rays. The blue colours of different intensity in the insert denote weberite domains in different crystallographic orientations. The light-blue bands denote disordered boundaries between the domains. Modified after [8].

Structural, calorimetric and computational analysis of the order/disorder transition

These new findings regarding the short-range ordering (SRO) of defect fluorite initiated a follow-up study [9] on a series of $Nd_{2x}Zr_{1-x}O_{2+x}$ samples and their structural and calorimetric investigation. The aim of these investigations was to detect the order/disorder transition in a non-stoichiometric pyrochlore and to measure the corresponding enthalpy effect. The knowledge of the enthalpy change, ΔH, together with the known temperature of the synthesis (T = 1873 K) allows the estimation of the configurational entropy change, $\Delta S = \Delta H/T$, from which the degree of SRO in the fluorite phase can be estimated.

The XRD analysis of a sample series in the $Nd_{2x}Zr_{1-x}O_{2+x}$ system allowed locating the order/disorder transition at x ~ 0.19. The transition from the pyrochlore to the defect fluorite structure is not only marked by the absence of the superstructure reflections, but also by a change in the slope of the unit cell parameter *a*. A series of the samples was studied by high-temperature oxide melt solution calorimetry in collaboration with Prof. Navrotsky at the Peter Rock Laboratory (UC Davis, USA).[9] The experimentally derived formation enthalpies allowed correlating the structural order/disorder transition with a step-like feature in the enthalpy vs. composition plot (Fig. 53) indicating an enthalpy increase of ~30 kJ/mol for the

defect fluorite structures. The enthalpy increase of ~30 kJ/mol can be interpreted as the enthalpy of the order/disorder transition. This value, coupled to the synthesis temperature of 1873 K implies a disordering entropy of ~16 J/K/mol, which is significantly smaller than the value of 22.4 J/K/mol that represents the complete cationic and anionic disorder. Our combined structural-calorimetric results are thus consistent with the results of Shamblin et al.[5] on the existence of a significant short-range ordering in non-stoichiometric defect fluorite samples.

The total neutron scattering and PDF analyses[5] have shown that weberite represents a better structural model for the cation and anion distribution in fluorite relative to a quasi-random structure that is built consistently with complete disorder. This result suggested that weberite might also be a better model for computing the enthalpy effects of pyrochlore/defect fluorite transitions. This possibility was tested by designing three series of quasi-random structures (QRS) which were based on a 2×2×2 supercell of fluorite containing 32 cation and 64 anion sites. The first series of these QRS was designed to emulate the cation distribution in the completely disordered fluorite solid solution of $Nd_{2x}Zr_{1-x}O_{2+x}$. The other two series of QRS were based on the pyrochlore and weberite structures, in which the disorder was allowed only within certain sublattices. This disorder must necessarily be introduced in these QRS to model the pyrochlore, weberite and defect fluorite solid solution over a wide compositional range. The total energies of these QRS were computed with the Density Functional Theory (DFT) based Quantum Espresso package[10] using the resources provided by the Jülich-Aachen Research Alliance for High-Performance Computing (JARA-HPC). The results of these calculations allowed for the computation of the formation enthalpies of the three solid solutions which are based on the defect fluorite, weberite and pyrochlore structures. The results of these calculations are compared to the experimentally derived calorimetric data (black squares) in Fig. 53. The calculations based on the series of the pyrochlore-type QRS (green) closely match the experimental calorimetric data within the pyrochlore domain. In the defect fluorite domain the calorimetric results fall between the formation enthalpies computed with the weberite- (blue) and defect fluorite-type (red) sets of QRS (Fig. 53).

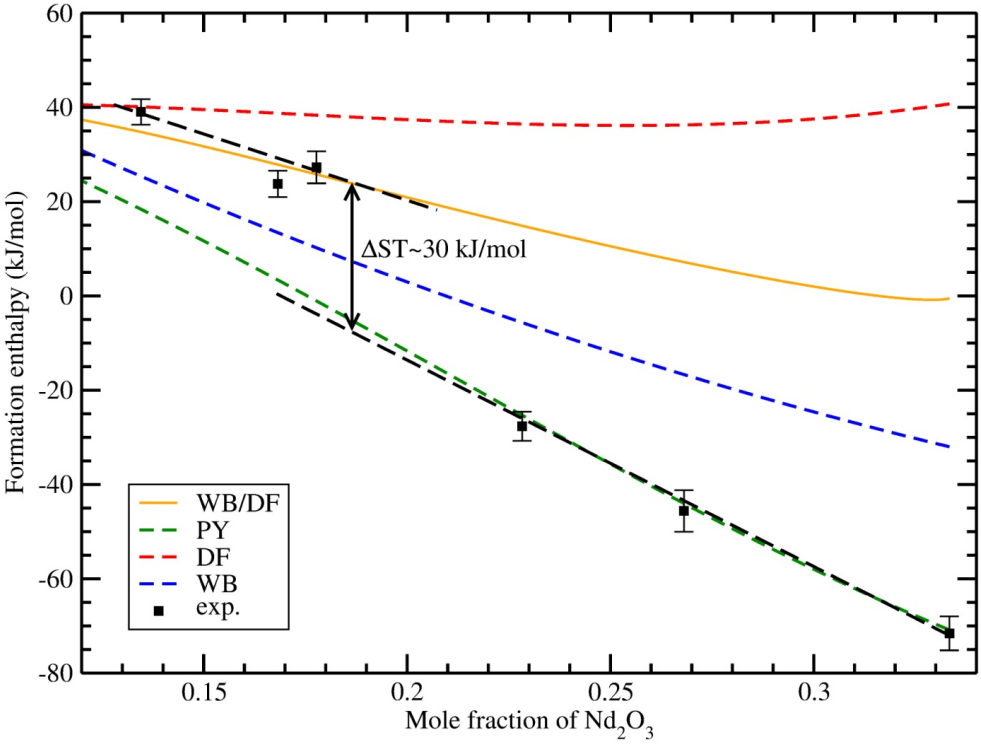

Fig. 53: Calorimetrically measured enthalpies of formation (from the oxides) of defect fluorites and pyrochlores (black squares) with the composition of $Nd_{2x}Zr_{1-x}O_{2+x}$. The step-like feature in the plot corresponds to the enthalpy effect of the order/disorder transition and the dashed lines represent the modeled formation enthalpies for various structural models, with PY for pyrochlore (green), WB for weberite (blue), DF for defect fluorite (red) and WB/DF representing the two state model of weberite and defect fluorite (orange). Modified after [9].

Therefore, the description of the enthalpy of formation data on defect fluorite samples requires a significant admixture of a structural component, which has a higher enthalpy of formation than weberite. At the present level of understanding of the nature of local ordering in fluorite, a 50:50 mixture of weberite- and fully disordered fluorite-type structural components appears to be a reasonable model representing the thermodynamic properties of the defect-fluorite phase. This model fits to the interpretation of Shamblin et al.[5] under the assumption that the high-enthalpy structural component of defect fluorite may represent disordered boundaries between the ordered weberite domains (Fig. 52).

In summary, our combined experimental and *ab initio* modeling approach has led us to a more detailed understanding of the order/disorder transition. Consistently with the interpretation of Shamblin et al.[5] our model implies that the transition occurs through the formation of ordered weberite-type domains, which then persist in the defect fluorite structure on a local scale. By correlating the experimentally measured enthalpy of the order/disorder transition in a non-stoichimetric sample with *ab initio* computed formation enthalpies of several model structures we were able to refine the weberite model of defect fluorite[5] by postulating the presence of another structural component, which is more disordered than weberite. A 50:50 “weberite”/“disordered fluorite” mixture fits the available data well. We are

fairly confident that the proposed model would be capable to adequately describe and predict structural and thermodynamic properties of pyrochlore and fluorite compounds not only for the $Nd_{2x}Zr_{1-x}O_{2+x}$ series, but also for other compositions, which may contain actinides. Future progress in modeling of the order/disorder transition in pyrochlore materials should be based on statistical-thermodynamic approaches able to take into account the predicted short-range order phenomena and the associated ordering energies.

Acknowledgements

We acknowledge the computing time on RWTH Aachen cluster awarded through Jülich-Aachen Research Alliance (JARA-HPC).

References

[1] Ewing, R.C.; Weber, W.J.; Lian, J.: *J. Appl. Phys*. 95 (**2004**) 5949-5971.
[2] Lumpkin, G.R.: *Elements* 2 (**2006**) 365-372.
[3] Neuefeind, J.; Feygenson, M.; Carruth, J.; Hoffmann, R.; Chipley, K.: *Nucl. Instrum. Methods Phys. Res. B* 287 (**2012**) 68-75.
[4] Proffen, Th.; Billinge, S.; Egami, T.; Louca, D.: *Z. Kristallogr.* 218 (**2003**) 132–143.
[5] Shamblin, J.; Feygenson, M.; Neuefeind, J.; Tracy, C.L.; Zhang, F.; Finkeldei, S.; Bosbach, D.; Zhou, H.; Ewing, R.C.; Lang, M.: *Nat. Mater.* 15 (**2016**) 507-511.
[6] Norberg, S.T.; Hull, S.; Eriksson, S.G.; Ahmed, I.; Kinyanjui, F.; Biendicho, J.J.: *Chem. Mat.* 24 (**2012**) 4294–4300.
[7] Bogicevic , A.; Wolverton, C.: *Phys. Rev. B* 67 (**2003**) 024106.
[8] Uberuaga, B.: *Nat. Mater.* 15 (**2016**) 496-497.
[9] Finkeldei, S.; Kegler, Ph.; Kowalski, P.M.; Schreinemachers, C.; Brandt, F.; Bukaemskiy, A.A.; Vinograd, V.L.; Beridze, G.; Shelyug, A.; Navrotsky, A.; Bosbach, D.: *Acta Mater*. 125 (**2017**) 166–176.
[10] Giannozzi, P., et al.: *J. Phys. Condens. Matter* 21 (**2009**) 395502.

6.14. Monazite-type ceramic waste forms for the immobilisation of tri- and tetravalent actinides

S. Neumeier, Y. Arinicheva, P. Kegler, P.M. Kowalski, H. Schlenz, G. Deissmann, D. Bosbach

Corresponding author: s.neumeier@fz-juelich.de

Introduction

In the last decades, various ceramic materials have been proposed as potential waste forms for the immobilisation of special nuclear waste streams, such as separated plutonium from civilian or military sources unsuitable for further use. Among these ceramics, monazite-type orthophosphates (LnPO$_4$; Ln = La – Gd) appear as promising candidates due to their specific physico-chemical properties including high structural flexibility, high chemical durability, and high radiation resistance[1-5].

The outstanding properties of monazites have been demonstrated by natural analogues being exposed to geological events for several hundred millions of years. Natural monazites can contain up to 27 wt.% natural radioelements, such as tetravalent Th and U without suffering from amorphization due to radiation damages[6] and chemical alteration by weathering[7].

Key factors for the development and application of monazite ceramics with tailor-made properties as nuclear waste forms comprise in particular a refined understanding of the incorporation mechanisms of radionuclides into the monazite structure as well as the demonstration of the long-term stability of the waste forms.

Structural flexibility of monazite-type solid solutions

The ABO$_4$ monazite-type structure (monoclinic, space group P2$_1$/n, Fig. 54, left) offers a high flexibility for incorporating a wide range of elements with variable size and charge such as tri- and tetravalent actinides which is correlated to the low symmetry of LnO$_9$ polyhedron (Fig. 54, left).

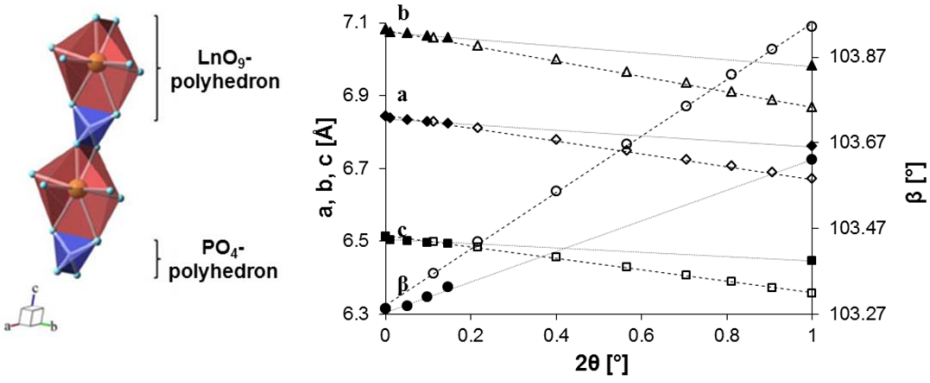

Fig. 54: Representation of the monazite structure and LnO$_9$ polyhedron connection (left). Linear dependency of lattice parameters on the chemical composition according to Vegard's law for La$_{1-x}$Eu$_x$PO$_4$ (open symbols) and La$_{1-x}$Pu$_x$PO$_4$ (closed symbols) solid solutions (right).

Trivalent actinides can be incorporated by direct substitution of trivalent lanthanides forming a single phase solid solution $Ln_{1-x}An_xPO_4$ (*Ln* = La-Gd, *An* = e.g. Pu^{3+}, Am^{3+}). This direct substitution was demonstrated for several monazite solid solutions using lanthanides as non-radioactive surrogates for actinides[8-10]. As expected, the incorporation of Nd, Eu, and Gd results in the formation of single phase monazite-type solid solutions, which is confirmed by the linear dependency of the lattice parameters on the chemical composition according to Vegard's law (Fig. 54, right).

For the immobilisation of actinides monazite-type $SmPO_4$ ceramics are of special interest due to their relatively low melting point[2, 11]. $Sm_x(Ca,An)_{1-x}PO_4$ (*An* = Th, U; x = 0.1 – 0.9) solid solutions were synthesised by solid state and co-precipitation reactions. Pellets were sintered under Ar atmosphere at T = 1450 °C (t = 12 h). The obtained material was investigated with respect to phase purity and composition by XRD, SEM, and IR-spectroscopy. Additionally, Rietveld refinements were performed and the lattice parameters determined. The X-ray diffraction data reveal that *a* and *b* cell constants of $Sm_x(Ca,U)_{1-x}PO_4$ decrease with increasing x value. This is perfectly sensitive, as the atomic radii of Sm(III) = 113.2 pm and (Ca(II) + U(IV))/2 = 111.5 pm are very similar in nine-fold coordination. Consistently, the Bragg reflections of $Sm_x(Ca,Th)_{1-x}PO_4$ shift to lower 2Θ values with increasing Th content. The unit cell becomes larger, as the mean size occupied by the cations is (Ca(II) + Th(IV))/2 = 113.5 pm. In both series the *c* lattice parameter decreases with increasing x. All IR spectra show significant signals attributed to the bending and stretching vibrations of the PO_4 tetrahedra in the range 400 – 1100 cm^{-1}, respectively, and the shift in wavenumbers seems to be rather small. This effect is already known from monazite-type $LnPO_4$ (*Ln* = La to Gd) ceramics[9].

However, the structural evolution of the solid solution $Sm_x(Ca,U)_{1-x}PO_4$ is almost comparable to that of single and binary lanthanide monazite-type structures. Uranium could be kept completely as U^{4+} using U-metal and an Ar-atmosphere during synthesis. Only U-rich phases showed additional U_4O_9. The structural evolution of the solid solution $Sm_x(Ca,Th)_{1-x}PO_4$ is by no means comparable to that of actinide-free monazite-type structures. The crystal structure develops continuously to that of pure cheralite $Ca_{0.5}Th_{0.5}PO_4$. Small changes of the average cation radius cause a rapid increase of the unit cell volume. Both $Sm_x(Ca,An)_{1-x}PO_4$ phases show opposite trends related to the change of the unit cell volume with increasing Sm-content.

Thermochemistry of monazite-type solid solutions

A reliable prediction of the long-term stability of a ceramic waste form requires systematic investigations of the thermochemistry of the solid solutions. These investigations allow for evaluating tendencies for destabilisation due to immiscibility gaps and/or phase separation of the solid solution induced by the incorporation of foreign ions and therefore, provide valuable information about the maximal loading of the waste form.

The enthalpies of formation and mixing of single phase monazite solid solution series ($La_{1-x}Ln_xPO_4$ (*Ln* = Pr, Nd, Eu and Gd) were directly measured utilising high temperature oxide melt drop solution calorimetry (Fig. 55, left), performed in collaboration with Prof. A. Navrotsky (Peter A. Rock Thermochemistry Laboratory, University of California Davis, Davis, CA, USA). For each measurement, 8 to 10 samples (50 - 60 mg) of the respective composition were dropped into 20 g of a $3Na_2O{\cdot}MoO_3$ solution at 700 °C. The integration of the thermal response of the system during the dissolution of the dropped sample provides the data to calculate the enthalpies of formation and the enthalpies of mixing of the solid solutions.

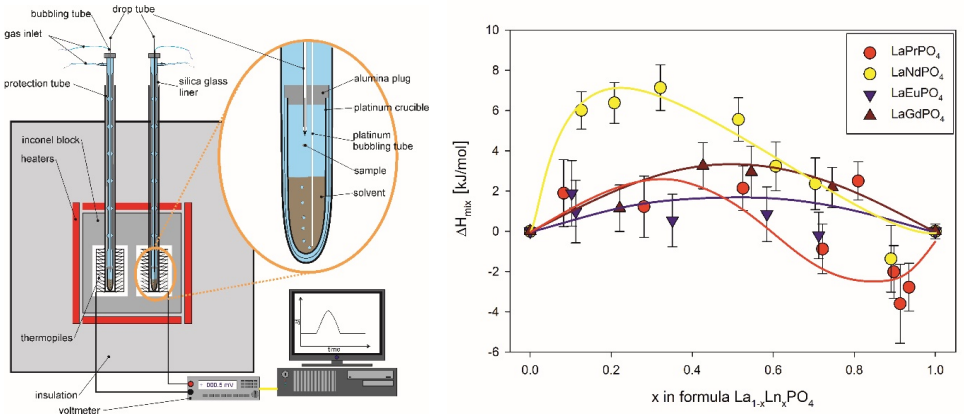

Fig. 55: Left: Scheme of the drop solution calorimetry set-up at UC DAVIS, CA, US. Right: Plot of the excess enthalpy of mixing as a function of *Ln*-content in $La_{1-x}Ln_xPO_4$ (*Ln* = Pr (red), Nd (yellow), Eu (blue) and Gd (brown)) solid solution series. The results are discussed in detail in [10] and [12].

An excess enthalpy of mixing was observed for all $La_{1-x}Ln_xPO_4$; *Ln* = Pr, Nd, Eu and Gd solid solution series (Fig. 55, right). The results from Eu and Gd-bearing solid solutions are in reasonable agreement with previous experimental[13] and DFT-based atomistic modeling studies[10, 14, 15]. It was shown that the excess enthalpies of mixing derived *ab initio* can be well described by a simple expression as a function of Young's modulus and the mismatch in measured/ calculated volumes of the endmembers (cf. 6.18). From the combined experimental and modeling studies it can be concluded that the excess enthalpy of mixing mainly depends on strain energy resulting from the difference in ionic radii of substituting and host cations. The effect of strain energy and difference in ionic radii on the structure of solid solution series was also examined in Raman[10, 16] and laser fluorescence[17] spectroscopy investigations. It was found that for the $La_{1-x}Gd_xPO_4$ system the bond length distribution in the solid solution systems results in the broadening of the fluorescence peaks which indicates homogeneity of the monazite-type solid solutions.

In contrast to the existing literature on excess properties of monazite-type ceramics, the enthalpy of mixing of the $(La,Nd)PO_4$ and $(La,Pr)PO_4$ solid solutions exhibit asymmetric and irregular excess properties. This effect cannot be explained with mismatch of ionic radii and lattice strain only, but rather by the way generating data by drop solution calorimetry. The literature data on excess enthalpies[13] were also derived from heat capacity measurements of these solid solutions. In contrast, the drop solution calorimetry measurements are based on the complete dissolution of the sample and thus include additional information such as the enthalpy of breaking chemical bonds. The unexpected variation of formation enthalpy along solution series containing Pr and Nd could possibly be explained by partially oxidation of $Pr^{+III} \rightarrow Pr^{+IV}$ in the solvent and magnetic effects of Nd.

These thermochemical data provide key parameters for the calculation of stability and solubility of the monazite solid solutions as a function of temperature[18].

Based on the results of the structural and thermodynamic investigations on surrogate doped monazite-type solid solution, the incorporation of trivalent actinides such as Am^{3+} and Pu^{3+} on defined lattice positions of the monazite structure should be generally feasible. As the ionic radii of Pu and minor actinides are in the range of the investigated *Ln* ions, a formation of a thermodynamically stable solid solution series with monazite structure can be expected. However, so far only few papers exist dealing with the incorporation of actinides into the monazite structure. Within a TALISMAN (Transnational Access to Large Infrastructure for a Safe Management of ActiNide) and ACTUSLAB (ACTinide USer LABoratory) activity together with JRC-Karlsruhe (former ITU) single-phase $La_{1-x}Pu^{III}_xPO_4$-monazite solid solutions with a molar fraction of Pu up to x = 0.15 were successfully synthesised by a solid state method at 1300 °C. Although $Pu^{IV}O_2$ was used as starting material for the solid state synthesis, no additional reducing agent was needed to reduce $Pu^{iV} \rightarrow Pu^{III}$ during synthesis since the reduction is induced by products from thermal decomposition of the PO_4-source ($(NH_4)_2HPO_4$) during solid state reaction[19, 20]. XRD and SEM analysis confirmed the formation of single phase solid solutions and their homogeneity (Fig. 56). X-ray absorption spectroscopy (XAS) analysis of the single phase (La,Pu)PO_4 solid solutions at the Pu-L_{III} and La-L_{III} edges proved the incorporation of Pu^{III} on defined lattice sites of the monazite structure. A comparison of XRD and EXAFS data reveals that the incorporation of Pu is adjusted by the local environment of $LaPO_4$. In contrast, the local environment of Pu remains $PuPO_4$-like for the entire solid solution range. This work demonstrates that monazite-type ceramics with a reasonable amount of Pu (10-15%) for nuclear waste applications can be fabricated by conventional solid state reaction at 1300 °C.[21]

At a higher Pu content (x = 0.50) residues of PuO_2 remained unreacted (Fig. 56). However, a decomposition of formed $PuPO_4$ or associate $La_{1-x}Pu^{III}_xPO_4$ solid solutions can be excluded because of the absence of Pu_2O_3 in refined XRD examinations. Moreover, the formation of single phase solid solutions with high Pu content can be expected after optimising the solid state synthesis conditions or utilizing wet chemistry methods, such as co-precipitation.

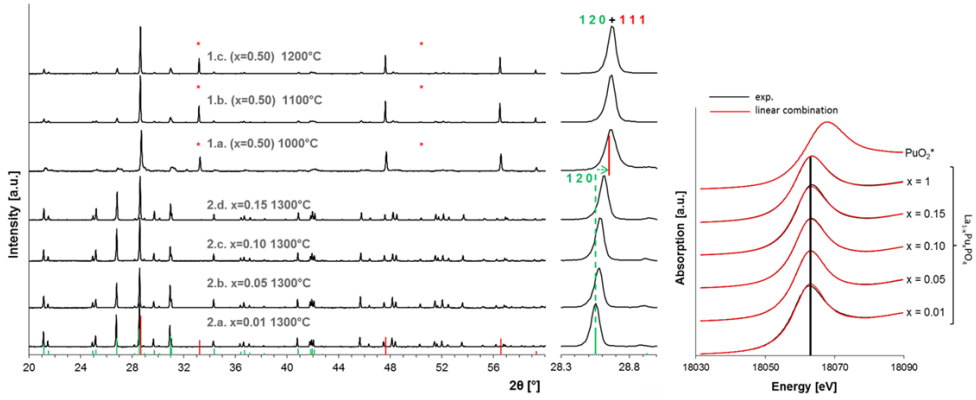

Fig. 56: Left: XRD patterns of $La_{1-x}Pu_xPO_4$ (x = 0.01, 0.05, 0.1, 0.15, 0.5) solid solutions; red asterisks indicate unreacted PuO_2. Right: XANES spectra of single phase (La,Pu)PO_4 solid solutions (x = 0.01 - 0.15 and 1[20]) as well as of the $Pu^{IV}O_2$ reference.

Conclusions

The flexibility of the monazite structure and the thermochemistry of monazite-type solid solutions have been investigated. Single phase solid solutions are formed by the incorporation of tri- and tetravalent actinides (Pu^{III}, Th^{IV}, U^{IV}) and non-radioactive trivalent surrogates. The enthalpies of mixing differ significantly between the investigated solid solutions ($La_{1-x}Ln_xPO_4$; *Ln* = Pr, Nd, Eu, Gd). It was found that for all solid solution the difference of the ionic radii and the lattice strain contribute to the excess properties. Apparently the redox chemistry and the magnetic properties play an additional role of the observed large excess effects for Pr and Nd, respectively. The incorporation of Pu^{III} into the monazite structure up to 15 mol% representing a reasonable amount of Pu for nuclear waste management applications was successfully achieved by solid state method and confirmed by XRD and XAS measurements. For higher Pu contents (50 mol%) unreacted PuO_2 was observed, but the incorporation of a higher Pu content into single phase monazites can be expected when varying and optimizing the synthesis method.
These results demonstrate on the one hand the thermodynamic stability of monazite-type solid solutions. On the other hand they reveal the uncertainties concerning the transferability of results from surrogate- to actinide-bearing solid solutions, particularly for actinides with very complex redox chemistry such as Pu. This emphasizes the need of research on actinide–bearing ceramic waste forms for a reliable predictability of the long-term stability of these materials.

Acknowledgements

This work was supported by the German Federal Ministry of Education and Research (BMBF); grant no.: 02NUK021, the German Research Foundation (DFG); grant-no.: SCHL 495/3-1, by the European FP7 TALISMAN project (JRP-No.: TALI-C06-11) under contract with the European Commission and bythe ACTUSLAB project (JRC-Karlsruhe; grant-no.: AUL-2016-18-195).

References

[1] Ewing, R.C. and Wang, L.M.: *Rev. Min. Geochem*. 48 (**2002**) 673-699.
[2] Lumpkin, G.R.: *Elements* 2 (**2006**) 365-372.
[3] Dacheux, N. et al.: *Am. Mineral*. 98 (**2013**) 833-847.
[4] Schlenz, H. et al.: *Z. Krist.* 228 (**2013**) 113-123.
[5] Neumeier et al.: *Radchim. Act*. 105 (**2017**) 961-984.
[6] Boatner, L.A.: *Rev. Min. Geochem.* 48 (**2002**) 87-120.
[7] Montel, J.M. et al.: *Eur. J. Mineral.* 23 (**2011**) 745-757.
[8] Arinicheva, Y. et al.: *Prog. Nucl. Energy* 72 (**2014**) 144-148.
[9] Heuser, J. et al.: *Prog. Nucl. Energy* 72 (**2014**) 149-155.
[10] Neumeier, S. et al.: *J. Chem. Thermodyn.* 105 (**2017**) 396-403.
[11] Hikichi, Y. & Nomura, T.: *J. Am. Ceram. Soc.* 70 (**1987**) C-252-C-253.
[12] Hirsch, A. et al.: *J. Solid State Chem.* 245 (**2017**) 82-88.
[13] Popa, K. et al.: *J. Chem. Thermodyn.* 39 (**2007**) 236-239.
[14] Li. Y. et al.: *J. Solid State Chem*. 220 (**2014**) 137-141.
[15] Kowalski, P.M. & Li, Y.: *J. Eur. Ceram. Soc*. 36 (**2016**) 2093-2096.
[16] Geisler, T.: *Front. Earth Sci*. 4 (**2016**).
[17] Huittinen, N. et al.: *J. Nucl. Mater*. 486 (**2017**) 148-157.
[18] Gorman-Lewis, D. et al.: *J. Chem. Thermodyn*. 39 (2007) 47-51.
[19] Bregiroux, D. et al.: *J. Nucl. Mater*. 366 (**2007**) 52-57.
[20] Popa, K. et al.: *J. Solid State Chem*. 230 (**2015**) 169-174.
[21] Arinicheva, Y. et al.: *J. Nucl. Mater*. 493 (**2017**) 404-431.

6.15. Structural investigations of amorphous geopolymers using synchrotron radiation and radial distribution functions

H. Schlenz, S. Weigelt, D. Bosbach

Corresponding author: h.schlenz@fz-juelich.de

Geopolymers based on metakaolin, a thermally treated kaolin clay, exhibit very promising properties as a potential nuclear waste form. By total scattering and pair distribution function (PDF) analyses we anticipated to get new insights into the structure of dominantly amorphous geopolymers on the atomic length scale. Together with results of Raman, IR, and MAS-NMR spectra a detailed picture of the geopolymers' network and its crystallographic features shall be drawn.

We investigated geopolymers of 14 different compositions containing Cs, Sr, Rb, K, Na or in combination ($K_{1-x}Cs_x$), ($Rb_{1-x}Cs_x$) or ($Ca_{1-x}Sr_x$) with x = 0.25, 0.50, and 0.75, respectively. For this purpose we have investigated all samples at the European Synchrotron Radiation Facility ESRF in Grenoble (France) and at Petra III / DESY in Hamburg (Germany), respectively, using 65.0 keV (ESRF) and 60.0 keV (Petra III) X-ray powder diffraction.

For each of these compositions an amorphous and two thermally treated samples heated to 150 °C or 1150 °C were prepared. The geopolymer samples that crystallized during the thermal treatment at 1150 °C served as reference for the identification of interatomic distance correlations. The powdered samples were filled into Kapton tubes provided by Goodfellow with an inner diameter of 0.5 mm and 25 µm wall thickness. The samples were rotated with 787 rpm and acquisition time for each sample was about half an hour. Subsequent data processing was conducted using the software suite PDFgetX3[1], where the absolute value of the scattering vector Q was restricted to the range of 0.53 to 27 $Å^{-1}$.

The total pair distribution functions G(r) of all geopolymers that cured at room temperature show very similar characteristics meaning similar peak positions as shown in Fig. 57. Also the degree of order is equal for the geopolymers with alkaline metal cations (Na, K, Rb, Cs), whereas the Sr-geopolymer shows a higher degree of order. All samples show a well-defined short-range order up to 5 Å, but only the Sr-geopolymer exhibits also a long-range order, while the other geopolymers have only a weak medium-range order between 5 Å and 8 Å.

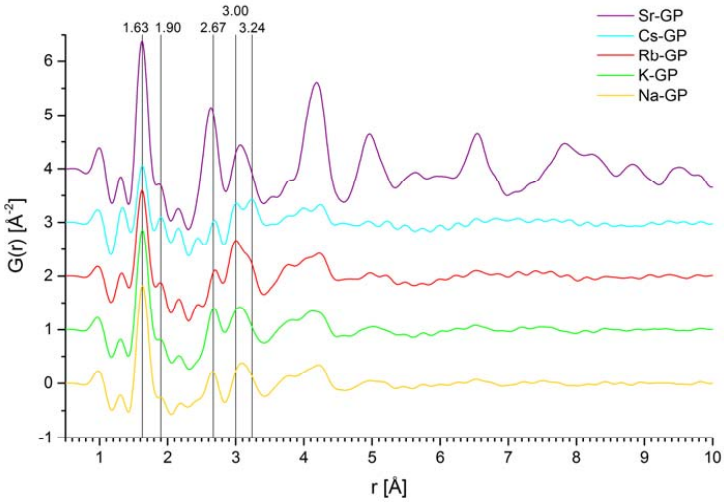

Fig. 57: Total pair distribution functions G(r) of geopolymers (GP) with the four different alkaline metal cations Na, K, Rb, and Cs as well as a geopolymer with the alkaline earth metal cation Sr. Marked r-values can be correlated to interatomic distances that can be found in the crystal structure of pollucite and its analogues.

Marked r-values in the plot are lengths that can be correlated with interatomic distances appearing typically in aluminosilicates like pollucite and its analogues, or kaolin. For example, the strong signal at 1.63 Å can be attributed to T–O bonds with T = Si, Al in tetrahedral silicate and aluminate groups. The much weaker signal at 1.90 Å, which is partly superimposed by the previous signal, corresponds to the Al–O distance in an AlO_6 octahedron. The O–O distance known from pollucite can be found at 2.67 Å. The following two broad signals at 3.00 Å and 3.24 Å can be interpreted as Si–Si, Al–Al, and Al–Si distances, explaining also the overlap of the signals. Additionally, the distance between oxygen and the alkaline metal or alkaline earth metal cation should be located around 3.3 Å. Following rather broad humps around 4 Å and 5 Å correspond to the distances between the cation to Si and Al or between the cations among each other, respectively.

In contrast to the alkaline metal geopolymers, the geopolymers with the alkaline earth metal cations Ca and Sr (Fig. 58) have already crystallized at room temperature while nearly the complete water content evaporated after opening the vials that served as sample containers. For these samples a long-range order up to 30 Å is observed, although it gets lost for the geopolymers with 50 % and more Ca on the cation position.

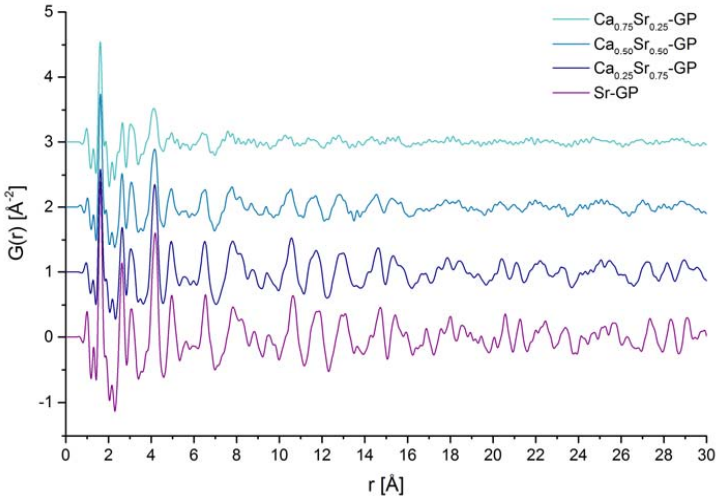

Fig. 58: Total pair distribution functions G(r) of ($Ca_{1-x}Sr_x$)-geopolymers. Fluctuating intensities up to 30 Å indicate a distinct long-range order.

In Fig. 59 the total pair distribution functions G(r) for the geopolymers with mixed cation compositions are plotted. The curves reveal a continuous change of intensities between the end members, while the peak positions and the general curve shapes do have significant similarities.

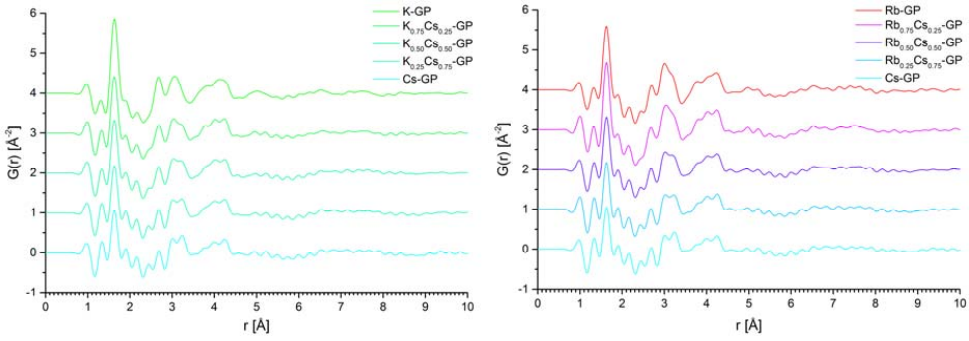

Fig. 59: Total pair distribution functions G(r) of ($K_{1-x}Cs_x$)- and ($Rb_{1-x}Cs_x$)-geopolymers.

References:

[1] P. Juhás, T. Davis, C.L. Farrow, S.J.L. Billinge, *J. Appl. Cryst.* 46 (**2013**) 560-566.

6.16. Stabilization of pentavalent uranium in oxo-phases

Ph. Kegler[1], B. Xiao[1], S.A. Novikov[1], I. Pidchenko[2], T. Vitova[2], T.E. Albrecht-Schmitt[3], E.V. Alekseev[1]

[1]Forschungszentrum Jülich GmbH, Institute of Energy and Climate Research – IEK-6: Nuclear Waste Management and Reactor Safety, 52425 Jülich, Germany

[2]INE, KIT, 76125 Karlsruhe, Germany

[3]Department of Chemistry and Biochemistry, Florida State University, Tallahassee, FL 32306, USA

Corresponding author: e.alekseev@fz-juelich.de

Introduction

According to current theory in natural and technical systems uranium is present in two oxidation states: as tetravalent (U(IV)) and hexavalent (U(VI)) uranium. In aqueous, geological and ecological systems U(VI) is the dominant valence state, whereas compounds with tetra- and hexavalent uranium are frequently described in solid-state chemistry.[1,2] In addition, the occurrence of bivalent (U(II)) and trivalent (U(III)) uranium is described under very reducing conditions.[3] Pentavalent uranium (U(V)) occurs rarely in the presence of oxygen, especially in solid state systems.[4,5] In recent years, however, it has become increasingly apparent that pentavalent uranium (U(V)) appears to play a more important role in natural and technical systems than previously assumed. This may have an important impact on the assumed stability of uranium in the repository as well as on the mechanisms involved in the mobilization of safety-related radionuclides and the formation of possible secondary phases during container and fuel corrosion.

In order to better estimate the relevance of pentavalent uranium, the processes leading to its stabilization as well as the range of its stability field have to be investigated more closely, as our knowledge in this field is very limited. A fundamental estimation of the relevance of U(V) compounds for the long-term safety of a prospective repository can only be obtained by a systematic investigation of the processes and conditions which lead to the stabilization of U(V).

Here we shortly want to present two experimental studies with different approaches to stabilize pentavalent uranium. The first method was successfully used for the preparation of a new U_2O_5 polymorph under extreme conditions of pressure and temperature. The second method was applied for the stabilization of U(V) in a series of Mo / W oxo salts by aliovalent substitution.

High pressure approach, preparation of U_2O_5

Up to now, four different polymorphs of U_2O_5 can be found in the literature (*α*-, *β*-, *λ*- and δ-U_2O_5).[6,7] Nevertheless, attributable to experimental challenges and sample instability, these U_2O_5 polymorphs have never been explicitly described and detailed crystallographic information of these polymorphs was not given and nor has there been any further experimental investigation since the original studies. It is a still an open question if *α*-, *β*-, and *λ*-polymorphs are existing. We were able to synthesize the first air-stable polymorph of pentavalent uranium oxide, named ε-U_2O_5. We succeeded in obtaining macroscopic single crystals of ε-U_2O_5, which allows the precise structural determination of highly condensed uranium(V)-oxygen arrangement on the basis of single-crystal X-ray diffraction.

The ε-U_2O_5 crystals were prepared by a high-temperature/high-pressure experiment using the walker type multi anvil module of a Voggenreiter LP 1000-540/50 in a 14/8 (TEL/OEL) assembly using a $LaCrO_3$ furnace. UO_3 and SiO_2 with the ratio of 1: 6 were used as the starting materials. The starting materials of UO_3, SiO_2 were weighed in with the desired ratio, then were mixed and finely grounded. Than the obtained mixture was filled into a Platinum capsule (outer diameter: 1.6 mm, wall thickness: 0.1 mm, length: 2.6 mm). After that the capsule was sealed with an impulse micro welding device (Lampert PUK U4) and placed into the center of 14/8 multi anvil assembly using a Cr stabilized MgO octahedron, a stepped $LaCrO_3$ heater and ZrO_2 as pressure medium outside the furnace and surrounding the capsule inside of the furnace. A type-C thermocouple was used. After assembling the total setup was dried at 200 °C for 12 hours. On the next day the octahedron was placed in the center of 8 tungsten carbide cubes (truncation length 8 mm). The whole assembly was inserted in the walker type multi anvil module and compressed to the desired pressure of 10 GPa within 5 hours. The sample was heated to 1290 ± 20 °C in 10 Minutes and then held at that temperature for 10 Minutes. Then the sample was cooled down to 450 ± 20 °C within 4 hours. After quenching to room temperature the pressure was released within 20 hours. After the experiment, black crystals of ε-U_2O_5 were obtained and isolated. The typical crystal size is around 60−100 µm (Fig. 60). To our surprise, the resulting ε-U_2O_5 crystals obtained under such extreme conditions are unusually durable. They can be stable at room-temperature ambient conditions over several weeks, with no evidence for the occurrence of decomposition or being oxidized.

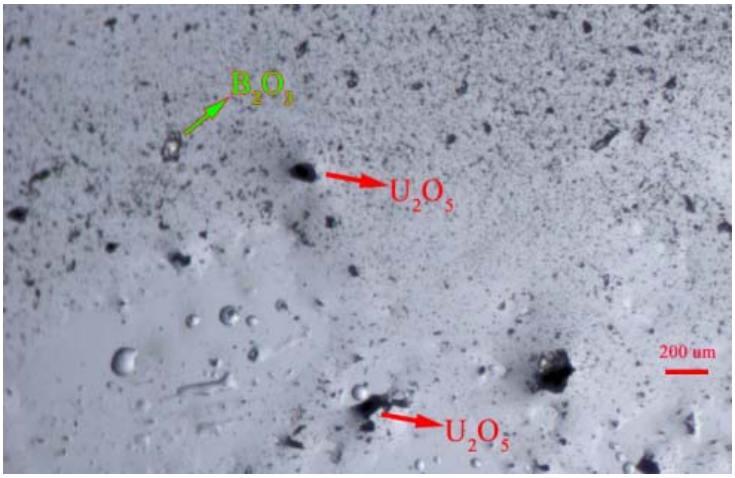

Fig. 60: Crystal of U_2O_5

Single-crystal X-ray diffraction shows that ε-U_2O_5 adopts a monoclinic structure with a = 6.6824(5) Å, b = 7.6380(5) Å, c = 12.6898(9) Å and β = 99.135(7). ε-U_2O_5 follows the same structural packing mode like the cubic UO_2, but much more distorted attributable to its lower crystal symmetry resulting from the incorporation of excessive oxygen atoms into the fluorite lattice (see Fig. 61 (a)). The complex framework of *ε*-U_2O_5 can be dissected into two more simple structural units (sub-layers). The two types of layers of *ε*-U_2O_5 (see Fig. 61 (b)) have the same uranium topological arrangement as that of the fluorite-typed UO_2 structure. These layers in *ε*-U_2O_5 are stacked, as shown in Fig. 61 (c, d), along the crystallographic *a*-axis in

the …ABAB… fashion. Adjacent layers are displaced with respect to each other such that the three-ring or four-ring cavity of one layer is resided on the uranium site of its next layer. This is also identical to the uranium sub-layer sequence in UO_2.

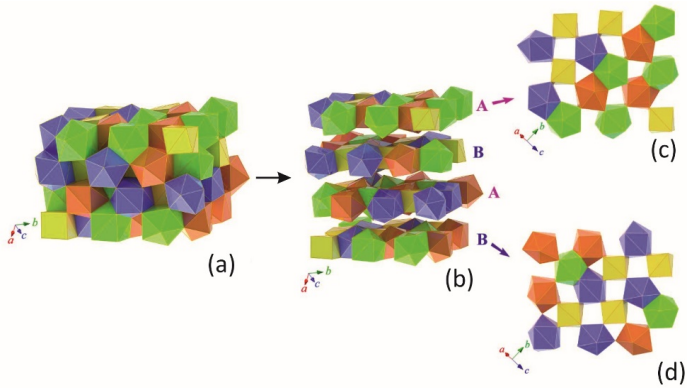

Fig. 61: View of crystal structure of ε-U_2O_5. (a) The framework of ε-U_2O_5 shows a close similarity to UO_2. (b) Dismantle the framework into simpler layers shows that ε-U_2O_5 is based on two different fluorite-typed layers illustrated in (c) and (d), respectively.

The distortion deviating from the idealized fluorite arrangement is dependent on geometric constraints of U^{5+} cations under high-pressure, which can be visualized by investigation of the local coordination environment of uranium cation. Fig. 62 shows the complete polyhedral depiction of all four symmetrically unique U^{5+} sites for ε-U_2O_5.

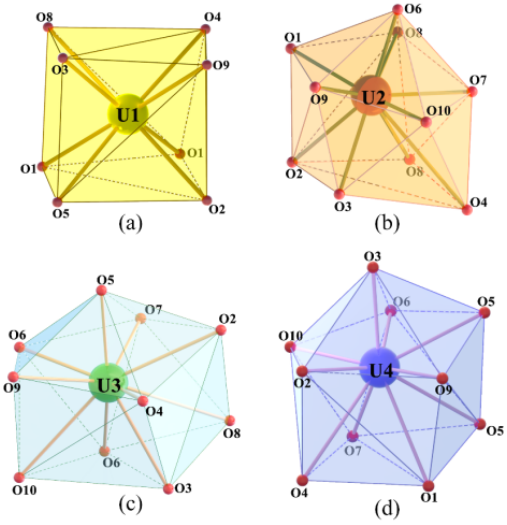

Fig. 62: The structure of ε-U_2O_5 has four crystallographically unique U^{+5} sites. (a) UO_4 cubic polyhedron. (b, c, d) tenfold distorted UO_{10} polyhedra.

The bond-valence summations (BVS) for these uranium sites are all close to 5 vu, with a range from 5.18 to 5.44 vu. This is in good accordance with the fact of U^{5+} in these sites. It is also worth to mention that even though the BVS parameters used from Burns [8] are actually designed for U^{6+}, they are still informative to discriminate U^{5+} from other uranium oxidations.
Actually, to the best of our knowledge, ε-U_2O_5 has the highest crystal density among all known uranium oxides. Other uranium oxides with high density are also based on the fluorite-typed structure, such as UO_2 (10.98 g/cm^3)[9], and α- β- and λ-U_2O_5 (around 11 g/cm^3).[7] The ambient meta-stable δ-U_2O_5 has the density of 8.22 g/cm^3 [10], while when the pressure is increased to 10 GPa, it jumps drastically to 11.62 g/cm^3, forming ε-U_2O_5. The nearly 41% of density increase from the ambient to the high-pressure polymorphs is associated with significant structural transformation from the layered δ-U_2O_5 to the more condensed fluorite-typed ε-U_2O_5. It is such large density increase under the high-pressure conditions that is mainly responsible for the stability of ε-U_2O_5. The enhanced structural stability due to increment of crystal density has also been observed in the recent study of fluorite-typed U_3O_8 at high-pressure[11]

Aliovalent substitution approach, stabilization of U(V) in a series of Mo / W complex oxides

Here we describe a more complex system where the oxidation state of uranium can be rationally altered through incorporation of cations with different sizes and charges. We demonstrate that the hexavalent uranium (U(VI)) and pentavalent uranium (U(V)) can be stabilized in two phases, namely $Ca(U^{VI}O_2)W_4O_{14}$ and $[Ln(U^{V}O_2)W_4O_{14}]$ (*Ln* = Nd-Tm and Y). The named materials were synthesized *via* high-temperature solid-state reaction under atmosphere conditions at 1200 °C, and formed well shaped crystals with a size up to 0.5 cm. $Ln(U^{V}O_2)W_4O_{14}$ (*Ln* = Nd-Tm and Y) is the first family of oxo-salts which are bearing pentavalent uranium and contain rare-earth metals. It is also an exceptional example of a uranyl(V) compound in which the apical O atoms of the uranyl unit interact with rare-earth polyhedra (highlighted in Fig. 63 (b)).
Single crystal analysis reveals that $Ln(U^{V}O_2)W_4O_{14}$ and $Ca(U^{VI}O_2)W_4O_{14}$ are isostructural. Both compounds crystallize in the monoclinic space group with two crystallographically independent W atoms, one U atom and one *Ln* or Ca atom in an asymmetric unit (see Fig. 63 (a)). They form in a condensed three-dimensional (3D) framework that can be reasonably separated into iriginite-type layers.[12] Part of the layers in $Ln(U^{V}O_2)W_4O_{14}$ and $Ca(U^{VI}O_2)W_4O_{14}$ are shown in Fig. 63 (b).The 5+ oxidation state of uranium in the structure of $Ln(U^{V}O_2)W_4O_{14}$ series have been confirmed with several methods including XANES and UV-vis-NIR spectroscopy as it shown in Fig. 63(e) and (f). The successful preparation of alkaline-earth-based $Ca(U^{VI}O_2)W_4O_{14}$ and lanthanide-based $Ln(U^{V}O_2)W_4O_{14}$ by adopting different starting reagents exhibits a rare example of complete aliovalent substitution of considerably different cations while keeping the overall structural topology. This shows that the $M(UO_2)W_4O_{14}$ (M = alkaline- or rare-earth) is a potential matrix with unusual structural stability which tolerates considerable modification in composition without structural alteration. The result, shown in Fig. 63 (c, d), demonstrate that when Ln^{3+} ions are introduced, they enter the crystal lattice substitutionally for Ca^{2+} sites, creating additional positive charge. The charge imbalance triggers the oxidation change of composition element of U(VI) to U(V) which plays the role of electron acceptor.

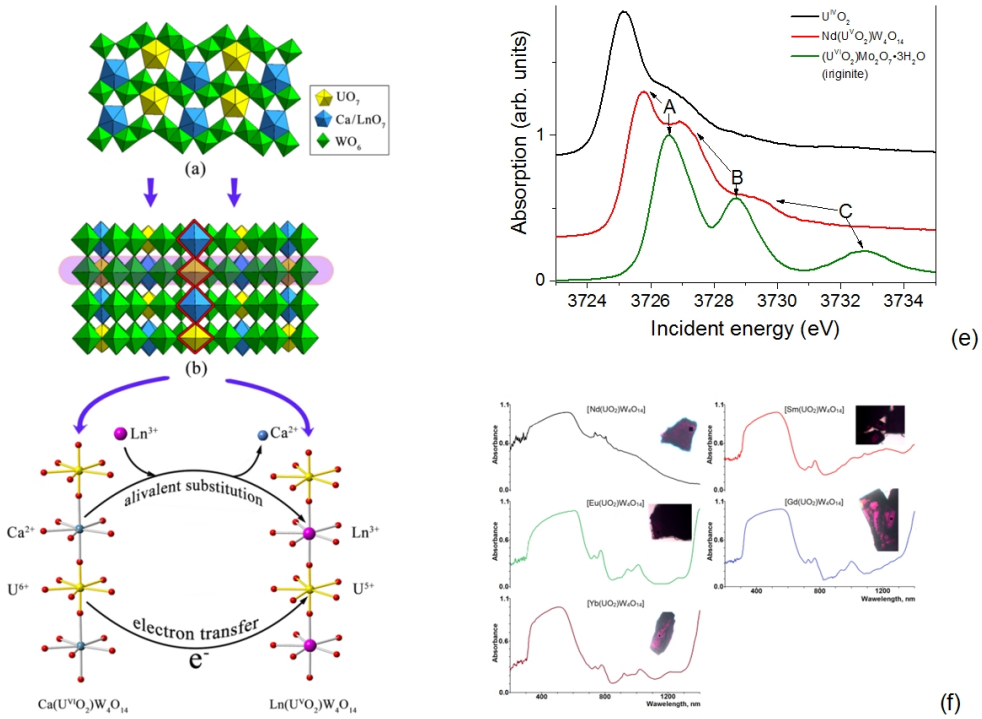

Fig. 63: (a) The polyhedral presentation of the three-dimensional framework in the isostructural *Ln*($U^{V}O_2$)W_4O_{14} and Ca($U^{VI}O_2$)W_4O_{14} compounds. Legends: The green and yellow colours are WO_6 and UO_7 polyhedra, respectively. The blue colour is CaO_7 or *Ln*O_7 in Ca($U^{VI}O_2$)W_4O_{14} or *Ln*($U^{V}O_2$)W_4O_{14}. (b) The framework can be subdivided into iriginite-type layers. (c, d) Representation of the charge-compensation mechanism when Ca^{2+} ions are substituted in the host phase of Ca($U^{VI}O_2$)W_4O_{14} with Ln^{3+} ions to result in *Ln*($U^{V}O_2$)W_4O_{14}. (e) U M_4-edge HR-XANES spectra of UO_2, Nd($U^{V}O_2$)W_4O_{14} and iriginite. (f) UV-vis-NIR absorption spectra and photographs of some *Ln*($U^{V}O_2$)W_4O_{14} members.

Conclusion

We demonstrated that it is possible to stabilize pentavalent uranium in complex oxides using different methods. Although both described experimental methods have no direct relevance for the processes and conditions of a future repository, the knowledge of mechanisms which can lead to a stable U(V) bearing phase and the range of its stability field could be of relevance for the long-term safety consideration and the modeling of a possible disposal site. Particularly, as recent works on systems which are more relevant for repository conditions[13-18] show that pentavalent uranium appears to play a more important role in natural and technical systems than previously assumed.

References

[1] Navrotsky, A.; Shvareva, T.; Guo, X.: In Burns, P.C. & Sigmon, G. (Eds.): Uranium-Cradle to Grave. *Min. Assoc. Can. Short Course* 43 (**2013**) 147-164.

[2] Morss, L.R.; Edelstein, N.M.; Fuger, J.: The chemistry of the actinide and transactinide elements. 4th ed. 2010, Dordrecht: Springer, Vol. 6 (**2010**).

[3]. MacDonald, M.R. et al.: *J. Amer. Chem. Soc.* 135(36) (**2013**) 13310-13313.

[4] Meyer, G. and Morss, L.R.: Topics in f-element chemistry. Dordrecht ; Boston: Kluwer Academic. XVI (**1991**) 367 p.

[5] Stritzinger, J.T. et al: *Inorg. Chem.* 53(10) (**2014**) 5294-5299.

[6] Rundle, R.E. et al.: *J. Am. Chem. Soc.* 70(1) (**1948**) 99-105.

[7] Hoekstra, H.R.; Siegel, S.; Gallagher, F.X.: *J. Inorg. Nucl. Chem.* 32(10) (**1970**) 3237-3248.

[8] Burns, P.C.; Ewing, R.C.; Hawthorne, F.C.: *Can. Mineral.* 35 (**1997**) 1551-1570.

[9] Allen, G.C.; Tempest, P.A.: *Proc. R. Soc. Lond. A Math. Phys. Sci,* 406(1831) (**1986**) 325---325.

[10] Brincat, N.A. et al.: *Dalton Trans.* 44(6) (**2015**) 2613-2622.

[11] Zhang, F.X. et al.: *J. Solid State Chem.* 213(0) (**2014**) 110-115.

[12] Serezhkin, V.; Efremov, V.; Trunov, V.: *Geokhim.* 13(19) (**1981**).

[13] Schindler, M.; Ilton, E.S.: In Burns, P.C. & Sigmon, G. (Eds.): Uranium-Cradle to Grave. *Min. Assoc. Can. Short Course* 43 (**2013**) 203-253.

[14] Kvashnina, K.O. et al., *Phys. Rev. Lett.*. 111(25) (**2013**).

[15] Garrido, F., et al., *Inorg. Chem.* 45(20) (**2006**) 8408-8413.

[16] Geng, H.Y. et al.: *Phys. Rev. B* 77(18) (**2008**).

[17] Cooper, M.W.D. et al.: *J. Nucl. Mater.* 443(1-3) (**2013**) 236-241.

[18] Kerisit, S., Liu, C.: *J. Phys. Chem. A* 117(30) (**2013**) 6421-6432.

6.17. Np^{IV} and Np^{VI} phase formation as a result of complex redox behaviour within aquatic Np-Se oxo-systems

E.M. Langer[1], O. Walter[2], E.V. Alekseev[1]

[1]Forschungszentrum Jülich GmbH, Institute of Energy and Climate Research – IEK-6: Nuclear Waste Management and Reactor Safety, 52425 Jülich, Germany

[2]European Commission, Directorate for Nuclear Safety and Security, Joint Research Centre, 76125 Karlsruhe, Germany

Corresponding author: e.alekseev@fz-juelich.de

Introduction

Neptunium shows a rich chemistry stably adopting a wide variety of oxidation states, ranging from +III to +VII, both in solutions as well as in solids. The variety of electronic structures is manifold due to the presence and availability of 5*f* orbitals.

Np occurs as a byproduct within the ^{235}U fuel cycle and the isotope ^{237}Np is considered as one of the most challenging actinides for final deep geologic waste disposal.[1,2] Reasons for this are the combination of a long half-life of 2.14×10^6 years, relatively weak complexing ability and a high solubility for compounds containing neptunyl ions resulting in a high mobility within the environment.[1-3] Next to Np, ^{79}Se is also considered crucial for the safe assessment of long-term nuclear waste disposal.[4] The combination of high radiotoxicity, geochemical mobility and a long half-life (3.27×10^5 years[5]) make ^{79}Se one of the radionuclides of greatest environmental impact.[6] The co-presence of these two elements within spent nuclear fuel makes it necessary to understand the fundamental reactions within these systems on a molecular level scale.

In solution, pentavalent Np is often erroneously considered to be the only viable oxidation state for Np in water with dissolved oxygen. This largely relies on the fact that comproportionation of Np^{IV} and Np^{VI} to Np^{V} is predicted due to standard reduction potentials.[7] This has however been proven wrong by many studies in which high concentrations, temperature influence, low pH and strong complexants all alter this equilibrium.[7-9] Disproportionation of Np^{V} into Np^{IV} and Np^{VI} in strong acidic conditions has been shown to be essential in Np^{V} chemistry.[10, 11]

Challenging handling issues and low availability of appropriate labs for transuranium elements, have led to thorium and uranium being used as structural surrogates. The chemical behaviour however can vary distinctly due to the different electronic configurations of the present 5*f* electrons between the surrogate systems and the real systems. In context of the GENTLE project funded by the European Commission, it was possible to conduct experiments in labs specifically designed to handle transuranium materials at JRC Karlsruhe (formerly known as ITU). Investigations in line of previous work conducted in the U-Se-O and Th-Se-O systems were transferred to the Np-Se-O system starting with very simple precipitation experiments investigating the influence of the initial oxidation state of Se on precipitate formation.

Experimental Setup and Procedure

Precipitation experiments were conducted utilizing a Np^{V} stock solution, alkali nitrates (K, Rb, and Cs), selenium dioxide and selenic acid. Hereby the influence of the initial oxidation state of Se was of keen interest. Two sets of experiments were carried out: the first set with Se in

initial oxidation state +IV (SeO_2) and the second with Se in initial oxidation state +VI (H_2SeO_4). The solutions were left to evaporate in air under slightly under-pressurized glove box conditions. Shortly before the majority of water evaporated, the precipitation containers were sealed with a lid, to reduce the crystallization speed for the final evaporation.
Structure determination was achieved by utilizing single crystal X-ray diffraction. Bond valence sum calculations and coordination behaviour was analyzed to validate the structure and to address the proposed oxidation states of the elements within the obtained phases.

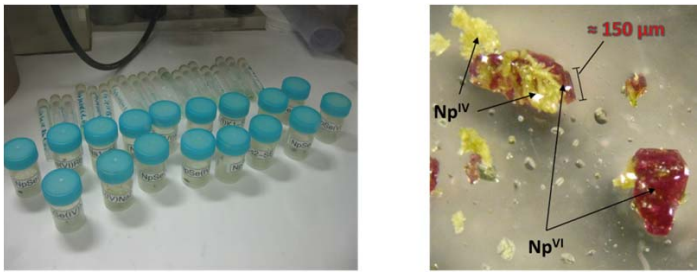

Fig. 64: Slow evaporation experiments. Left shows the whole set of experiments and the right shows an exemplary photo for the simultaneous formation of Np^{IV} and Np^{VI} phases. Hereby the former is visible as the yellow-green $Rb_{4-x}[Np^{IV}(SeO_3)_{4-x}(HSeO_3)_x](H_2O)$ and the latter as ruby-red $Rb(Np^{VI}O_2)(NO_3)_3$[12]

Results

The experimental regimes with different initial selenium valence show distinctly different results. Using Se^{IV} in the initial solution resulted in Np^{IV} selenites (Se^{IV}) and surprisingly using Se^{VI} resulted in Np^{VI} selenates (Se^{VI}).

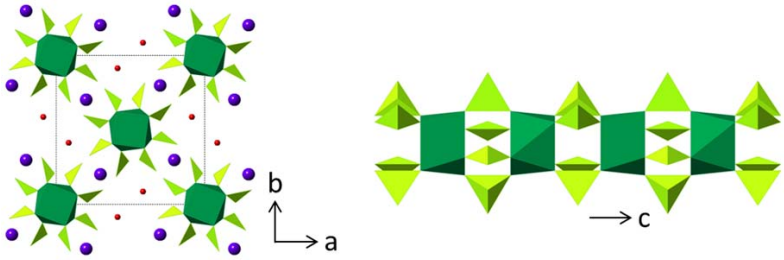

Fig. 65: $A_{4-x}[Np(SeO_3)_{4-x}(HSeO_3)_x](H_2O)$ (A = K, Rb). The left shows a top view parallel to [001] with square antiprismatic NpO_8 polyhedra in dark green, trigonal pyramidal SeO_3 in light green, alkali metal (K, Rb) in purple and water in red. The one-dimensional chains of $[Np(SeO_3)_{4-x}(HSeO_3)_x]^{(4-x)-}$ are shown on the right.

Neptunium Selenites

The experiments with selenium in initial oxidation state +IV resulted in the formation of Np^{IV} selenites and simultaneously in Np^{VI} nitrates. Fig. 64 shows an exemplary photo of the simultaneous presence of Np^{IV} and Np^{VI} indicated by the different colours, hereby yellow-green is the Np^{IV} phase and ruby-red the Np^{VI} phase. The structure of these selenites $A_{4-x}[Np(SeO_3)_{4-x}(HSeO_3)_x](H_2O)$ (A = K, Rb) can be described as one-dimensional chain

structures of NpO_8 square antiprisms connected by four selenite trigonal pyramids (Fig. 65). A similar structural coordination has previously been reported for Ce, Np and Pu iodates.[8, 13] The structure is stabilized by interspace alkali cations acting as counter cations. It can be assumed that the stereochemically active lone pair of electrons present atop the selenite trigonal pyramid is also acting as a stabilizing factor.

Neptunium Selenates

In contrast to the experiments with Se^{IV}, the Se^{VI} experiments did not yield in Np^{IV} and Np^{VI}; it only yielded in Np^{VI}. Four novel neptunyl selenate phases were obtained within this set of experiments: $K(H_3O)[(NpO_2)_2(SeO_4)_3(H_2O)_2]\cdot(H_2O)_{3.5}$, $Rb_2[(NpO_2)_2(SeO_4)_3(H_2O)_2]\cdot(H_2O)_4$, $Cs_2[(NpO_2)_2SeO_4)_3]$ and $K_6(H_3O)_3[(NpO_2)_9(SeO_4)_{13.5}(H_2O)_6]\cdot(H_2O)_{15}$ (Fig. 66). To our knowledge, this was the first report of Np^{VI} selenates to date.

All four phases show distinctive two-dimensional layered structures. The first three show monolayer structures, whereas the last shows a quasi-double-layer structure. The first two phases have a strong structural resemblance as the layers are found to be orientational geometric isomers. The interspace between the layers is filled with alkali metal cations, hydronium ions and/or water molecules. This is necessary to compensate the effective charges of the single layers. The determination of hydrogen positions cannot be determined with standard X-ray diffraction methods, making it difficult to differentiate hydronium and water molecules precisely, the presence can however be indicated by bond valence sums and due to charge balance considerations.

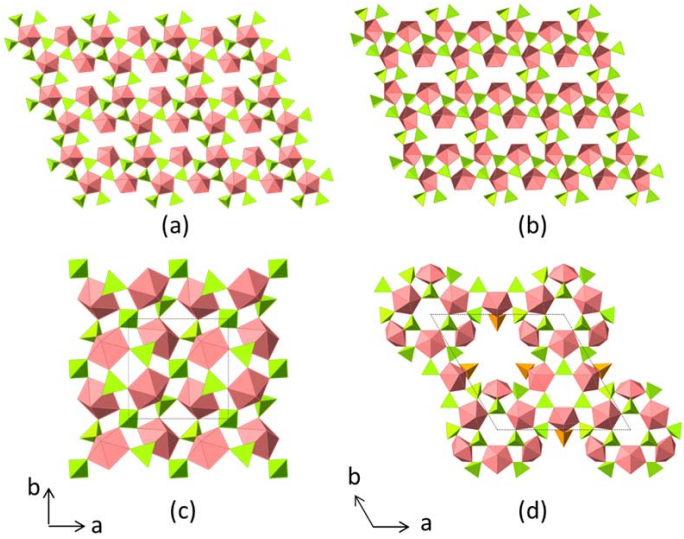

Fig. 66: Two-dimensional sheet layers of (a) $K(H_3O)[(NpO_2)_2(SeO_4)_3(H_2O)_2]\cdot(H_2O)_{3.5}$ (parallel to the (0 1 0) plane), (b) $Rb_2[(NpO_2)_2(SeO_4)_3(H_2O)_2]\cdot(H_2O)_4$ (parallel to the (1 0 -1) plane), (c) $Cs_2[(NpO_2)_2SeO_4)_3]$ and (d) $K_6(H_3O)_3$ $[(NpO_2)_9(SeO_4)_{13.5}(H_2O)_6]\cdot(H_2O)_{15}$. Hereby the NpO_7 pentagonal bipyramids are depicted in rose and the SeO_4 tetrahedra in light green. In (d) the orange tetrahedra show partially occupied selenate tetrahedra via which the two-layers are quasi-connected.

All layers are based upon NpO_7 pentagonal bipyramids vertex sharing with selenate tetrahedra to form two-dimensional sheets. Different connection patterns can be distinguished by a topologic description, which allows a systematic classification of 0D, 1D and 2D structures.
For three of the above mentioned selenates, uranium analogs exist. Hereby the $Cs_2[(NpO_2)_2SeO_4)_3]$ analog was not reported to date, but prepared in-house. Only for the more complex double layer structure no uranium analog has been found to date.

Discussion

The results obtained from the slow evaporation experiments show a very strong dependence on the initial oxidation state of Se. The addition of Se^{IV} in form of SeO_2 resulted in Np^{IV} selenites as well as Np^{VI} nitrates. This kinetically driven phenomenon can be explained by the disproportionation of Np^{V} in acidic conditions, first reported by Sjoblom and Hindman in the 1950's.[10]

$$2\,[NpO_2]^+ + 4\,H^+ \;\rightleftharpoons\; Np^{4+} + \,[NpO_2]^{2+} + 2\,H_2O \quad (I)$$

The Np^{IV} selenites precipitate first due to their expected lower solubility compared to corresponding nitrates. In the later process, with decreasing solution volumes and hence higher super-saturations, also the present Np^{VI} precipitates in form of nitrates.
In case of initial Se^{VI} being used, the first ever reported Np^{VI} selenate phases have been stabilized. To best of our knowledge, only one Np^{VI} oxo-selenium compound has been reported: $(NpO_2)(SeO_3)$[7], a neptunyl selenite. It was prepared by hydrothermal methods and formed simultaneously with the Np^{IV} bearing $Np(SeO_3)_2$, this concurrent precipitation being explained by the disproportionation of Np^{V}. The formation of several different selenates, as well as the inability to find any Np^{IV} or Np^{V} species, indicates at a complete oxidation of the initial Np^{V} within the solution (reaction (II)[14]). Possible reaction pathways could be:

Oxidation: $$2\,[NpO_2]^+ \;\rightleftharpoons\; [NpO_2]^{2+} + 2\,e^- \qquad (II) \qquad E^0 = -1.159\,V\,[14]$$

Reduction: $$NO_3^- + 3\,H^+ + 2\,e^- \rightleftharpoons\; HNO_2 + H_2O \qquad (III) \qquad E^0 = +0.934\,V\,[15]$$

$$SeO_4^{2-} + 2\,H^+ + 2\,e^- \rightleftharpoons\; SeO_3^{2-} + H_2O \qquad (IV) \qquad E^0 = +0.880\,V\,[16]$$

The most likely source for oxidation is the presence of the high nitrate concentration (reaction (III)[15]), present due to the addition of alkali nitrates and the Np^{V} solution being based on nitric acid. Oxidation via reduction of Se^{VI} to Se^{IV} (reaction (IV)[16]) seems unlikely, as no selenites were found within the according experiments.
As previously described, the 1D structural units of the obtained neptunium selenites show distinct similarities to neptunium and plutonium iodates, indicating a possible coprecipitation of these phases. This can especially be of importance for the safe assessment of nuclear waste, as iodine in form of the long-lived fission product ^{129}I ($t_{1/2}$ 1.6 x 10^7 years) is, similar to ^{79}Se, considered a radionuclide of greatest environmental impact within spent nuclear fuel.[6]
The structural behaviour of the reported structures is in accordance with expected behaviour for potential Np^{VI} selenates. The neptunyl ion is well known to cause two-dimensional layered structures, similar to U^{VI}.
The absence of cation-cation interactions within these structures is also expectable. The O-Np bond in Np^{VI} is stronger as in the weaker Np^{V}, where this permits linkages of the neptunyl polyhedra through the neptunyl ion oxygen atom.[17]

Conclusion

Two aqueous Np-Se systems have been investigated. Six novel alkali neptunium oxo-selenium phases with different oxidation states of Np and Se were prepared via slow evaporation experiments. Experiments conducted with Se in the initial oxidation state Se^{IV} lead to the formation of Np^{IV} selenites and simultaneously Np^{VI} nitrates due to disproportionation of Np^{V} in acidic media. It was possible to prepare the first Np^{VI} selenates to date by using initial Se^{VI} in form of selenic acid. Hereby the Np^{V} oxidation to Np^{VI} was addressed due to the presence of a high nitrate concentration. A possible oxidation via reduction of selenium was rejected as no selenite presence was detected. Bond-valence sum calculations and coordination behaviour support the oxidation state assignments.
The structures of the reported Np^{VI} selenates resemble the expected structural behaviour similar to the U^{VI} analogs. This can be seen due to the existence of two previously reported isostructural uranyl bearing phases and one uranyl isostructural phase we recently found in-house. The reaction pathway however was very much unexpected and does not resemble the chemical behaviour of U^{V}/U^{VI} due to the big differences between Np and U redox behaviour. The unexpected behaviour of Np within this very simple system shows the necessity to further investigate this system.
To further understand the influence of the nitrate, experiments on the basis of alkali chlorides instead of nitrates have been prepared and are currently under investigation. Furthermore investigations at higher pH range (neutral to slightly basic) and at less oxidizing/reducing conditions are planned.

Acknowledgements

We are grateful for the support provided by the European Commission in funding the experiments under the scheme of GENTLE SRE Funding at JRC Karlsruhe, Directorate G (former Institute for Transuranium Elements, ITU). The work has additionally been supported by the Helmholtz Association within the VH-NG-815 grant.

References

[1] Kaszuba, J.P.; Runde, W.H.: *Environ. Sci. Technol.* (**1999**) 4427-4433.
[2] Silva, R.J.; Nitsche, H.: *Radiochim. Acta* (**1995**) 396.
[3] Antonio, M.R.; Soderholm, L., Williams, C.W., et al.: *Radiochim. Acta* (**2001**) 17.
[4] Barney, G.S.; Wood, B.J.: (**1980**) p. Medium: ED.
[5] Jörg, G.; Bühnemann, R.; Hollas, S. et al.: *Appl. Radiat. Isot.* (**2010**) 2339-2351.
[6] Bruno, J.; Ewing, R.C.: *Elements* (**2006**) 343-349.
[7] Diefenbach, K.; Lin, J.; Cross, J.N. et al.: *Inorg. Chem.* (**2014**) 7154-7159.
[8] Bray, T.H.; Ling, J.; Choi, E.S. et al.: *Inorg. Chem.* (**2007**) 3663-3668.
[9] Jin, G.B.: *Inorg. Chem.* (**2013**) 12317-12319.
[10] Sjoblom, R.; Hindman, J.: *J. Am. Chem. Soc.* (**1951**) 1744-1751.
[11] Sarsfield, M.J.; Taylor, R.J.; Maher, C.J.: *Radiochim. Acta* (**2007**) 677-682.
[12] Alcock, N.W.; Roberts, M.M.; Brown, D.: *J. Chem. Soc., Dalton Trans*. (**1982**) 33-36.
[13] Cromer, D.; Larson, A.: *Acta Cryst.* (**1956**) 1015-1018.
[14] Edelstein, N.M.; Fuger, J.; Morss, L.R.: The Chemistry of the Actinide and Transactinide Elements, (**2010**).
[15] Vanysek, P.: CRC handbook of chemistry and physics (**1998**).
[16] Bouroushian, M.: Electrochemistry of Metal Chalcogenides. Springer Berlin, Heidelberg (**2010**).
[17] Forbes, T.Z.; Burns, P.C.: *J. Solid State Chem.* (**2007**) 106-112.

6.18. Atomistic modeling in nuclear waste management

P.M. Kowalski[1], G. Beridze[1], Y. Ji[1], Y. Li[1], G.L. Murphy[2], Z. Zhang[2], B.J. Kennedy[3], E. Alekseev[1], B. Xiao[1]

[1]Forschungszentrum Jülich GmbH, Institute of Energy and Climate Research – IEK-6: Nuclear Waste Management and Reactor Safety, 52425 Jülich, Germany

[2]Australian Nuclear Science and Technology Organisation, Lucas Heights, New South Wales 2234, Australia

[3]School of Chemistry, The University of Sydney, Sydney, New South Wales 2006, Australia

Corresponding author: p.kowalski@fz-juelich.de

Abstract

Over the last two decades atomistic modeling techniques become popular research tools in various research fields, including research on nuclear materials. Having excellent supercomputing infrastructure available at Forschungszentrum Jülich GmbH we apply the state of the art methods of computational chemistry and materials science to the research on nuclear waste materials, including the ceramic waste forms and the actinide-bearing secondary phases. Because f-elements are computationally challenging, besides strictly applied research, we are involved in the improvement of the description of strongly correlated f-electrons and the force-fields for molecular dynamics simulations. We show here that a combination of the fundamental research on computation of f-elements with the applied investigation that consists of derivation of the important structural, energetics and thermodynamic parameters, having access to the new experimental data, results in superior characterization of nuclear materials and allows for tackling scientific questions that without such a joint investigation could not be easily answered. Such an integrated approach to the research enhanced the capability of the structural research performed at IEK-6.

Introduction

The computational methods of quantum chemistry and materials science have been successfully applied in various research fields in order to study the atomic-scale properties of materials of chemically complex compositions.[1] They are also frequently used in nuclear waste management-related research.[2] Here we discuss the selected applications of atomistic modeling to investigation of the materials that are investigated at IEK-6 and by NUSAFE partners with the strong emphasis on the cases where modeling side contribution was crucial to obtain full characterization of the investigated systems and to correctly interpret the experimental data. The discussed materials include the ceramic waste forms (phosphates and zirconates), secondary phases and new actinide-compounds. We discuss the atomic level characterization of the structural, thermodynamic, elastic and energetic parameters of these compounds. Last, but not least, we demonstrate the fundamental knowledge gain obtained from joint atomistic modeling and experimental investigation that results in significant improvement of the modeling techniques.

Materials and Methods

Although the Density Functional Theory (DFT) is the work-horse of the computational materials science,[1] its applicability to actinide- and lanthanide-bearing materials is

questionable. This is because the exchange correlation functionals have been designed to reproduce properties of weakly correlated systems (homogeneous electron gas approximation) or light elements, and should not be expected to perform equally well for heavy elements that contain strongly correlated electrons.

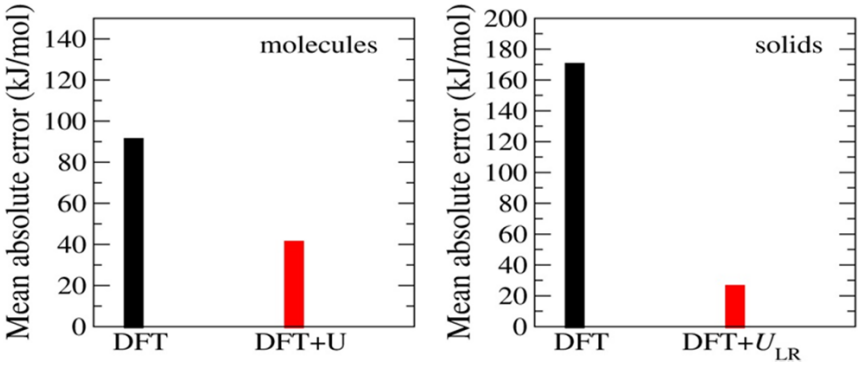

Fig. 67: The mean absolute error of the reaction enthalpies derived using DFT (PBE) and DFT+*U* methods with the Hubbard *U* parameter derived using the linear response method of [11]. The reference data are experimental measurements.[5] Left and right panels show results for molecular and solid compounds, respectively.

This shortcoming is visible for AnO_2 solids (*An* = U, Np and Pu) which are predicted to be metals, while these materials are insulators,[3] and in the overestimation of the reaction enthalpies for actinide-bearing molecular complexes,[4] to name all but two cases. We thus extensively benchmarked and subsequently applied the DFT+U method, with the Hubbard U parameter derived *ab initio* and derived a computational setup which results in significantly improved description of structures and energetics of actinide- and lanthanide-bearing compounds.[2,5,6] In Fig. 67 we show the improvement over DFT obtained for thermochemistry of *An*-bearing molecular and solid compounds. The key to the excellent result is to consider variation of the Hubbard U parameter between different actinides (lanthanides), which is usually omitted by others. The studies of ceramic materials revealed that the DFT calculations performed using pseudopotentials with f-electrons frozen in the core can result in a better agreement with the DFT+U method than DFT when f-electrons are treated explicitly.[5,6] Because such an approach is computationally very stable we used it in subsequent calculations of some materials properties. The obtained *ab initio* results were used to improve the force-fields for molecular-dynamics simulations (see [7]).

The *ab initio* calculations were performed with quantum-espresso DFT plane wave code (www.quantum-espresso.org), with ultrasoft pseudopotentials to represent the core electrons.[8] The energy cutoff was usually set at 50 Ry and we used the PBE[9] and PBEsol[10] generalized gradient approximation (GGA) exchange-correlation functionals with the former resulting in better energetics and the later in improved structures. The Hubbard U parameter for DFT+U method was determined self-consistently for each specific compound using the linear response[11] or cRPA methods[12].

Results and Discussion

Characterization of phosphate-type solid solutions

One important aspect of a nuclear waste form material is its ability to form a stable, homogeneous solid solution with radionuclides. Therefore, various structural, thermochemical and thermodynamic properties have been experimentally investigated within the BMBF "Conditioning" project by IEK-6 and co-partners (cf 6.14). Having access to fresh measurements on phosphate systems in the last four years we have significantly contributed to this research with atomistic modeling. The joint investigation includes the structural characterization,[6,13] the thermochemistry,[14] derivation of the thermodynamic parameters such as heat capacities,[15] the thermal conductivities[16] and the excess enthalpies of mixing,[17,18] investigation of the radiation damage resistance[7] and the elastic parameters[16,18,19]. All these joint studies resulted in improved characterization of the investigated materials and additional knowledge gain that could not be obtained from independent experimental or modeling studies.

In Fig. 68 we compare the derived and measured Young's modulus of the $La_{1-x}Eu_xPO_4$ monazite-type solid solution. The atomistic simulations were performed with the aid of special quasi-random structures that resemble the homogeneous solid solutions and the perfect match of the simulated to the experimental data provided indirect confirmation of the homogeneity of the solid solution, which could be questionable from the alone *ab initio* studies of thermodynamic parameters of solid solutions. On the other hand, good prediction of the elastic properties allows for modeling of the excess properties of solid solutions using strain energy-based model (cf. 6.14).

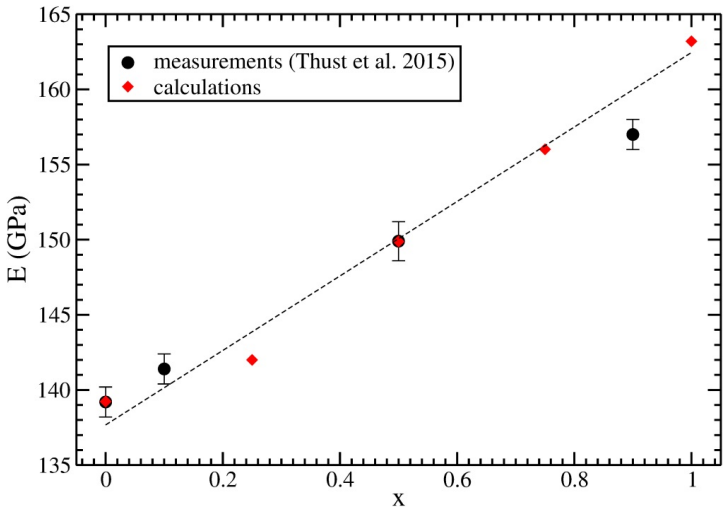

Fig. 68: The Young's modulus for $La_{1-x}Eu_xPO_4$ solid solution. The points represent the simulated values[19] (red) and measurements (black) of Thust et al.[26]. The solid dashed line is plotted to show the trend.

Table 5: The thermal conductivity computed and measured for xenotime-type ceramics.[16]

Composition	Calculated	Measured
$ErPO_4$	10.51	12.01
$YbPO_4$	11.58	11.71
$LuPO_4$	11.75	11.97

The elastic properties could be used to deliver information on the thermal conductivities of the investigated materials using for instance Slack model for thermal conductivity.[20] In Table 5. we compare the computed and measured thermal conductivities for selected xenotime-type ceramics ($LnPO_4$ phosphates for *Ln* = Tb,...,Lu). Because of the usage of well tested computational method with simulations we are able to produce results with the experimental level accuracy. This is an important test, showing that simulations can successfully deliver information of thermal properties of materials, which we plan to subsequently explore in the follow up studies.

Energetics of defects formation in pyrochlore-type ceramics

Pyrochlore-type ceramics are of interest for immobilization of actinides because certain pyrochlores under irradiation transform to a disordered fluorite, which is a solid phase, rather than becoming amorphous.[21] However, the origin of this order-disorder transition of selected pyrochlores is not well understood. The determination of the energetics of simple defects formation in pyrochlore is a first step in a quest to understand the process. Our *ab initio* calculations of cation-antisite and anion Frenkel pair defect formation energies in pyrochlores indicate that the formation of defect fluorite is associated with small or even negative anion Frenkel pair defect formation energies,[22] which is different from the conclusion of other studies (e.g. [23]) where cation antiside defects are considered the drivers of the transition. As illustrated in Table 6 our calculations are able to reproduce the experimentally measured O-diffusion barriers in selected pyrochlores, which confirms that we catch correctly the energetics of the defect formation and diffusion.

Table 6: The energy barriers (in eV) for oxygen diffusion in pyrochlore-type ceramics (all data are from [27] and references hereafter).

Composition	Activation Energy	Measured O diffusion barrier
$Nd_2Zr_2O_7$	0.90	0.76-0.84
$Gd_2Zr_2O_7$	0.58	0.73-0.90
$Er_2Ti_2O_7$	0.73	0.93

Solid state chemistry of actinides

After testing the *ab initio* methods for *An*-bearing compounds we applied them to the real systems investigated at IEK-6 and partner institutions. One example of a successful research in the investigation of the O-defects driven phase transition in the $USrO_4$ system performed in collaboration with scientists from ANSTO and University of Sydney.[24] It has been experimentally observed that under introduction of vacancies the structure of $USrO_4$ transforms from orthorhombic to rhombohedral phase. The computed energetics of the defect

formation in this system, illustrated in Fig. 69, shows that defects stabilize the rhombohedral $USrO_4$ compound and the subsequent electronic structure analysis indicates that formation of U(V) species in $USrO_{4-x}$ is responsible for this behaviour.

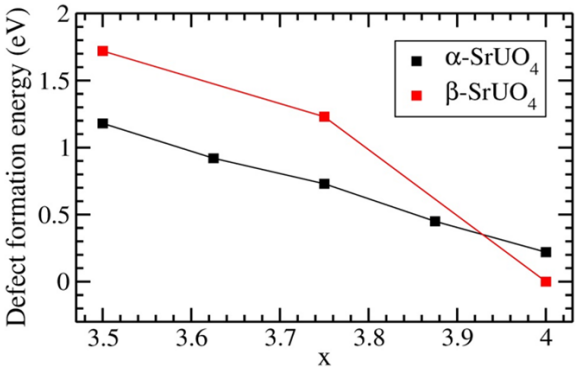

Fig. 69 The vacancy formation energies in $USrO_x$ system.[25]

In general, atomistic modeling tools are very useful not only for the interpretation of experimental data, but for the extension of understanding of the materials behaviour beyond the experimental conditions. On regular basis we deliver the information on the relative phase stability and phase diagrams. One such example is the phase diagram of $ThMo_2O_7$ system, shown in Fig. 70, which allowed for understanding of the formation of the HP-orthorhombic phase under experimental conditions (P = 3.5 GPa, T = 1200 K) and prediction of the formation of other phases at specific temperatures and pressures.[25] With the subsequent studies of incorporation and stability of U in different oxide-phases – studies related to spent nuclear fuel – we aim into improvement and development of the force-fields for molecular dynamics simulations that would allow for large scale simulation of kinetically driven processes such as diffusion, corrosion and dissolution in these systems.

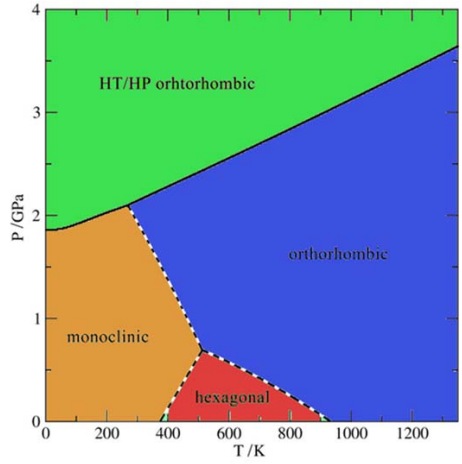

Fig. 70: The phase diagram of $ThMo_2O_8$ system.[25]

Conclusions

We have presented a selection of our atomistic modeling studies that contributed to characterization of nuclear waste-related materials. Our experience shows that with an appropriate choice of the computational method the structural, thermochemical, thermodynamic, elastic, defect formation and radiation damage properties of nuclear waste materials can be accurately computed. On many occasions joint experimental and modeling studies resulted in a superior characterization of the investigated materials that could not be achieved by independent experimental or atomistic modeling studies. Moreover, the broader impact and importance to scientific community of our studies are reflected by the fact that the studies on monazite-type ceramics[6] and $ThMo_2O_8$ system[25] were recognized as highlight stories with cover pages in well-respected journals. We thus expect that the popularity of the atomistic modeling in the research on nuclear waste materials will increase in the future and that jointly with the experimental efforts this research will bring new insights into understanding of nuclear waste related-materials.

Acknowledgments

We acknowledge the computing time on RWTH Aachen and Forschungszentrum Jülich GmbH supercomputers, awarded through Jülich-Aachen research alliance (JARA-HPC).

References

[1] Jahn, S.; Kowalski, P.M.: *Rev. Mineral. Geochem.* 78 (**2014**) 691-743.
[2] Chrones, A.; Rushton, M.J.D.; Jiang, C.; Tsoukalas, L.H.: *J. Nucl. Mater.* 441 (**2013**) 29-39.
[3] Wen, X. D.; Martin R. L.; Henderson T. M.; Scueria G. E.: *Chem. Rev.* 113 (**2013**) 1063-1096.
[4] Shamov, G.A.; Schreckenbach, G.; Vo, T.N.: *Chem. Eur. J.* 13 (**2007**) 4932-4947.
[5] Beridze, G.; Kowalski, P.M.: *J. Phys. Chem. A,* 118 (**2014**) 11797-11810.
[6] Blanca-Romero, A.; Kowalski, P.M.; Beridze, G.; Schlenz, H.; Bosbach, D.: *J. Comput. Chem.* 35 (**2014**) 1339-1346.
[7] Ji, Y.; Kowalski, P.M.; Neumeier, S.; Deismann, G.; Kulriya, P.K.; Gale, J.D.: *Nucl. Instrum. Meth. B.* 393 (**2017**) 54-58.
[8] Vanderbilt, D.: *Phys. Rev. B* 41 (**1990**) 7892-7895.
[9] Perdew, J.P.; Burke, K.; Ernzerhof, M.: *Phys. Rev. Lett.* 77 (**1996**) 3865-3868.
[10] Perdew, J.P.; Ruzsinszky, A.; Csonka, G.I.; Vydrov, O.A.; Scuseria, G E.; Constantin, L.A.; Zhou, X.; Burke, K.: *Phys. Rev. Lett.* 100 (**2008**) 136406.
[11] Cococcioni, M.; de Gironcoli, S.: *Phys. Rev. B* 71 (**2005**) 035105.
[12] Aryasetiawan, F.; Karlsson, K.; Jepsen, O.; Schönberger, U. *Phys. Rev. B* 74 (**2006**) 125106.
[13] Beridze G.; Birnie, A.; Koniski, S.; Ji, Y.; Kowalski, P.M.: *Prog. Nucl. Energ.* 92 (**2016**) 142-146.
[14] Finkeldei, S.; Kegler, Ph.; Kowalski, P.M.; Schreinemachers, C.; Brandt, F.; Bukaemskiy, A.A.; Vinograd, V.L.; Berdize, G.; Shelyug, A.; Navrotsky, A.; Bosbach, D.: *Acta Mater.* 125 (**2017**) 166-176.
[15] Kowalski, P. M.; Beridze, G.; Vinograd, V. L.; Bosbach, D.: *J. Nucl. Mater.* 464 (**2015**) 147-154.
[16] Ji, Y.; Beridze, G.; Kowalski, P.M.: *Energy Procedia* XX (**2017**) XX-XX.
[17] Li, Y.; Kowalski, P.M.; Blanca-Romero, A.; Vinograd, V.; Bosbach, D.: *J. Solid State Chem.* 220 (**2014**) 137-141.
[18] Kowalski, P.M.; Li, Y.: *J. Eur. Ceram. Soc.* 36 (**2016**) 2093-2096.
[19] Kowalski, P.M.; Ji, Y.; Li,Y.; Arinicheva, Y.; Beridze, G.; Neumeier, S.; Bukaemskiy, A.; Bosbach, D.: *Nucl. Instrum. Meth. B* 393 (**2017**) 68-72.
[20] Slack, G.A.: *J. Phys. Chem. Solids*. 34 (**1973**) 321-335.
[21] Ewing, R.C.; Weber, W.J.; Lian, J.: *J. Appl.Phys.* 95 (**2004**) 5949.
[22] Li, Y.; Kowalski, P.M.; Beridze G.; Birnie, A.; Finkeldei, S.; Bosbach, D.: *Scripta Mater.* 107 (**2015**) 18-21.
[23] Sickafus, K.E.; Minervini, L.; Grimes, R. W.; Valdez, J. A.; Ishimaru, M.; Li, F.; McClellan, K. J.; Hartmann, T.: *Science,* 289 (**2000**) 748–751.
[24] Murphy, G.L.; Kennedy, B.J.; Kimpton, J.A.; Gu, Q.; Johannessen, B.; Beridze, G.; Kowalski, P.M.; Bosbach, D.; Avdeev, M.; Zhang, Z.: *Inorg. Chem.* 55 (**2016**) 9329-9334.
[25] Xiao, B.; Kegler, Ph.; Gesing, T.M.; Robben, L.; Blanca-Romero, A.; Kowalski, P.M.; Li, Y.; Klepov, V.; Bosbach, D.; Alekseev, E.V.: *Chem. Eur. J.* 22 (**2016**) 946-958.
[26] Thust, A.; Arinicheva, Y.; Haussuehl, Y. E.; Bayarjagal, L.; Vogel, S. C.; Neumeier, S.; Winkler, B.: *J. Am. Ceram. Soc.* 98 (**2015**) 4016-4021.
[27] Li, Y.; Kowalski, P.M.: *J. Nucl. Mater. XX* (**2017**) XX-XX.

6.19. Joint atomistic modeling and experimental investigation of ceramic waste materials

P.M. Kowalski[1], G. Beridze[1], Y. Li[1], Y. Ji[1], S. Neumeier[1], N. Huittinen[2], H. Schlenz[1], Y. Arinicheva[1], S. Finkeldei[1], D. Bosbach[1].

[1]Forschungszentrum Jülich GmbH, Institute of Energy and Climate Research – IEK-6: Nuclear Waste Management and Reactor Safety, 52425 Jülich, Germany

[2]Helmholtz-Zentrum Dresden - Rossendorf, Institute of Resource Ecology, Bautzner Landstraße 400, 01328 Dresden, Germany

Corresponding author: p.kowalski@fz-juelich.de

Abstract

Ceramic waste forms have been considered as a potential radionuclide immobilization barrier in the prospective repository concepts. Because of this, materials such as phosphate- (monazite, xenotime and rhabdophane) or pyrochlore-type ceramics have been investigated at IEK-6 with the world-wide partners. Here we discuss the results of the investigation of the structural, thermochemical and thermodynamic parameters of these ceramics. In particular we discuss the importance of the atomistic modeling in probing the stability of solid solutions, disordering phenomena and formation of short-range ordering in these materials.

Introduction

Phosphate- (e.g. monazite) and zirconate- (e.g. pyrochlore) ceramics have been for long time considered as potential nuclear waste forms.[1,2] Because many properties that lead to radiation damage resistance enhancement in these materials have not been well characterized, IEK-6 performed extended investigation of these materials as part of the BMBF *"Conditioning"* project. We contributed to this research with the atomistic modeling and here we discuss the results of selected, successful joint atomistic modeling and experimental investigations of the materials properties that are important for the assessment of long-term stability of ceramic nuclear waste forms. In particular we discuss the derivation of the structural, thermochemical and thermodynamic parameters such as formation and excess mixing enthalpies, homogeneity of solid solutions and formation of short-range ordering. All the discussed parameters are important for the characterization of ceramic nuclear waste forms and some of the crucial information is only accessible by application of the atomistic simulations to interpret the experimental data.

Materials and Methods

Because of the strongly correlated nature of *f*-electrons that constitute lanthanide and actinide elements, for the applied, atomistic modeling studies we apply the DFT+*U* method with the Hubbard *U* parameter derived *ab initio*. Prior to application, we extensively benchmarked these methods on various molecular and solid systems, including phosphate-type ceramics.[3,4] The *ab initio* calculations were performed with Quantum-ESPRESSO DFT plane wave code (www.quantum-espresso.org), which uses ultrasoft pseudopotentials to represent core electrons.[5] The energy cutoff was set at 50 Ry. In these studies, along with the standard generalized gradient approximation (GGA) functionals, such as the PBE[6] and PBEsol[7], we used the DFT+*U* method, which utilizes a Hubbard model to account for a

strong on-site coulomb repulsion between *f*-electrons[8]. The Hubbard *U* parameter was determined self-consistently for each specific compound using the linear response[8] or cRPA methods[9]. The force-field calculations of the extended systems were performed using LAMMPS code (lammps.sandia.gov) with the force-fields (inter-atomic interactions) parameters fitted to reproduce the *ab initio* structural and energetics data.

Results and Discussion

Structural and thermochemical characterization of phosphate-type waste forms.

As a first step in atomistic modeling of ceramic nuclear waste forms we computed *ab inito* the structural and thermochemical parameters of monazite- and xenotime-type ceramics. We derived the lattice parameters and formation enthalpies and compared them to the available experimental data.[3,4] The comparison of the *Ln*-O bond lengths and the formation enthalpies from oxides are given in Fig. 71. We obtained excellent match to the measured bond length and formation enthalpies, which indicates that the selected atomistic modeling technique could be successfully applied to study the parameters and properties that have not been yet measured or if measured, require interpretation. The so computed properties include the heat capacities[10], the elastic moduli[11,12,13], the excess enthalpies of mixing[11,14] and the threshold displacement energies[15]. Some of these results are discussed in the next sections.

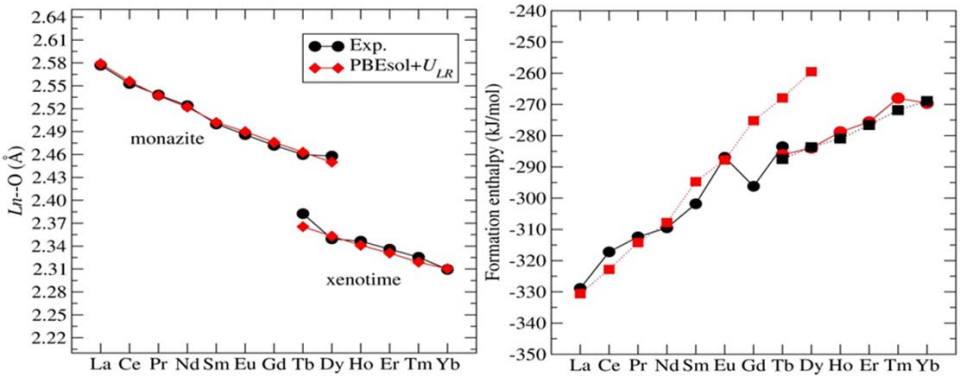

Fig. 71: Average *Ln*-O distance predicted by the DFT+*U* method with the Hubbard U parameter derived using the linear response method of [8], and measured experimentally. Right: the computed and measured formation enthalpies for these systems.

Excess enthalpies of mixing.

One important aspect of a nuclear waste form material is its ability to form a stable solid solution with radionuclides. The excess enthalpy of mixing H^E and the related Margules interaction parameter, *W*, are important indicators of the thermodynamic stability of a solid solution, because they drive the potential formation of the miscibility gap.[14] In case of regular solid solution, such as monazite-type solutions case, the enthalpy of mixing is given as $H^E = W$x(1-x).[15] The miscibility gap, indicating demixing and phases separation, forms if $W > 2RT$, where *R* is the gas constant and *T* is the temperature.[14] We have computed the interaction parameters for a series of $Ln_{1-x}(Ln,An)_xPO_4$ solid solutions and concluded that *W* [kJ/mol] = $0.618(\Delta V\ [cm^3/mol])^2$, where ΔV is the difference in volumes of the solution endmembers.[11,14] We found that this relationship is independent on lanthanide and actinide

substituting cations, which also indicates that lanthanides are good surrogates for investigation of the excess mixing properties of actinide-bearing monazites. Because the derived *ab initio W* parameters[14] for solutions such as $La_{1-x}Eu_xPO_4$ or $La_{1-x}Gd_xPO_4$ indicate that these solid solutions should not be thermodynamically stable for temperatures below 800K, we decided to investigate these systems further, using direct measurements (TRLFS, drop solution calorimetry) and theoretical considerations. Because TRLFS studies combined with atomistic modeling show homogeneity of these solid solutions ($La_{1-x}Gd_xPO_4$, see next section) in collaboration with Prof. Alexandra Navrotsky we obtained excess enthalpies of mixing for these systems.[16] Because the measured *W* parameters were about half the computed values, we derived an independent from *ab initio* simulations strain energy-based model that allows for computation of Margules interaction parameters using Young's moduli, *E*, and volumes *V* of endmembers.[11] We have shown that

$$W = \frac{E}{6V}\Delta V^2 \qquad (1)$$

This relationship explains the $W \sim \Delta V^2$ dependence deducted from the *ab initio* data and allows for understanding the discrepancy between the *ab initio* and experimental data. Because Young modulus is accurately derived by *ab initio* methods (see Kowalski et al., this volume), the cause of the discrepancy lies in the *ab initio* volumes, that are slightly off the experimental values (for La:Gd system $\Delta V(DFT) = 36$ Å^3, while $\Delta V(exp) = 26$ Å^3). The *ab* initio volumes, thus, when applied to Eq. 1 propagate into significant overestimation of the W parameters. As indicated in Fig. 72, when the experimental volumes are used instead, the Eq. 1 reproduces the excess enthalpy of mixing of $La_{1-x}Gd_xPO_4$ system that has been directly measured. The joint experimental and atomistic modeling investigation resulted thus is precise estimation of the Margules interaction parameters and construction of well justified and tested model for this parameter. The model indicates that the monazite-type solid solutions, including important from the nuclear waste management point of view $La_{1-x}Pu_xPO$# solid solution, are thermodynamically stable, i.e. there is no thermodynamical force affecting their stability in the long disposal time.

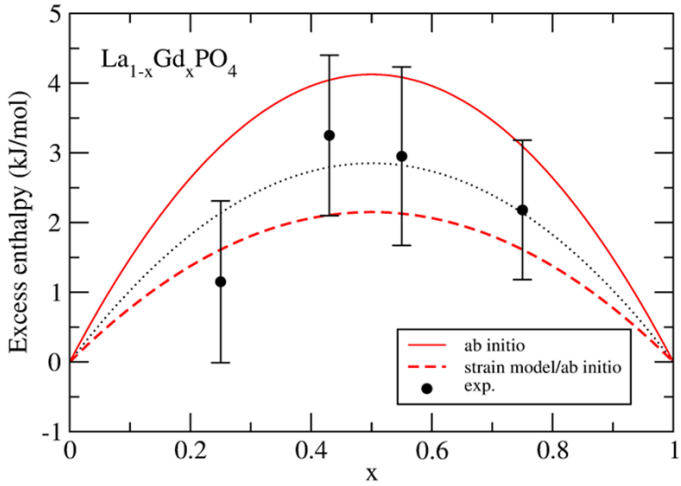

Fig. 72: The excess enthalpies of mixing for Gd:La monazite-type solid solution.[16]

Probing homogeneity of solid solutions: short-range ordering

The homogeneity of the monazite-type solid solutions have been demonstrated by a combination of different experimental techniques (TRLFS, calorimetry) and atomistic modeling.[17] The studies performed on the characterization of the monazite-type solid solutions indicate their homogeneous character and no apparent formation of the miscibility gap. The structural arrangements of the cations in a solid solution have been checked by the incorporation of Eu cations and TRLFS technique (laser fluorescence). The obtained profiles for $La_{1-x}Gd_xPO_4$ solid solutions, given in Fig. 73, are substantially broadened for the intermediate compositions, compared with the pure phases. The underlying origin of this behaviour was shown by atomistic simulations performed using force fields on large special quasi random structures. As illustrated in Figure 3., we found a good correlation between the broadening of the distribution of the Eu-O bond lengths and the broadening of the TRLFS profiles, which indirectly confirms homogeneous (not preferential) incorporation of the cations into the solid solution matrix, showing thus the homogeneity of the solid solution.

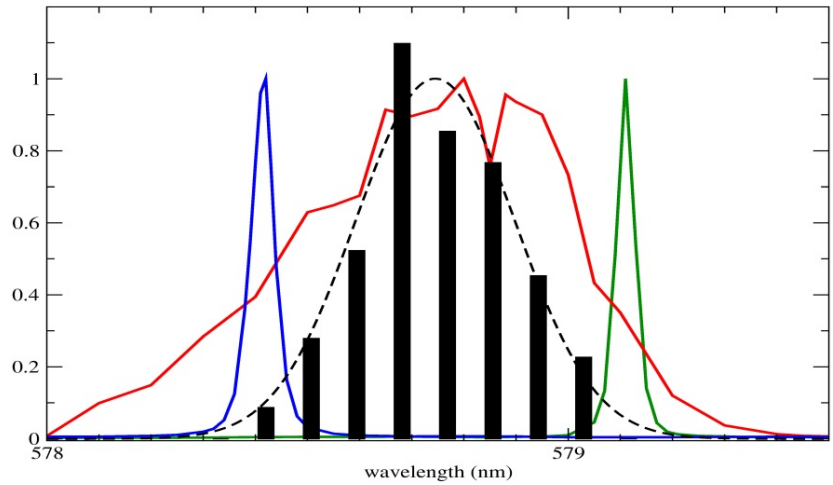

Fig. 73: The correlation between the distribution of the Eu-O bond-length and the measured TRLFS profiles for Gd:La monazite-type solid solutions.[17]

The double substitutions solid solutions with tetravalent actinides are also of interest for nuclear waste management. In these cases the substitution of tetravalent actinides (Th(IV) or U(IV)) is accompanied by substitution of M^{2+} cation (e.g. $CaThPO_4$). Because of the different charges of the substituting cations (4+ and 2+ vs. 3+) significant ordering tendency occurs in these systems. This results in computed ordered $CaThPO_4$ structure being the most stable endmember form. This is in contradiction to some experimental measurements of homogeneous solution of this phase[18] and large excess enthalpy of mixing[19] that could not be reconciled with synthesis of the relevant homogeneous solutions series. On the other hand, the calculated formation enthalpy of the ordered structure (H_f = 504 kJ/mol) matches much better the experimental value (H_f = 506 +/-10 kJ/mol,[20]) than the computed formation enthalpy of the disordered structure (H_f = 473 kJ/mol). This discrepancy shows that short-range ordering plays an important role in the structures with strong ordering tendencies.

Disordering in pyrochlore-type ceramics

The potential applications of pyrochlores in nuclear waste management comes from the fact that selected pyrochlores under irradiation, rather than becoming amorphous transfer to a disordered fluorite, which is a crystalline phase.[2] The disordering and partial ordering are thus important phenomena in pyrochlore-type ceramic waste forms. We have investigated this order-disorder transition in the $Nd_xZr_{1-x}O_{2-0.5x}$ system. In Finkeldei et al. (2017)[21] our computed formation enthalpies match very well the measured formation enthalpies for pyrochlore series, but the disordered fluorite domain could not be equally well reproduced. Only the consideration of the Weberite-type cation arrangements as representation of short-range ordering, as found by Shamblin et al. (2016)[22], and application of a defect fluorite/weberite two state model reconciled the data. The fact that defect fluorite is not a good representation of short structure of disordered pyrochlore is illustrated by comparing the computed and measured differences in formation enthalpies of ordered and disordered $Eu_2Zr_2O_7$ and $Gd_2Hf_2O_7$ pyrochlores. As illustrated in Fig. 74, the enthalpy of formation from oxides computed assuming the defect fluorite structure is positive (thus prohibiting formation of such a phase) and substantially larger than the measured value, which is much better reproduced by the computed formation enthalpy of weberite-type structure. This is yet another example showing the importance of short-range ordering on behaviour of ceramic waste forms. Because this topic is well suited for the atomistic modeling, we expect more such studies in the future.

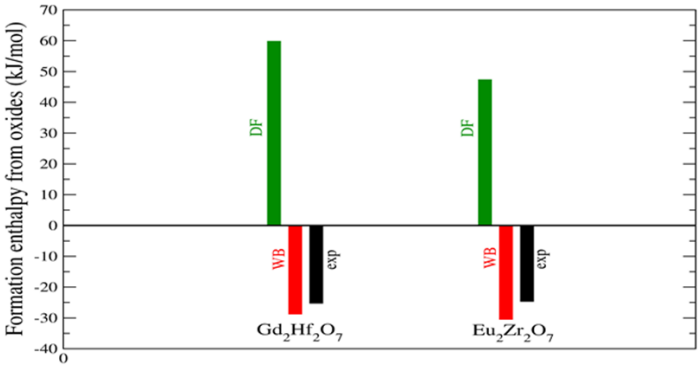

Fig. 74: The measured and computed formation enthalpies from oxides of $Gd_2Hf_2O_7$ and $Eu_2Zr_2O_7$ defect fluorite phases. The experimental data come from [23,24].

Conclusions

Here we have presented an overview of our recent joint investigation of the phosphate- and pyrochlore-type ceramic waste forms. We show selected results of joint atomistic modeling and experimental investigations of these materials. These include research on structural, thermochemical, thermodynamic and ordering/disordering properties. All these cases show the importance of atomistic modeling in obtaining a more complete and comprehensive characterization of the investigated materials. In particular, combination of modeling and experimental techniques helped in understanding the long-term thermodynamic stability of monazite-type ceramic waste forms and formation of short-range ordering in ceramic materials. We expect that the later effect will be further investigated by the atomistic modeling techniques that are best suited for studies of such atomic-scale phenomena.

Acknowledgments

We acknowledge the computing time on RWTH Aachen and Forschungszentrum Jülich GmbH supercomputers, awarded through Jülich-Aachen research alliance (JARA-HPC).

References

[1] Ewing, R.; Wang, L.: *Rev. Mineral. Geochem.* 48 (**2002**) 673.
[2] Ewing, R.C.; Weber, W.J.; Lian, J.: *J. Appl.Phys.* 95 (**2004**) 5949.
[3] Blanca-Romero, A.; Kowalski, P.M.; Beridze, G.; Schlenz, H.; Bosbach, D.: *J. Comput. Chem.* 35 (**2014**) 1339-1346.
[4] Beridze G.; Birnie, A.; Koniski, S.; Ji, Y.; Kowalski, P.M.: *Prog. Nucl. Energ.* 92 (**2016**) 142-146.
[5] Vanderbilt, D: *Phys. Rev. B* 41 (**1990**) 7892-7895.
[6] Perdew, J.P.; Burke, K.; Ernzerhof, M.: *Phys. Rev. Lett.* 77 (**1996**) 3865-3868.
[7] Perdew, J.P.; Ruzsinszky, A.; Csonka, G.I.; Vydrov, O.A.; Scuseria, G.E.; Constantin, L.A.; Zhou, X.; Burke, K.: *Phys. Rev. Lett.* 100 (**2008**) 136406.
[8] Cococcioni, M.; de Gironcoli, S.: *Phys. Rev. B* 71 (**2005**) 035105.
[9] Aryasetiawan, F.; Karlsson, K.; Jepsen, O.; Schönberger, U.: *Phys. Rev. B* 74 (**2006**) 125106.
[10] Kowalski, P.M.; Beridze, G.; Vinograd, V.L.; Bosbach, D.: *J. Nucl. Mater.* 464 (**2015**) 147-154.
[11] Kowalski, P.M.; Li, Y.: *J. Eur. Ceram. Soc.* 36 (**2016**) 2093-2096.
[12] Ji, Y.; Beridze, G.; Kowalski, P.M.: *Energy Procedia* XX (**2017**) XX-XX.
[13] Kowalski, P.M.; Ji, Y.; Li, Y.; Arinicheva, Y.; Beridze, G.; Neumeier, S.; Bukaemskiy, A.; Bosbach, D.: *Nucl. Instrum. Meth. B* 393 (**2017**) 68-72.
[14] Li, Y.; Kowalski, P.M.; Blanca-Romero, A.; Vinograd, V.; Bosbach, D.: *J. Solid State Chem.* 220 (**2014**) 137-141.
[15] Ji, Y.; Kowalski, P.M.; Neumeier, S.; Deismann, G.; Kulriya, P.K.; Gale, J.D.: *Nucl. Instrum. Meth. B.* 393 (**2017**) 54-58.
[14] Glynn, P.: *Rev. Mineral. Geochem.* 40 (**2000**) 481–511.
[15] Popa, K.; Konings, R.J.M.; Geisler, T.: J. Chem. Thermodyn. 39 (**2007**) 236–239.
[16] Neumeier, S.; Kegler, Ph.; Arinicheva, Y.; Shelyug, A.; Kowalski, P.M.; Schreinemachers, C.; Navrotsky, A.; Bosbach, D.: *J. Chem. Thermodyn.* 105 (**2017**) 396-403.
[17] Huittinen, N.; Arinicheva, Y.; Kowalski, P.M.; Vinograd, V.L.; Neumeier, S.; Bosbach, D.: *J. Nucl. Mater.* 486 (**2017**) 148-157.
[18] Popa, K.; Wallez, G.; Raison, P.E.; Bregiroux, D.; Apostolidis, C.; Lindqvist-Reis, P.; Könings, R.J.M.: *Inorg. Chem.* 49 (**2010**) 6904-6908.
[19] Konings, R.J.M.; Walter, M.; Popa, K.: *J. Chem. Thermodyn.* 40 (**2008**) 1305-1308.
[20] Popa, K.; Shvareva, T.; Mazeina, L.; Colineau, E.; Wastin, F.; Konings, R.J.M.; Navrotsky, A.: *Am. Mineral.* 93 (**2008**) 1356-1362.
[21] Finkeldei, S.; Kegler, Ph.; Kowalski, P.M.; Schreinemachers, C.; Brandt, F.; Bukaemskiy, A.A.; Vinograd, V.L.; Berdize, G.; Shelyug, A.; Navrotsky, A.; Bosbach, D.: *Acta Mater.* 125 (**2017**) 166-176.
[22] Shamblin, J.; Feygenson, M.; Neuefeind, J.; Tracy, C.L.; Zhang, F.X.; Finkeldei, S.; Bosbach, D.; Zhou, H. D.; Ewing, R.C.; Lang, M.: Nat. Mater. 15 (**2016**) 507-511.
[23] Ushakov, S.V.; Navrotsky, A; Tangeman, J.A.; Helean, K.B.: *J. Am. Ceram. Soc.* 90 (**2007**) 1171-1176.
[24] Saradhi, M.P.; Ushakov, S.V.; Navrotsky, A.: *RSC Adv.* 2 (**2012**) 3328-3334.

6.20. Neutron based analytical techniques for radioactive waste assay

E. Mauerhofer[1], F. Mildenberger[1], T.Nicol[1,2], C. Carasco[2], B. Perot[2], G. Kemmerling[3]

[1]Forschungszentrum Jülich GmbH, Institute of Energy and Climate Research – IEK-6: Nuclear Waste Management and Reactor Safety, 52425 Jülich, Germany

[2]CEA, DEN, Cadarache, Nuclear Measurement Laboratory, 13108 Saint-Paul-Lez-Durance, France

[3]Forschungszentrum Jülich GmbH, Jülich Centre for Neutron Science – JCNS-2/PGI-4: Scattering Methods, 52425 Jülich, Germany

Corresponding author: e.mauerhofer@fz-juelich.de

Introduction

This paper summarizes the main results obtained in the application of prompt and delayed gamma neutron activation analysis for determination of nonradioactive elements and fissile nuclides in radioactive waste. Furthermore the development of a detection system based on scintillating fibers for fast neutron imaging is presented.

Prompt and Delayed Gamma Neutron Activation Analysis

In a previous article[1] dedicated to the development of the analytical facility MEDINA (Multi Element Determination based on Instrumental Neutron Activation) we showed that prompt gamma neutron activation analysis (PGNAA) with 14 MeV neutrons is suitable to identify nonradioactive elements in 200 L radioactive waste drums. The methodology developed to determine the elemental composition of a waste matrix was verified first through the analysis of a 200 L steel drum homogeneously filled with concrete of well-known composition.[2] The analytical results were found to agree well with the expected values, the differences lying between -9 and +5%. Detection limits of 4 and 145 mg/kg were achieved for the toxic elements cadmium and mercury, respectively for an assay time of 30 min. However radioactive waste may be heterogeneous over a wide range of composition including neutron and absorbing elements as well as gamma absorbing elements affecting the reliability and accuracy of analytical results. Thus, the performance of PGNAA was investigated for 200 L steel drums filled with various amounts and arrangements of concrete and polyethylene blocks.[3] Polyethylene was chosen to simulate the presence of neutron moderating and absorbing material in the waste and to study its influence on the determination of the whole sample elemental composition. The latter was evaluated using the method proposed for the analysis of large homogeneous samples[2] assuming that the drum is filled only with a concrete matrix having the apparent density of the heterogeneous samples. The analytical results were found to agree with the expected values within ± 34% (Fig. 75) which is quite reasonable with regards to the samples heterogeneity; the deviations observed being mainly due to the different neutron properties of the materials leading to a perturbation of the thermal neutron energy distribution in each sample region.

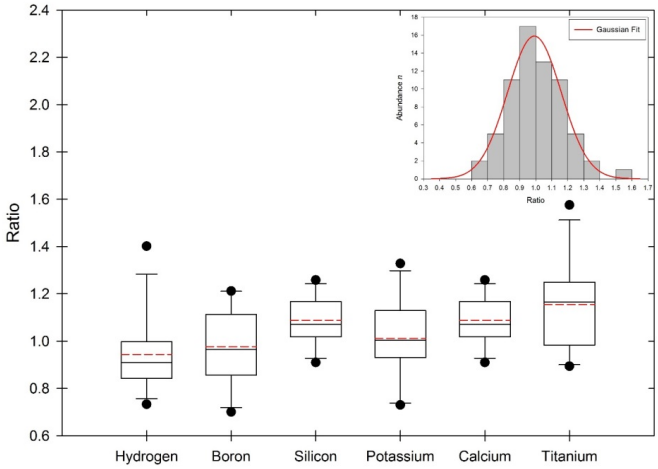

Fig. 75: Results for the PGNAA of 200 L drums filled with concrete and polyethylene. Box-and whisker plots of the ratios of measured to expected amount for each detected element and Gaussian distribution of all data. Continuous and dashed lines in the boxes represent the median and arithmetic mean, respectively. The close symbols represent the outliers.[3]

In the PGNAA studies, the irradiation and counting conditions were set preferentially for the detection of prompt gamma-rays induced by thermal neutron capture though additional information on the waste composition may be gained measuring delayed gamma-rays from fast and thermal neutron activation products. The sensitive detection of these delayed gamma-rays requires that thermal neutrons have almost vanished. From the measurements of the thermal neutron die-away times we showed in [4] that a waiting time of about 12 ms from the end of neutron pulses is necessary to record delayed gamma-ray spectra without appreciable prompt gamma-ray contribution. The performance of cyclic neutron activation analysis (CNAA) was investigated for drums filled with concrete, polyethylene or a mix of concrete and polyethylene.[5] We showed that knowledge on the thermal neutron die-away time is required to correct for prompt gamma background interferences as well as to determine the thermal neutron flux in neutron pulses. We showed also that the fast neutron flux may be estimated from the results obtained by thermal neutron capture (prompt gamma-rays measurement) with some assumption on the sample composition with regards to the detected delayed gamma rays. The method proposed to evaluate the sample composition by CNAA provided for the homogeneous samples a good agreement between measured and expected values, differences lying between -3 and 15%. For the heterogeneous samples the determined elemental contents were found to agree with the expected values within ±39%, (Fig. 76) the large deviations observed being associated to local perturbation of the fast and neutron flux owing different neutron and absorption properties of the materials. Depending on the polyethylene content of the samples detection limits ranging between 14 and 24 mg/kg for cadmium, 520 and 740 mg/kg for mercury and 5.5 and 53 g/kg for lead were achieved for an assay time of about 30 min.

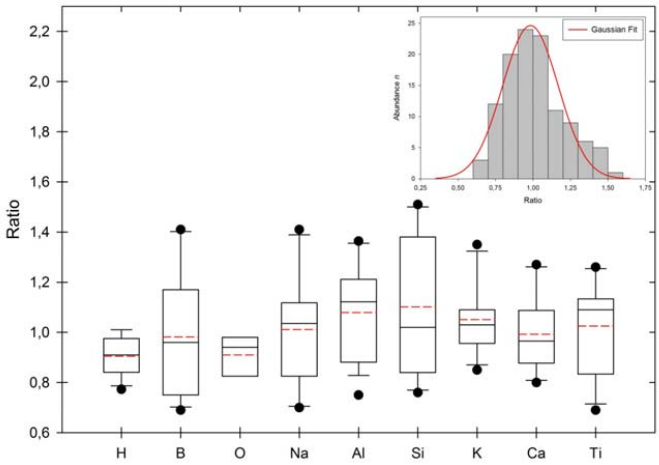

Fig. 76: Results for CNAA of 200 L drums filled with concrete and polyethylene. Box-and whisker plots of the ratios of measured to expected amount for each detected element and Gaussian distribution of all data. Continuous and dashed lines in the boxes represent the median and arithmetic mean, respectively. The close symbols represent the outliers.[5]

The use of neutron activation analysis for radioactive waste characterization was further investigated in the framework of cooperation between CEA Cadarache and FZJ. In a first study the validation of the numerical model of the facility MEDINA using MCNP Monte Carlo particle code was carried out.[6] Simulations and measurements of prompt capture gamma rays from small samples measured in MEDINA were compared for some elements of interest (beryllium, aluminium, chlorine, copper, selenium, strontium, and tantalum). The comparison was performed using different nuclear databases, resulting in satisfactory agreement within ±20% and thus validation the numerical model of MEDINA in view of following studies. Then, the feasibility of fission delayed gamma-ray measurements of ^{239}Pu and ^{235}U in 225 L waste drums was studied, considering bituminized or concrete matrixes representative of wastes produced in France and Germany.[7] The delayed gamma-ray emission yields were first determined from U and Pu metallic samples measurements in the neutron activation cell REGAIN at CEA Cadarache, showing satisfactory consistency with literature data. The useful delayed gamma-ray signals of ^{239}Pu and ^{235}U, homogeneously distributed in 225 L matrixes, were then determined from MCNP simulations using the numerical model of the MEDINA facility. Weak signals of about one hundred counts per gram of ^{239}Pu or ^{235}U after 2 hours irradiation were obtained (Fig. 77). Because of the high gamma emission in the bituminized waste produced in France (about 1 TBq of ^{137}Cs per drum), the use of detector collimator and/or shielding is mandatory to avoid electronic saturation, making fission gamma-ray undetectable. However German concrete waste being of lower activity, their corresponding active background was measured in MEDINA with a concrete mock-up, leading to limit of detection between 10 and 310 g of ^{239}Puor ^{235}U, depending on the delayed gamma-ray. In order to improve these performances, the shielding of MEDINA germanium detector was optimized using MCNP calculations, resulting in a gamma and neutron background reduction factors of 4 and 5, respectively.[8] The experimental validation of the shielding efficiency was performed by implementing easy-to-build shielding configurations in MEDINA, which

confirmed the expected background reduction factors predicted by MCNP simulations. Thanks to an optimized detector shielding, it will also to use a higher neutron emissions source, like a high flux neutron generator or an electron LINAC with appropriate targets for neutron production, in view to further reduce detection limits.

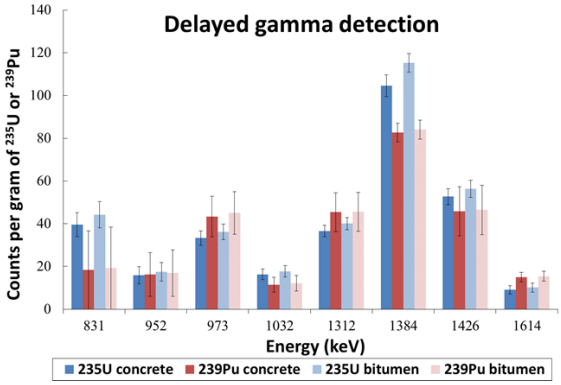

Fig. 77: Delayed gamma signal per fissile isotope mass evaluated with MCNPX for 225 L bituminized and concrete drum assays in MEDINA with a neutron emission of 2 10^8 n/s and a 7200 s pulsed irradiation for the 831 keV ($^{90g+m}$Rb), 952 keV (^{95}Y), 973 keV ($^{132g+m}$Sb,), 1312 keV ($^{136g+m}$I) and 1426 keV (^{94}Sr) gamma rays, followed by 6300 s, 18900s or 48600 s post-irradiation measurements for the 1032 keV (^{89}Rb), 1384 keV (^{92}Sr) and 1614 keV (^{104}Tc, ^{134}I) gamma rays.[7]

Fast Neutron Imaging

In a previous work [9] the performances of a compact fast neutron radiography system using a 14 MeV neutron generator and an amorphous silicon (aSi) photodiode flat panel detector (XRD 1642 CPO, PerkinElmer) linked to a 3 mm thick plastic convertor (EJ-260, Eljen Technology) as imaging detector were described. In order to increase the scintillation efficiency and the light output an additional scintillator was built using scintillating fibers (SCF) of type SCF-3HF(1500)M (Kuraray) having a diameter of 1 mm and a length of 10 mm as prototype. The scintillating fibers consist of a core of polystylene doped with 1500 μg/g of hydroyflavone for radiation hardness and a multilayer cladding acting as light guide (polymethylmetacrylate for inner cladding, fluorinated polymer for outer cladding). These scintillating fibers emit green light but a peak emission at a wavelength of 530 nm matching well the wavelength absorption range of α-Si. For practical reasons, single bundles of closely packed scintillating fibers with an area of 25×25 mm^2 as shown in Fig. 78 were first fabricated.

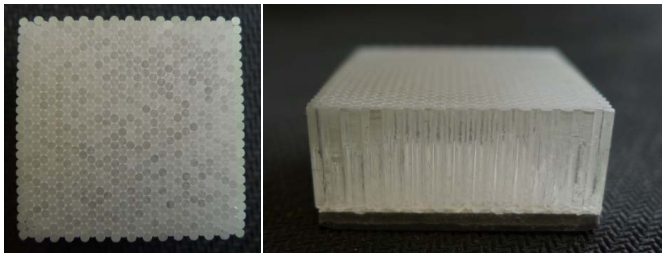

Fig. 78: Single bundles of closely packed scintillating fibers of type SCF-3HF(1500)M.

After polishing, the initial length of the fibers (10 mm) was reduced to 8 mm. Finally, 64 single bundles were assembled jointly in an aluminium frame to form a scintillator with an area of 20×20 cm^2 (Fig. 79) covering partially the α-Si flat panel. The scintillator was mounted light tight directly on the plastic scintillator EJ-260 (Fig. 79) avoiding so the risk to damage the sensitive photodiode array by the replacement of the scintillator.

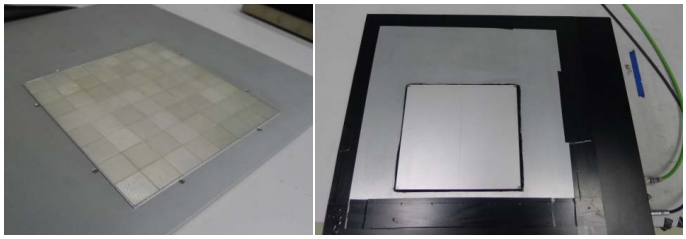

Fig. 79: Assembling of the single bundles on the aluminium frame (left) and mounting on the α-Si flat panel (right).

The neutron radiographs of an eye bolt M52 lying on two aluminium bricks recorded with the two types of neutron converters, the plastic scintillator EJ-260 and the scintillating fibers, respectively are compared in Fig. 80. As expected, the use of scintillating fibers increases the light production and particularly the image contrast since the light is guided to the photodiodes of the α-Si flat panel. Thus they are well appropriated as neutron converter for fast neutron imaging. According to simulations[10], the thickness of a SCF based converter could be extended up to 50 cm to enhance the probability of neutron interaction and therefore the light output.

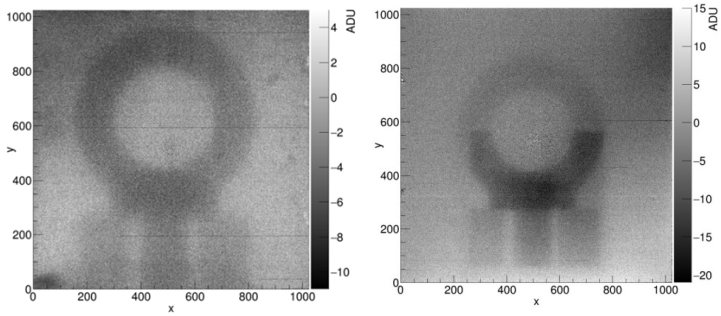

Fig. 80: Neutron radiographs of an eye bolt M52 lying on two aluminium bricks recorded with the plastic scintillator EJ-260 (left) and the additional scintillating fibers SCF-3HF(1500)M covering partially the α-Si flat panel (right). Radiographs were recorded for 900 s under the same conditions regarding the distance between object, detector and neutron source (40 and 1 cm) and the fast neutron emission (1.6 10^8 n/s).

Acknowledgements

Financial support for research on Neutron Imaging was provided by the German Federal Ministry of Education and Research (Contract No. 0S9022B).

References

[1] Mauerhofer, E., Havenith, A.: *J. Radioanal. Nucl. Chem.* 302 (**2014**) 483-488.

[2] Mauerhofer, E., Havenith, A., Kettler, J.: *J. Radioanal. Nucl. Chem*. 309 (**2016**) 273-278.

[3] Mildenberger, F., Mauerhofer, E.: *J. Radioanal. Nucl. Chem.* 309 (**2016**) 1264-1269.

[4] Mildenberger, F., Mauerhofer, E.: *J. Radioanal. Nucl. Chem.* 307 (**2016**) 661-667.

[5] Mildenberger, F., Mauerhofer, E.: *J. Radioanal. Nucl. Chem.* 311 (**2017**) 917-927.

[6] Nicol, T., Carasco, C., Perot, B., Ma, J.L., Mauerhofer, E., Havenith, A., Collot, J.: *J. Radioanal. Nucl. Chem*. 308 (**2016**) 671-67.7

[7] Nicol, T., Perot, B., Carasco, C., Brackx, E., Mariani, A., Passard, C., Mauerhofer, E.: J. Collot, *Nucl. Instrum. Methods Phys. Res A* 832 (**2016**) 85-94.

[8] Nicol, T., Mauerhofer, E., Carasco, C., Perot, B., Collot, J.: *J. Radioanal. Nucl. Chem*. 31 (**2016**) 865-874.

[9] Schumann, M., Mauerhofer, E., Kemmerling, G., Willenbockel, M.: Institute of Energy and Climate Research, IEK-6: Nuclear Waste Management, Report 2013/2014, Energy & Environment Volume 327, ISBN 978-3-95806-155-2

[10] Engels, R., Frank, M., Furletov, S., Furletova, J., Havenith, A., Kemmerling, G., Kettler, J., Klapdor-Kleingrothaus, T., Mauerhofer, E., Schitthelm, O., Schumann, M., Vasques, R., Voß, D.: Abschlussbericht, BMBF-Vorhaben 02S9022A-C, Radiographie mittels schneller Neutronen zur Charakterisierung radioaktiver Abfälle (Neutron Imaging)

6.21. Treatment of nuclear graphite for the safe management

N. Shcherbina[1], A. Bukaemskiy[1], E. Petrova[2], D. Bosbach[1]

[1]Forschungszentrum Jülich GmbH, Institute of Energy and Climate Research – IEK-6: Nuclear Waste Management and Reactor Safety, 52425 Jülich, Germany

[2]Department of Theoretical and Experimental Reactor Physics, NRNU MEPhI, Moscow, Russian Federation Affiliation

Corresponding author: n.shcherbina@fz-juelich.de

Abstract

The effect of soft milling on structural of nuclear graphite was investigated using XRD. Using the refined fitting of XRD data we were able to separate contributions of two different phases: porous binder and more ordered filler phase. Their lattice parameters, a and c, as well as the graphitization degrees were determined with a very good precision. The Gaussian fitting routine allowed quantification of binder and filler in every fraction. The finer fractions, <100 µm, revealed higher binder concentration compared to non-fractionated original graphite, whereas fractions with bigger particle size exhibit higher filler content. Calculated distribution of binder in the graphite fractions was shown to correlate with relative distribution of ^{14}C. The applied approach of soft milling and fractionation have demonstrated a possibility of ^{14}C to be mechanically redistributed, which is due to the fact that ^{14}C is associated with the porous structure of nuclear graphite. The fractionation undertaken in this work can be a complimentary step to the thermal decontamination methods applied for selective separation of ^{14}C from irradiated nuclear graphite.

Introduction

Decommissioning is a final step in the lifetime of every nuclear facility, which involves removal of the fuel, dismantling of the plant and equipment, decontamination of the plant constructions etc. Decommissioning is always concerned with generation of nuclear wastes, so-called “problematic” nuclear wastes, which properties are different from the wastes arising from the routine operation of nuclear facility. Handling of these wastes requires special attention in order to ensure their safe management and provide for the systematic reduction of radiological hazards. Since many decades nuclear graphite has been widely used in the nuclear reactors (e.g. gas-cooled reactors, Russian RBMK, etc.) as a moderator, reflector, construction material and fuel matrix. During decommissioning retrieved irradiated graphite represent the waste stream of high volume with a relatively low specific inventory of long- and short-lived radionuclides, and therefore is classified as problematic nuclear waste. Presently, more than 250,000 tons of irradiated nuclear graphite are accumulated worldwide, and due to the lack of established waste management routes awaiting further management.[1,2] In Germany, about 1,000 tons of irradiated graphite and carbon bricks will have to be disposed of as non-heat generating radioactive waste.[3] Up to date a few management options for irradiated nuclear graphite were considered, including heat treatment, incineration and direct geological disposal.[2,4] Regardless from the disposal option, irradiated graphite (i.e. bricks, blocks, sleeves, etc.) has to be crushed in order to be encapsulated for interim storage or immobilized for final disposal (e.g. in cement). According to the earlier report, the process of graphite crushing can be accompanied by an uneven distribution of radionuclides among different particle size fractions,[5] therefore the

fundamental understanding of nuclear graphite structure, radionuclide distribution and retention in irradiated graphite is essential for safety of nuclear facility decommissioning. This work represents a systematic study of graphite structure before and after mechanical treatment and gains an insight into the ^{14}C distribution in irradiated graphite. A performance of mechanical treatment as an approach for volume reduction of irradiated graphitic wastes is evaluated to be a complimentary step to the decontamination method reported earlier.[6]

Experimental

Crushing and fractionation was performed using inactive (virgin) nuclear graphite from Siberian Chemical Combine, i.e. the material of the same origin as in [5]. The crushing of graphite was performed under water in order to prevent an uncontrolled release of the fine dust particles. An ultrasonic treatment was applied for better segregation of graphite particles. In following the separation of graphite in 6 fractions (i.e. 450, 315, 140, 80, 25 mkm and <25 mkm) was performed using the set of sieves. The sieving was carried out under water as well. Afterwards the fractions were dried at 90 °C within 24 hours. Characterization of graphite fractions included particle mass distribution and structural examination using powder X-ray diffraction (D8 Advance by Brucker AXS GmbH). A 2Θ diffraction angle from 10 to 100° was recorded with 0.02° increment. Measurements were performed at room temperature. In order to define precise reflex position (2Θ) a deconvolution of XRD reflexes was performed using Gaussian routine. The fitting was carried out for reflexes 002, 004 and 006, shown in Fig. 81, for determination of lattice parameter c; correspondingly reflexes 100, 110 and 200 were used for evaluation of lattice parameter a (which is equal to b).

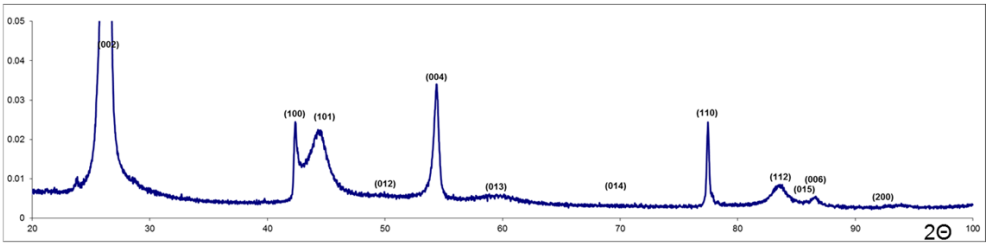

Fig. 81: A typical XRD diffractogram of nuclear graphite.

The lattice parameters of the crystal structure, a (b = a) and c of every component of nuclear graphite (binder or filler), were determined using Nelson-Riley method[7] for correction of a reflex position at the small angles (eq. 1), where lattice parameter is determined by interpolation of c(f_Θ) function to the zero (i.e. at Θ = 180°):

$$f(\theta) = 0.5\left(\frac{(cos\theta)^2}{sin\theta} + \frac{cos\theta}{\theta}\right) \quad \text{(Eq. 1)}$$

Here Θ is an diffraction angle in °.

The lattice parameter c was used to define the degree of graphitization (G_f) as follows[8]:

$$G_f = \frac{3.425 - {}^{c}/_{2}}{3.425 - 3.356} \quad \text{(Eq. 2)}$$

Where c – is a lattice parameter of graphite component (filler or binder), 3.425 and 3.356 – respective distances between the graphene sheets in turbostatic (i.e. disoredered) and hexagonal (highly ordered) graphite.

Results and discussion

Crushing and fractionation of nuclear graphite:

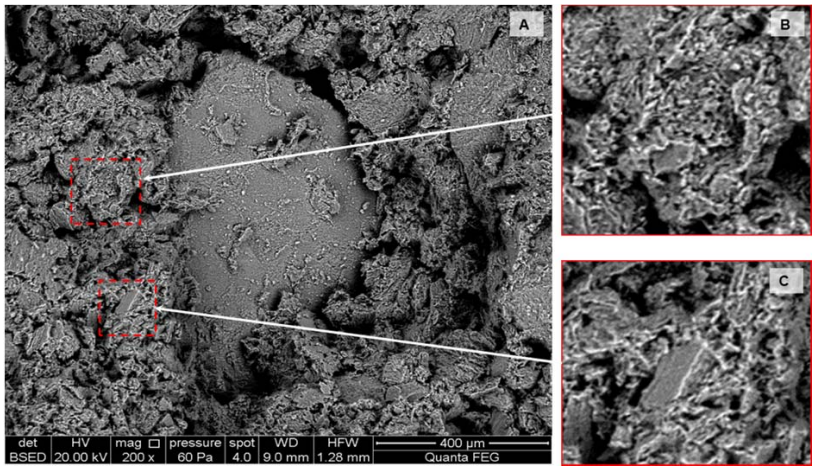

Fig. 82: A typical structure of nuclear graphite: SEM image of nuclear graphite (A) and corresponding magnification of a binder region (B) and filler particle (C).

Nuclear graphite is a complex composite material manufactured from petroleum or pitch coke as filler using pitch tar as a binder material. The major fabrication steps are coke calcination, blending, mixing with the binder (e.g. tar), isostatic pressing/moulding/extrusion into bricks or blocks.[9] Subsequently, the blocks are graphitised at about 2800 °C, additionally impregnated with tar for improving the graphite density, and graphitised again. One of the last steps is purification of graphite from metallic impurities using of gaseous chlorine or freons [1] The long graphitization of nuclear graphite is applied in order to form thermodynamically more stable graphite lattice, and as a result the alignment of properties of both component. Despite of that, filler particles and binder material are still to be distinguished in the final product (cf. Fig. 82 A). Binder material (cf. Fig. 82 C) exhibits very distinctive porous structure with spherical pores of ca. 10 μm in diameter, whereas filler particles (Fig. 82 C) are of 10 μm – 500 μm in size, having typical layered structure (i.e. stucks of graphene layers). Typical for filler material is longitudinal cracks, which follow the directions of basal planes in filler particles, and a very few pores. Besides the differences in structure, binder and filler materials originally vary in their composition. In contrast to filler, binder material contains higher amount of solid impurities (e.g. Li, Fe, Co) and gases (e.g. N_2 or O_2) trapped in closed pores or adsorbed to the internal and external graphite surface, which results in higher radionuclide inventory, produced through neutron activation. Some of these activation products, like ^{60}Co (half-life 5.27 a) and ^{3}H (half-life 12.33 a), are in particular relevant during reactor decommissioning and dismantling, whereas some long-lived activation products such ^{14}C (half-life 5700 a), or ^{36}Cl (half-life $3.01 \cdot 10^5$ a) can be specifically important with respect to interim storage, and operational as well as long-term safety of disposal facilities.[10,11] The dominant activation product in irradiated nuclear graphite, ^{14}C, is produced preferentially from (adsorbed) nitrogen by the nuclear reaction $^{14}N(n,p)^{14}C$ and to a significantly lesser extent by activation of stable ^{13}C (via $^{13}C(n,\gamma)^{14}C$) in the graphite or from

oxygen ($^{17}O(n,\alpha)^{14}C$). The distribution of ^{14}C is mainly following that of its precursor ^{14}N, i.e. most of ^{14}C is localized in pores originated from binder material, whereas a little fraction of ^{14}C, originated from ^{13}C, is evenly distributed in the graphite. After milling of irradiated graphite the ^{14}C, to a large extent, was shown to be associated with the fine particle fraction.[5] It was suggested that such fractionation occurs because most of ^{14}C is accumulated in the porous regions of nuclear graphite, which are easier to crush and mill compared to the crystalline filler particles. In order to investigate the correlation between ^{14}C distribution and structure of graphite fractions, which may potentially be responsible for retention of ^{14}C in irradiated nuclear graphite, present investigations on crushing and fractionation was carried out in the same way as in [5] using inactive graphite. Fig. 83 represents the average particle size in graphite fractions in comparison to the data obtained in [5]. The comparison shows that fractions with a rather close particle size were obtained in our work and experiments performed with irradiated graphite,[5] and allows considering the similar properties of respective fractions.

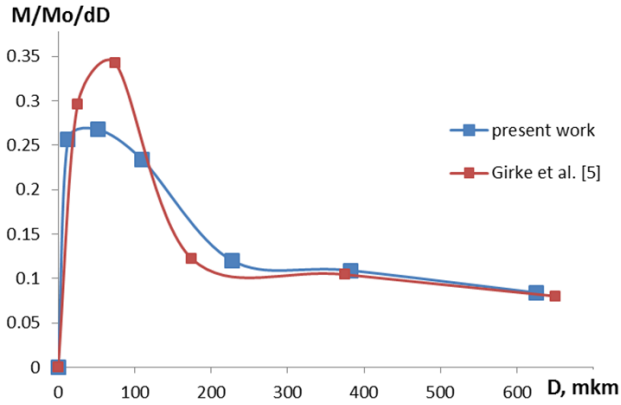

Fig. 83: A comparison of particle size distribution in graphite fractions obtained by "crushing&fractionation" in our work and in [5].

Structural characterization of graphite fractions

Characterization of untreated graphite as well as fractionated graphite with XRD method have demonstrated that all graphite reflexes are asymmetric and can be described as a sum of two Gaussian functions, as shown in Fig. 84. This is presumably a result of contribution of two graphitic components having different structures – binder material, a less ordered graphite, and filler with higher crystallinity degree. The peak of binder (phase 1) has systematically larger FWHM (Full Width at Half Maximum) than that of filler (phase 2), which indicates a more disordered structure of binder. Based on an assumption of two contributions from binder and filler the values for lattice parameters of every component (i.e. c_1 and a_1, as well as c_2 and a_2) were obtained for original (none-treated) graphite sample. Also these lattice parameters of binder and filler were determined for each graphite fraction separately.

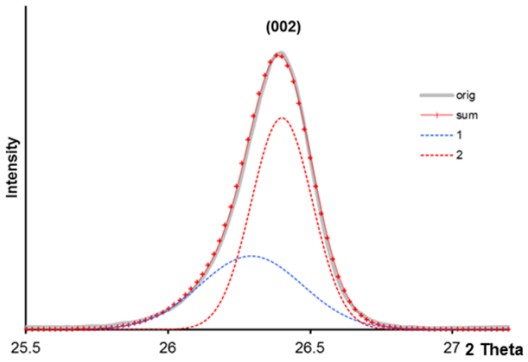

Fig. 84: An example of deconvolution of an XRD-reflex into two Gaussian functions: orig – recorded XRD-reflex, 1 – binder phase, 2 – filler phase, sum – superposition of two peaks.

The values for original graphite and averaged value over all graphite fractions are summarizes in Table 7. Obviously the values for c_1 and a_1, as well as c_2 and a_2 for binder and filler correspondingly were obtained with a rather high accuracy, which confirms a correctness of our assumption and reliability of applied approach for XRD-data evaluation. Interestingly that parameters a of binder and filler lie close to each other, whereas values of c differ more significantly. This demonstrates a c-axis crystal expansion in binder phase compared to filler phase.

Table 7: Lattice parameters of original (none-treated) and fractionated graphite (averaged over 7 graphite fractions).

Sample	Phase 1 (binder)		Phase 2 (filler)	
	$a_1 = b_1$	c_1	$a_2 = b_2$	c_2
Original graphite	2.463±0.003	6.762±0.007	2.454±0.001	6.736±0.006
Fractionated graphite (average)	2.463±0.001	6.762±0.005	2.455±0.001	6.736±0.002

In following, the values of lattice parameter c were used for calculation of the graphitization degree G_f of both components in corresponding graphite fractions. These results are plotted in Fig. 85 along with G_f of original none-fractionated graphite sample (dashed-line). Obviously the lower value of G_f is characteristic for phase 1, i.e. 0.641±0.037, whereas G_f of phase 2 is systematically higher, 0.827±0.015. Typically, the value of G_f is used for evaluation of the quality of graphitization process and refers to the distance between the graphene sheets in turbostatic (i.e. disordered) and hexagonal (highly ordered) graphite (see Eq. 2). Accordingly, the G_f may vary between 0 and 1, whereas the higher the G_f, the more ordered the graphite is and the closer its structure approaches to the ideal structure of hexagonal graphite. These values correlate very good with the suggestion of the phase 1 being a disordered binder phase, and phase 2 being more ordered filler phase. Besides that corresponding G_f values for filler and binder determined for fractionated graphite lie rather close to that of original (none-fractionated) graphite. This, once again, proves the reliability of applied approach for separation of individual contributions of binder and filler phases into XRD pattern.

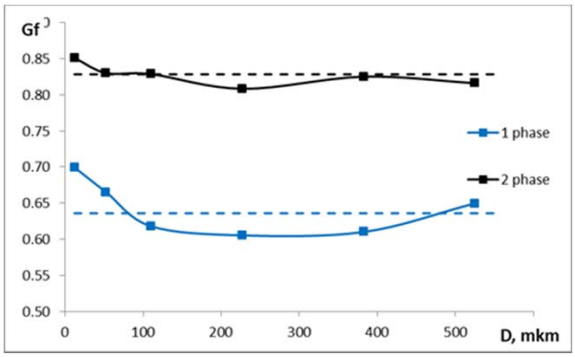

Fig. 85: Graphitization degree (G_f) of binder (phase 1) and filler (phase 2) evaluated for every fraction of nuclear graphite.

^{14}C distribution among graphite fractions

Using peak deconvolution approach we were able to estimate the relative amount binder (Fr_b) in every graphite fraction applying following equation:

$$Fr_b = \frac{S_b}{(S_b+S_f)\cdot S_{b0}} \qquad \text{(Eq. 3)}$$

Where S_b and S_f are respective peak areas of binder and filler component in a graphite fraction, and S_{b0} - peak areas of binder of none-fractionated graphite.

The results, shown in Fig. 86, are plotted against the average particle size in every fraction and compared to the corresponding relative amount of ^{14}C derived from Girke et al.[5]. Dashed line demonstrates the amount of binder and ^{14}C in none-fractionated graphite and shown as a reference for better visibility. The finest fraction (<25 μm) contains almost twice as much ^{14}C as in original non-fractionated sample. Obviously, an enrichment of the fine graphite fractions of <100 μm with ^{14}C occurs, and increases with decreasing of average particle size. At the same time, relative content of ^{14}C in fractions <100 μm is lower compared to none-fractionated graphite. Apparently a soft milling of graphite entails redistribution of ^{14}C, so that most of ^{14}C is bond to the fine graphite fraction.

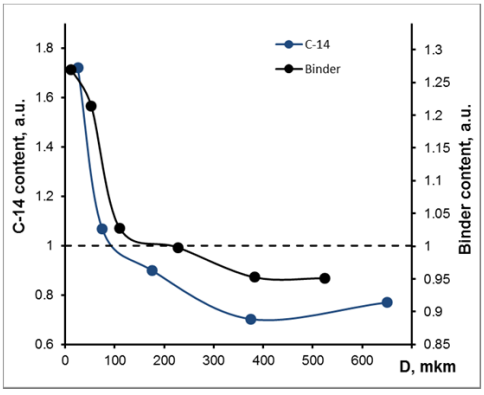

Fig. 86: Relative distribution of binder (black) and ^{14}C in fractionated nuclear graphite; relative amount of binder in non-fractionated graphite is given as a reference (dashed line).

Last but not least, the shape of both curves is rather similar, which points out at the linear correlation between ^{14}C distribution and relative amount of binder. This is, in fact, in agreement with an initial suggestion that ^{14}C resides in the porous regions of nuclear graphite and can be mechanically separated.

Conclusions

Structural characterization of mechanically treated nuclear graphite was performed using XRD. The evaluation of XRD data refined with the data fitting allowed the separation contribution of two different phases: porous binder and more ordered filler phase. Their lattice parameters, a and c, were derived with the very good precision. Based on that the graphitization degrees of binder and filler were determined to be 0.641±0.037 and 0.827±0.015 respectively. Calculated distribution of binder in the graphite fractions was demonstrated to be in a very good agreement with relative distribution of ^{14}C reported earlier.[5] The applied approach of soft milling and fractionation have demonstrated a possibility of ^{14}C to be mechanically redistributed, which is evidently due to the fact that ^{14}C is associated with the porous particles in nuclear graphite. The separation efficiency of fractionation undertaken so far on the lab scale in the manual regime may be further improved by using, e.g. appropriate industrial equipment.[5] Mechanical treatment can serve as a complimentary step to the thermal decontamination used to selective separation of ^{14}C from irradiated nuclear graphite.

References:

[1] Electric Power Research Institute (EPRI). Graphite decommissioning: Options for graphite treatment, recycling, or disposal, including a discussion of safety-related issues. EPRI Technical Report 1013091 (**2006**). pp. 156.
[2] International Atomic Energy Agency (IAEA) Characterization, treatment and conditioning of radioactive graphite from decommissioning of nuclear reactors. IAEA-TECDOC-1521, Vienna, (**2006**) pp. 71.
[3] Kuhne, L.; Rizzato, C.; Baginski, K.; Trigubowitsch, N.; Petrova, E.; Vulpius, D.; Nabbi, R.; Neumann, A.; Steinmetz, H.-J.; von Lensa, W. Entsorgung von bestrahltem Graphit (CarboDISP) – Abschlussbericht zum BMBF-Vorhaben FKZ 02S8790. Forschungszentrum Jülich GmbH, pp. 146, (**2015**) pp. 146.
[4] IAEA-TECDOC-1647. Progress in radioactive graphite waste management. IAEA, (**2010**).
[5] Girke, N.A.; Bushuev, A.V.; Koyhin, A.F.; Petrova, E.V.; Aleeva, T.B.; Yubarev, V.N.: *Atomic Energy* 112(1) (**2012**) 63-66.
[6] Vulpius, D.; Baginski, K.; Kraus, B.; Thomauske, B.: *Nucl. Eng. Des.* 265 (**2013**) 294-309.
[7] Nelson, J.B.; Riley, D.P.: *Proc. Phys. Soc. Lond.* 57 (**1945**) 160-177.
[8] Vyatkin, S.E. et al.: *Atomizdat*, 1967 (*In Russian*).
[9] Burchell, T.D.: Radiation effects in graphite. Chapter 4.10 in: Konings, R.J.M. (ed.) Comprehensive nuclear materials. 4 (**2012**) 299-324.
[10] Chadwick, M.B. et al.: *Nuclear Data Sheets* 112 (**2011**) 2887-2996.
[11] Beghein, Ph. et al.: *Nucl. Eng. Des.* 251 (**2012**) 146-149.
[12] http://www.selfrag.com/explorer-examples.php

6.22. Safeguards systems analysis: Further development of quantitative methods

Th. Krieger, J. Rutkowski, I. Niemeyer
Corresponding author: t.krieger@fz-juelich.de

The project “Further Development of Quantitative Methods in Safeguards” was initiated in December 2016. The work within the period 2017-2018 focuses mainly on the three topics

- Inspection sampling plans
- Inspection games over time – Fundamental models and approaches
- Acquisition path analysis (APA)

which are elaborated in the following sections.

Inspection sampling plans

One of the tasks assigned to International Atomic Energy Agency (IAEA) inspectors is to independently verify nuclear material accountancy information declared by the facility operators or reported by a State. In this context inspectors verify information associated with nuclear material items at a facility such as net (gross, tare) weight, concentration, enrichment, element or isotope weight.[1,2] In order to detect nuclear material diversion (and corresponding operator data falsification), specialized equipment is used to measure bulk quantities of nuclear material.[3,4] Understanding the instrumentation used is essential to evaluate the resulting data and associated measurement errors.[5-7]

Because time and financial constraints make it impossible for inspectors to verify 100% of the items present in a facility at the time of the inspection, inspectors verify a sample of these items, and, based on the verification results, draw a conclusion about all the declared nuclear material at the facility. The sample of items inspected must be large enough to represent the population in order to allow a meaningful conclusion. On the other hand, it must also be as small as possible to minimize expense.[1]

More formally, consider a stratum[1] with N items, two measurement verification methods[2] with relative standard deviations (RSDs, the coefficient of variation) δ_i together with the number of items n_i verified with method $i, i = 1,2$, a diverted goal amount of M (usually one significant quantity[3]), and an average item size of $\bar{x}$, that depends on the operator’s declared nuclear

[1] Grouping of items and/or batches having similar physical and chemical characteristics (e.g. isotopic composition) made for the purpose of facilitating statistical sampling [8].

[2] Methods used by the IAEA to independently verify nuclear material accounting information, e.g., identification, weighing, volume determination, sampling and analysis, Non-destructive assay (NDA, an item is assayed by using a neutron or gamma detector), Destructive analysis (DA, a sample of item material is analyzed by mass spectrometry in an analytical chemistry laboratory) [8].

[3] The approximate amount of nuclear material for which the possibility of manufacturing a nuclear explosive device cannot be excluded [8].

material. Then the detection probability (DP), i.e., the probability to detect at least one falsified item, as a function of the number r of falsified items, is given by (see [1])

$$1-\sum_{i=Max(0,\,n_1-(N-r))}^{Min(r,\,n_1)}\mathbb{P}(N,r,n_1,i)\left(\Phi\left(\frac{3\delta_1-\frac{M}{\bar{x}r}}{\left(1\pm\frac{M}{\bar{x}r}\right)\delta_1}\right)\right)^{i}\cdot \left(\sum_{j=Max(0,\,n_1+n_2-(N-(r-i)))}^{Min(r-i,n_2)}\mathbb{P}(N-n_1,r-i,n_2,j)\left(\Phi\left(\frac{3\delta_2-\frac{M}{\bar{x}r}}{\left(1\pm\frac{M}{\bar{x}r}\right)\delta_2}\right)\right)^{j}\right), \quad (1)$$

where the selection probability $\mathbb{P}(N,r,n,i)$ is the probability that i defective items out of r defective items are in a sample of size n from a stratum with N items, and $\Phi()$ is the distribution function of a standard normally-distributed random variable.

To illustrate Eq. (1), Fig. 87 presents the DP curves for six sampling plans (n_1,n_2), where $N=116$, $\delta_1=15\%$ and $\delta_2=5.52\%$, $M=8$ [kg] (for plutonium), and $\bar{x}=0.5$ [kg] is chosen.

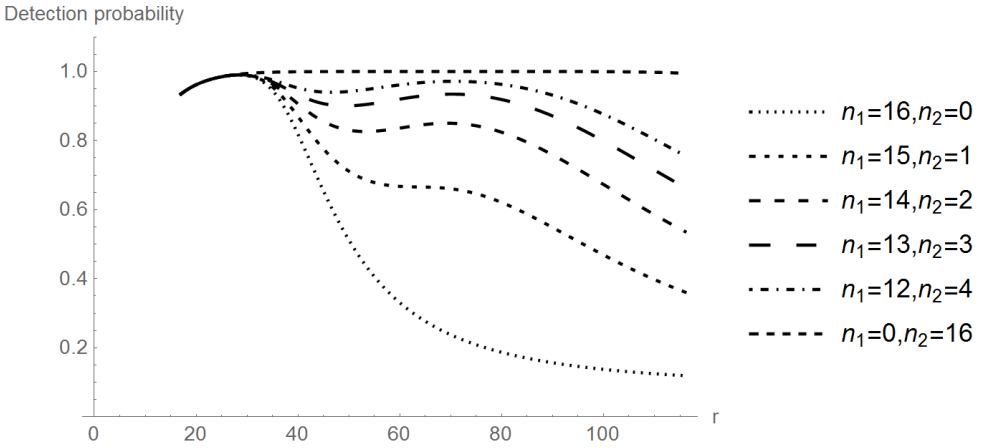

Fig. 87: DP curves as a function of the number r of falsified items.

To derive Eq. (1), several assumptions have to be made, such as (see [1]):

- The relative difference statistics are approximately normally distributed
- The average amount of nuclear material in each item is $\bar{x}$ (constant mass assumption)
- the amount M/r is removed from each of the r falsified items (equal diversion assumption)
- the inspector performs n_1+n_2 individual one-at-a-time item tests to test the null hypothesis (no diversion) against the alternative hypothesis (diversion of the goal amount M)
- a multiplicative error model with purely random errors is considered, i.e. the measurement X is modelled as $X=\mu(1+R)$, where μ is the true unknown mass and R is the random error with zero expectation and a finite variance

If one or more of these assumptions is violated, Eq. (1) and thus, the resulting DP curves will change. Because IAEA's verification sampling plans are based on the minimum achievable DP, i.e. the global minimum of a DP curve for the plotted range of falsified items r, the assumptions used for deriving Eq. (1) need to be considered carefully. In this context, the sensitivity of these and other assumptions on IAEA verification sampling plans need to be studied. A first attempt is made in [9,10].

Inspection games over time – Fundamental models and approaches

In the last thirty years a large number of game theoretical models have been developed and analyzed which describe similar or related inspection problems. An inspection game is a mathematical model of a situation where a person or an organization verifies that another party adheres to certain agreed or legal rules (e.g., an international treaty). The verified party may, however, have an interest in violating these agreed or legal rules. Because the verifying organization's resources are limited, verification can only be partial. A mathematical analysis helps in designing an optimal inspection scheme, where it must be assumed that an illegal action is executed strategically.

Because of the large number of existing game theoretical models, it has become increasingly difficult to maintain an overview on 1) what models have already been analyzed, and 2) how these models are related to each other. More than that in many cases the model assumptions are not well documented, which means in particular for practitioners who want to use these models, that it is very difficult to decide whether they describe their inspection procedures properly.

To classify the existing inspection models a list of assumptions was developed:

- Inspection philosophy: The objective of the Inspectorate may be to detect any illegal activity as soon as possible (playing for time), or it may be to detect it within a given time interval (critical time).
- Time: Interim inspections and the start of an illegal activity may start at any point of time during the reference time interval, or both the inspections and the start of an illegal activity may start only at discrete points of time during the reference time interval.
- Planning: The Operator may plan his illegal activity (if at all) at the beginning of the reference time interval, or sequentially, during the reference time interval. The same possibilities exist for the Inspectorate and its inspection planning.
- Sampling: Inspections may be performed 1) without committing statistical errors, or 2) errors of the second kind (no detection of illegal behaviour) may occur, or 3) errors of the first kind (false alarms) and errors of the second kind may occur. The second case is relevant, if only items are counted on a random sampling basis (attribute sampling procedures). The third case is given when quantitative measurements are performed.

Using this list of assumptions, in [11] – a book written for practitioners and theoreticians – the existing game theoretical inspection models are categorized, and equivalences, relations and differences between them and their Nash equilibria are identified (issue 1) and 2) mentioned above). Also, game theoretical analyses of quite a few new inspection models are included.

Acquisition path analysis (APA)

Since safeguards challenges are growing and becoming more complex, the IAEA has further developed and applied its concept for safeguards implementation at the State level, the so-called 'State Level Concept'. Whereas the safeguards focus formerly had been exclusively on declared nuclear material and facilities, the new approach concentrates on the overall capabilities of a State, making extensive use of open source information as well as inspection results, thereby migrating from a more or less mechanistic verification procedure to a risk-based prioritization of inspection activities.

Since emphasis must nevertheless be placed on ensuring that no State will be discriminated against, the concept has to be objective, transparent, reproducible, standardized, and documented. As part of this approach, the technical objectives of safeguards measures and safeguards activities should be established by applying structured and technically based analytical methods (i.e. acquisition or diversion path analyses).

A structured methodology and a software implementation for acquisition path analysis was developed which supports analyzing acquisition paths including establishing and prioritizing technical objectives, identifying applicable safeguards measures, and conducting a strategic assessment (game theoretical analysis). To perform the game theoretical analysis, two types of quantities are required: Technical quantities (such as non-detection probabilities and the total amount of inspection effort involved) and nontechnical quantities. The nontechnical quantities are the State's overall incentive to choose an acquisition path, State's perceived sanctions in the event of detection, State's false alarm cost for false accusation, Inspectorate's loss in the event of detection (failed deterrence), Inspectorate's false alarm cost (credibility loss) and Inspectorate's loss in the event of non-detection.[12-13]

The results of the game theoretical analysis are Nash equilibrium strategies and equilibrium payoffs. Because they depend on the specific values assigned to the two types of quantities (expert judgment), a sensitivity analysis is recommended in order to investigate the effect of a small change in one of the quantities on the game theoretical results.[14]

At present such a sensitivity analysis seems to be unfeasible for realistic acquisition path models so simpler acquisition path models including a sensitivity analysis regarding the influence of the payoff parameters on the Inspectorate's equilibrium strategy and payoff need to be investigated. This research started in [15]. Future research focuses on the analysis of realistic acquisition path models. The results are expected to increase the acceptance of the benefits game theoretical considerations have at all. For that purpose, existing models (e.g., for Germany's nuclear fuel cycle) can be analyzed with the APA software developed in Jülich, and a comprehensive sensitivity analysis can be performed.

Acknowledgements

This work was supported by the Federal Ministry for Economic Affairs and Energy, Germany, through the German Safeguards Support Programme to the IAEA under task B.24/JNT C 1871 and B.26/D1925.

References

[1] IAEA: *Statistical Methods for Verification Sampling Plans*, *Safeguards Technical Report*. IAEA (**2017)**.
[2] Bonner, E.R.; Burr, T.L.; Krieger, Th.; Norman, C.F.: Statistical Methods in Nuclear Material Safeguards, Wiley StatsRef: Statistics Reference Online (**2014**), DOI: 10.1002/9781118445112.stat00104.pub2.
[3] Burr, T.L.; Krieger, Th.; Norman, C.F.; Zhao, K.: *EPJ Nucl. Sci. Technol.* 2 (**2016**) https://doi.org/10.1051/epjn/2016026.
[4] Bonner, E.R.; Burr, T.L.; Krieger, Th.; Norman, C.F.; Zhao, K.; Laughter, M.; Geist, W.: *J. Nucl. Mater. Manag.* XLIV(2) (**2016**) 53-61.
[5] Burr, T.L; Croft, S.; Krieger, Th.; Martin, K.; Norman, C.; Walsh, S.J: *Appl. Radiat. Isot.* 108 (**2016**) 49-57.
[6] Walsh, S.J.; Macsik, Z.; Wegrzynek, D.; Krieger, Th.; Boulyga, S.: *J. Anal. At. Spectrom* 31 (**2016**) 686-699.
[7] Bonner, E.R.; Burr, T.L.; Krieger, Th.; Martin, K.; Norman, C.F.: *Sci. Techn. Nucl. Install.* (**2017**) https://doi.org/10.1155/2017/2679243.
[8] IAEA: *IAEA Safeguards Glossary, 2001 Edition. International Nuclear Verification Series, No. 3*.
[9] Krieger, Th.; Burr, T.L.: *J. Nucl. Mater. Manag.*, XLIX(3) (**2016**) 45-48.
[10] Krieger, Th.; Burr, T.L.; Norman, C.F.: *Consequences of non-zero item variability on the IAEA's inspection sampling plans*. Proc. INMM 58th Annual Meeting (**2017**).
[11] Avenhaus, R.; Krieger, Th.: *Inspection Games over Time – Fundamental Models and Approaches*. (in preparation), to be published in 2018.
[12] Listner, C.; Niemeyer, I.; Canty, M. J.; Murphy, C. L.; Stein, G.; Rezniczek, A.: *J. Nucl. Mater. Manag.* XLIII(4) (**2015**) 49-59.
[13] Listner, C.; Niemeyer, I.; Canty, M. J.; Stein, G.: *Nav. Res. Log.* 63(3) (**2016**) 260-271.
[14] Avenhaus, R.; Canty, M.J.; Krieger, Th.: *J. Nucl. Mater. Manag.* XL(4) (**2012**) 130-144.
[15] Krieger, Th.; Canty, M. J.; Rutkowski, J.; Niemeyer, I.; Stein, G.; Rezniczek, A.: Proc. 39th ESARDA Annual Meeting (**2017**) 830-841.

6.23. Production of U_3O_8 microparticle reference materials for nuclear safeguards

M. Dürr[1], R. Middendorp[1], A. Knott[1,2], S. Neumeier[1,*], M. Klinkenberg[1], I. Niemeyer[1], D. Bosbach[1]

[1]Forschungszentrum Jülich GmbH, Institute of Energy and Climate Research – IEK-6: Nuclear Waste Management and Reactor Safety, 52425 Jülich, Germany

[2]European Commission, Joint Research Centre Karlsruhe (JRC), 76344 Karlsruhe, Germany

*Corresponding author: s.neumeier@fz-juelich.de

Introduction

To verify the commitment of member states to the Treaty on Non-Proliferation of Nuclear Weapons, the International Atomic Energy Agency (IAEA) performs inspections in nuclear facilities. During such inspections, collection of environmental swipe samples is used as a means that is able to detect undeclared activities within the inspected facility. Such collected swipe samples are shipped to the IAEA's network of analytical laboratories (NWAL), which consists of a number of dedicated analytical laboratories world-wide capable of analyzing the elemental and isotopic composition of individual microparticles on such swipe samples.

Especially with the introduction of a large geometry-secondary ionization mass spectrometer (LG-SIMS) for the analysis of individual particles, there is a great need for dedicated particulate reference materials which can be used for quality control measurements, method calibration, validation and optimization. In framework of the cooperative agreement between the IAEA and FZJ, a particle production facility was established within the controlled area of the IEK-6 which is capable of producing micrometer-sized, spherical uranium oxide particles with a monodisperse particle size distribution which are intended to be certified for the uranium isotopic composition and the amount of uranium per particle.

Production of microparticles

The production of monodisperse uranium oxide microparticles is based on the spray-pyrolysis of monodisperse aerosol droplets, where the aerosol droplets are generated using a vibrating orifice aerosol generator (VOAG). The VOAG is capable of producing monodisperse droplets from aqueous solutions containing uranium with the desired isotopic composition.[1] The aerosol droplets are passed through a drying column and an aerosol heater using a pre-filtered stream of air, during which the solvent evaporates and the dried particles decompose into solid particles.

Particles were produced starting from uranyl nitrate, uranyl chloride and uranyl acetate precursor solutions and the effect of the treatment temperature onto the final particle morphology was investigated.[2] The experiments showed that both uranyl nitrate and uranyl acetate resulted in the production of spherical particles with a monodisperse particle size distribution whereas particles produced from uranyl chloride consisted of highly irregular shaped. Milling of the particles by means of a focused ion beam (FIB) followed by secondary electron microscopy (SEM) image acquisition (Fig. 88) shows that particles obtained from uranyl chloride precursor solutions consisted of a hollow core whereas particles produced from uranyl nitrate and uranyl acetate contained a porous particle core.

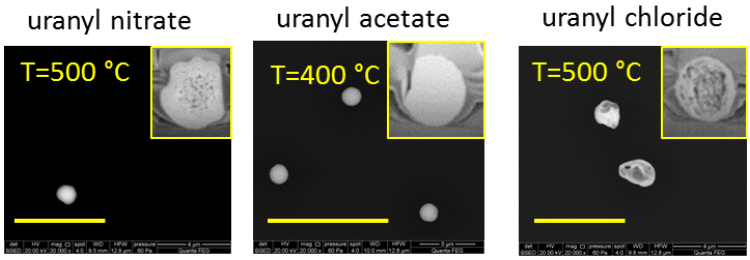

Fig. 88: SEM micrographs of uranium oxide particles produced from uranyl nitrate, acetate and chloride. The yellow bar corresponds to a length of 1 µm, the insets show cross-sections of the particles, prepared by FIB milling.

The temperature of the aerosol heater was also found to strongly affect the particle morphology. The thermal decomposition of the particles could be followed by SEM/EDX investigations and showed a similar trend as observed for large amounts of materials, although the various decomposition stages appear to proceed at lower temperatures. At temperatures exceeding 500 °C, an increased amount of fusion of multiple particles was found (Fig. 89), leading to a widening of the particle size distribution.

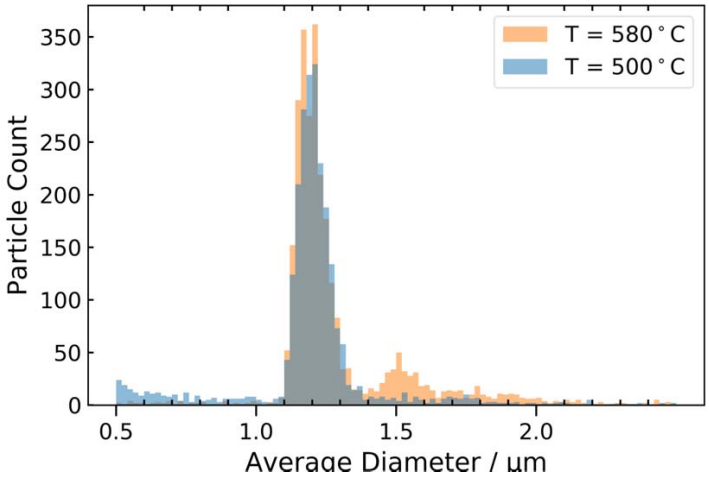

Fig. 89: Particle size distribution of particles produced from uranyl nitrate solutions treated at 500 °C and 580 °C.

Structural characterization of particles

The produced microparticles were investigated by µ-X-ray diffraction (µ-XRD) at the microXAS beamline of the Swiss Light Source (PSI, Villigen, Switzerland) to obtain information regarding the chemical structure of the produced particles.[2] The collected µ-XRD patterns of particles produced from uranyl nitrate solutions with treatment temperatures of 400, 500 and 580 °C all showed a single orthorhombic U_3O_8 phase (Fig. 90), which is normally only encountered for temperatures exceeding 600 °C.[3] To verify the presence of a

U_3O_8 phase instead of the expected β-UO_3 phase, µ-XANES measurements were performed, which confirmed the presence of U_3O_8. In addition to the particles produced from uranyl nitrate precursor solutions, particles produced from uranyl nitrate solutions were investigated, which were also found to consist of a U_3O_8 phase.

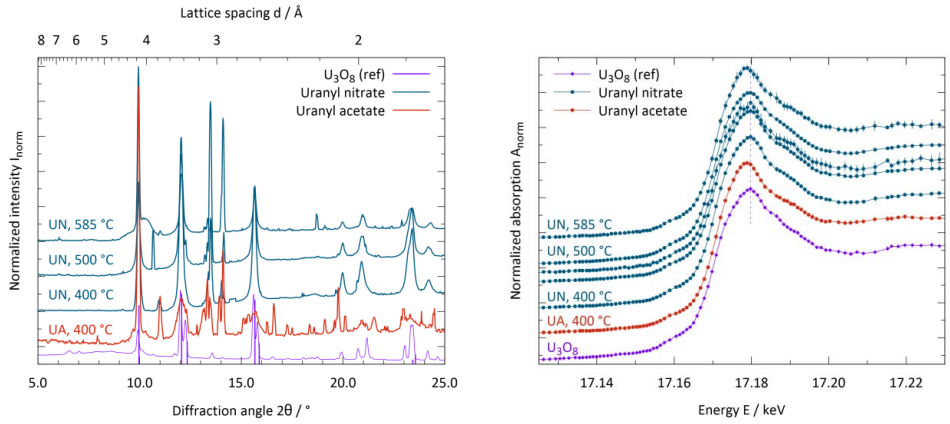

(a) µ-XRD **(b) µ-XANES**

Fig. 90: µ-XRD and µ-XANES measurements of particles produced from uranyl nitrate and uranyl acetate precursor solutions.

In addition to the µ-XRD and µ-XANES measurements, µ-Raman spectroscopic measurements were performed at CEA/DAM/DIF. During the µ-Raman studies, particles produced from uranyl nitrate, uranyl acetate and uranyl chloride were investigated, all of which resulted in similar spectra. Although comparison with reference spectra did not yield any clear match, the µ-Raman measurements show the value of having well characterized materials which can be used as standards.

In addition, to the µ-Raman studies of uranium oxide particles produced from different precursor solutions, particles consisting of a homogeneous mixture of uranium and cerium were investigated. The collected spectra of particles containing a cerium weight fraction of 10 % were comparable to the spectra collected for the pure uranium oxide particles, whereas the spectra collected for particles containing 50 wt.% cerium showed a different phase. µ-XRD measurements of particles containing 25 wt.% cerium showed a cubic phase, from which can be concluded that with an increasing amount of cerium, a cubic uranium/cerium oxide solid-solution is formed. During the µ-Raman measurements of particles containing 10 wt.% cerium, an irreversible phase transformation was observed upon increasing the laser power, which indicates that the cubic solid-solution is thermodynamically more stable than the (presumable) mixed CeO_2/U_3O_8 phase. The formation of a uranium/cerium oxide solid-solution is highly advantageous towards the production of particles consisting of a mixture of multiple actinides and/or lanthanides, as such solid solutions can be assumed to be perfectly homogeneous.

Stability of particles in solution

The stability of particles in various liquid media was investigated to determine the suitability of using particle suspensions as further processing step. At first, produced particles were stored in different media, after which the stability was assessed by SEM investigations.[4] In water, both with and without surfactant (PVP-20000), significant dissolution was observed within 16 days (Fig. 91). The dissolution was found to proceed via the particle core, indicating that the solvent is capable of penetrating the dense shell and infiltrates the pores at the core of the particles.

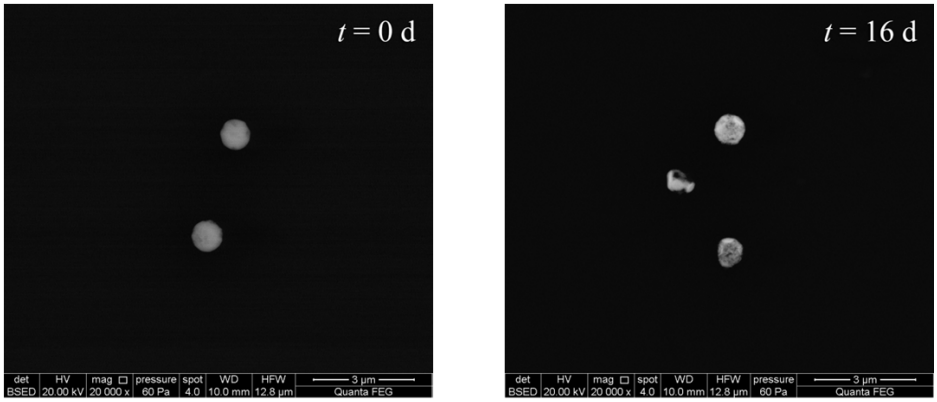

Fig. 91: SEM micrographs of particles stored in water. Reprinted from [4].

Of the investigated media (ethanol, 2-propanol, n-decane and dimethyl formamide), ethanol was found to be most suitable as media to process particles as no alteration of the particles was observed and particle detachment from the collection substrate into the media were highly efficient. SEM studies of particles stored in an ethanol suspension for up to 455 days (Fig. 92) did not show any alteration of the particles. Additionally, the amount of dissolved uranium was measured by Q-ICP-MS analysis, from which no significant dissolution was measured after 228 days.

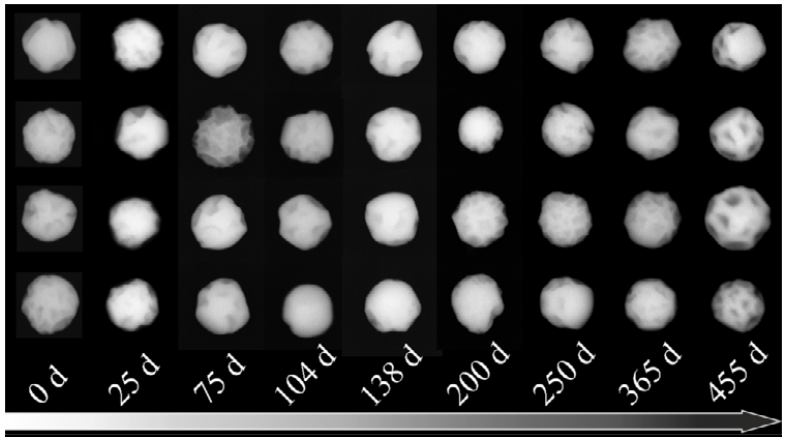

Fig. 92: SEM micrographs of particles stored in ethanol for up to 455 d. Reprinted from [5].

In addition to the dissolution studies, the isotopic exchange of uranium between different types of particles in an ethanol suspension was studied. Particles consisting of depleted uranium and low-enriched uranium were stored in ethanol and in time the isotopic composition of both particles was investigated. The results indicate that no exchange occurred within 202 days. To further investigate the isotopic exchange of uranium between U_3O_8 and dissolved uranium, milligram amounts of U_3O_8 containing depleted uranium were contacted with water and ethanol saturated with low-enriched uranium. In the aqueous system, a significant exchange was observed following first-order kinetics (Fig. 93).

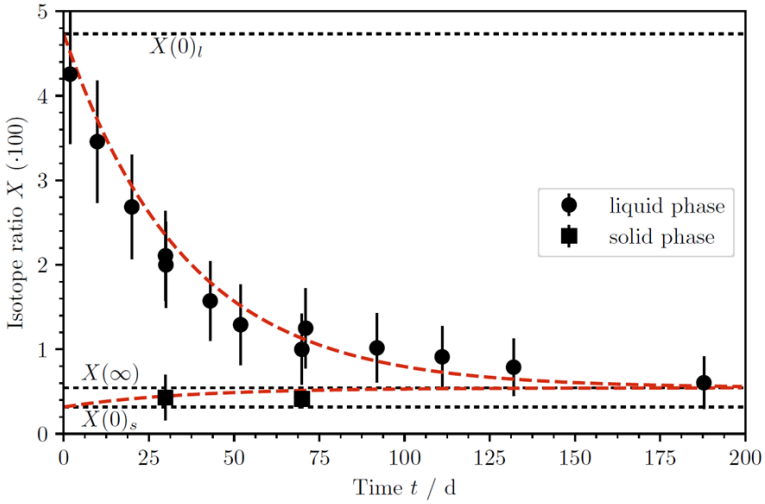

Fig. 93: Isotope exchange between U_3O_8 and uranium-saturated water. Reprinted from [5].

The experiments were performed at 14, 21 and 50 °C, from which the activation energy of the reaction could be estimated using Arrhenius equation. An activation energy of 35 kJ mol^{-1} was determined, which indicates that the exchange reaction occurs via surface reactions. Based on comparable experiments performed with different solid and liquid phases, the exchange is expected to occur via the formation of a uranyl hydroxide surface layer. Similar experiments performed in ethanol showed no exchange between the solid U_3O_8 and the uranium dissolved in the ethanol. These results indicate that no hydroxide layer is formed and any exchange proceeds via diffusion.

Particle suspensions

In order to increase the homogeneity, the produced particles were transferred into ethanol suspensions, as it was shown that the particles remain stable within such suspensions. Such suspensions could not only be used to increase the between-particle homogeneity, but also offers new possibilities towards the production of reference materials, such as particle mixtures, as was demonstrated using cerium and uranium oxide particles and the production of cotton swipe samples, as shown in Fig. 94.

Fig. 94: SEM micrographs of cotton swipe loaded with uranium (red) and cerium (yellow) oxide microparticles. Reprinted from [6].

Conclusion

Over the recent years, a method was developed to produce spherical microparticles with a monodisperse particle size distribution which can be used for quality control purposes. The production method was investigated with respect to the precursor solution and thermal treatment temperature, which allowed the method to be optimized. μ-XRD, μ-XANES and μ-Raman spectroscopy were employed to investigate the chemical structure of the produced particles, from which was found that the particles consist of an orthorhombic U_3O_8 phase. The presence of the U_3O_8 phase is of advantage towards the stability of particles in suspensions, which was demonstrated in ethanol; no dissolution and uranium isotopic exchange were observed. Particle suspensions were used to produce particle mixtures consisting of uranium and cerium oxide particles and to produce different types of samples, such as cotton swipe samples.

The isotopic composition of the produced particles was found to be similar to the isotopic composition of the precursor solution and, after thorough cleaning, samples free of any memory-effects were produced. A project is currently ongoing to produce particles which will be certified as certified reference material with respect to the uranium isotopic composition and the uranium content of single particles.

Acknowledgements

We thank F. Pointurier from CEA/DAM/DIF for the μ-Raman measurements and D. Ferreira-Sanchez, V. Samson and D. Grolimund from PSI for their support during the μ-XRD and μ-XANES measurements.

This work was supported by German Support Program to the IAEA under task C.43/A1960 and task C.45/A1961 and the Federal Ministry for Economic Affairs and Energy (FKZ 02W6263).

The μ-XRD and μ-XANES measurements leading to these results have received funding from the European Community's Seventh Framework Programme (FP7/2007-2013) under the Talisman project. We acknowledge the Paul Scherrer Institut, Villigen, Switzerland for provision of synchrotron radiation beam time at the microXAS beamline of the SLS.

References

[1] Knott, A.: *Production and Characterization of Monodisperse Uranium Particles for Nuclear Safeguards Applications.* (**2016**).
[2] Middendorp, R. et al. : *Anal. Chem.* 89 (**2017**) 4721-4728.
[3] Hoekstra, H.R.; Siegel, S.: *J. Inorg. Nucl. Chem.* 18 (**1961**) 154-165.
[4] Middendorp, R.; Dürr, M.; Bosbach, D.: *Procedia Chem.* 21 (**2016**) 285-292.
[5] Middendorp, R.: *Synthesis of Calibration Standards and Reference Materials for Nuclear Safeguards Applications.* (**in preparation**).
[6] Middendorp, R et al.: *ESARDA Bull.* 54 (**2017**) 23-30.

6.24. Non-nuclear applications

Non-nuclear applications of Prompt and Delayed Gamma Neutron Activation Analysis

Prompt and Delayed Gamma Neutron Activation Analysis (P&DGNAA) based on neutron generator or isotopic neutron sources is a versatile and powerful non-destructive analytical technique which may found applications in relevant fields such as safeguards (specific detection of nuclear materials), home-land security (detection of dangerous substances like chemicals or explosive), primary natural resources prospection (in situ borehole-logging, analysis of drilling core) and secondary natural resources assay (analysis of baring material, urban-mining, sludge, characterization of Waste Electrical and Electronic Equipment (WEEE) for recycling). Furthermore P&DGNAA may be implemented in industrial processes for parameter optimization and for quality control of products and also to determine the toxicity level of residues.

The MEDINA technology[1,2] based on P&DGNAA and developed for the characterization of radioactive waste has attracted quite some interest in recycling industry. The performance of MEDINA to determine the elemental composition of various large samples such as catalytic converters (Umicore AG & Co. KG, Belgium), CRT-glass (3S International, USA), Fluorescent powder (BLUBOX Company, Switzerland) and material from remedial activities (Eberhard Recycling AG, Switzerland) were investigated. In cooperation with RWE Power AG application of P&DGNAA for online elemental analysis of brown coal for firing optimization is also investigated.

References

[1] E. Mauerhofer, A. Havenith: *J. Radioanal. Nucl. Chem.* 302 (**2014**) 483-488.
[2] Patent AU2011282018; Forschungszentrum Jülich GmbH, E. Mauerhofer, J. Kettler

Application of safeguards methods and techniques in the context of monitoring BWC compliance

Many of the technologies and methodologies originally developed for safeguards verification in the context of the Nuclear Non-proliferation Treaty (NPT) could also be used for verifying or monitoring compliance with other non-proliferation or arms control treaties. In this context, IEK-6 has collaborated with the Research Group for Biological Arms Control at Carl Friedrich von Weizsäcker-Centre for Science and Peace Research (ZNF), University of Hamburg, on biological arms control. Due to the lack of an agreed verification mechanism in the Biological Weapons Convention (BWC), new approaches are required to support compliance monitoring and proliferation control. The main focus has been on the application of satellite imagery for off-site inspection of potential BW production facilities as well as mathematical models to analyse all potential paths by which a State could acquire biological warfare agents. In future, IEK-6 will collaborate with the newly established junior group “Biological threats: Analysis and integrated assessment of risks” (acronym: BIGAUGE) at the ZNF on mathematical modelling and open source information analysis for assessing biological risks.

Rare earth element separation by solvent extraction

During the last decades the demand for rare earth elements (REE) increases as a result of rising technology applications (e.g. hybrid cars, wind turbines, industrial catalyst, etc.). China has, beside Australia and the United States, the largest rare earth deposits and has a global monopoly on rare earths mining.[1] Since last years, caused by a Chinese export restriction, a significant increase in rare earth prices was observed. Expecting a rising demand for rare

earth metals a shortage of rare earths is upcoming. The separation of rare earth elements, the last step of rare earth mineral beneficiation, is the most value creating procedure. The most challenging separation is the separation of two directly neighboring rare earth elements.[2] There have been major developments in the technology for the separation of high purity rare earths. One advantageous technique for rare earth purification involves hydrometallurgical processes, such as those developed at IEK-6 for actinide(III) partitioning.[3] Both families of f-elements have very similar physical and chemical properties. Many extraction systems with relatively low rare earth separation factors were described in the literature. Neighboring rare earth elements, being chemically similar, show in Satos report separation factors from 1.03-2.58.[4] Satos data were reproduced and for heavier rare earth elements (e.g. Er, Yb) a higher extraction at lower concentrations can be observed. In collaboration with an industrial partner, the IEK-6 will use its expertise to develop more efficient extraction systems for the mutual lanthanide separation.

References

[1] Kynicky, J., Smith, M. P., Xu, C.: *Elements* 8 (**2012**) 361-367.
[2] Gupta, C.K., Krishnamurthy, N.: *Extractive metallurgy of rare earths.* CRC Press, Boca Raton, Florida, (**2005**).
[3] Modolo, G., Odoj, R.: *J. Alloy. Compd*. 271-273 (**1998**) 248-251.
[4] Sato, T.: *Hydrometallurgy* 22 (**1989**) 121-140.

7 Education and training activities

Education in nuclear safety research in particular with RWTH Aachen University is supported by IEK-6. Prof. Dirk Bosbach holds the chair for the disposal of nuclear waste. Further, an accredited Master Curriculum "Nuclear Safety Engineering" was established at RWTH Aachen University in 2010 and in the meantime several students participated this two years programme. A practical course on nuclear measuring techniques in the radiochemistry laboratories of IEK-6 as well as the lecture "Introduction to Nuclear Chemistry" was launched in 2010 and has attracted students from nuclear safety engineering, chemistry, computational engineering science and nuclear technology at RWTH Aachen University. Lectures are also given at the Aachen University of Applied Science by IEK-6 staff.

In the framework of the JARA cooperation Prof. Evgeny Alekseev is teaching at the Institute of Crystallography / RWTH Aachen University. Additionally Prof. Giuseppe Modolo and Dr. Holger Tietze-Jaensch were appointed as adjunct professor at RWTH Aachen University, Faculty of Georesources and Materials Engineering, Aachen, Germany in 2016 and as guest professor at the University of South China, Hengyang, Hunan, China for the period of 2015-2017, respectively.

The IEK-6 also participates in the new graduate school Energy and Climate HITEC, which was founded in 2011 in Jülich. The IEK-6 supports HITEC Theme Days “Nuclear waste disposal and reactor safety” held at RWTH Aachen University, HITEC Methods Days “Application of X-ray diffraction methods in energy research” as well as HITEC Labs “Synthesis methods for immobilizing radioactive elements in ceramic host phases” and “Structural characterization of ceramics by spectroscopic and diffraction methods”, which are hands-on practical training lasting two to three days for small groups of PhD students from various HITEC fields. Furthermore, biannual Orientation Days (in March and October) are organized for new HITEC participates. Second-year PhD students organize a three-day retreat; where they present their projects and the scientific methods employed and discuss them with their fellow PhD students.

7.1. Courses taught at universities by IEK-6 staff

Prof. Dr. D. Bosbach

RWTH Aachen University
Faculty of Georesources and Materials Engineering
Topic: Grundlagen der Kernchemie, Hours: 2 SWS, since WS 2010
Topic: Langzeitsicherheit der Endlagerung, Hours: 2 SWS, WS 2012/2013 2013/2014
Topic: Kerntechnisches Messpraktikum, 1 week, since WS 2010

Prof. Dr. E. Alekseev

RWTH Aachen University
Faculty of Georesources and Materials Engineering
Topic: Some aspects of solid state and coordination chemistry of actinides, Hours: 4 SWS, SS 2014
Topic: Single-crystal diffraction on actinide compounds, Hours: 4 SWS, SS 2014
Topic: Grundzüge der Kristallographie, Hours: 4 SWS, Since WS 2012

Dr. Piotr Kowalski

KIT, Karlsruhe
ThUL School in Actinide Chemistry
Topic: How challenging is it to compute actinides? Atomistic modeling of nuclear materials relevant for nuclear waste management. 2h lecture, Oct 2015

RWTH Aachen, German Research School on Simulation Sciences
Simulation Science Seminar
Topic: Computational Science in Nuclear Waste Management: Atomistic Modeling of Nuclear Materials, 1h Seminar lecture, Dec 2016

Prof. Dr. G. Modolo

Aachen University of Applied Science, Fachbereich Chemie und Biotechnologie
European Master of Science in Nuclear Applications
Topic: Nuclear Fuel Cycle, Hours: 2 SWS since 2010

RWTH Aachen University
Faculty of Georesources and Materials Engineering
Topic: Brennstoffe, Wiederaufbereitung und Konditionierung, Hours: 2 SWS, since 2011
Topic: Sicherheit in der Wiederaufarbeitung, Hours: 3 SWS, since 2011
Topic Die Wertschöpfungskette der Seltenen Erden(SE)- Gewinnung und Recycling, 3.5 SWS, since 2015

Dr. I. Niemeyer

Rheinische Friedrich-Wilhelms-Universität Bonn
Faculty of Mathematics and Natural Sciences
Topic: The role of remote sensing in disaster management and conflict prevention, Hours: 2 SWS, WS 2015/16

Dr. H. Tietze-Jaensch

Institute for Nuclear Chemistry and Technology (INCT), Warsaw, Poland; June 2015
JRC, Ispra, Italy, 7th/8th International Summer School on Nuclear Decommissioning and Waste Management
University of South China, Hengyang, Hunan, China, October 2015 and 2016
Warsaw University of Technology, Faculty of Physics, Warsaw, Poland

7.2. Appointment

In 2016 RWTH Aachen University, Faculty 5- Georesources and Materials Engineering awarded **Giuseppe Modolo** as adjunct professor.

For the period of 2015-2017 the University of South China, Hengyang, Hunan, China awarded **Dr. Holger Tietze-Jaensch** as guest professor.

7.3. Graduates

12 PhD students are currently (Dec. 2016) working on research projects related to the safe management of nuclear waste in Jülich. 7 PhD candidates have successfully defended their theses during the last 2 years and 3 PhD candidates will finish in 2017. Furthermore, 12 diploma, bachelor, and master theses were finished in 2015 / 2016. Currently, 8 students are working on their theses. 6 students passed an internship at IEK-6 during the last 2 years.

7.3.1 Bachelor, Diploma, Master thesis

J. Dellen: Incorporation of tetravalent F-elements into the crystal structures of samarium orthophosphates and related phosphosilicates. Master thesis (2016), Aachen University of Applied Sciences – FH, Campus Jülich.

R. Engelmann: Synthese und Charakterisierung von UO_2-basierten Modellsystemen. Bachelor thesis (2016) Aachen University of Applied Sciences – FH, Campus Jülich.

C. Gatzen: Phasenbeziehungen im System $YbPO_4$ – $GdPO_4$. Master thesis (2015) RWTH Aachen University.

P. Haaß: U/Gd oxide system – studies on the influence of gadolinium on the oxide system via internal gelation and co-precipitation. Master thesis (2016) Aachen University of Applied Sciences – FH, Campus Jülich.

A. Hable: Wirkungsquerschnittsbestimmung (n,f) von ^{238}U, ^{237}Np und ^{242}Pu mit Spaltneutronen am FRMII, Garching. Master thesis (2016), TU Vienna, Austria.

J. Holthausen: Synthesis, pelletization and characterization of a monoclinic lanthanum gadolinium phosphate solid solution system. Bachelor thesis (2016), Zuyd Hoogeschool, Heerlen, Netherland.

L. Klaß: Modified diglycolamides for a selective separation on Am(III): complexation, structural investigations and process applicability. Master thesis (2016), RWTH Aachen University.

B. Kraus: Selective separation of americium(III) from PUREX raffinate using diglycolamide-based solvents combined with hydrophilic complexants. Master thesis (2015), Aachen University of Applied Sciences – FH, Campus Jülich.

N. Lieck: Study on the determination of Fe-55 in neutron activated steel components by X-ray spectrometry. Bachelor thesis (2016), Zuyd Hoogeschool, Heerlen, Netherland.

7.3.2 Doctoral thesis

G. Beridze: Feasible and reliable *ab initio* atomistic modeling for nuclear waste management. Schriften des Forschungszentrums Jülich Reihe Energie & Umwelt / Energy & Environment 325, 128 p. (2016) RWTH Aachen University.

J. Heuser: Keramiken des Monazit-Typs zur Immobilisierung von minoren Actinoiden und Plutonium. Schriften des Forschungszentrums Jülich Reihe Energie & Umwelt / Energy & Environment 278, 212 p. (2015) RWTH Aachen University.

C. Genreith: Partial neutron capture cross sections of actinides using Cold Neutron Prompt Gamma Activation Analysis. Schriften des Forschungszentrums Jülich Reihe Energie & Umwelt / Energy & Environment 250, 166 p. (2015) RWTH Aachen University

A. Knott: Production and characterization of monodisperse uranium particles for nuclear safeguards applications. Schriften des Forschungszentrums Jülich Reihe Energie & Umwelt / Energy & Environment 336, 184 p. (2016) RWTH Aachen University.

T. Nicol: Caractérisation des colis de déchets radioactifs par activation neutronique. (2016) Université Grenoble Alpes, France.

B. Xiao: The Crystal Chemistry of Thorium and Uranium Compounds with Oxo-anions from Group VI of Periodic Table (S, Se, Te, Cr, Mo and W). (2016) RWTH Aachen University.

N. Yu: New insights into thorium and uranium oxo-arsenic(III/V) and oxo-phosphates(V) crystal chemistry. (2015) RWTH Aachen University.

7.4. Vocational training

Forschungszentrum Jülich offers different vocational training programs. The 3 years lasting education is supported by IEK-6 in nuclear- / radio-chemistry. In 2015/16 five laboratory assistants were trained in the laboratories of IEK-6. Three of them finished their education successfully in 2015/2016 and received a certificate of apprenticeship.

7.5. Further education and information events

IEK-6 is committed to support the education of young people including schoolchildren in nuclear safety research. Forschungszentrum Jülich participates in the nationwide **"Girls and Boys Day".** Girls from 5th to 13th class have the opportunity to become familiar with different professions such as chemist, physicist, or firewoman as well as the working conditions at laboratories, garages and offices. At IEK-6, the topic "No fear of radioactive materials" was presented. Basics about radioactivity in the environment and radioactive decay as well as different measuring techniques were explained. Measurements of different sample were carried out by the girls themselves to get a feeling for radioactivity and attract children's interest in science.

In February 23 – 25, 2015, the "**25th Seminar on Activation Analysis and Gamma Spectroscopy (SAAGAS)**" was organized by IEK-6 in Aachen, Germany to provide an exchange forum for beginners and experienced scientists in this field. The international seminar comprised 32 oral presentations and a poster session addressing important topics such as nuclear waste characterization, development of advanced techniques and data analysis tools as well as industrial applications.

From November 30 to December 01, 2015, the "**6th Workshop of the PhD Network on Reactive Transport - Modeling and Experiments**" was held at Forschungszentrum Jülich, organized by IEK-6. These workshops serve as a platform for PhD students working within the field of reactive transport (modeling and experiments) to present and discuss their work, exchange their knowledge and ideas, and share their experience. The workshop was attended by 18 participants representing 8 academic institutions (i.e. research centres and universities) from Germany, Belgium and Spain. During the workshop 13 oral presentations were given covering topics from pore scale modeling of concrete degradation, porosity evolution in porous media due to mineral dissolution/precipitation, to catchment scale simulations of reactive transport and applications of High Performance Computing (HPC) in reactive transport modelling. The workshop was concluded with a guided tour to the Jülich Supercomputing Centre to obtain information on their HPC infrastructure, in particular, the supercomputers JUQUEEN and JUROPA.

7.6. Institute seminar

The IEK-6 organizes an institute seminar with internal talks and invited speakers, to present the recent research activities. Further information on www.fz-juelich.de/iek/iek-6.

7.6.1 Internal talks 2015

27.01.2015 **H. Curtius:** Endlagersicherheit
S. Neumeier: Innovative Entsorgungsstrategien (Keramik)
E. Alekseev: Festkörperchemie der Actiniden
P. Kowalski: Atomistische Modellrechnung
H. Schlenz: Strukturforschung
G. Modolo: Innovative Entsorgungsstrategien (Partitioning)
E. Mauerhofer: Abfallcharakterisierung
M. Rossbach: Nukleare Daten
H.-J. Steinmetz: Entsorgungskonzepte für radioaktive Abfälle
I. Niemeyer: Safeguards

04.02.2015 **B. Xiao:** New aspects of Th chemistry in oxo-molybdate and oxo-tungstate systems

11.03.2015 **S. Weigelt:** Synthesis and characterization of geopolymers as nuclear waste forms for the save disposal of fission products ^{137}Cs and ^{90}Sr
Y. Arinicheva: Structural and microstructural investigations on monazite type ceramics

18.03.2015 **M. Schumann:** Fast neutron imaging with an a Si Detector for nuclear waste assay
F. Mildenberger: Thermal neutron die-away-time studies for P&DGNAA of large samples at the MEDINA-facility

22.04.2015 **A. Bukaemskiy:** Some aspects of phase stability in zirconia-neodymia system

06.05.2015 **S. Finkeldei:** Fabrication and structural characterisation of plutonium-pyrochlore ceramics
L. Kuhne: ^{14}C release from reactor graphite

20.05.2015 **I. Fast:** Determination of uncertainties of PWR spent fuel radionuclide inventory based on real operational history data
N. Yu: Further insight into uranium and thorium metaphosphate chemistry and the effect of Nd^{3+} incorporation into uranium(IV) metaphosphate

17.06.2015 **T. Randriramalala:** FaNGaS: A new instrument for the (n,n'gamma) reaction measurements at FRM II

T. Nicol: ^{235}U and ^{239}Pu characterization in radioactive waste using neutron fission delayed gamma rays

19.08.2015 **M. Dürr:** Die Qualität von Messdaten in der nuklearen Verifikation - aktuelle Forschungs- und Entwicklungsarbeiten am Forschungszentrum Jülich

26.08.2015 **E. Ebert:** Dissolution studies on Mo- and MgO-based inert matrix fuels for the transmutation of minor actinides

16.09.2015 **Y. Hao:** Further exploration on synthetic and structural chemistry of Actinide Borates

23.09.2015 **S. Hadic:** Chemical degradation studies on a series of dithiophosphinic acids

G. Beridze: Fast and reliable calculations of f-elements from first principles

30.09.2015 **S. Neumeier:** Structural investigations on $(La,Gd)PO_4$ solid solutions under heavy ion irradiation

28.10.2015 **H. Schmidt:** Radiolytic stability of the highly selective nitrogen donor ligands $CyMe_4BTBP$ and $CyMe_4BTPhen$

A. Wilden: Gamma-radiolytic stability of new methylated TODGA derivatives for minor actinide recycling

04.11.2015 **Y. Ji:** Large scale atomistic simulations of radiation damage in monazite-type ceramics

R. Middendorp: Preparation of uranium oxide microparticles for nuclear safeguards

18.11.2015 **P. Kaufholz:** Selective separation of Am(III) from PUREX-raffinates

25.11.2015 **I. Niemeyer:** Nuclear arms control and disarmament verification: Technical challenges and solutions

B. Kraus: Selective separation of americium(III) from PUREX raffinate using diglycolamide-based solvents combined with hydrophilic complexants

02.12.2015 **C. Rizzato:** Radiocarbon on Spent Ion Exchange Resins (SIERs) arising from BWRs

7.6.2 Internal talks 2016

20.01.2016 **N. Shcherbina:** Irradiated graphite and it´s safe disposal

V. Vinograd: Thermodynamics of mixing in the ternary (Ba,Sr,Ra)SO_4 solid solution

27.01.2016 **K. Aymanns:** Technical challenges of safeguards implementation in Germany

24.02.2016 **G. Murphy:** Examination of high temperature structural phase transformations in strontium uranium oxides using neutron and synchrotron scattering

03.03.2016 **F. Brandt:** Sekundärphasen

G. Deissmann: Simulation des Reaktiven Stofftransports

E. Alekseev: Festkörperchemie

P. Kowalski: Atomistische Simulation

N. Shcherbina: Abfallbehandlung

G. Modolo: Hydrometallurgische Trennverfahren

E. Mauerhofer: Abfallcharakterisierung

M. Rossbach: Nukleare Daten

I. Niemeyer: Internationale Kernmaterialüberwachung

09.03.2016 **E. Langer:** Investigation of phase formation by structural and topologic characterization within Th/U oxo-selenium systems

16.03.2016 **H. Schlenz:** Structural features and thermodynamic properties of some selected oxides, phosphates and aluminosilicates relevant for nuclear waste disposal.

27.04.2016 **L. Klaß:** Modified diglycolamides for a selective separation of Am(III): complexation, structural investigations and process applicability

20.05.2016 **P. Haaß:** U/Gd oxide system - studies on the influence of gadolinium on the oxide system via internal gelation and co-precipitation

01.06.2016 **I. Fast:** Realistic bandwidth estimation in the theoretically predicted radionuclide inventory of PWR-UO_2 spent fuel derived from reactor design and operating data

15.06.2016 **Y. Ji:** Complementary atomistic modeling and experimental studies of radiation damage in monazite-type ceramic nuclear waste forms

15.06.2016 **T. Koubsky**: DFT simulations of chemical stability of ligands used in liquid-liquid extraction of actinides

22.06.2016 **M. Isaacs:** Uptake and retention of selenium and iodine in cementitious systems

29.06.2016 **P. Kegler:** High temperature drop solution calorimetry of $La_{1-x}Ln_xPO_4$-monazites and $Nd_xZr_{1-x}O_{2-0.5x}$ pyrochlores

07.09.2016 **A. Baena:** UO_2 and ThO_2 doped nuclear fuel

14.09.2016 **Y. Li:** *Ab initio* simulations of ceramics relevant for nuclear waste management: Cases of monazite and pyrochlore

28.09.2016 **F. Mildenberger:** Charakterisierung von Mischabfällen mittels der Zyklischen Neutronen-Aktivierungs-Analyse (CNAA)

26.10.2016 **J. Poonoosamy:** Benchmarking of reactive transport codes for a 2D setup with mineral dissolution/precipitation reactions and feedback of transport parameters

07.12.2016 **J. Weber**: Fundamental insights into the radium uptake into barite by atom probe tomography and electron microscopy

7.6.3 Invited talks 2015

26.02.2015 **Prof. D. Read:** Challenges posed by industrial radioactivity
Loughborough University, UK

21.04.2015 **Prof. D. Shoesmith:** The influence of composition and lattice properties on the electrochemical reactivity and corrosion behaviour of uranium dioxide under waste disposal conditions
University of Western Ontario, Canada

30.06.2015 **Dr. J.S. Poonoosamy:** Multi-scale investigation of porosity change due to mineral dissolution and precipitation
PSI, Switzerland

30.06.2015 **M. Isaacs:** Synthesis of superplasticisers and an assessment of their suitability for use in a GDF
Loughborough University, UK

01.09.2015 **M. Sailer:** Entsorgung und Endlagerung in Deutschland – Situation und Fragen
Öko-Institut e.V., Berlin, Germany

29.10.2015 **C.R. Scales:** Technology development for the immobilisation of plutonium containing residues
National Nuclear Laboratory, UK

24.11.2015 **R.J. Baker:** Uranyl minerals as models for the long term storage of spent nuclear fuels
Trinity College, University of Dublin, Ireland

7.6.4 Invited talks 2016

12.01.2016 **Dr. S. Wu:** The effect of substituted ions on the retention of Se, U and Tc by pyrite
Helmholtz-Zentrum Dresden-Rossendorf, Dresden, Germany

17.02.2016 **Dr. R. Hellmann:** Nanoscale interfacial science applied to mineral-water and glass-water interactions

19.04.2016 **Dr. J. Tits:** Die Immobilisierung von Selen durch Zement unter Endlager-bedingungen
PSI, Switzerland

18.05.2016 **W. Filbert / S. Dörr:** Safeguardskonzepte für die Endlagerung ausgedienter Kernbrennstoffe in verschiedenen Wirtsgesteinen unter Berücksichtigung der Rückholungs- und Bergungsoption
DBE Technology GmbH, Peine, Germany

19.09.2016 **B.P. Uberuaga:** A generalized view of amorphization resistance in complex oxides
Los Alamos National Laboratory, USA

09.11.2016 **Dr. A.G. Kalinichev**: Molecular computer simulation of the multi-scale dynamics of water and Ions in the nanopores of cementitious materials
L'Ècole des Mines de Nantes, France

09.11.2016 **I. Androniuk**: Interaction of gluconate and uranyl ions with calcium silicate hydrate phases
L'Ècole des Mines de Nantes, France

14.11.2016 **Prof. Dr. U. Becker**: Quantifying kinetic bottlenecks in mineral-catalyzed redox reactions
University of Michigan, USA

23.11.2016 **Prof. Dr. M. Gottschalk**: Beyond the Margules-equation: A universal thermodynamic equation for solid solutions including coupled substitution, long- and short-range order
German Research Centre for Geosciences (GFZ), Potsdam, Germany

02.12.2016 **Prof. Dr. H.L. Hall:** The Institute for Nuclear Security at the University of Tennessee: Objectives, capabilities, activities
University of Tennessee, Knoxville, USA

7.7. Visiting scientists / Research visits

Visiting scientists

Jose Jorge Rios Ramirez — Aug. 2014 - Jan. 2015
University of Puebla, Mexico

Rebecka Forward — June - Aug. 2015
Queen's University, Kingston, Canada

Gabriel Murphy — Jan. - Mar. 2015
University of Sydney, Australia
Australian Nuclear Science and Technology Organisation (ANSTO), Sydney, Australia

Simon Blouin — May - Aug. 2016
University of Montreal, Montreal, Canada

Tomas Koubsky — June 2016
Czech Technical University, Prague, Czech Rep.

Guojun Yuan — Mar. 2016 - Feb. 2017
China Institute of Atomic Energy, Beijing, China

Research visits of IEK-6 staff

Ronald Middendorp, Alexander Knott — Oct. 2015
Paul-Scherrer-Institute, Villigen, Switzerland

Philip Kegler; Christian Schreinemachers — Mar. - Apr. 2015
University of California Davis, CA, USA

Yulia Arinicheva
JRC-Karlsruhe (former ITU), Germany — Nov. - Dec. 2015
University of Bergen, Norway — Mar. – Aug. 2016

Ronald Middendorp — May 2016
Paul-Scherrer-Institute, Villigen, Switzerland

Holger Tietze-Jaensch
University of South China, Hengyang, Hunan, P.R. China — Oct. 2015 & Oct. 2016
University of Bristol, UK — Jan. - Mar. 2016

Sarah Finkeldei
University of Sheffield, UK — Feb. & Apr. 2015
Australian Nuclear Science and Technology Organisation (ANSTO), Sydney, Australia — Nov. - Dec. 2015
The University of Tennessee, Knoxville, USA — Apr. & Oct. - Dec. 2016

8 Awards

Sarah Finkeldei received the Cutting-Edge-Idea Award of the Forschungszentrum Jülich for her Projekt “COCO-SNUF: Unravelling the Corrosion Complexity of Spent Nuclear Fuel: “Understanding fundamental reaction mechanisms using UO_2 based model systems”, 2015.

Sarah Finkeldei received the Ph.D Award of the German Chemical Society, Nuclear Chemistry Division (Promotionspreis der Fachgruppe Nuklearchemie der Gesellschaft Deutscher Chemiker (GDCh)) for her thesis "Pyrochlore as nuclear waste form: actinide uptake and chemical stability”, 2015.

Thomas Krings, Julia Heuser, and Sarah Finkeldei received the Borchers Award of the RWTH Aachen for their Ph.D. theses rated “summa cum laude”.

Sarah Finkeldei received the Excellence Award of the Forschungszentrum Jülich for her Ph.D. thesis, 2016.

Fig. 95: Award ceremony „JuDocs 2016“. The Excellence Award of Forschungszentrum Jülich GmbH was awarded to Dr. Sarah Finkeldei.

8.1. Poster awards

George Beridze, Yan Li and Piotr Kowalski won a prestigious poster prize awarded by the European Mineralogical Union at Goldschmidt conference 2015 for the poster "*Ab initio* modeling of computationally challenging Earth (f-) materials" (see EMU Poster Prizes at eurominunion.org). This poster was presented in „Crystal Chemistry of Earth and Planetary Materials" session (2015).

Steve Lange, Guido Deissmann and Dirk Bosbach received a poster prize at the "4th International Workshop on Mechanisms and Modelling of Waste/Cement Interactions" in Murten, Switzerland, for his contribution on "Uptake and retention of safety relevant radionuclides in cementitious systems".

Ivan Fast, Yulia Aksyutina, Holger Tietze-Jaensch and Dirk Bosbach were awarded best Track-2 poster at the Waste Management Symposium, WMS2015, Phoenix, USA, Mar 2015, for the contribution on the "NPP Operational History and the Uncertainties of Radionuclides Relevant for the Final Disposal of PWR Spent Fuel"; WM Proceedings 2015, 15149 pp. (2015).

8.2. Scholarships

Rebecka Forward, Queen's University, Kingston, Canada received a 3-months fellowship of the DAAD-Rise (Research Internships in Science and Engineering) foundation to perform atomistic simulations in the Young Investigator Group of **Dr. Piotr Kowalski** (IEK-6).

Jose Jorge Rios Ramirez, University of Puebla, Mexico, won a 6-months Mexican National Council of Science and Technology (CONACYT) scholarship to perform PhD dissertation research on the atomistic simulations of Pu-oxides surfaces in the Young Investigator Group of **Dr. Piotr Kowalski** (IEK-6).

Simon Blouin from University of Montreal, Canada, won 4 months DAAD scholarship for research stay to perform simulations of IR spectra in the Young Investigator Group of **Dr. Piotr Kowalski** (IEK-6).

Tomas Koubsky, Czech Technical University in Prague, won a 1 month DAAD scholarship for research stay in the Young Investigator Group of **Dr. Piotr Kowalski** (IEK-6).

Yulia Arinicheva (IEK-6) was awarded with a half-year international scholarship in collaboration with the University of Bergen supported by the German-Norwegian Scholarship Programme in "Energy Sciences" of E.ON Stipendienfonds. The joint research project focused on basic studies of properties of rare-earth-element orthophosphates with respect to their capability in sustainable energy technology applications.

9 Selected R&D projects

9.1. EU projects

ANNETTE – Advanced Networking for Nuclear Education and Training and Transfer of Expertise; 01/2016 - 12/2019.

ASGARD - Advanced fuelS for Generation IV reActors: Reprocessing and Dissolution, 10/2011 - 10/2015, Work package leader: Dr. G. Modolo, FZJ

CEBAMA – Cement-based materials, properties, evolution, barrier functions; 06/2015 - 05/2019

G-SEXTANT – Geospatial Intelligence Services in Support of EU External Action; 01/2013 - 03/2015; Work package leader: Dr. I. Niemeyer

SACSESS - Safety of Actinide Separation Processes; 03/2013 - 02/2016; Work package leader: Dr. G. Modolo, FZJ

9.2. More projects

ImmoRad - Grundlegende Untersuchungen zur Immobilisierung langlebiger Radionuklide durch die Wechselwirkung mit endlagerrelevanten Sekundärphasen; 02/2012 - 01/2015, Bundesministerium für Bildung und Forschung (BMBF)

Radiographie mittels schneller Neutronen zur Charakterisierung radioaktiver Abfälle (**Neutronen Imaging**); 05/2012 - 04/2015
Bundesministerium für Bildung und Forschung (BMBF)

Untersuchungen zum grundlegenden Verständnis der selektiven Komplexierung von f-Elementen (**f-KOM**); 07/2012 - 06/2015
Bundesministerium für Bildung und Forschung (BMBF)

Bestimmung und Validierung nuklearer Daten von Actiniden zur Zerstörungsfreien Spaltstoffanalyse in Abfallproben durch prompt Gamma Neutronenaktivierungsanalyse (**PGAA-Actinide**); 08/2012 - 07/2015
Bundesministerium für Bildung und Forschung (BMBF)

Conditioning - Grundlegende Untersuchungen zur Immobilisierung langlebiger Radionuklide mittels Einbau in endlagerrelevante Keramiken; 10/2012 - 06/2016
Bundesministerium für Bildung und Forschung (BMBF)
Coordination: Dr. S. Neumeier, FZJ

Synthese und Charakterisierung keramischer Samarium-Phosphat- und Samarium-Phosphosilicat-Phasen zur Immobilisierung von Actinoiden; 04/2012 - 06/2015
Deutsche Forschungsgemeinschaft (DFG)

Koordinierung und fachliche Betreuung des deutschen IAEO-Safeguards-Unterstützungsprogramms (**Scientific Coordination of the German Safeguards Support Programme to the IAEA**); 07/2013 - 06/2017
Bundesministerium für Wirtschaft und Energie (BMWi)

Neu- und Weiterentwicklung von Safeguardstechniken und –methoden (**Safeguards techniques and methods**); 10/2013 - 09/2017
Bundesministerium für Wirtschaft und Energie (BMWi)

PROMETEUS – PROcess of radioactive MErcury Treatment under EU Safety-standards; 06/2016-05/2019
Bundesministerium für Bildung und Forschung (BMBF)

Material properties of depleted U_3O_8
Urenco, Germany

Thermogravimetric and radiochemical analysis of activated graphite
Jülicher Entsorgungsgesellschaft für Nuklearanlagen mbH (JEN), Germany

Aufklärung von Thermodynamik und Speziation von Actiniden bei höheren Temperaturen in Kombination von Schätzmethoden, spektroskopischen und quantenchemischen Methoden (**ThermAc3**); 03/2015 - 03/2018
Bundesministerium für Bildung und Forschung (BMBF)

10 Committee work

Prof. Dr. Dirk Bosbach:

- Speaker of the Helmholtz research program "Nuclear Waste Management, Safety and Radiation Research"
- Member of the Berlin-Brandenburg Academy of Science (BBAW)
- Member of the advisory board of the Nuclear chemistry division of the German Chemical Society (GDCh)
- Member of the scientific advisory boards of the TALISMAN network
- Representative of FZJ in the German Alliance for Competence in Nuclear Technology
- Representative of FZJ in the Impelementation of Geological Disposal - Technology Plattform (IGD-TP)
- Representative of FZJ in the Sustainable Nuclear Energy - Technology Platform (SNETP) incl. the NUGENIA network

Dr. Martin Dürr

- Representative of FZ Jülich in the German Safeguards Coordination Committee (AG Kernmaterialüberwachung, AKÜ)

Dr. Sarah Finkeldei

- Member of the Structure Committee for IEK-13
- Member of the Appointment Committee for IEK-13

Dr. Clemens Listner

- Institute of Nuclear Materials Management (INMM): Associate Editor of the Journal of Nuclear Materials Management (JNMM)

Dr. Eric Mauerhofer

- Member of International Committee on Activation Analysis
- Scientific Consultant for RWE Power AG in the field on online coal-analytics
- Scientific and organization Committee of 25th Seminar on Activation Analysis and Gamma Spectroscopy, Aachen, Germany (2015)

Prof. Dr. Giuseppe Modolo:

- Technical Programm Committee of the First SACSESS International Workshop 2015
- Technical Conference Committee of International Global 2015 conference, Paris, France
- Technical Conference Committee of the International ATALANTE 2016 conference, Montpellier, France
- Editorial Board of the Journal Solvent Extraction and Ion Exchange
- Distinguished reviewers board of the Journal of Radioanalytical and Nuclear Chemisty

Dr. Irmgard Niemeyer:

- Standing Advisory Group on Safeguards Implementation (SAGSI): German member
- European Safeguards Research and Development Association (ESARDA): Vice President 2015/16, Representative of FZ Jülich in the Steering Committee, Chair Symposium Committee 2015
- Institute of Nuclear Materials Management (INMM): Vice-Chair WG Open-source and Geospatial Information (2015), Associate Editor Journal of Nuclear Materials Management
- Representative of FZ Jülich in the German Safeguards Coordination Committee (AG Kernmaterialüberwachung, AKÜ)
- Women in Nuclear (WiN) Germany, Member of the Board (Education) (2016)
- International Partnership for Nuclear Disarmament Verification (IPNDV): Technical Expert for Germany
- International Society for Photogrammetry and Remote Sensing (ISPRS): Member of the International Policy Advisory Committee (IPAC)

Dr. Matthias Rossbach:

- International Committee on Activation Analysis
- International Scientific Advisory Committee for the Budapest Neutron Centre, Hungarian Academy of Sciences
- Review Panel Imaging, Analysis, Nuclear and Particle Physics for Beam-time at all Instruments hosted at FRM II Research Reactor, Garching
- Scientific Advisory Committee of the 2016 Int. Conf. on Nuclear Data for Science and Technology, Bruges, Belgium
- WPEC sub-group SG-41: Improving nuclear data accuracy of ^{241}Am and ^{237}Np capture cross sections

Priv.-Doz. Dr. Hartmut Schlenz:

- Member of the NEA TDB Iron II expert group

Dr. Holger Tietze-Jaensch:

- IAEA - Labonet: accredited German representative at the IAEA network LABONET on issues of the Characterization of Radioactive Waste
- ENTRAP-SC: Member and elected chairman of the Steering Committee of the European working group ENTRAP (European Network of Testing facilities for the quality checking of Radioactive waste Packages)
- iPAC & PAC -WM: Member of the International Advisory Committee (IPAC) and of the Program Advisory Committee (PAC) of Waste Management, Phoenix, AZ, USA

Dr. Hans-Jürgen Steinmetz:

- International Program Advisory Committee (IPAC) of the Annual Arizona Waste Management Conference

Katharina Aymanns:

- Deputy chairperson in the DIN Standards Committee Materials Testing

11 Publications

The scientific and technical results of the work carried out at IEK-6 are published in relevant journals and presented to interested specialist audience at national and international conferences on the subject.

Table 8: Publications 2015/2016

Year		2015	2016
Publications	Peer reviewed journals	42	40
	Books	1	3
	Proceedings	19	4
Conferences	Presentations	65	51
	Poster	34	20

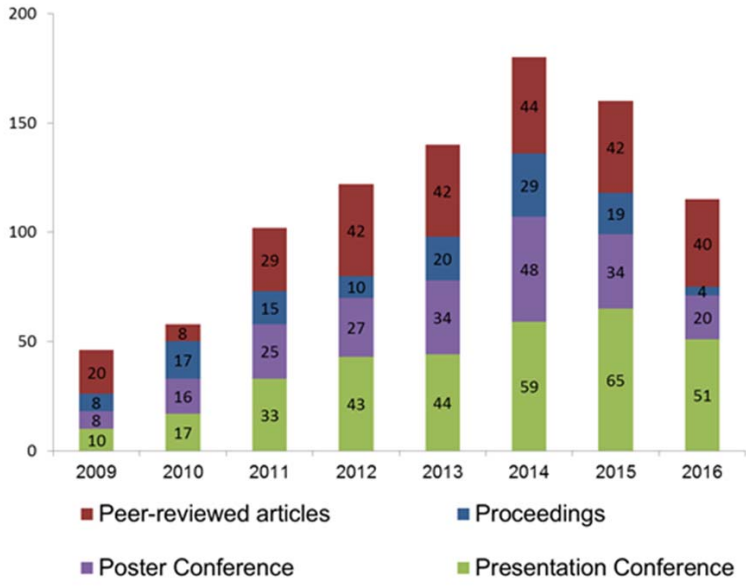

Fig. 96: Publications 2009 - 2016.

11.1. Publications 2015

11.1.1 Journal papers

Peer-reviewed journals

Allen, K., Deicer, M., Cliff, C., Niemeyer, I., Listner, C., 2015: Systems approach to arms control verification. ESARDA Bulletin, 53: 83-91.

Aneheim, E., Ekberg, C., Modolo, G., Wilden, A., 2015: Single centrifugal contactor test of a proposed group actinide extraction process for partitioning and transmutation purposes. Separation Science and Technology, 50(10): 1554-1559.

Brandt, F., Curti, E., Klinkenberg, M., Rozov, K., Bosbach, D., 2015: Replacement of barite by a $(Ba,Ra)SO_4$ solid solution at close-to-equilibrium conditions: A combined experimental and theoretical study. Geochimica et Cosmochimica Acta, 155: 1-15.

Carrott, M., Geist, A., Hères, X., Lange, S., Malmbeck, R., Miguirditchian, M., Modolo, G., Wilden, A., Taylor, R., 2015: Distribution of plutonium, americium and interfering fission products between nitric acid and a mixed organic phase of TODGA and DMDOHEMA in kerosene, and implications for the design of the "EURO-GANEX" process. Hydrometallurgy, 152: 139-148.

Curtius, H., Kaiser, G., Lieck, N., Güngör, M., Klinkenberg, M., Bosbach, D., 2015: Spent UO_2 TRISO coated particles - instant release fraction and microstructure evolution. Radiochimica Acta, 103(6): 433-442.

Degueldre, C. and Alekseev, E., 2015: Uranium trioxide behavior during electron energy loss spectroscopy analysis. Radiation Physics and Chemistry, 108: 7-12.

Ebert, E., Bukaemskiy, A., Sadowski, F., Lange, S., Wilden, A., Modolo, G., 2015: Reprocessability of molybdenum and magnesia based inert matrix fuels. First SACSESS International Workshop, 60(4-Pt.II): 871-878.

Fischer, C., Finkeldei, S., Brandt, F., Bosbach, D., Luttge, A., 2015: Direct measurement of surface dissolution rates in potential nuclear waste forms: The example of pyrochlore. ACS Applied Materials & Interfaces, 7(32): 17857-17865.

Galán Montano, H., Zarzana, C., Groenewold, G. S., Mincher, B. J., Wilden, A., Núñez Gómez-Aleixandre, A., Schmidt, H., Egberink, R., Leoncini, A., Cobos Sabate, J., Verboom, W., Modolo, G., 2015: Gamma-radiolytic stability of new methylated TODGA derivatives for minor actinide recycling. Dalton Transactions, 44(41): 18049-18056.

Göbbels, C., Krings, T., Mauerhofer, E., 2015: On the applicability of $LaBr_3$ detectors in the non-destructive characterization of radioactive waste drums. Journal of Radioanalytical and Nuclear Chemistry, 303(3): 2399-2405.

Göttsche, M., Kütt, M., Neuneck, G., Niemeyer, I., 2015: Advancing disarmament verification tools: a task for Europe? Non-Proliferation and Disarmament Studies, 47: 1-18.

Guo, X., Szenknect, S., Burns, P.C., Dacheux, N., Navrotsky, A., Mesbah, A., Labs, S., Clavier, N., Poinssot, C., Ushakov, S.V., Curtius, H., Bosbach, D., Ewing, R.C., 2015:

Thermodynamics of formation of coffinite, $USiO_4$. Proceedings of the National Academy of Sciences of the United States of America, 112(21): 6551-6555.

Hinz, K., Altmaier, M., Gaona, X., Rabung, T., Schild, D., Richmann, M., Reed, D.T., Alekseev, E., Geckeis, H., 2015: Interaction of Nd(III) and Cm(III) with borate in dilute to concentrated alkaline NaCl, $MgCl_2$ and $CaCl_2$ solutions: solubility and TRLFS studies. New Journal of Chemistry, 39(2): 849-859.

Kaufhold, S., Dohrmann, R., Klinkenberg, M., Noell, U., 2015: Electrical conductivity of bentonites. Applied Clay Science, 114: 375-385.

Kaufholz, P., Sadowski, F., Wilden, A., Modolo, G., Lewis, F.W., Smith, A.W., Harwood, L.M., 2015: TS-BTPhen as a Promising Hydrophilic Complexing Agent for Selective Am(III) Separation by Solvent Extraction: First SACSESS International Workshop, 60(4-Pt.II): 815-820.

Klobes, B., Finkeldei, S., Brandt, F., Bosbach, D., Bessas, D., Embs, J.-P., Hermann, R., 2015: A general and Eu specific perspective on lattice dynamics in pyrochlore and defect fluorite $(Eu_{1-x}Nd_x)_2Zr_2O_7$: Physica Status Solidi / B, 252(9): 1940-1645.

Klobes, B., Finkeldei, S., Röhrig, W., Bosbach, D., Hermann, R.P., 2015: Hyperfine interactions in and lattice parameters of pyrochlore and defect fluorite $(Eu_{1-x}Nd_x)_2Zr_2O_7$. Journal of Physics and Chemistry of Solids, 79: 43-48.

Kowalski, P., Beridze, G., Vinograd, V., Bosbach, D., 2015: Heat capacities of lanthanide and actinide monazite-type ceramics. Journal of Nuclear Materials, 46: 147-154.

Lelet, M.I., Suleimanov, E.V., Golubev, A.V., Geiger, C.A., Bosbach, D., Alekseev, E., 2015: A calorimetric and thermodynamic investigation of $A_2[(UO_2)_2(MoO_4)O_2]$ compounds with A = K and Rb and calculated phase relations in the system $(K_2MoO_4+UO_3+H_2O)$. The Journal of Chemical Thermodynamics, 90: 270-276.

Li, Y., Kowalski, P., Beridze, G., Birnie, A. R., Finkeldei, S., Bosbach, D., 2015: Defect formation energies in $A_2B_2O_7$ pyrochlores. Scripta Materialia, 107: 18-21.

Listner, C., Niemeyer, I., Canty, M., Murphy, C., Stein, G., Rezniczek, A., 2015: Acquisition path analysis quantified – Shaping the success of the IAEA's state-level concept. Journal of Nuclear Materials Management, 43(4): 49-59.

Mildenberger, F. and Mauerhofer, E., 2015: Thermal neutron die-away times in large samples irradiated with a pulsed 14 MeV neutron source. Journal of Radioanalytical and Nuclear Chemistry, 307(1): 661-667.

Randriamalala, T., Rossbach, M., Mauerhofer, E., Révay, Z., Söllradl, S., Wagner, F.M., 2015: FaNGaS: A new instrument for (n,n'y) reaction measurements at FRM II. Nuclear Instruments & Methods in Physics Research / A, 806(C): 370-377.

Revay, Z., Kudejova, P., Kleszcz, K., Söllradl, S., Genreith, C., 2015, In-beam activation analysis facility at MLZ, Garching: Nuclear Instruments & Methods in Physics Research / A, 79: 114-123.

Rossbach, M., 2015: Letter to the editor of JRNC: Journal of Radioanalytical and Nuclear Chemistry, 304(2): 965-966.

Rossbach, M., Genreith, C., Hurst, A.M., Bernstein, L., Sleaford, B., Escher, J.E., Randriamalala, T., Mauerhofer, E., Revay, Z., Kudejova, P., Söllradl, S., Belgya, T.,

Szentmiklosi, L., and Firestone, R.B., 2015: TANDEM: a mutual cooperation effort for transactinide nuclear data evaluation and measurement. Journal of Radioanalytical and Nuclear Chemistry, 304(3): 1359-1363.

Rossbach, M. and Mauerhofer, E., 2015: FaNGaS - Fast Neutron Gamma Spectroscopy instrument for prompt gamma signature of inelastic scattering reactions. Journal of Large-Scale Research Facilities, 1: A32.

Rozov, K., Curtius, H., and Bosbach, D., 2015: Preparation, characterization and thermodynamic properties of Zr-containing Cl-bearing layered double hydroxides (LDHs). Radiochimica Acta, 103(5): 369–378.

Schmidt, H., Wilden, A., Modolo, G., Švehla, J., Grüner, B., Ekberg, C., 2015: Gamma radiolytic stability of $CyMe_4BTBP$ and effect of nitric acid. First SACSESS International Workshop, 60(4-Pt.II): 879-884.

Taylor, R., Bourg, S., Glatz, J.-P., Modolo, G., 2015: Development of actinide separation processes for future nuclear fuel cycles in Europe. Nuclear Future, 11(4): 38-43.

Thust, A., Arinicheva, Y., Haussühl, E., Ruiz-Fuertes, J., Bayarjargal, L., Vogel, S.C., Neumeier, S., Winkler, B., 2015: Physical properties of $La_{1-x}Eu_xPO_4$,$0 \leq x \leq 1$, monazite-type ceramics. Journal of the American Ceramic Society, 98(12): 4016–4021.

Tietze-Jaensch, H., Van Iseghem, P., Steyer, S., Van Velzen, L., del Cerro, E.V., Boucher, L., Dodaro, A., Fuks, L., Guisset, J.P., Koivuranta, S., Lierse, C., Neckel, W., Piña, G., 2015: ENTRAP and its potential interaction with European networks. Mineralogical Magazine, 79(6): 1515-1520.

Wilden, A., Modolo, G., Kaufholz, P., Sadowski, F., Lange, S., Munzel, D., Geist, A., 2015: Process development and laboratory-scale demonstration of a regular-SANEX process using C5-BPP (2,6-Bis(5-(2,2-dimethylpropyl)-1H-pyrazol-3-yl)pyridine). Separation Science and Technology, 50(16): 2467-2475.

Wilden, A., Modolo, G., Kaufholz, P., Sadowski, F., Lange, S., Sypula, M., Magnusson, D., Müllich, U., Geist, A., Bosbach, D., 2015: Laboratory-scale counter-current centrifugal contactor demonstration of an innovative-SANEX process using a water soluble BTP. Solvent extraction and ion exchange, 33(2): 91-108.

Xiao, B., Gesing, T.M., Robben, L., Bosbach, D., Alekseev, E., 2015: Dinuclear face-sharing bi-octahedral tungsten(VI) core and unusual thermal behavior in complex Th tungstates. Chemistry - a European Journal. 21(21): 7746-7754.

Xiao, B., Klinkenberg, M., Bosbach, D., Suleimanov, E. V., Alekseev, E., 2015: Effects of Te(IV) oxo-anion incorporation into thorium molybdates and tungstates. Inorganic Chemistry, 54(12): 5981-5990.

Xiao, B., Langer, E., Dellen, J., Schlenz, H., Bosbach, D., Suleimanov, E.V., Alekseev, E., 2015: Chemical and structural evolution in the $Th–SeO_3^{2-}/SeO_4^{2-}$ system: from simple selenites to cluster-based selenate compounds: Inorganic Chemistry, 54(6): 3022-3030.

Xiao, B., Schlenz, H., Dellen, J., Bosbach, D., Suleimanov, E.V., Alekseev, E., 2015: From two-dimensional layers to three-dimensional frameworks: Expanding the structural diversity of uranyl compounds by cation-cation interactions. Crystal Growth & Design, 15(8): 3775-3784.

Yu, N., Kegler, P., Klepov, V., Dellen, J., Schlenz, H., Langer, E., Bosbach, D., Alekseev, E., 2015: Influence of extreme conditions on formation and structures of caesium uranium (VI) arsenates. Dalton Transactions, 44(47): 20735-20744.

Yu, N., Klepov, V., Neumeier, S., Depmeier, W., Bosbach, D., Suleimanov, E.V., Alekseev, E., 2015: Further insight into uranium and thorium metaphosphate chemistry and the effect of Nd^{3+} incorporation into uranium(IV) metaphosphate. European Journal of Inorganic Chemistry, 2015(9): 1562-1568.

Zarzana, C.A., Groenewold, G.S., Mincher, B.J., Mezyk, S.P., Wilden, A., Schmidt, H., Modolo, G., Wishart, J.F., and Cook, A.R., 2015: A comparison of the γ-radiolysis of TODGA and T(EH)DGA using UHPLC-ESI-MS analysis. Solvent Extraction and Ion Exchange, 33(5): 1-17.

Zhao, P., Mangir Murshed, M., Huq, A., Grossmann, H.K., Mädler, L., Alekseev, E., Gesing, T.M., 2015: Nanoscale building blocks in a novel lithium arsenotungsten bronze: Synthesis and characterization. Journal of Solid State Chemistry, 226: 81-87.

11.1.2 Proceedings/Books

Proceedings

Aksyutina, Y., Fast, I., Tietze-Jaensch, H., Guillaumin, F., Pinson, P., 2015: The German product quality control of the compacted metallic nuclear waste. Proc WM2015 Conference: Phoenix, USA, pp. 15311

Allen, K., Chen, C., Dreicer, M., Niemeyer, I., Listner, C., Stein, G., 2015: Systems approach to arms control verification. Proceedings of 37th ESARDA Symposium on Safeguards and Nuclear Non-Proliferation: Manchester, UK, 974-981.

Chen, C., Dreicer, M., Allen, K., Niemeyer, I., Listner, C., Stein, G., 2015: Developing a systems concept to arms control verification — Results from the ESARDA VTM WG Workshop. Proceedings Institute of Nuclear Materials Management (INMM), 56th Annual Meeting: Indian Wells, USA.

Curtius, H., Bosbach, D., Deissmann, G., 2015: Corrosion of spent fuel from research and prototype reactors under conditions relevant to geological disposal. Key Topics in Deep Geological Disposal, DAEF; Köln, Germany: KIT Scientific Publishing, 176-80.

Dürr, M., Middendorp, R., Knott, A., 2015: Preparation of uranium micro-particles as reference material for nuclear safeguards. Proceedings of 37th ESARDA Symposium on Safeguards and Nuclear Non-Proliferation: Manchester, UK, 488 - 497.

Ebert, E., Bukaemskiy, A., Modolo, G., 2015: Dissolution behavior of MgO- and Mo-based inert matrix fuel for the transmutation of plutonium and minor actinides. GLOBAL2015 - Nuclear Fuel Cycle for a Low-Carbon Future: Paris, France. pp. 5199.

Ebert, E., Modolo, G., Bukaemskiy, A., Sadowski, F., Bosbach, D., 2015: Dissolution behavior of MgO- and Mo-based inert matrix fuel for the transmutation of plutonium and minor actinides. 13th Information Exchange Meeting on Actinide and Fission Product Partitioning and Transmutation – IEMPT13: Seoul, Korea, 314-321.

Fast, I., Aksyutina, Y., Tietze-Jaensch, H., Bosbach, D., 2015: Determination of uncertainties of PWR spent fuel radionuclide inventory based on real operational history data. 4th International Conference on Advancements in Nuclear Instrumentation Measurement Methods and their Applications (ANIMMA): Lisbon, Portugal, IEEE, 1-5.

Fast, I., Tietze-Jaensch, H., Aksyutina, Y., Bosbach, D., 2015: On the Influence of the power plant operational history on the inventory and the uncertainties of radionuclides relevant for the final disposal of PWR spent fuel. WM Symposium: Phoenix, USA, pp. 15149.

Fossati, L., Bagnulo, S., Haswell, C.A., Patel, M.R., Busuttil, R., Kowalski, P. et al., 2015: Polarimetry as a tool to find and characterise habitable planets orbiting white dwarfs. From the Sun to Stars and Stellar Environments: Punta Leona, Costa Rica, 325-332.

Jussofie, A., Graf, W., van Beveren, K., Geißler, W., Niemeyer, I., Rezniczek, A. et al., 2015: An update on the implementation of remote data transmission (RDT) in the dry interim storage facilities in Germany. Proceedings of 37th ESARDA Symposium on Safeguards and Nuclear Non-Proliferation: Manchester, UK, 296-301.

Listner, C., Canty, M., Stein, G., Rezniczek, A., Niemeyer, I., 2015: Formalizing acquisition path analysis for the IAEA's state-level concept. Proceedings of 37th ESARDA Symposium on Safeguards and Nuclear Non-Proliferation: Manchester, UK, 372-382.

Listner, C., Niemeyer, I., Canty, M., Stein, G., Rezniczek, A., 2015: Formalizing acquisition path analysis for the IAEA's state-level concept. Proceedings Institute of Nuclear Materials Management 56th Annual Meeting: Indian Wells, USA, 372 -382.

Mank, G., Damm, G., Modolo, G., Wilden, A., Pierce, R., Maxted, M. et al., 2015: Management of spent high temperature reactor graphite pebble bed fuel. IAEA International Conference on Research Reactors: Safe Management and Effective Utilization: Vienna, Austria, 7 p.

Marie, C., Duchesne, M.-T., Russello, E., Kaufholz, P., Wilden, A., Modolo, G. et al., 2015: Development of a selective americium separation process using TPAEN as a water-soluble stripping agent. GLOBAL2015 - Nuclear Fuel Cycle for a Low-Carbon Future: Paris, France, pp. 5101.

Merk, B., Geist, A., Modolo, G., Knebel, J., 2015: The German P&T study: Results and conclusions in the view of the contributing Helmholtz research centres. 13th Information Exchange Meeting on Actinide and Fission Product Partitioning and Transmutation – IEMPT13: Seoul, Korea, 56-62.

Nicol, T., Perot, B., Carasco, C., Brackx, E., Mariani, A., Passard, C. et al., 2015: ^{235}U and ^{239}Pu characterization in radioactive waste using neutron-induced fission delayed gamma rays. IEEE Nuclear Science Symposium & Medical Imaging Conference: Seattle, USA, p. 6.

Niemeyer, I., 2015: Nuclear verification from space – Satellite imagery within nuclear non-proliferation and arms control verification regimes. Proceedings of 37th ESARDA Symposium on Safeguards and Nuclear Non-Proliferation: Manchester, UK, 646-653.

Niemeyer, I., 2015: Spaceborne verification: Satellite imagery within nuclear non-proliferation and arms control verification regimes. Proceedings Institute of Nuclear Materials Management (INMM) 56th Annual Meeting: Indian Wells, USA.

Niemeyer, I., Canty, M., Lagrange, J.-M., Listner, C., Schwartz, D., Uruñuela, S. et al., 2015: Integrated analysis of satellite imagery for nuclear monitoring - G-SEXTANT findings. Proceedings of 37th ESARDA Symposium on Safeguards and Nuclear Non-Proliferation: Manchester, UK, 674-685.

Rozov, K., Curtius, H., Bosbach, D., 2015: Preparation and estimation of thermodynamic properties of Fe(II)-, Co(II)-, Ni(II)- and Zr(IV)-containing layered double hydroxides. Key Topics in Deep Geological Disposal, DAEF: Köln, Germany; KIT Scientific Publishing; pp. 141.

Wilden, A., Modolo, G., Geist, A., 2015: Development and demonstration of innovative partitioning processes (i-SANEX and 1-cycle SANEX) for actinide partitioning. 13th Information Exchange Meeting on Actinide and Fission Product Partitioning and Transmutation: Seoul, Korea, 138-147.

Wilden, A., Modolo, G., Geist, A., Rothe, J., Dardenne, K., Schäfer, S. et al., 2015: Complex structure of *An* and *Ln* complexes with modified diglycolamides in solution and solid state using different analytical techniques. GLOBAL2015 - Nuclear Fuel Cycle for a Low-Carbon Future: Paris, France, pp. 5179.

Books

Modolo, G., Geist, A., Miguirditchian, M., 2015: Minor actinide separations in the reprocessing of spent nuclear fuels: recent advances in Europe. Reprocessing and Recycling of Spent Nuclear Fuel. Burlington: Elsevier Ltd., 245-280.

11.1.3 Reports

Beele, B.B., Bremer, A., Geist, A., Magnusson, D., Müllich, U., Panak, P.J. et al., 2015: Separation of long-lived minor actinides. Report. Karlsruhe, Germany: KIT Scientific Publishing.

Modolo, G., Gerdes, M., Kaufholz, P., Kraus, B., Sadowski, F., Schmidt, H. et al., 2015: EU-Projekt SACSESS, HYBAR 5 - Half Yearly Beneficiary Activity Report No. 5: Internal report

Modolo G, Kaufholz P, Sadowski F, Schmidt H, Wilden A. EU-Projekt SACSESS, HYBAR 4 - Half Yearly Beneficiary Activity Report No. 4: Internal report

Möller, T., Thierfeldt, S., Filby, A., Bosbach, D., Deissmann, G., Modolo, G., Wilden, A., 2015: Gutachten zum Thema “Transmutation”. Im Auftrag der Geschäftsstelle GSt StandAG, Kommission Lagerung hoch radioaktiver Abfallstoffe (K-MAT 45). Deutscher Bundestag, Berlin, Germany.

Verhoef, E., Neeft, E., Deissmann, G., Filby, A., Wiegers, R., Kers, D., 2015: Waste families in OPERA. Report. Vlissingen: COVRA.

11.1.4 Poster

Altmaier, M., Gaon, X., Brandt, F., Krüger, S., Colàs, E., Grivé, M. et al., 2015: Thermac - a joint project on aquatic actinide chemistry and thermodynamics at elevated temperature conditions. Migration 2015: Santa Fe, NM, USA.

Arinicheva, Y., Huittinen, N., Neumeier, S., Clavier, N., Stumpf, T., Dacheux, N. et al., 2015: Time resolved and in-situ studies on monazite-type phosphate ceramics for nuclear waste immobilization. RACIRI Summer School: Sellin/Rügen, Germany.

Arinicheva, Y., Lozano-Rodriguez, M.J., Scheinost, A.C., Clavier, N., Dacheux, N., Bosbach, D. et al., 2015: Structural studies on (La,Eu)PO_4 solid solutions by Infrared, Raman and X-ray Absorption Spectroscopy. 25th Seminar on Activation Analysis and Gamma Spectroscopy (SAAGAS): Aachen, Germany.

Arinicheva, Y., Neumeier, S., Bosbach, D., 2015: Monazite-type phosphate ceramics for nuclear waste immobilization. HITEC Mid-term Evaluation: Jülich, Germany.

Beridze, G., Blanca-Romero, A., Li, Y., Kowalski, P., 2015: Computing lanthanide- and actinide-bearing materials with DFT+U method. 9th International Conference on f-Elements: Oxford, United Kingdom.

Beridze, G., Li, Y., Blanca-Romero, A., Kowalski, P., 2015: Calculation of f-electrons-bearing materials using DFT+U method. PSI-k 2015 Conference: San Sebastian, Spain.

Beridze, G., Li, Y., Kowalski, P., 2015: *Ab initio* modeling of computationally challenging earth (f-) materials. Goldschmidt 2015: Prague, Czech Republic.

Brandt, F., Rozov, K., Klinkenberg, M., Bosbach, D., 2015: The solubility of $RaSO_4$ and uptake of radium by $BaSO_4$ at T = 25 – 90 °C. Migration 2015: Santa Fe, NM, USA.

Brandt, F., Rozov, K., Klinkenberg, M., Bosbach, D., 2015: Replacement of Barite by (Ba, Ra)SO_4 at T = 25 – 90 °C. Goldschmidt 2015: Prague, Czech Republic.

Brykala, M., Rogowski, M., Deptula, A., Schreinemachers, C., Modolo, G., 2015: Co-conversion from solution to uranium dioxide or uranium carbide by powder-free INCT methods. First SACSESS International Workshop: Warsaw, Poland.

Cheng, M., Steppert, M., Ebert, E., Walther, C., 2015: How does iron influence the dissolution behavior of Mo based generation IV reactor fuel? New insights using nano ESI-TOF-MS. GDCh Wissenschaftsforum Chemie: Dresden, Germany.

Deissmann, G., Filby, A., Neumeier, S., Bosbach, D., 2015: Solubility of lanthanide-phosphates (*Ln*PO_4) and aqueous lanthanide speciation under repository-relevant conditions. MRS 2015 - Scientific Basis for Nuclear Waste Management Symposium XXXIX Montpellier, France.

Deissmann, G., Haneke, K., Filby, A., Wiegers, R., Bosbach, D., 2015: Evaluation of waste form behaviour in a geological repository for high-level radioactive waste in Boom Clay in the Netherlands. Clays in Natural and Engineered Barriers for Radioactive Waste Confinement - 6th International Conference: Brussels, Belgium.

Deissmann, G., Haneke, K., Filby, A., Wiegers, R., Bosbach, D., 2015: Corrosion behaviour of high-level radioactive waste forms in a geological repository in Boom Clay in the Netherlands. Goldschmidt 2015: Prague, Czech Republic.

Filby, A., Deissmann, G., Wiegers, R., 2015: Evaluation of LILW degradation processes and products in a geological repository for radioactive waste in Boom Clay in the Netherlands. Clays in Natural and Engineered Barriers for Radioactive Waste Confinement - 6th International Conference: Brussels, Belgium.

Filby, A., Kunz, R., Möller, T., Deissmann, G., Neumeier, S., Bosbach, D., 2015: A computational study of heavy ion irradiation of phosphate ceramics. MRS 2015 - Scientific Basis for Nuclear Waste Management Symposium XXXIX Montpellier, France.

Forward, R., Ji, Y., Beridze, G., Liang, Y., Kowalski, P., 2015: Atomistic simulations of monazite-type ceramic as prospective nuclear waste form. CECAM Workshop - Multi-Scale Modelling of Matter under Extreme Irradiation: Dublin, Ireland.

Ji, Y., Beridze, G., Li, Y., Kowalski, P., 2015: Atomistic simulations of materials relevant for nuclear waste management. 79th Annual Meeting of the DPG and DPG Spring Meeting: Berlin, Germany.

Ji, Y., Li, Y., Beridze, G., Kowalski, P., 2015: Large scale simulations of nuclear materials. Goldschmidt 2015: Prague, Czech Republic.

Kaufholz, P., Wilden, A., Modolo, G., Sadowski, F., Harwood, L.M., Lewis, F. et al., 2015: Investigations on a TODGA-based liquid-liquid extraction system using SO_3Ph-BTPhen for the separation of americium(III) from a simulated PUREX raffinate. First SACSESS International Workshop: Warsaw, Poland.

Klinkenberg, M., Brandt, F., Vinograd, V., Weber, J., Rozov, K., Kulik, D. et al., 2015: Phase equilibrium in the ternary (Ba,Sr,Ra)SO_4 solid solution - aqueous solution system. GDCh Wissenschaftsforum 2015: Dresden, Germany.

Klinkenberg, M., Brandt, F., Weber, J., Vinograd, V., Rozov, K., Kulik, D. et al., 2015: Experimental and simulation study of phase equilibrium in the system (Ba,Sr,Ra)SO_4 + H_2O. Migration 2015: Santa Fe, NM, USA2015.

Kowalski, P., Beridze, G., Li, Y., Ji, Y., Vinograd, V., Bosbach, D., 2015: Atomistic modeling of nuclear materials. PSI-k 2015 Conference: San Sebastian, Spain.

Li, Y., Beridze, G., Blanca-Romero, A., Ji, Y., Vinograd, V., Bosbach, D. et al., 2015: Characterization of nuclear waste materials by a novel computational approach. E-MRS Spring Meeting: Lille, France.

Li, Y., Kowalski, P., Beridze, G., Finkeldei, S., Vinograd, V., Bosbach, D., 2015: *Ab initio* simulations of pyrochlores ($A_2B_2O_7$): the energetics of defect formation and the excess properties of pyrochlore-type solid solutions. PSI-k 2015 Conference: San Sebastian, Spain.

Li, Y., Kowalski, P., Beridze, G., Vinograd, V., Bosbach, D., 2015: Atomistic simulations of novel nuclear waste forms: Cases of monazite and pyrochlore ceramics. Goldschmidt 2015: Prague, Czech Republic.

Mank, G., Damm, G., Modolo, G., Wilden, A., Pierce, R., Maxted, M. et al., 2015: Management of spent high temperature reactor graphite pebble bed fuel. IAEA International Conference on Research Reactors - Safe Management and Effective Utilization: Vienna, Austria.

Middendorp, R., Dürr, M., Bosbach, D., 2015: Production and characterization of uranium oxide microparticle reference materials for nuclear safeguards applications. GDCh Wissenschaftsforum 2015: Dresden, Germany.

Molinero, J., Deissmann, G., Trinchero, P., Ebrahimi, H., Bosbach, D., Gylling, B. et al., 2015: High performance reactive transport modeling for understanding radionuclide behaviour in fractured crystalline rocks at sub-millimeter scale. Migration 2015: Santa Fe, NM, USA.

Randriamalala, T., Rossbach, M., Genreith, C., Revay, Z., Kudejova, P., Söllradl, S. et al., 2015: FaNGaS: a new instrument for Fast Neutron Gamma Spectroscopy at FRM II research reactor at Garching. Advancements in Nuclear Instrumentation: Lisabon, Portugal.

Ríos Ramírez, J.J., Beridze, G., Li, Y., Blanca Romero, A., Kowalski, P., 2015: Feasible and reliable *ab initio* calculations of materials relevant for nuclear waste management. International Workshop on Computational Physics and Materials Science: Total Energy and Force Method (ICTP): Trieste, Italy.

Schmidt, M., Peschel, S., Hofmann, S., Walther, C., Bosbach, D., Stumpf, T., 2015: Retention of trivalent actinides by structural incorporation. Migration 2015: Santa Fe, NM, USA.

Schumann, M., Engels, R., Kemmerling, G., Mauerhofer, E., Willenbockel, M., 2015: Performance study of an amorphous-silicon flat panel detector for fast neutron imaging of nuclear waste. Advancements in Nuclear Instrumentation Measurement Methods and their Applications: Lisbon, Portugal.

Shcherbina, N., Franzen, C., Walther, C., 2015: Application of layered double hydroxides for Tc-99 immobilization. Goldschmidt 2015: Prague, Czech Republic.

Tushingham, J., Niemeyer, I., Sevini, F., 2015: ESARDA – The European Safeguards Research and Development Association. 23rd WiN Global Annual Conference: Women in Nuclear meet Atoms for Peace: Vienna, Austria.

Weigelt, S., Schlenz, H., König, A., Heise, H., Bosbach, D., 2015: Structural characterization of geopolymers for the safe disposal of the fission products ^{137}Cs and ^{90}Sr. Wissenschaftsforum Chemie 2015: Dresden, Germany.

Wilden, A., Modolo, G., Geist, A., Rothe, J., Dardenne, K., Schäfer, S. et al., 2015: Complex structure of *An* and *Ln* complexes with modified diglycolamides in solution and solid state using different analytical techniques. Second Joint Student Workshop on f-Element Chemistry: Karlsruhe, Germany.

11.1.5 Presentations

Conferences:

Arinicheva, Y., Bukaemskiy, A.A., Neumeier, S., Modolo, G., Roth, G., Bosbach, D., 2015: Studies on thermal and mechanical properties of monazite-type ceramics for the conditioning of minor actinides. E-MRS Spring Meeting: Strasbourg, France.

Allen, K., Chen, C., Dreicer, M., Niemeyer, I., Listner, C., Stein, G., 2015: Systems approach to arms control verification. Proceedings of 37th ESARDA Symposium on Safeguards and Nuclear Non-Proliferation: Manchester, UK.

Arinicheva, Y., Clavier, N., Huittinen, N., Bukaemskiy, A., Neumeier, S., Stumpf, T. et al., 2015: Structural studies on rhabdophane-monazite phase transition in (La,Eu)PO_4. MRS 2015 - Scientific Basis for Nuclear Waste Management XXXIX: Montpellier, France.

Arinicheva, Y., Neumeier, S., Clavier, N., Bukaemskiy, A., Podor, R., Dacheux, N. et al., 2015: Synthesis, crystallization and microstructural evolution by sintering of monazite-type ceramics. E-MRS Spring Meeting: Lille, France.

Beridze, G., Li, Y., Blanca-Romero, A., Kowalski, P., 2015: Efficient calculations of f-materials relevant for nuclear waste management using DFT+U. Cracow Colloquium on f-Electron Systems: Cracow, Poland.

Beridze, G., Li, Y., Blanca-Romero, A., Kowalski, P., 2015: Feasible and reliable modeling of f-element-bearing materials with DFT+U method. Second Joint Student Workshop on f-Element Chemistry: Karlsruhe, Germany.

Beridze, G., Li, Y., Kowalski, P., 2015: Feasible and reliable computation of properties of novel ceramic waste forms. E-MRS Spring Meeting: Lille, France.

Gausse, C., Szenknect, S., Mesbah, A., Clavier, N., Neumeier, S., Bosbach, D., 2015: Solubility of the rhabdophane ($Ln$$PO_4$.n$H_2O$): A low temperature precursor of the monazite. Goldschmidt 2015: Prague, Czech Republic.

Chen, C., Dreicer, M., Allen, K., Niemeyer, I., Listner, C., Stein, G., 2015: Developing a systems concept to arms control verification — Results from the ESARDA VTM WG workshop. Institute of Nuclear Materials Management (INMM) 56th Annual Meeting: Indian Wells, USA.

Dürr, M., 2015: Preparation of Uranium Micro-Particles as Reference Material for Nuclear Safeguards. Proceedings of 37th ESARDA Symposium on Safeguards and Nuclear Non-Proliferation: Manchester, UK.

Dürr, M., 2015: Die Qualität von Messdaten in der nuklearen Verifikation – aktuelle Forschungs- und Entwicklungsarbeiten am Forschungszentrum Jülich. 7 Symposium „Nukleare und radiologische Bedrohungen“, Fraunhofer INT: Euskirchen, Germany.

Ebert, E., Bukaemskiy, A., Modolo, G., 2915: Dissolution behavior of MgO- and Mo-based inert matrix fuel for the transmutation of plutonium and minor actinides. GLOBAL2015 - Nuclear Fuel Cycle for a Low-Carbon Future: Paris, France.

Ebert, E., Modolo, G., Bosbach, D., Cheng, M., Steppert, M., Walther, C., 2015: Dissolution studies on molybdenum-based inert matrix fuels for the transmutation of minor actinides. First SACSESS International Workshop: Warsaw, Poland.

Finkeldei, S., Brandt, F., Stennett, M., Holliday, K., Bukaemskiy, A., de Visser-Tynova, E. et al., 2015: Fabrication and structural characterisation of actinide-pyrochlore ceramics. E-MRS Spring Meeting: Lille, France.

Gausse, C., Mesbah, A., Szenknect, S., Clavier, N., Neumeier, S., Bosbach, D. et al., 2015: Study of dissolution of monazite: kinetic point of view. MRS 2015 - Scientific Basis for Nuclear Waste Management XXXIX: Montpellier, France.

Grambow, B., Suzuki, T., Bosbach, D., Kulik, D.A., Spahiu, K., Duro, L., 2015: Impact of slow processes close to equilibrium on radionuclide migration. Migration 2015: Santa Fe, NM, USA.

Huittinen, N., Arinicheva, Y., Holthausen, J., Neumeier, S., Stumpf, T., 2015: Incorporation of Cm^{3+} and Eu^{3+} in $LnPO_4$ ceramics – A site-selective TRLFS study. MRS 2015 - Scientific Basis for Nuclear Waste Management XXXIX: Montpellier, France.

Huittinen, N., Arinicheva, Y., Holthausen, J., Schmidt, M., Neumeier, S., Stumpf, T., 2015: Curium(III) and Europium(III) incorporation in lanthanide phosphate ceramics for conditioning of radioactive waste. Migration 2015: Santa Fe, NM, USA.

Lozano-Rodriguez, M.J., Arinicheva, Y., Heuser, J., Kvashnina, K., Neumeier, S., Scheinost, A.C., 2015: Determination of local structure in mixed lanthanoid phosphate solid solutions by X-ray absorption spectroscopy. E-MRS Spring Meeting: Lille, France.

Jussofie, A., Graf, W., van Bevern, K., Geißler, W., Niemeyer, I., Rezniczek, A. et al., 2015: An update on the implementation of remote data transmission (RDT) in the dry interim storage facilities in Germany. Proceedings of 37th ESARDA Symposium on Safeguards and Nuclear Non-Proliferation: Manchester, UK.

Kaufholz, P., Wilden, A., Modolo, G., Harwood, L.M., Lewis, F., Wagner, C. et al., 2015: Selective separation of Am(III) using the hydrophilic complexing agent SO_3Ph-BTPhen. First SACSESS International Workshop: Warsaw, Poland.

Kowalski, P., 2015: Atomistic modelling of materials relevant for nuclear waste management. 9th International Conference on f-Elements: Oxford, UK.

Kowalski, P., 2015: Feasible and reliable *ab initio* approach to computation of materials relevant for nuclear waste management. 11th International Conference on Ceramic Materials and Components for Energy and Environmental Applications: Vancouver, Canada.

Li, Y., Beridze, G., Kowalski, P., 2015: Energetics of defects formation and origin of selective disordering in pyrochlores. E-MRS Spring Meeting: Lille, France.

Listner, C., Canty, M., Niemeyer, I., Stein, G., Rezniczek, A., 2015: Entdeckungswahrscheinlichkeiten von Proliferationsaktivitäten: Möglichkeiten der Quantifizierung. 7 Symposium „Nukleare und radiologische Bedrohungen“, Fraunhofer INT: Euskirchen, Germany.

Listner, C., Canty, M., Stein, G., Rezniczek, A., Niemeyer, I., 2015: Formalizing acquisition path analysis for the IAEA's state-level concept. Proceedings of 37th ESARDA Symposium on Safeguards and Nuclear Non-Proliferation: Manchester, UK.

Listner, C., Niemeyer, I., Canty, M., Stein, G., Rezniczek, A., 2015: Formalizing acquisition path analysis for the IAEA's state-level concept. Institute of Nuclear Materials Management (INMM) 56th Annual Meeting: Indian Wells, USA.

Listner, C., Stein, G., Canty, M., Rezniczek, A., Niemeyer, I., 2015 Systems approach to arms control verification. DPG Frühjahrstagung 2015: Berlin, Germany.

Lozano-Rodriguez, M.J., Arinicheva, Y., Holthausen, J., Neumeier, S., Scheinost, A., 2015: Structural stability study of the mixed $La_{0.7-x}Lu_xEu_{0.3}PO_4$ solid solutions by Extended X-ray Absorption Spectroscopy. MRS 2015 - Scientific Basis for Nuclear Waste Management XXXIX: Montpellier, France.

Marie, C., Duchesne, M.-T., Russello, E., Kaufholz, P., Wilden, A., Modolo, G. et al., 2015: Development of a selective americium separation process using TPAEN as a water-soluble stripping agent. GLOBAL2015 - Nuclear Fuel Cycle for a Low-Carbon Future: Paris, France.

Marie, C., Rusello, E., Duchesne, M.T., Kaufholz, P., Wilden, A., Modolo, G. et al., 2015: Development of a selective Am separation process using TPAEN. First SACSESS International Workshop: Warsaw, Poland.

Mauerhofer, E., Havenith, A., Kettler, J., 2015: PGNAA of a 200 L steel drum filled with concrete. 14th International Conference on Modern Trends in Activation Analysis: Delft, The Netherlands.

Mildenberger, F., Mauerhofer, E., 2015: Thermal neutron Die-Away-Time studies for P&DGNAA of large samples at the MEDINA facility. 25th Seminar on Activation Analysis and Gamma Spectroscopy (SAAGAS): Aachen, Germany.

Mildenberger, F., Mauerhofer, E., 2015: Thermal neutron Die-Away-Time studies for P&DGNAA of large samples at the MEDINA facility. Advancements in Nuclear Instrumentation Measurement Methods and their Applications: Lisbon, Portugal.

Mildenberger, F., Mauerhofer, E., 2015: Influence of neutron moderating materials in the characterization of 200 L radioactive waste drums by neutron activation analysis. 14th International Conference on Modern Trends in Activation Analysis: Delft, The Netherlands.

Mincher, B.J., Zarzana, C.A., Groenewold, G.S., Mezyk, S.P., Wilden, A., Modolo, G., 2015: A comparison of the radiation chemistry of several diglycolamides. MARC X: Methods and Applications of Radioanalytical Chemistry: Kailua-Kona, Hawaii, USA.

Neumeier, S., Arinicheva, Y., Clavier, N., Podor, R., Huittinen, N., Dacheux, N. et al., 2015: Advanced investigation on microstructure evolution and on solid solution formation during sintering of monazite-type ceramics. Materials Science & Technology (MS&T2015): Columbus, OH, USA.

Neumeier, S., Bosbach, D., 2015: Conditioning of long-lived radionuclides in ceramic waste forms – A German joint research project. MRS 2015 - Scientific Basis for Nuclear Waste Management XXXIX: Montpellier, France.

Neumeier, S., Huittinen, N., Arinicheva, Y., Holthausen, J., Bosbach, D., Stumpf, T., 2015: TRLFS – Probing f-element incorporation in ceramic materials on a molecular level. 25th Seminar on Activation Analysis and Gamma Spectroscopy (SAAGAS): Aachen, Germany.

Neumeier, S., Kulriya, P.K., Arinicheva, Y., Deissmann, G., Avasthi, D.K., Bosbach; D., 2015: In-situ structural investigations on monazite-type $La_{0.2}Gd_{0.8}PO_4$-ceramics under heavy ion irradiation. MRS 2015 - Scientific Basis for Nuclear Waste Management XXXIX: Montpellier, France2015.

Niemeyer, I., 2015: Nuclear verification from space – Satellite imagery within nuclear non-proliferation and arms control verification regimes. Proceedings of 37th ESARDA Symposium on Safeguards and Nuclear Non-Proliferation: Manchester, UK.

Niemeyer, I., 2015: Spaceborne verification: Satellite imagery within nuclear non-proliferation and arms control verification regimes. Institute of Nuclear Materials Management (INMM) 56th Annual Meeting: Indian Wells, USA.

Niemeyer, I., Canty, M., Lagrange, J.-M., Listner, C., Schwartz, D., Urunela Hernández, S. et al., 2015: Integrated analysis of satellite imagery for nuclear monitoring - G-SEXTANT findings. Proceedings of 37th ESARDA Symposium on Safeguards and Nuclear Non-Proliferation: Manchester, UK.

Rossbach, M., Randriamalala, T., Revay, Z., Kudejova, P., Söllradl, S., Wagner, F.M., 2015: Prompt and delayed inelastic scattering reactions from fission neutron PGAA – first results of FaNGaS. Advancements in Nuclear Instrumentation: Lisbon, Portugal.

Rossbach, M., Randriamalala, T., Revay, Z., Söllradl, S., Wagner, F.M., 2015: Fission Neutron PGAA from inelastic scattering reactions – first results of FaNGaS. Modern Trends in Activation Analysis: Delft, The Netherlands.

Schausten, C., Thust, A., Hirsch, A., Arinicheva, Y., Wätjen, A., Neumann, A. et al., 2015: Sintering behaviour and microstructure of rare earth phosphates $REPO_4$ (with RE = La, Ce, Pr). MRS 2015 - Scientific Basis for Nuclear Waste Management XXXIX: Montpellier, France.

Schausten, C., Wätjen, A., Arinicheva, Y., Neumeier, S., Hirsch, A., Roth, G. et al., 2015: Untersuchung des Sinterverhaltens und der Gefüge von Seltenerd-Phosphaten $SEPO_4$ (mit SE = La, Ce, Pr). 90. DKG Jahrestagung: Bayreuth, Germany.

Schmidt, H., Modolo, G., Wilden, A., Ekberg, C., Halleröd, J., Grüner, B. et al., 2015: Radiolytic and hydrolytic stability of the highly selective nitrogen donor ligands $CyMe_4BTBP$ and $CyMe_4BTPhen$. First SACSESS International Workshop: Warsaw, Poland.

Schmidt, H., Modolo, G., Wilden, A., Ekberg, C., Halleröd, J., Grüner, B. et al., 2015: Radiolytic stability of the highly selective nitrogen donor ligands $CyMe_4BTBP$ and $CyMe_4BTPhen$. Radical Behavior Workshop: Idaho Falls, Idaho, USA.

Schreinemachers, C., Middendorp, R., John, J., Bukaemskiy, A., Modolo, G., Brykala, M. et al., 2015: Conversion of actinides into oxide pre-cursors for innovative fuel fabrication. TopFuel 2015: Zürich, Switzerland.

Schumann, M., Engels, R., Kemmerling, G., Mauerhofer, E., Willenbockel, M., 2015: Performance study of an amorphous-silicone flat panel detector for fast neutron imaging of nuclear waste. Advancements in Nuclear Instrumentation Measurement Methods and their Applications: Lisbon, Portugal.

Schumann, M., Engels, R., Schitthelm, O., Vasques, R., Voß, D., Willenbockel, M. et al., 2015: Fast neutron imaging with an α-Si detector for nuclear waste assay. 25th Seminar on Activation Analysis and Gamma Spectroscopy (SAGAAS): Aachen, Germany.

Thust, A., Arinicheva, Y., Haussühl, E., Ruiz-Fuertes, J., Bayarjargal, L., Vogel, S.C. et al., 2015: Physical properties and microstructures of monazite-type ceramics for the immobilization of nuclear waste. 14th International Conference European Ceramic Society: Toledo, Spain.

Thust, A., Hirsch, A., Haussühl, E., Arinicheva, Y., Klinkenberg, M., Neumeier, S.,et al., 2015: Physical and microstructural properties of monazite-type ceramics. MRS 2015 - Scientific Basis for Nuclear Waste Management XXXIX: Montpellier, France.

Vinograd, V., Brandt, F., Klinkenberg, M., Weber, J., Rozov, K., Kulik, D. et al., 2015: Phase equilibria in the system (Ba, Sr, Ra)SO_4 + H_2O. Goldschmidt 2015: Prague, Czech Republic.

Weber, J., Brandt, F., Klinkenberg, M., Barthel, J., Breuer, U., Savenko, A. et al., 2015: Characterization of (Ba,Ra)SO_4 solid solutions with true nm-scale resolution. Goldschmidt 2015: Prague, Czech Republique.

Weber, J., Brandt, F., Klinkenberg, M., Barthel, J., Breuer, U., Savenko, A. et al., 2015: Characterization of (Ba,Ra)SO_4 solid solutions on the atomic level by atom probe tomography and transmission electron microscopy. Gesellschaft deutscher Chemiker Wissenschaftsforum: Dresden, Germany.

Weber, J., Brandt, F., Klinkenberg, M., Breuer, U., Savenko, A., Barthel, J. et al., 2015: Advanced microanlytical characterization of the (Ba,Ra)SO_4 solid solution with ATP and TEM. Migration 2015: Santa Fe, NM, USA.

Weigelt, S., Schlenz, H., König, A., Heise, H., Bosbach, D., 2015: Structural characterization of geopolymers for the safe disposal of the fission products ^{137}Cs and ^{90}Sr. MRS 2015 - Scientific Basis for Nuclear Waste Management XXXIX: Montpellier, France.

Wilden, A., Galán, H., Groenewold, G.S., Mincher, B.J., Zarzana, C.A., Núñez, A. et al., 2015: Gamma-radiolytic stability of new methylated TODGA derivatives for minor actinide recycling. Radical Behavior Workshop: Idaho Falls, Idaho, USA.

Wilden, A., Modolo, G., Geist, A., Rothe, J., Dardenne, K., Schäfer, S. et al., 2015: Complex structure of *An* and *Ln* complexes with modified diglycolamides in solution and solid state using different analytical techniques. First SACSESS International Workshop: Warsaw, Poland.

Wilden, A., Modolo, G., Geist, A., Rothe, J., Dardenne, K., Schäfer, S. et al., 2015: Complex structure of *An* and *Ln* complexes with modified diglycolamides in solution and solid state using different analytical techniques. Second Joint Student Workshop on f-Element Chemistry: Karlsruhe, Germany.

Wilden, A., Modolo, G., Geist, A., Rothe. J., Dardenne, K., Schäfer, S. et al., 2015: Complex structure of *An* and *Ln* complexes with modified diglycolamides in solution and solid state using different analytical techniques. GDCh Wissenschaftsforum Chemie: Dresden, Germany.

Wilden, A., Modolo, G., Geist, A., Rothe, J., Dardenne, K., Schäfer, S. et al., 2015: Complex structure of *An* and *Ln* complexes with modified diglycolamides in solution and solid state using different analytical techniques. GLOBAL2015 - Nuclear Fuel Cycle for a Low-Carbon Future: Paris, France.

Wilden, A., Modolo, G., Hupert, M., Santiago-Schübel, B., Löfstrom-Engdahl, E., Halleröd, J. et al., 2015: Gamma-radiolytic stability of solvents containing C5-BPP for actinide(III)/lanthanide(III) separation. Radical Behavior Workshop: Idaho Falls, Idaho, USA.

Zarzana, C.A., Groenewold, G.S., Mincher, B.J., Mezyk, S.P., Wilden, A., Schmidt, H., Wilden, A. et al., 2015: A comparison of the gamma-radiolysis of TODGA and T(EH)DGA using UHPLC-ESI-MS analysis. Radical Behavior Workshop: Idaho Falls, Idaho, USA.

Invited Talks

Arinicheva, Y., Neumeier, S., Bosbach, D., 2015: Monazite ceramics as nuclear waste matrix: Structural investigations. 2. Projektstatusgespräch zur BMBF geförderten Nuklearen Sicherheitsforschung: Dresden, Germany.

Beridze, G., 2015: Nuclear waste management on supercomputers: reliable modeling of experimentally challenging materials. HITEC Symposium: Jülich, Germany.

Dacheux, N., Szenknect, S., Den Auwer, C., Lozano-Rodriguez, J., Bosbach, D., Burns, P.C. et al., 2015: Synthesis and determination of the thermodynamic properties of coffinite. Migration 2015: Santa Fe, NM, USA.

Finkeldei, S., 2015: Pyrochlore für die nukleare Entsorgung: struktureller Einbau von Actiniden und chemische Beständigkeit. GDCh-Wissenschaftsforum Chemie 2015: Dresden, Germany.

Finkeldei, S., Brandt, F., Stennett, M., Holliday, K., Hyatt, N., Bosbach, D., 2015: Actinide pyrochlores: Fabrication and new structural insights. Goldschmidt 2015: Prague, Czech Republic2015.

Kowalski, P., 2015: Atomistic modeling of matter at extreme conditions: selected applications in nuclear waste management, isotope geochemistry and stellar astrophysics. Institute for Mineralogy and Geoscience Colloquium: Köln University; Cologne, Germany.

Kowalski, P.: How challenging is it to compute actinides? - Atomistic modeling of nuclear materials relevant for nuclear waste management. PGI-1 Institute Colloquium: Jülich Germany.

Kowalski, P., Li, Y., Vinograd, V., 2015. *Ab initio* modeling of excess mixing parameters of solid solutions relevant for nuclear waste management. Goldschmidt 2015: Prague, Czech Republic.

Kowalski, P., Neumeier, S., 2015: Feasible and reliable atomistic simulations - Approach to modeling materials relevant for nuclear waste management. Materials Science & Technology (MS&T) 2015, Columbus, OH, USA.

Listner C, Canty M, Stein G, Rezniczek A, Niemeyer I., 2015: Evolution of Safeguards – What can formal Acquisition Path Analysis contribute? Workshop Acquisition Path Analysis, IAEA; Vienna, Austria.

Listner, C., Niemeyer, I., 2015: Fernerkundung als Werkzeug für die Verifikation von Rüstungskontroll- und Abrüstungsverträgen. Kolloquium „Frieden und Sicherheit“, IFSH & ZNF: Universität Hamburg, Hamburg, Germany.

Modolo, G., Wilden, A., Geist, A., 2015: Demonstration of innovative partitioning processes for minor actinide recycling from high active waste solutions. Pacifichem 2015: Honolulu, Hawaii, 2015.

Neumeier, S., Arinicheva, Y., Bosbach, D., 2015: Investigations on monazite-type solid solutions for nuclear waste management applications. Seminar - University of Tennessee 2015: Knoxville, TN, USA.

Neumeier, S., Arinicheva, Y., Schreinemachers, C., Finkeldei, S., Brandt, F., Bukaemskiy, A.A. et al., 2015: Immobilisation of actinides in ceramic materials for innovative waste management strategies. Institutsseminar Institut für Angewandte Physik, Frankfurt, Germany.

Neumeier, S., Arinicheva, Y., Huittinen, N., Lozano-Rodriguez, M.J., Holthausen, J., Modolo, G. et al., 2015: Spectroscopic studies on monazite-type ceramics for the conditioning of radioactive waste: Infrared, Raman, X-ray absorption and site-selective time resolved laser fluorescence spectroscopy. E-MRS Spring Meeting: Lille, France.

Neumeier, S., Bosbach, D., 2015: Grundlegende Untersuchungen zur Immobilisierung langlebiger Radionuklide mittels Einbau in endlagerrelevante Keramiken (Conditioning). 2. Projektstatusgespräch zur BMBF geförderten Nuklearen Sicherheitsforschung: Dresden, Germany.

Niemeyer, I., 2015: Object-based image analysis using KOMPSAT-3 Imagery. SI Imaging Services: Daejeon, Republic of Korea.

Niemeyer, I., Listner, C., Canty, M., Rezniczek, A., Stein, G., 2015: Quantifying detection probabilities for proliferation activities outside declared nuclear facilities. INMM International Safeguards Division (ISD) Meeting: Manchester, UK.

Niemeyer, I., Trautwein, W., 2015: Joint research and development – Member states support programmes (MSSPs) as a vehicle for the technical development and further improvement of IAEA safeguards. 23rd WiN Global Annual Conference: Women in Nuclear meet Atoms for Peace: Vienna, Austria.

Randriamalala, T., Rossbach, M., 2015: Prompt gamma-rays from neutron inelastic scattering at FaNGaS: Benchmark spectrum analysis. Modern Trends in Activation Analysis: Delft, The Netherlands.

Rossbach, M., Revay, Z., 2015: NAA advanced methods and techniques – the neutron is a valuable probe. 25th Seminar on Activation Analysis and Gamma Spectroscopy (SAAGAS 2015): Aachen, Germany.

Sadowski, F. , 2015: Validierung der Methodenparameter für die Konzentrationsbestimmung von Multielementlösungen mittels ICP-MS. FC25 Projektpräsentation: Berufskolleg Simmerath/Stolberg der Städteregion Aachen: Stolberg, Germany.

Additional Talks

Arinicheva, Y., 2015: Matryoshka for nuclear waste. RACIRI Summer School: Sellin/Rügen, Germany.

Aymanns, K., 2015: Tamper indicating enclosure EOSS and NGSS. European Safeguards Research & Development Association (ESARDA) - Working Group: Ispra, Italy.

Aymanns, K., 2015: Assesment of lifecycle challenges for the Electronic Optical Sealing System (EOSS). European Safeguards Research & Development Association (ESARDA) - Working Group: Manchester, Great Britain.

Dreicer, M., Chen, C., Allen, K., Niemeyer, I., Listner, C., Stein, G., 2015: Applying state-level approaches to arms control verification – a systems concept. Meeting of the ESARDA Working Group on Verification Technologies and Methodologies (VTM); Manchester, UK.

Dürr, M., 2015: Update on DA-related activities at Forschungszentrum Jülich. Meeting of the ESARDA Working Group on Techniques and Standards for Destructive Analysis, Manchester, UK.

Finkeldei, S., Holliday, K., Brandt, F., de Visser-Tynova, E., Bruin, J., Stennett, M. et al., 2015: Structural uptake of actinides by zirconia based pyrochlores. Seminar - Waste Immobilization Laboratory: Sheffiled, UK.

Kaufholz, P., Wilden, A., Modolo G., 2015: Americium selective separation using hydrophilic complexing agents. SACSESS Meeting on EXAm hot-test: Paris, France.

Klass, L., 2015: Selective separation of Am(III) from a PUREX raffinate. 6. Halbjahrestreffen, BMBF Projekt f-Kom 02NUK020E: Aachen, Germany.

Kowalski, P., 2015: Atomistische Modellrechnungen für die sichere Entsorgung radioaktiver Abfälle. IEK-JSC Meeting: Jülich, Germany.

Kowalski P. Atomistische Modellrechnung - Presentation of Atomistic Modeling Group (IEK-6). Jülich, Germany.

Kowalski, P., 2015: An overview of atomistic modelling activities at IEK-6. Helmholtz-Koordinierungstreffen (Trilateral meeting: FZJ, KIT & HZDR): Jülich, Germany.

Li, Y., Kowalski, P., 2015: Progress in computational modelling of ceramic materials. 5th BMBF Project-meeting Conditioning (02NUK021A): Dresden, Germany.

Marie, C., Duchesne, M.-T., Russello, E., Kaufholz, P., Miguirditchian, M., 2015: SACSESS Report. SACSESS Second Annual Meeting: Warsaw, Poland.

Modolo, G., 2015: SACSESS Meeting on EXAm hot-test: Paris, France.

Neumeier, S., 2015: Combined experimental & atomistic modelling research approach for studies on monazite ceramics for nuclear waste immobilisation. Midterm Evaluation - YIG "Atomistic Modelling": Jülich, Germany.

Rozov, K., Curtius, H., Dahmen, K.. 2015: Aufklärung von Thermodynamik und Speziation von Actiniden und Spaltprodukten bei höheren Temperaturen in Kombination von Schätzmethoden, spektroskopischen und quantenchemischen Methoden - Focus: Zr(IV) LDHs. Project meeting ThermAc: Jülich, Germany.

Rutkowski, J., 2015: Digital declaration site maps for the additional protocol. European Safeguards Research & Development Association (ESARDA) Working Group Meetings: Ispra, Italy.

Schmidt, H., Kaufholz, P., Modolo, G., Wilden, A., Sadowski, F., Gerdes, M. et al., 2015: JUELICH contribution in 3rd and 4th semester, WP 1.1 – 1.2 – 1.4, in collaboration with CEA, CHALMERS and IIC. SACSESS Second annual meeting: Warsaw, Poland.

Schmidt, H., Modolo, G., Wilden, A., 2015: Radiolysis/ hydrolysis of $CyMe_4BTBP$ and $CyMe_4BTPhen$. SACSESS Meeting on Radiolysis: Prague, Czech Republic.

Schmidt, H., Modolo, G., Wilden, A., Ekberg, C., Halleröd, J., Grüner, B. et al., 2015: Product identification of radiolysis products from $CyMe_4BTBP$ and $CyMe_4BTPhen$. Meeting on Modeling of Radiolysis Products: Jülich, Germany.

Weber, J., Brandt, F., Klinkenberg, M., Barthel, J., Breuer, U., Savenko, A. et al., 2015: Nano-scale analysis of Ra uptake into barite by TEM and APT. Second Joint Student Workshop on f-Element Chemistry: Karlsruhe, Germany.

Weber, J., Brandt, F., Klinkenberg, M., Barthel, J., Breuer, U., Savenko, A. et al., 2015: Ra retention by barite APT and TEM characterization of the $(Ba,Ra)SO_4$ solid solution with nm-scale resolution. HITEC Theme Day on Nuclear Waste Management: Jülich, Germany.

Weber, J., Brandt, F., Klinkenberg, M., Breuer, U., Barthel, J., Savenko, A, et al., 2015: Combined atom probe tomography and scanning transmission electron microscopy characterization of $Ba_xRa_{1-x}SO_4$ solid solutions - enabling the process understanding of Ra uptake into barite. European APT Workshop: Leoben, Austria.

Wilden, A., Assenmacher, J., Schmidt, H., Modolo, G., Gerdes, M., Hupert, M. et al., 2015: Überblick über die FZJ-IEK6 Aktivitäten im Verbundprojekt f-Kom. 6. Halbjahrestreffen, BMBF Projekt f-Kom 02NUK020E: Aachen, Germany.

11.2. Publications 2016

11.2.1 Journal paper

Peer-reviewed journals

Beele, B., Skerencak-Frech, A., Stein, A., Trumm, A., Wilden, A., Lange, S., Müllich, U., Schimmelpfennig, B., Geist, A., Panak, P., 2016: 2,6-bis(5,6-diisopropyl-1,2,4-triazine-3-yl)pyridine: A highly selective N-donor ligand studied by TRLFS, liquid-liquid extraction and molecular dynamics. New Journal of Chemistry, 40(12): 10389-10397.

Beridze, G., Birnie, A., Koniski, S., Ji, Y., and Kowalski, P., 2016: DFT + U as a reliable method for efficient *ab initio* calculations of nuclear materials. Progress in Nuclear Energy, 92: 142-146.

Fast, I., Aksyutina, Y., Tietze-Jaensch, H., and Bosbach, D., 2016: Determination of bandwidths of PWR-UO_2 spent fuel radionuclide inventory based on real operational history data. IEEE Transactions on Nuclear Science, 63(4): 2331-2335.

Gausse, C., Szenknect, S., Qin, D. W., Mesbah, A., Clavier, N., Neumeier, S., Bosbach, D., and Dacheux, N., 2016: Determination of the Solubility of Rhabdophanes $Ln PO_4 \cdot 0.667 H_2O$ (*Ln* = La to Dy). European Journal of Inorganic Chemistry, 2016(28): 4615-4630.

Geist, A., Taylor, R., Ekberg, C., Guilbaud, P., Modolo, G., Bourg, S., 2016: The SACSESS hydrometallurgy domain — An overview. ATALANTE 2016 - Conference on Nuclear Chemistry for Sustainable Fuel Cycles, 21: 218-222.

Hao, Y., Klepov, V.V., Murphy, G.L., Modolo, G., Bosbach, D., Albrecht-Schmitt, T.E., Kennedy, B.J., Wang, S., Alekseev, E., 2016: Influence of synthetic conditions on chemistry and structural properties of alkaline earth uranyl borates. Crystal Growth & Design, 16(10): 5923-5931.

Huittinen, N., Arinicheva, Y., Schmidt, M., Neumeier, S., Stumpf, T., 2016: Using Eu^{3+} as an atomic probe to investigate the local environment in $LaPO_4$–$GdPO_4$ monazite end-members. Journal of Colloid and Interface Science, 483: 139-145.

Kaufholz, P., Modolo, G., Wilden, A., Sadowski, F., Bosbach, D., Wagner, C., Geist, A., Panak, P., Lewis, F., Harwood, L., 2016: Solvent extraction and fluorescence spectroscopic investigation of the selective Am(III) complexation with TS-BTPhen: Solvent Extraction and Ion Exchange: 34(2): 126-140.

Klepov, V.V., Serezhkina, L.B., Serezhkin, V.N., Alekseev, E., 2016: Synthesis and crystal structure analysis of uranyl triple acetates: Journal of Solid State Chemistry, 244: 100-107.

Klobes, B., Arinicheva, Y., Neumeier, S., Simon, R.E., Jafari, A., Bosbach, D., Hermann, R.P., 2016: Quadrupole splitting and Eu partial lattice dynamics in europium orthophosphate $EuPO_4$. Hyperfine Interactions, 237(1): 31.

Koubský, T., Schmidt, H., Modolo, G., Kalvoda, L., 2016: Simulation of UV/Vis spectra of $CyMe_4BTBP$ and some of its degradation products. ATALANTE 2016 - Conference on Nuclear Chemistry for Sustainable Fuel Cycles, 21: 509-516.

Kowalski, P., Li, Y., 2016: Relationship between the thermodynamic excess properties of mixing and the elastic moduli in the monazite-type ceramics. Journal of the European Ceramic Society, 36(8): 2093-2096.

Listner, C., Niemeyer, I., Canty, M., Stein, G., 2016: A strategic model for state compliance verification. Naval Research Logistics, 63(3): 260-271.

McLachlan, F., Greenough, K., Geist, A., McLuckie, B., Modolo, G., Wilden, A., Taylor, R., 2016: Nitric acid extraction into the TODGA/TBP solvent: Solvent Extraction and Ion Exchange, 34(4): 334-346.

Middendorp, R., Dürr, M., Bosbach, D., 2016: The stability of uranium microspheres for future application as reference standard in analytical measurements, ATALANTE 2016 - Conference on Nuclear Chemistry for Sustainable Fuel Cycles, 21: 285-292.

Mildenberger, F., Mauerhofer, E., 2016: Prompt gamma neutron activation analysis of large heterogeneous samples composed of concrete and polyethylene: Journal of Radioanalytical and Nuclear Chemistry, 309(3): 1265-1269.

Murphy, G.L., Kennedy, B.J., Kimpton, J.A., Gu, Q., Johannessen, B., Beridze, G., Kowalski, P., Bosbach, D., Avdeev, M., Zhang, Z., 2016: Nonstoichiometry in strontium uranium oxide: Understanding the rhombohedral–orthorhombic transition in $SrUO_4$. Inorganic Chemistry, 55(18): 9329-9334.

Murshed, M.M., Zhao, P., Fischer, M., Huq, A., Alekseev, E., Gesing, T.M., 2016: Thermal expansion modeling of framework-type $Na[AsW_2O_9]$ and $K[AsW_2O_9]$. Materials Research Bulletin, 84: 273-282.

Neumeier, S., Arinicheva, Y., Clavier, N., Podor, R., Bukaemskiy, A., Modolo, G., Dacheux, N., Bosbach, D., 2016: The effect of the synthesis route of monazite precursors on the microstructure of sintered pellets. Progress in Nuclear Energy, 92: 298-305.

Neumeier, S., Kegler, P., Arinicheva, Y., Shelyug, A., Kowalski, P., Schreinemachers, C., Navrotsky, A., Bosbach, D., 2016: Thermochemistry of $La_{1-x}Ln_xPO_4$-monazites (*Ln* = Gd, Eu): The Journal of Chemical Thermodynamics, 105: 396-403.

Nicol, T., Carasco, C., Perot, B., Ma, J.L., Payan, E., Mauerhofer, E., Havenith, A., Collot, J., 2016: Quantitative comparison between PGNAA measurements and MCNPX simulations. Journal of Radioanalytical and Nuclear Chemistry, 308(2): 671-677.

Peterman, D., Geist, A., Mincher, B., Modolo, G., Galán, M.H., Olson, L., McDowell, R., 2016: Performance of an i-SANEX system based on a water-soluble BTP under continuous irradiation in a γ-radiolysis test loop. Industrial & Engineering Chemistry, 55(39): 10427-10435.

Prieto, M., Heberling, F., Rodríguez-Galán, R.M., Brandt, F., 2016: Crystallization behavior of solid solutions from aqueous solutions: An environmental perspective. Progress in Crystal Growth and Characterization of Materials, 6(3): 29-68.

Roscioli-Johnson, K.M., Zarzana, C.A., Groenewold, G.S., Mincher, B.J., Wilden, A., Schmidt, H., Modolo, G., Santiago-Schübel, B., 2016: A study of the γ-radiolysis of N,N-didodecyl-N',N'-dioctyldiglycolamide using UHPLC-ESI-MS analysis. Solvent Extraction and Ion Exchange, 34(5): 439-453.

Rossbach, M., Randriamalala, T., Mauerhofer, E., Revay, Z., Söllradl, S., 2016: Prompt and delayed inelastic scattering reactions from fission neutron irradiation - first results of FaNGaS. Modern Trends in Activation Analysis, 309(1): 149-154.

Rutkowski, J., Steinmaus, K., Dahl, F., Robb, S.W., Kirkgoeze, R., 2016: The implementation and use of the geospatial exploitation system within the IAEA's department of safeguards. Journal of Nuclear Materials Management, 44(2): 39-44.

Schmidt, H., Wilden, A., Modolo, G., Bosbach, D., Santiago-Schübel, B., Hupert, M., Švehla, J., Grüner, B., Ekberg, C., 2016: Gamma radiolysis of the highly selective ligands $CyMe_4BTBP$ and $CyMe_4BTPhen$: Qualitative and quantitative investigation of radiolysis products. ATALANTE 2016 - Conference on Nuclear Chemistry for Sustainable Fuel Cycles, 21, 32-37.

Shamblin, J., Feygenson, M., Neuefeind, J., Tracy, C.L., Zhang, F., Finkeldei, S., Bosbach, D., Zhou, H., Ewing, R.C., Lang, M., 2016: Probing disorder in isometric pyrochlore and related complex oxides. Nature Materials, 15(5): 507-511.

Siidra, O.I., Kabbour, H., Mentre, O., Nazarchuk, E.V., Kegler, P., Zinyakhina, D.O., Colmont, M., Depmeier, W., 2016: Lead oxychloride borates obtained under extreme conditions. ChemInform, 47(47).

Siidra, O.I., Kabbour, H., Mentre, O., Nazarchuk, E.V., Kegler, P., Zinyakhina, D.O., Colmont, M., Depmeier, W., 2016: Lead oxychloride borates obtained under extreme conditions. Inorganic Chemistry, 55(17): 9077-9084.

Silber, D., Kowalski, P., Traeger, F., Buchholz, M., Bebensee, F., Meyer, B., Wöll, C., 2016: Adsorbate-induced lifting of substrate relaxation is a general mechanism governing titania surface chemistry. Nature Communications, 7: 12888.

Vanel, V., Marie, C., Kaufholz, P., Montuir, M., Boubals, N., Wilden, A., Modolo, G., Geist, A., Sorel, C., 2016: Modeling and flowsheet design of an Am separation process using TODGA and H_4TPAEN. ATALANTE 2016 - Conference on Nuclear Chemistry for Sustainable Fuel Cycles, 21: 223-230.

Weber, J., Barthel, J., Brandt, F., Klinkenberg, M., Breuer, U., Kruth, M., Bosbach, D., 2016: Nano-structural features of barite crystals observed by electron microscopy and atom probe tomography. Chemical Geology: 424: 51-59.

Wilden, A., Modolo, G., Hupert, M., Santiago-Schübel, B., Löfström-Engdahl, E., Halleröd, J., Ekberg, C., Mincher, B.J., and Mezyk, S.P., 2016: Gamma-radiolytic stability of solvents containing C5-BPP (2,6-Bis(5-(2,2-dimethylpropyl)-1H-pyrazol-3-yl)pyridine) for actinide(III) / lanthanide(III) separation. Solvent Extraction and Ion Exchange, 34(1), 1-12.

Xiao, B., Kegler, P., Bosbach, D., Alekseev, E., 2016: Rich non-centrosymmetry in a Na-U-Te oxo-system achieved under extreme conditions. ChemInform, 47(29).

Xiao, B., Kegler, P., Bosbach, D., Alekseev, E., 2016: Investigation of reactivity and structures formation in K-Te-U oxo-system under high-temperature/high-pressure conditions. Dalton transactions, 45(38): 15225-15235.

Xiao, B., Kegler, P., Bosbach, D., Alekseev, E., 2016: Rich non-centrosymmetry in a Na-U-Te oxo-system achieved under extreme conditions. Inorganic Chemistry, 55(9): 4626-4635.

Xiao, B., Kegler, P., Gesing, T. M., Robben, L., Blanca-Romero, A., Kowalski, P., Li, Y., Klepov, V., Bosbach, D., Alekseev, E., 2016: Giant volume change and topological gaps in temperature- and pressure-induced phase transitions: Experimental and computational study of $ThMo_2O_8$. Chemistry - a European Journal, 22(3): 946-958.

Xiao, B., Schlenz, H., Bosbach, D., Suleimanov, E.V., Alekseev, E., 2016: The structural effects of alkaline- and rare-earth elements incorporation into the thorium molybdates. Crystal Engineering Communications, 18(1): 113-122.

Xu, X., Liu, Z., Yang, S., Chen, L., Diwu, J., Alekseev, E., Chai, Z., Albrecht-Schmitt, T.E., Wang, S., 2016: Potassium uranyl borate 3D framework compound resulted from temperature directed hydroborate condensation: Structure, spectroscopy, and dissolution studies. Dalton Transactions, 45(39): 15464-15472.

11.2.2 Proceedings/Books

Proceedings

Ebrahimi, H., Trinchero, P., Molinero, J., Deissmann, G., Bosbach, D., Hammond, G. et al., 2016: PFLOTRAN grain-scale simulations of oxygen intrusion and radionuclide sorption in a heterogeneous rock sample. JUQUEEN Extreme Scaling Workshop 2016: Jülich, Germany, 55-62.

Niemeyer, I., Aymanns, K., Dürr, M., Rutkowski, J., Bosbach, D, Trautwein, W., 2016: Joint programme on the technical development and further improvement of IAEA safeguards - The German MSSP. Institute of Nuclear Materials Management (INMM) - 57th Annual Meeting: Atlanta, USA, p. 10.

Niemeyer, I., Deissmann, G., Bosbach, D., 2016: Bridging nuclear safety, security and safeguards at geological disposal of high-level radioactive waste and spent nuclear fuel. International Conference on the Safety of Radioactive Waste Management: Vienna, Austria. p. 5.

Rutkowski, J., Canty, M., Niemeyer, I., Stein, G., Rezniczek, A., 2016: Acquisition path analysis: JCPOA case study. Institute of Nuclear Materials Management (INMM) - 57th Annual Meeting: Atlanta, Georgia, USA, p. 8.

Books

Neumeier, S., Klinkenberg, M., Bosbach, D., 2016: Institute of energy and climate research - IEK-6: Nuclear waste management report 2013 / 2014: Material science for nuclear waste management. Forschungszentrum Jülich GmbH, Energy & Environment, 328: 219 p.

Kowalski, P., Beridze, G., Li, Y., Ji, Y., Friedrich, C., Şaşioğlu, E. et al., 2016: Feasible and reliable *ab initio* approach to computation of materials relevant for nuclear waste management. In: Shimamura, Kiyoshi (ed.): Additive manufacturing and strategic technologies in advanced ceramics. Hoboken, NJ, USA: John Wiley & Sons, Inc., p. 205-17.

Li, Y., Kowalski, P., Beridze, G., Blanca-Romero, A., Ji, Y., Vinograd, V. et al., 2016: Atomistic simulations of ceramic materials relevant for nuclear waste management: Cases of monazlte and pyrochlore. In: Pfeifer, Thomas (ed.): Ceramics for energy conversion, storage, and distribution systems. Hoboken, NJ, USA: John Wiley & Sons, Inc., p. 165-75.

11.2.3 Reports

Deissmann, G., Haneke, K., Filby, A., Wiegers, R., 2016: Dissolution behaviour of HLW glasses under OPERA repository conditions. Report, Vlissingen: COVRA.

Deissmann, G., Haneke, K., Filby, A., Wiegers, R., 2016: Corrosion behaviour of spent research reactor fuel under OPERA repository conditions. Report, Vlissingen: COVRA.

Filby, A., Deissmann, G., Wiegers, R., 2016: LILW degradation processes and products. Report, Vlissingen: COVRA.

Modolo, G., Gerdes, M., Klass, L., Sadowski, F., Schmidt, H., Schneider, D. et al., 2016: EU-Projekt SACSESS, HYBAR 6 - Half Yearly Beneficiary Activity Report No. 6: Internal Report.

Modolo, G., Wilden, A., 2016: Fachlicher Schlussbericht des BMBF Forschungsvorhabens Verbundprojekt „Untersuchungen zum grundlegenden Verständnis der selektiven Komplexierung von f-Elementen (f-Kom)“ Teilprojekt E, 02NUK020E: Report.

Verhoef, E.V., Neeft, E.A., Deissmann, G., Filby, A., Wiegers, R.B., Kers, D., 2016: Waste families in OPERA. Report,. Vlissingen: COVRA.

11.2.4 Poster

Kowalski, P., Beridze, G., Li, Y., Ji, Y., 2016: Towards reliable modeling of challenging f-electrons bearing materials: Experience from modeling of nuclear materials. MRS Fall Meeting: Boston, USA.

Middendorp, R., Dürr, M., Bosbach, D., 2016: The stability of uranium microspheres for future application as reference standard in analytical measurements. ATALANTE 2016 - Conference on Nuclear Chemistry for Sustainable Fuel Cycles: Montpellier, France.

Beridze, G., Kowalski, P., Alekseev, E., Xiao, B., Kegler, P., Baker, R. et al., 2016: Parameter free DFT+U method for efficient modelling of nuclear materials. NUMAT 2016 - The Nuclear Materials Conference: Montpellier, France.

Brandt, F., Weber, J., Klinkenberg, M., Breuer, U., Barthel, J., Povstugar, I. et al., 2016: Radium retention by $Ba_xRa_{1-x}SO_4$ solid solution formation: an electron microscopy and atom probetomography investigation. MRS Fall Meeting 2016: Boston, USA.

Deissmann, G., Haneke, K., Filby, A., Wiegers, R., Bosbach, D., 2016: Geological disposal of high-level radioactive wastes in Boom Clay in the Netherlands: Evaluation of waste form corrosion behaviour for the generic OPERA safety case. 2nd Conference on Key Topics in Deep Geological Disposal: Cologne, Germany.

Gylling, B., Trinchero, P., Molinero, J., Deissmann, G., Svensson, U., Ebrahimi, H. et al., 2016: A DFN-based High Performance Computing approach to the simulation of radionuclide transport in mineralogically heterogeneous fractured rocks. AGU Fall Meeting: San Francisco, USA.

Huittinen, N., Scheinost, A.C., Wilden, A., Arinicheva, Y., 2016: Cm^{3+} Incorporation in $La_{1-x}Gd_xPO_4$ monazites: A TRLFS and XAFS study. 9th International Conference on Nuclear and Radiochemistry: Helsinki, Finland.

Ji, Y., Beridze, G., Li, Y., Forward, R., Kowalski, P., 2016: Large scale simulations of nuclear materials. NIC Symposium 2016: Jülich, Germany.

Johnson, K., Zarzana, C.A., Groenewold G.S., Mincher B.J., Wilden A., Schmidt, H. et al., 2016: A study of the γ-radiolysis of di-dodecyl di-octyl diglycolamide (D3DODGA) using UHPLC-ESI-MS analysis. 64th ASMS Conference on Mass Spectrometry and Allied Topics: San Antonio, Texas, USA.

Kowalski, P., Beridze, G., Li, Y., Xiao, B., Alekseev, E., 2016: Feasible and reliable *ab initio* calculation of f-elements-bearing materials relevant for nuclear waste management. MMM2016 Conference – 8th International Conference on Multiscale Materials Modeling: Dijon, France.

Lange, S., Deissmann, G., Bosbach, D., 2016: Uptake and retention of safety relevant radionuclides in cementitious systems. 4th International Workshop on Mechanisms and Modelling of Waste/Cement Interactions: Murten, Switzerland.

Lange, S., Deissmann, G., Bosbach, D., 2016: Interaction of long-lived safety relevant radionuclides with cementitious materials. 2nd Conference on Key Topics in Deep Geological Disposal: Cologne, Germany.

Mossini, E., Kaufholz, P., Wilden, A., Modolo, G., Macerata, E., Mariani, M. et al., 2016: i-SANEX single-stage centrifugal contactor experiment with a novel hydrophilic complexing agent. ATALANTE 2016 - Conference on Nuclear Chemistry for Sustainable Fuel Cycles: Montpellier, France.

Schmidt, H., Wilden, A., Modolo, G., Bosbach, D., Santiago-Schübel, B., Hupert, M. et al., 2016: Gamma-radiolysis of the nitrogen donor ligands $CyMe_4BTBP$ and $CyMe_4BTPhen$. International Conference on Ionizing Processes: Brookhaven National Laboratory, USA.

Szreder, T., Schmidt, H., Modolo, G., 2016: Early stages of $CyMe_4BTPhen$ radiation chemistry in 1-octanol. ATALANTE 2016 - Conference on Nuclear Chemistry for Sustainable Fuel Cycles: Montpellier, France.

Weber, J., Brandt, F., Klinkenberg, M., Barthel, J., Breuer, U., Bosbach, D., 2016: Ra uptake into barite. 252nd American Chemical Society National Meeting & Exhibition: Philadelphia, USA.

Wilden, A., Galán, H., Groenewold, G.S., Mincher, B.J., Zarzana, C.A., Nunez, A. et al.: Gamma-radiolytic stability of new methylated TODGA derivatives for minor actinide recycling. Sustainable Nuclear Energy Conference: Nottingham, UK.

Wilden, A., Galán, H., Groenewold, G.S., Mincher, B.J., Zarzana, C.A., Nunez, A. et al., 2016: Gamma-radiolytic stability of new methylated TODGA derivatives for minor actinide recycling. ATALANTE 2016 - Conference on Nuclear Chemistry for Sustainable Fuel Cycles: Montpellier, France.

Wilden, A., Geist, A., Gerdes, M., Müllich, U., Modolo, G., 2016: Influence of temperature on the extraction of trivalent actinides and lanthanides by diglycolamide ligands. Sustainable Nuclear Energy Conference: Nottingham, UK.

11.2.5 Presentations

Conferences:

Arinicheva, Y., Clavier, N., Huittinen, N., Bukaemskiy, A., Neumeier, S., Stumpf, T. et al., 2016: Structural studies on rhabdophane-monazite phase transformation in $La_{1-x}Ln_xPO_4 \cdot 0.667\ H_2O$ (*Ln*=Eu, Gd). Goldschmidt 2016: Yokohama, Japan.

Arinicheva, Y., Huittinen, N., Popa, K., Somers, J., Neumeier, S., Rossberg, A. et al., 2016: Structural incorporation of Cm^{3+} and Pu^{3+} in phosphate ceramics with monazite structure. E-MRS Fall Meeting: Warsaw, Poland.

Arinicheva, Y., Kegler, P., Schreinemachers, C., Huittinen, N., Neumeier, S., Shelyug, A., Navrotsky, A., Bosbach, D.: Studies on solid solution formation and thermochemistry of $La_{1-x}Ln_xPO_4$-monazites (*Ln*= Gd, Eu). ATALANTE 2016 - Conference on Nuclear Chemistry for Sustainable Fuel Cycles: Montpellier, France.

Beridze, G., Kowalski, P., Li, Y., Alekseev, E., Xiao, B., Kegler, P. et al., 2016: Reliable atomistic modeling for nuclear waste management. MRS Fall Meeting: Boston, USA.

Bosbach, D., Brandt, F., Klinkenberg, M., Vinograd, V., Deissmann, G., 2016: The relevance of solid solution – aqueous solution systems to the safety case for deep geological disposal of nuclear wastes. 2nd Conference on Key Topics in Deep Geological Disposal: Cologne, Germany.

Bosbach, D., Shcherbina, N., Mauerhofer, E., Deissmann, G., 2016: Radioaktive Sonderabfälle kerntechnischer Anlagen: Charakterisierung und Konditionierung. VDI Fachkonferenz Rückbau kerntechnischer Anlagen: Düsseldorf, Germany.

Finkeldei, S., Brandt, F., Deissmann, G., Baena Velez, A.M., Bukaemskiy, A., Lang, M. et al., 2016: UO_2 based model systems – a complementary approach for research into spent nuclear fuel corrosion. MRS Fall Meeting: Boston, USA.

Finkeldei, S., Kowalski, P., Kegler, P., Brandt, F., Vinograd, V., Lang, M. et al., 2016: Pyrochlore disorder: a combined experimental and atomistic simulation study. Goldschmidt 2016: Yokohama, Japan.

Gausse, C., Mesbah, A., Szenknect, S., Clavier, N., Neumeier, S., Bosbach, D. et al.: Kinetics and thermodynamics of monazite dissolution. ATALANTE 2016 - Conference on Nuclear Chemistry for Sustainable Fuel Cycles: Montpellier, France.

Gausse, C., Mesbah, A., Szenknect, S., Clavier, N., Neumeier, S., Bosbach, D. et al., 2016: Synthèse et dissolution de matrices phosphatées de structure monazitique. Journées Nationales de Radiochimie: Nice, France.

Geist, A., Taylor, R., Ekberg, C., Guilbaud, P., Modolo, G., Bourg, S., 2016: The SACSESS hydrometallurgy domain - an overview. ATALANTE 2016 - Conference on Nuclear Chemistry for Sustainable Fuel Cycles: Montpellier, France.

Ji, Y., Kowalski, P., Neumeier, S., Li, Y., Beridze, G., Bosbach, D., 2016: Complementary atomistic modeling and experimental studies of radiation damage in monazite-type ceramic nuclear waste forms. COSIRES - Computer Simulation of Radiation Effects in Solids Conference 2016: Loughborough, UK.

Ji, Y., Li, Y., Beridze, G., Kowalski, P., 2016: Large scale simulations of monazite-type ceramic nuclear waste forms. 8th International Conference on Multiscale Materials Modeling: Dijon, France.

Kowalski, P., Beridze, G., Ji, Y., Li, Y., 2016: Reliable and efficient *ab initio* simulations of computationally challenging materials. EMC - Second European Mineralogical Conference 2016: Rimini, Italy.

Kowalski, P., Blouin, S., Dufour, P., 2016: Infrared opacities in dense atmospheres of cool white dwarf stars. 20th European Workshop on White Dwarfs: Warwick, UK.

Kowalski, P., Ji, Y., Xiao, B., Bosbach, D., Beridze, G., Vinograd, V. et al., 2016: Simulation of ceramic materials relevant for nuclear waste management. COSIRES - Computer Simulation of Radiation Effects in Solids 2016: Loughborough, UK.

Kowalski, P., Li, Y., Beridze, G., Finkeldei, S., Kegler, P., Neumeier, S. et al., 2016: Reliable atomistic modeling of monazite and pyrochlore ceramics as matrices for immobilization of nuclear waste. Goldschmidt 2016: Yokohama, Japan.

Kowalski, P., Li, Y., Ji, Y., 2016: Progress made in computational modeling of ceramic materials in the scope of BMBF "Conditioning" project. 5th Meeting BMBF Verbundprojekt: Fundamental studies on immobilization of long-lived radionuclides after incorporation into repository relevant ceramics (Conditioning): Aachen, Germany.

Lange, S., Klinkenberg, M., Deissmann, G., Bosbach, D., 2016: Understanding the behaviour of safety relevant radionuclides in cementitious systems: First results on the uptake of radium and technetium by CSH, AFm and AFt. Cebama 1st Annual Workshop: Barcelona, Spain.

Li, Y., Kowalski, P., Beridze, G., Birnie, A., Vinograd, V., Finkeldei, S. et al., 2016: *Ab initio* simulations of ceramics relevant for nuclear waste management: Cases of monazite and pyrochlore. E-MRS Fall Meeting: Warsaw, Poland.

Marie, C., Duchesne, M.-T., Russello, E., Kaufholz, P., Wilden, A., Modolo, G. et al., 2016: Development of a selective americium separation process using TPAEN as a water-soluble stripping agent. ATALANTE 2016 - Conference on Nuclear Chemistry for Sustainable Fuel Cycles: Montpellier, France.

Middendorp, R., Dürr, M., 2016: The stability of uranium microspheres for future application as reference standards. ESARDA 38th Annual Meeting: Luxembourg, Luxembourg.

Mildenberger, F., Mauerhofer, E., 2016: Cyclic neutron activation analysis of large samples with a pulsed 14 MeV neutron source. 1st International Conference on Radioanalytical and Nuclear Chemistry: Budapest, Hungary.

Neumeier, S., Kowalski, P., Bukaemskiy, A., Arinicheva, Y., Beridze, G., Bosbach, D., 2016: Monazite ceramics for nuclear waste management strategies: An experimental and modeling study. ATALANTE 2016 - Conference on Nuclear Chemistry for Sustainable Fuel Cycles: Montpellier, France.

Niemeyer, I., Aymanns, K., Dürr, M., Rutkowski, J., Bosbach, D., Trautwein, W., 2016: Joint programme on the technical development and further improvement of IAEA safeguards - The German MSSP. Institute of Nuclear Materials Management (INMM), 57th Annual Meeting: Atlanta, USA.

Niemeyer, I., Rutkowski, J., 2016: Satellite imagery processing for the verification of nuclear non-proliferation and arms control. European Association of Remote Sensing Laboratories (EARSeL) Symposium 2016: Bonn, Germany.

Rohmen, S., 2016: Pore-scale reactive transport modelling based on the Lattice-Boltzmann-Method. Cebama, 1st Annual Workshop: Barcelona, Spain.

Roscioli-Johnson, K.M., Zarzana, C.A., Groenewold, G.S., Mincher, B.J., Wilden, A., Schmidt, H. et al., 2016: A study of the gamma-radiolysis of di-dodecyl di-octyl diglycolamide using UHPLC-MS analysis. ATALANTE 2016 - Conference on Nuclear Chemistry for Sustainable Fuel Cycles: Montpellier, France.

Rutkowski, J., Canty, M., Niemeyer, I., Rezniczek, A., Stein, G., 2016: Acquisition path analysis: JCPOA case study. INMM, 57th Annual Meeting: Atlanta, Georgia, USA.

Schmidt, H., Wilden, A., Modolo, G., Bosbach, D., Santiago-Schübel, B., Hupert, M. et al., 2016: Gamma-radiolysis of the nitrogen donor ligands $CyMe_4BTBP$ and $CyMe_4BTPhen$. International Conference on Ionizing Processes: Brookhaven National Laboratory, USA.

Schmidt, H., Wilden, A., Modolo, G., Bosbach, D., Santiago-Schübel, B., Hupert, M. et al., 2016: Gamma-radiolysis of the highly selective ligands $CyMe_4BTBP$ and $CyMe_4BTPhen$: Qualitative and quantitative investigation of radiolysis products. ATALANTE 2016 - Conference on Nuclear Chemistry for Sustainable Fuel Cycles: Montpellier, France.

Szreder, T., Kocia, R., Schmidt, H., Modolo, G., 2016: Selected aspects of the SANEX system radiation chemistry. 13th DAE-BRNS Biennial Trombay Symposium on Radiation & Photochemistry (TSRP-2016) incorporating 6th Asia Pacific Symposium on Radiation Chemistry (APSRC-2016): Mumbai, India.

Taylor, R., Carrott, M., Rhodes, C., Sarsfield, M., Wilden, A., Galan, H. et al., 2016: The EURO-GANEX process: current status of flowsheet development and process safety studies. ATALANTE 2016 - Conference on Nuclear Chemistry for Sustainable Fuel Cycles: Montpellier, France.

Trinchero, P., Iraola, A., Ebrahimi, H., Molinero, J., Svensson, U., Patrik, V., Deissmann, G., 2016: Modelling the field experiments of REPRO and LTDE-SD using iDP. 34th SKB Task Force modelling of Ground Water Flow and Transport of Solutes Meeting: Prague, Czech Republic.

Trinchero, P., Puigdomenech, I., Molinero, J., Ebrahimi, H., Gylling, B., Svensson, U., Bosbach, D., Deissmann, G., 2016: Continuum-based DFN-consistent simulations of oxygen ingress in fractured crystalline rocks. AGU Fall Meeting: San Francisco, USA.

Vanel, V., Marie, C., Kaufholz, P., Montuir, M., Boubals, N., Wilden, A. et al., 2016: EuroEXAm - modeling and flowsheet design of an Am separation process using TODGA and H_4TPAEN. ATALANTE 2016 - Conference on Nuclear Chemistry for Sustainable Fuel Cycles: Montpellier, France.

Weber, J., Brandt, F., Klinkenberg, M., Barthel, J., Breuer, U., Povstugar, I. et al., 2016: $Ba_xRa_{1-x}SO_4$ - nano-structural and chemical investigation by electron microscopy and APT. Atom Probe Tomography & Microscopy: Gyeongju, South Korea.

Weigelt, S., Schlenz, H., König, A., Heise, H., Bosbach, D., 2016: Structural characterization of geopolymers for the safe disposal of the fission products ^{137}Cs and ^{90}Sr. ATALANTE 2016 - Conference on Nuclear Chemistry for Sustainable Fuel Cycles: Montpellier, France.

Wilden, A., Klass, L., Verboom, W., Modolo, G., 2016: Evaluation of modified aqueous complexants for Am/Cm separation in the EXAm system. Sustainable Nuclear Energy Conference: Nottingham, UK.

Wilden, A., Schmidt, H., Modolo, G., Hupert, M., Santiago-Schübel, B., Svehla, J. et al., 2016: Gamma-radiolytic degradation of N-donor extractants, solvent extraction, mass spectrometric investigations and the influence of nitric acid. Sustainable Nuclear Energy Conference: Nottingham, UK.

Invited Talks

Bosbach, D., Finkeldei, S., Brandt, F., Kowalski, P., Bukaemskiy, A., Kegler, P. et al., 2016: Pyrochlore-related zirconates: New insights into nuclear waste form performance. MRS 2016 - Scientific Basis for Nuclear Waste Management Symposium: Boston, USA.

Deissmann, G., 2016: Waste packaging and degradation. 2nd Petrus-OPERA PhD and Early-Stage Researchers Conference - Radioactive Waste Management and Disposal: Delft, The Netherlands.

Deissmann, G., 2016: Corrosion of HLW waste matrices - input safety assessment. KIVI - OPERA Symposium: The Hague, The Netherlands.

Finkeldei, S., Kowalski, P., Lumpkin, G., Bosbach, D., Thorogood, G.J., Kegler, P. et al., 2016: The order/disorder transition in pyrochlores: a combined experimental and atomistic simulation study. ATALANTE 2016 - Conference on Nuclear Chemistry for Sustainable Fuel Cycles: Montpellier, France.

Ji, Y., Beridze, G., Li, Y., Kowalski, P., 2016: Large scale simulations of nuclear waste materials. International Youth Nuclear Congress: Hangzhou, China.

Kowalski, P., 2016: How challenging, useful and enjoyable is it to compute actinides? - Atomistic modelling of nuclear materials relevant for nuclear waste management. Seminar at Aachen Institute for Advanced Study in Computational Engineering Science – AICES: RWTH Aachen University, Germany.

Lang, M., Shamblin, J., Tracy, C., Finkeldei, S., Bosbach, D., Ewing, R., 2016: Characterization of radiation effects in complex-oxide nuclear waste forms: New application of neutron total scattering. Materials Science & Technology 2016: Salt Lake City, USA.

Modolo, G., 2016: Partitioning of minor actinides - an essential requirement for Transmutation. Summer Physics School on "Radiation Exposure and Disposal Options for Nuclear Waste": Bad Honnef, Germany.

Niemeyer, I., 2016: Overview on the activities at Forschungszentrum Jülich in support of non-proliferation, arms control and disarmament. Seminar at Research Center for Nuclear Weapons Abolition (RECNA): Nagasaki University, Nagasaki, Japan.

Niemeyer, I., 2016: Overview of safeguards activities and interests at Forschungszentrum Jülich. Cooperation meeting at DoE/NNSA: Washington D.C., USA.

Popa, K., Raison, P., Martel, L., Somers, J., Konings, R.J.M., Wallez, G., Arinicheva, Y., Neumeier, S., 2016: Recent progress in actinide phosphates chemistry. Plutonium Futures - The Science: Baden-Baden, Germany.

Weber, J., Brandt, F., Klinkenberg, M., Barthel, J., Breuer, U., Bosbach, D., 2016: Ra uptake into barite. 252nd American Chemical Society National Meeting & Exhibition: Philadelphia, USA.

Additional Talks

Aymanns, K., 2016: Assessment of lifecycle challenges for the Electronic Optical Sealing System (EOSS). European Safeguards Research & Development Association (ESARDA) - Working Group: Luxembourg, Luxembourg.

Niemeyer, I., 2016: Training and Knowledge Management (TKM). ESARDA 38th Annual Meeting: Luxembourg, Luxembourg.

Niemeyer, I., 2016: Systembasierte Ansätze zur Rüstungskontrolle und Abrüstungsverifikation. FONAS-Jahrestagung 2016: Osnabrück, Germany.

Niemeyer, I., 2016: Aktivitäten des Forschungszentrums Jülich zur nuklearen Nichtverbreitung, Kernmaterialüberwachung und Abrüstungsverifikation. FONAS-Jahrestagung 2016: Osnabrück, Germany.

Rutkowski, J., Canty, M., Niemeyer, I., Rezniczek, A., Stein, G., 2016: Acquisition path analysis: JCPOA case study. ESARDA 38th Annual Meeting: Luxembourg, Luxembourg.

12 How to reach us

By car:

Coming from Cologne (Köln) take the A 4 motorway (Cologne – Aachen), leave the motorway at the Düren exit, and then turn right towards Jülich (B 56). After about 10 km, turn off to the right onto the L 253, and follow the signs for "Forschungszentrum".

Coming from Aachen take the A 44 motorway (Aachen – Düsseldorf) and leave the motorway at the Jülich-West exit. At the first roundabout turn left towards Jülich, and at the second roundabout turn right towards Düren (B 56). After about 5 km, turn left onto the L 253 and follow the signs to "Forschungszentrum".

Coming from Düsseldorf Airport take the A 52 motorway (towards Düsseldorf/Mönchengladbach), followed by the A 57 (towards Cologne). Turn off at Neuss-West, and continue on the A 46 until you reach the crossroads "Kreuz Wanlo". Take the A 61 (towards Koblenz/Aachen) until you reach "Dreieck Jackerath" where you should take the A 44 (towards Aachen). Continue as described in "Coming from Düsseldorf".

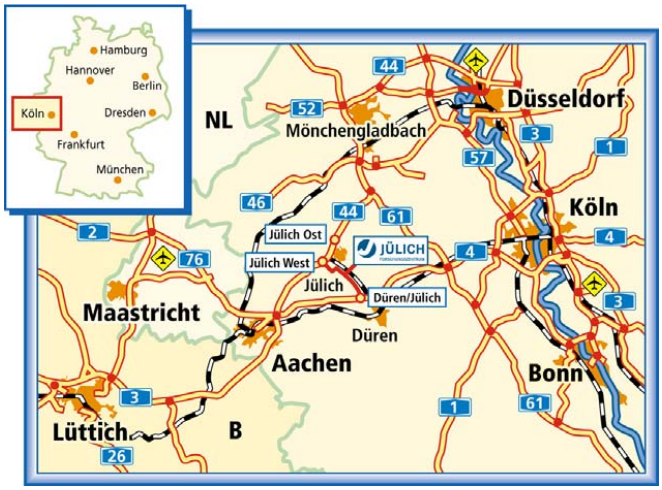

Fig. 97: Euregio Rheinland map.

Coming from Düsseldorf on the A44 motorway (Düsseldorf – Aachen) you have two options:

1. (Shorter route but more traffic) turn right at the Jülich-Ost exit onto the B 55n, which you should follow for approx. 500 m before turning right towards Jülich. After 200 m, before the radio masts, turn left and continue until you reach the "Merscher Höhe" roundabout. Turn left here, drive past the Solar Campus belonging to the University of Applied Sciences and continue straight along Brunnenstrasse. Cross the Römerstrasse junction, continue straight ahead onto Wiesenstrasse and then after the roundabout and the caravan dealers, turn left towards "Forschungszentrum" (signposted).
2. (Longer but quicker route) drive until you reach the "Jülich-West" exit. At the first roundabout turn left towards Jülich, and at the second roundabout turn right towards Düren (B 56). After about 5 km, turn left onto the L 253 and follow the signs to "Forschungszentrum".

Navigation systems

In your navigation system, enter your destination as "Wilhelm-Johnen-Strasse". From there, it is only a few hundred metres to the main entrance – simply follow the signs. The Research Centre itself is not part of the network of public roads and is therefore not recognised by navigation systems.

By train from Cologne Bonn Airport

From the railway station at the airport, take the S13 to Cologne main train station (Hauptbahnhof) and then continue with the regional express to Düren, or go to Köln-Ehrenfeld by regional express and then take the S12 to Düren. Continue from Düren as described in "By train".

By train from Düsseldorf International Airport

From the railway station at the airport, travel to Cologne main train station and then continue on to Düren. Some trains go directly to Düren whereas other connections involve a change at Cologne main train station. Continue from Düren as described in "By train".

Fig. 98: Forschungszentrum Jülich campus map.

By train:

Take the train from Aachen or Cologne to the train station in Düren. From here, take the local train ("Rurtalbahn" [RTB]) for Jülich and get out at the "Forschungszentrum" stop. To make sure that the train stops at "Forschungszentrum" you should press the request stop button (Haltewunsch) in good time after the "Selgersdorf" stop. Bus number 11 leaves from this stop for the Research Centre (for bus timetables, see "Aachen - Jülich bus connections"). If you walk, it will take you approximately 20 minutes to reach the Research Centre's main entrance.

By bus:

Aachen - Jülich bus connection

The SB11 bus line connects the Research Centre to the local public transport system. Commuters from Aachen travelling to the Research Centre have 19 options every day of reaching their destination and 18 in the other direction to get back to Aachen.

Institute:

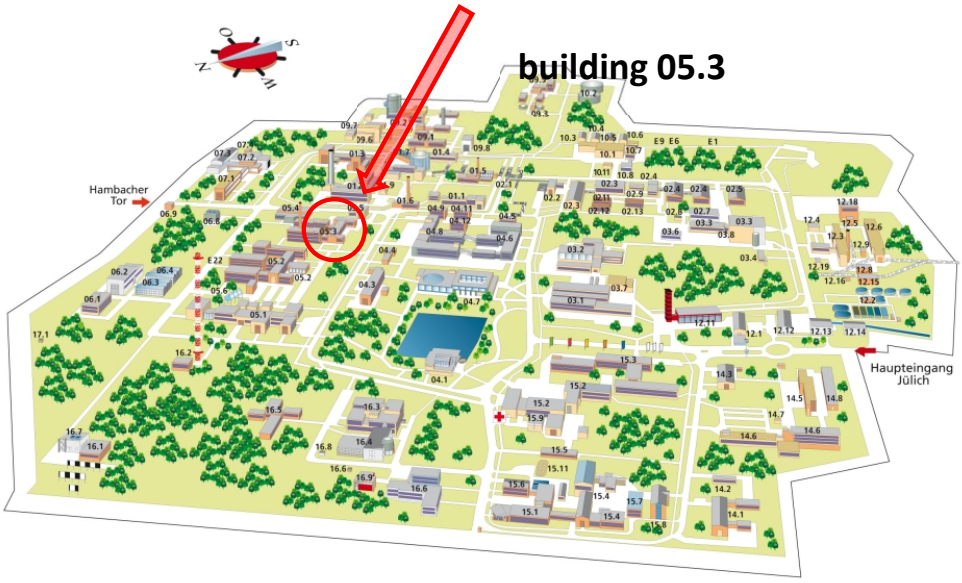

Fig. 99: Map showing the Institute, Helmholtz-Ring H18, building no. 05.3.

13 List of figures

14 List of tables

Band / Volume 392
Microcrystalline Silicon Carbide for Silicon Heterojunction Solar Cells
M. B. Pomaska (2017), 150 pp
ISBN: 978-3-95806-267-2

Band / Volume 393
Einfluss der Kristallisation auf das Fließverhalten oxidischer Schmelzen
S. Seebold (2017), 168 pp
ISBN: 978-3-95806-268-9

Band / Volume 394
Water vapour in the UTLS – Climatologies and Transport
P. R. Neis (2017), x, 124 pp
ISBN: 978-3-95806-269-6

Band / Volume 395
Neutronenaktivierungsanalyse mit gepulsten 14 MeV Neutronen zur Charakterisierung heterogener radioaktiver Abfälle
F. Mildenberger (2017), vi, 128 pp
ISBN: 978-3-95806-271-9

Band / Volume 396
Coupled biotic-abiotic mechanisms of nitrous oxide production in soils during nitrification involving the reactive intermediates hydroxylamine and nitrite
S. Liu (2017), xvii, 148 pp
ISBN: 978-3-95806-272-6

Band / Volume 397
Mixed-phase and ice cloud observations with NIXE-CAPS
A. Costa (2017), xviii, 117 pp
ISBN: 978-3-95806-273-3

Band / Volume 398
Deposition Mechanisms of Thermal Barrier Coatings (TBCs) Manufactured by Plasma Spray-Physical Vapor Deposition (PS-PVD)
W. He (2017), ix, 162 pp
ISBN: 978-3-95806-275-7

Band / Volume 399
Carbonyl Sulfide in the Stratosphere: airborne instrument development and satellite based data analysis
C. Kloss (2017), vi, 84, 1-14 pp
ISBN: 978-3-95806-276-4

Band / Volume 400
Lagrangian transport of trace gases in the upper troposphere and lower stratosphere (UTLS)
P. Konopka (2017), 70 pp
ISBN: 978-3-95806-279-5

Band / Volume 401
Numerical Simulation of Plasma Spray-Physical Vapor Deposition
P. Wang (2017), IX, 127 pp
ISBN: 978-3-95806-282-5

Band / Volume 402
The Selective Separation of Am(III) from Highly Radioactive PUREX Raffinate
P. Kaufholz (2017), IV, 173 pp
ISBN: 978-3-95806-284-9

Band / Volume 403
Spatio-Temporal Estimation and Validation of Remotely Sensed Vegetation and Hydrological Fluxes in the Rur Catchment, Germany
M. Ali (2018), xvi, 116 pp
ISBN: 978-3-95806-287-0

Band / Volume 404
Thermomechanical Characterization of Advanced Ceramic Membrane Materials
Y. Zou (2018), xvi, 168 pp
ISBN: 978-3-95806-288-7

Band / Volume 405
Betrachtung der Kristallinitätsentwicklung in mikrokristallinem Dünnschicht-Silizium mit in-situ Raman-Spektroskopie
T. Fink (2018), XI, 166 pp
ISBN: 978-3-95806-289-4

Band / Volume 406
Institute of Energy and Climate Research
IEK-6: Nuclear Waste Management
Report 2015 / 2016
Material Science for Nuclear Waste Management
S. Neumeier, H. Tietze-Jaensch, D. Bosbach (Eds.)
(2018), 223 pp
ISBN: 978-3-95806-293-1

Weitere ***Schriften des Verlags im Forschungszentrum Jülich*** unter
http://wwwzb1.fz-juelich.de/verlagextern1/index.asp

Energie & Umwelt / Energy & Environment
Band / Volume 406
ISBN 978-3-95806-293-1

Mitglied der Helmholtz-Gemeinschaft

JÜLICH
Forschungszentrum